IN VIVO EVALUATION OF A NOVEL DONUT-SHAPED MINITABLET FOR INTRAOCULAR IMPLANTATION

YAHYA ESSOP CHOONARA

A thesis submitted to the Faculty of Health Sciences, University of the Witwatersrand,

in fulfillment of the requirements for the degree of

Doctor of Philosophy

Supervisors:

Professor Michael Paul Danckwerts

University of the Witwatersrand, Department of Pharmacy and Pharmacology, Johannesburg, South Africa

and

Professor Viness Pillay

University of the Witwatersrand, Department of Pharmacy and Pharmacology, Johannesburg, South Africa

2009

DECLARATION

I, Yahya Essop Choonara declare that this thesis is my own work. It has been submitted for the degree of Doctor of Philosophy in the Faculty of Health Sciences at the University of the Witwatersrand, Parktown, Johannesburg, South Africa. It has not been submitted before for any degree or examination at this or any other University.

……

Signed this……...day of October 2009

RESEARCH PUBLICATIONS ARISING FROM THIS WORK

1. An *in vitro* study of the design and development of a novel donut-shaped minitablet for intraocular implantation, Yahya E. Choonara, Viness Pillay, Trevor R. Carmichael and Michael P. Danckwerts, *International Journal of Pharmaceutics, 310, 15-24, 2006.*

2. Studies on a novel donut-shaped minitablet for intraocular drug delivery, Yahya E. Choonara, Viness Pillay, Trevor R. Carmichael and Michael P. Danckwerts, *AAPS PharmSciTech, 8(4), 1-7, 2007.*

3. A review of implantable intravitreal drug delivery technologies for the treatment of posterior segment eye diseases, Yahya E. Choonara, Viness Pillay, Michael P. Danckwerts, Trevor R. Carmichael and Lisa C. du Toit, *Journal of Pharmaceutical Sciences, in press, October 2009.*

4. Characterization of a donut-shaped minitablet: The effects of irradiation sterilization on the physical and chemical stability of the device, Yahya E. Choonara, Viness Pillay, Michael P. Danckwerts, Riaz A. Khan, Lisa C. du Toit and Trevor R. Carmichael, *AAPS PharmSciTech, submitted, October 2009.*

5. *In vivo* evaluation of a donut-shaped minitablet in the rabbit eye model, Yahya E. Choonara, Viness Pillay, Michael P. Danckwerts, Trevor R. Carmichael, Lisa C. du Toit, Carla Wanblad and Simon J. Naylor, *Journal of Controlled Release, submitted, October 2009.*

6. Exploratory data analysis from a donut-shaped minitablet device employing compartmental and non-compartmental pharmacokinetic modeling analysis, Yahya E. Choonara, Viness Pillay, Michael P. Danckwerts, Trevor R. Carmichael and Lisa C. du Toit, *Current Drug Delivery, submitted, October 2009.*

(See Appendix A)

RESEARCH PRESENTATIONS ARISING FROM THIS WORK

1. The influence of gamma-irradiation sterilization on a PLGA-based intraocular drug delivery device, Yahya E. Choonara, Viness Pillay, Michael P. Danckwerts and Trevor R. Carmichael, American Association of Pharmaceutical Scientists, Los Angeles Convention Centre, Los Angeles, California , United States of America, November 16-20, 2009.

2. A biodegradable donut-shaped minitablet for sustained intraocular release of ganciclovir, Yahya E. Choonara, Viness Pillay, Michael P. Danckwerts, Trevor R. Carmichael, Simon J. Naylor, Carla Wanblad and Valence M.K. Ndesendo, American Association of Pharmaceutical Scientists, Atlanta World Congress Centre, Atlanta, Georgia, United States of America, November 16-20, 2008.

3. A ganciclovir-loaded intraocular device implanted in rabbit eyes for the potential treatment of human cytomegalovirus retinitis, Yahya E. Choonara, Viness Pillay, Michael P. Danckwerts, Trevor R. Carmichael, Simon J. Naylor and Carla Wanblad, 29th Annual Conference of the Academy of Pharmaceutical Sciences of South Africa, Hunters Rest Resort, Magaliesburg, Johannesburg, South Africa, September 22-26, 2008.

4. Development of a highly sensitive UPLC assay method for the determination of ganciclovir in rabbit serum and vitreous humor, Yahya E. Choonara, Viness Pillay, Michael P. Danckwerts and Trevor R. Carmichael, 29th Annual Conference of the Academy of Pharmaceutical Sciences of South Africa, Hunters Rest Resort, Magaliesburg, Johannesburg, South Africa, September 22-26, 2008.

5. A ganciclovir-loaded intraocular device implanted in rabbit eyes for the potential treatment of human cytomegalovirus retinitis, Yahya E. Choonara, Viness Pillay, Michael P. Danckwerts, Trevor R. Carmichael, Simon J. Naylor and Carla Wanblad, Faculty of Health Sciences Research Day, University of the Witwatersrand, Johannesburg, South Africa, 20th August 2008.

6. An *in vivo* investigation into a novel biodegradable device for intravitreal insertion, Trevor R. Carmichael, Yahya E. Choonara, Viness Pillay, Michael P. Danckwerts and Simon J. Naylor, 2008 Annual Meeting of the Association for Research in Vision and Ophthalmology, Fort Lauderdale, Florida, United States of America, April 27-May 1, 2008.

7. An *in vivo* investigation into the intraocular implantation and histomorphological characterization of a novel biodegradable polymeric device, Yahya E. Choonara, Viness Pillay, Michael P. Danckwerts, Trevor R. Carmichael and Simon J. Naylor, 28th Annual Conference of the Academy of Pharmaceutical Sciences of South Africa, Club Mykonos Resort, Langebaan, Cape Town, September 4-7, 2007.

8. Direct compression of a novel intra-ocular poly(DL-lactide-co-glycolide) (PLGA) implant: Investigation of the micromeritic parameters, Yahya E. Choonara, Viness Pillay and Michael P. Danckwerts, Annual Meeting of the American Association of Pharmaceutical Scientists, San Antonio, Texas, United States of America, October 29-November 2, 2006.

9. A novel donut-shaped minitablet for intra-ocular implantation in HIV+ patients, Yahya E. Choonara, Viness Pillay and Michael P. Danckwerts, 1st Symposium on Biomaterials Science and Applications in South Africa, University of the Witwatersrand, 4th September, 2006.

(See Appendix B)

PATENT FILED

A biodegradable implantable drug delivery device. Inventors: Yahya E. Choonara, Viness Pillay and Michael P. Danckwerts. United States Patent Application (11/288,035) filed on 28.11.2005 and published on 31.05.2007 (US-2007-0122449-A1). Field of the invention relates to a biodegradable, implantable device for the *in situ* delivery of a pharmaceutical composition and to a method of manufacturing such a device.

(See Appendix C)

SUMMARY

The therapeutic advantages offered by the use of implantable intraocular devices are numerous and significant. Intravitreal drug delivery technologies that provide continuous controlled drug release may in time find significant application in the treatment of ophthalmic diseases that are otherwise difficult to treat effectively. Disease due to cytomegalovirus retinitis (CMV-R) is among the most common opportunistic infection in patients with the Acquired Immune Deficiency Syndrome (AIDS). The virus can give rise to multiple organ disease and retinitis accounts for 75-85% of CMV-R disease in patients. It is a serious sight-threatening infection that occurs in approximately 25% of patients with AIDS. If left untreated the disease follows a relentless course which inevitably results in blindness. Several intraocular devices have been developed for the treatment of posterior segment eye diseases. However, these have significant limitations in providing effective treatment. This research was approached from a pharmaceutical technology development and formulation viewpoint aimed at the development and optimization of a biodegradable ganciclovir (GCV)-loaded Donut-Shaped MiniTablet (DSMT) device for the efficacious treatment of posterior segment eye diseases. This research was performed in the New Zealand White Albino (NZWA) rabbit eye model. A GCV-loaded DSMT device using various poly(lactic-co-glycolic acid) (PLGA) combinations was prepared on a Manesty F3 tableting press using a novel central rod and punch setup developed in our laboratories. The effect of irradiation sterilization on the physical and chemical stability of the DSMT device was investigated employing structural transition analysis, porositometry, thermal analysis, textural profiling and chemometric modeling. In addition, a blueprint surgical procedure for implantation of the device in the rabbit eye model and a sensitive Ultra Performance Liquid Chromatography (UPLC) assay method employing 3D chromatography was developed. The safety, biocompatibility or potential toxicity of the device was examined via direct and indirect ophthalmoscopy, slit lamp examination, intraocular pressure measurements, histopathological examinations and clinical observations to assess any changes in the vitreous (vitreous haze) and retina (edema, chorio-retinal atrophy, vascular changes, exudative changes, and necrosis) adjacent to the implanted device. The *ex vivo* micro-environmental pH variation in close proximity to the DSMT was monitored and variations were evaluated from pH-time profiles. Twelve NZWA rabbits (divided in two groups of six rabbits each) were used for the *in vivo* study. The DSMT was implanted into the rabbit through the pars plana/peripheral retina of the right eye and sutured with 9-0 nylon. Vitreous humor (VH) from the left eye was used as controls. Two rabbits from each group of six were euthanized on days 3, 7, 14, 28, 48 and 72. The residual devices, VH, plasma samples and ocular tissue were retrieved and stored at -70ºC prior to GCV concentration analysis by 3D UPLC technology. The *in vivo* release of GCV from the DSMT device was pharmacokinetically evaluated employing compartmental and non-compartmental pK models. Results revealed that the affected transitions during γ-irradiation sterilization favored the DSMT to be employed as an implantable intraocular device. PLGA was regarded as suitably stable under compression and γ-sterilization for manufacture of the DSMT device. The DSMT device was well tolerated in the rabbit eye model without any adverse effects or toxicity to intraocular tissue structures over the entire duration reaching 72 days in this study as confirmed by histopathological examination. GCV release in the VH of the rabbits from the DSMT device was maintained within the ED_{50} range for the treatment of human CMV-R. Our study has shown that constant drug release can be obtained with the DSMT device due to its unique geometry as well as the use of PLGA with varying molecular mass, lactide:glycolide ratios, drug-loading capacities and compressive forces during tableting. GCV exhibited superior prolonged release characteristics without any dose dumping. On average 2.02±0.01µg/h of GCV was released into the VH from every 5mg GCV-loaded DSMT device over 72 days. Results also indicated that the method adopted for the previous *in vitro* drug release study was sufficiently powerful, convenient and discriminating for predicting the *in vivo* release of GCV from the device. An *in vitro-in vivo* (IVIVC) was obtained in keeping with the complexities of the study conditions and described by a Levy plot with a time-scaled Level A IVIVC correlation obtained (R^2=0.90). The DSMT device was found to be sufficiently flexible and may be used for the effective long-term intravitreal delivery of drugs for the treatment of various posterior segment eye diseases.

ACKNOWLEDGMENTS

At the time of completion of this research I have worked with a great number of people whose contribution in various ways to this research and the making of this thesis deserve special mention. It is a pleasure to convey my gratitude to them all in my humble acknowledgement. Firstly I would like to record my gratitude to Professor Viness Pillay for his impeccable supervision, advice, mentorship and guidance from the very early stages of this research as well as giving me extraordinary experiences throughout the work. Above all and the most needed, he provided me with unflinching encouragement, leadership and support in numerous ways. His true scientist intuition has made him a constant oasis of ideas and passion in science, which exceptionally inspires and enriches my growth as a student, and researcher. His involvement in this research with his originality has triggered and nourished my intellectual maturity that I will benefit from, for a long time to come. I am thankful to him more than he knows and I am proud to record that I had several opportunities to work closely with an exceptionally experienced pharmaceutical scientist like him who is regarded as a world leader in the field. I also gratefully acknowledge Professor Michael P. Danckwerts for his constant advice, supervision, and contribution, which made him also a backbone of this research and so to this thesis. Many thanks go to Professor Trevor R. Carmichael for his valuable clinical expertise and using his precious time to undertake the surgical implantation procedure in the rabbits that was necessary for completion of this thesis. I am grateful in every possible way and hope to keep up our collaboration in the future. I have also benefited by advice and guidance from Dr. Leith Meyer and his team at the Central Animal Services (CAS) at the University of the Witwatersrand who granted me their time regarding the logistical procedures for undertaking the animal studies. Many thanks also to Professor Alan D. Rothberg for his continual encouragement and support during the course of completing this research. I would also like to thank Mr. Sello Ramarumo and the rest of the technical and support team at the Department of Pharmacy and Pharmacology for their kind assistance in ensuring that this research could be undertaken in a clean and conducive environment. To Professor Simon J. Naylor and Dr. Carla Wanblad and the team at the School of Anatomical Pathology who assisted with the preparation of the histology slides of this research, I thank you. It is also a pleasure to pay tribute to Dr. Riaz A. Khan at Integral University, India, for collaborating on the chemometric and molecular modeling aspects of this research. I would also like to convey special acknowledgement to the Biotechnology Partnerships and Development (BioPAD) team and the Department of Science and Technology of South Africa, in particular to, Dr. Joe Molete (CEO: BioPAD), Dr. Bonginkosi Gumede (Health Portfolio Manager) and Ms. Kefiloe Monageng (Health Portfolio Administrator) for their indispensable assistance in funding so that I could optimally perform this research. To Dr. Robert Caveney, Ms. Cristina Pinto and Ms. Barbara Herweg at the Wits Enterprise (Pty) Ltd., thank you for your kind help in persevering to take this research to the commercialization stage. Furthermore, I would also like to thank Dr. Llewellyn Parker and his team at Bowman Gilfillan Attorneys for their hearty assistance in filing the patent arising from this research. I also benefited from the technical teams at the following companies, Microsep (Pty) Ltd., Lasec (Pty) Ltd., PA Cuthbert (Pty) Ltd., Labotec (Pty) Ltd., Wirsam Scientific (Pty) Ltd., Micron Scientific (Pty) Ltd., Perkin Elmer (Pty) Ltd., Advanced Laboratory Solutions (Pty) Ltd., Apollo Scientific (Pty) Ltd., Poretech (Pty) Ltd. and Isotron SA (Pty) Ltd. and would like to thank them for guiding me through the precise handling of delicate cutting-edge equipment that was also pivotal to the completion of this research. It is also a pleasure to mention the entire postgraduate team for creating a pleasant and vibrant research ambiance at our Research Discussion Group meetings as well as in the laboratories and for all the dry humor about the life of a scientist. Collective acknowledgments are also owed to my colleagues within the Department of Pharmacy and Pharmacology. I was also extraordinarily fortunate to have met Professor Patrick de Luca (President: American Association of Pharmaceutical Sciences) and I am grateful to him for the stimulating science discussion we had and advice given to me on my visit to Kentucky, USA, and thank you. It also brings me much happiness to unequivocally express my deepest gratitude wholeheartedly to my entire family. My parents deserve special mention for their inseparable support and prayers. To my Uncles Mr. Mahomed Farid Choonara, Mr. Yunus Choonara and Cousin Mr. Imraan Choonara. In the first place these are the people who fundamentally raised me, shaped my learning character and showed me the joy of intellectual pursuit ever since I was a child when my dad passed away. Thank you for your sacrifices, for always being the best you can be for me and your unconditional love and support. To my Mother, Rabia Choonara, for her never-ending care, encouragement and gentle love. Words fail me to express my appreciation to her for her persistent prayers and confidence in me that has made me the person I am today. Thank you all for always pushing me far beyond my limits. To my brothers and cousins thanks for being supportive and compassionate. I would like to thank everybody who was just as important to the successful realization of this thesis, as well as expressing my apology that I could not mention everyone personally or to those that I may have forgotten. Finally, but undoubtedly not the least, I would like to thank the Almighty for every bounty He has bestowed upon me.

DEDICATION

This thesis is dedicated to all those who believe in the richness of acquiring knowledge and concur that without action any idea is only as big as the brain cell in which it was conceived

TABLE OF CONTENTS

CHAPTER 1
INTRODUCTION

CHAPTER 2
A LITERATURE REVIEW OF INTRAVITREAL IMPLANTABLE DEVICE TECHNOLOGIES FOR THE TREATMENT OF POSTERIOR SEGMENT EYE DISEASES

CHAPTER 3
CHARACTERIZATION OF THE DONUT-SHAPED MINITABLET: THE EFFECTS OF IRRADIATION STERILIZATION ON THE PHYSICAL AND CHEMICAL STABILITY OF THE DEVICE

CHAPTER 4
IN VIVO EVALUATION OF THE DONUT-SHAPED MINITABLET IN THE RABBIT EYE MODEL

CHAPTER 5
EXPLORATORY DATA ANALYSIS EMPLOYING COMPARTMENTAL AND NON-COMPARTMENTAL PHARMACOKINETIC MODELING ANALYSIS

CHAPTER 6
CONCLUSIONS, RECOMMENDATIONS AND FUTURE OUTLOOK

LIST OF FIGURES

Figure 3.7: Chemometric energy paradigms and molecular structural models depicting the influence of the sterilization process on the DSMT device matrix and pore formation after irradiation where, a) constant energy requirement by the DSMT matrix during irradiation, b) energy decay through decoiling with minimal energy retained after irradiation and c) instant energy decay profile of the matrix, where, E_{ID}= instant energy decay, E_{HD}=hold energy decay, E_{TD}=energy decay point with E_{HD}., E_{TBM} energy requirement till irradiation complete, TBM= irradiation time, E_{Tn} end-point energy relationship at n point of time.

Figure 3.8: A schematic depicting the forces and pressures operating on the powder blend under compression in a punch and die assembly with the protrusion of the novel central rod employed for producing the DSMT device. Where, $F_a(P_a)$=applied force (pressure) by the upper punch, $F_b(P_b)$=force transmitted by the lower punch (in a single-punch press), F_d=force lost to the die (i.e. the axial frictional force operating during compression), $F_r(P_r)$=radial force arising from the horizontal expansion of the mass in response to the axial compressive force (pressure) and is reduced as a result of the residual force absorbed by the central rod, F_e=ejection force on the lower punch during expulsion of the DSMT out of the die, *D*=die diameter and *d*=diameter of the central rod, *L*=height of the compact.

Figure 3.9: Theoretical radial pressure cycles for an ideal elastic body, a body with constant yield stress and a Mohr body, where A-A'= yield points, B-B'=maximum applied pressure, C-C'= yield points of decompression and D-D'= residual die-wall pressures (Source: Long, 1960).

Figure 3.10: Schematic diagrams depicting the differences in surfaces available for interaction and subsequent consolidation during compression between a) a conventional tablet matrix and b) a donut shaped tablet matrix of equal diameter.

Figure 3.11: A model depicting typical digitalized signals from an instrumented tablet press of the compression/decompression tableting cycles of a) a conventional tablet matrix and b) a DSMT device, where, *1a* and *b*=upper punch forces, *2a* and *b*=lower punch forces, *3a* and *b*=upper punch displacements, *4a* and *b*=lower punch displacements, *5a* and *5b*=die-wall force of conventional tablet matrix and DSMT device, respectively, *6a*=residual lower punch force, *6b*=central rod friction during DSMT compression and decompression, *7a*=ejection force of conventional tablet matrix, *7b*=residual lower punch force after DSMT compression and *8*=ejection force after DSMT compression.

Figure 3.12: Superimposed thermal profiles for native GCV, native PLGA, a GCV:PLGA physical mixture, a non-sterilized GCV-loaded DSMT device and a sterilized GCV-loaded DSMT device, at a temperature range of 30-400°C and a heating rate of 10°C/min (N=3).

Figure 3.13: Superimposed FTIR spectra of a) native GCV, b) native PLGA, c) a GCV:PLGA physical mixture, d) a non-sterilized DSMT device and e) a sterilized DSMT device.

Figure 3.14: Schematic depicting the molecular geometrical changes of PLGA strands after γ-irradiation showing a) a PLGA strand segment at initial stages, b) irradiation-induced energy perturbations resulting in bond re-orientation, ordering and patterning, c) energy emission-stimulated stereochemical changes toward a more stable PLGA conformation, d) intermediatary energy variable conformation between structures c) and e), where e) represents the most stable and least energetic PLGA strand conformation along with patterning of all methylene hydrogens at similar levels of geometrical coordination.

LIST OF TABLES

LIST OF EQUATIONS

CHAPTER 1

INTRODUCTION

1.1. Background and Rationale for this Research

Disease due to cytomegalovirus (CMV) is among the most common opportunistic infections in patients with HIV/AIDS. It is a serious sight-threatening infection and if left untreated the disease follows a relentless course which inevitably results in blindness (Smith et al., 1992; Jabs et al., 2003). Treatment of CMV retinitis (CMV-R) requires chronic suppressive maintenance therapy with antiviral bioactives to prevent relapse. In the last decades delivery of antiviral drugs to the vitreous cavity for treating CMV-R has been attempted by various routes which suffer from some weakness or the other. As outlined later in Chapter 2 of this thesis, promising developments are polymeric implants designed to deliver drugs intravitreally. They allow for higher intraocular drug levels than could be achieved by systemic administration and avert the inconvenience of direct intravitreal injection therapy.

The Vitrasert® implant (Chiron Vision Inc, Irvine, CA, USA) which was approved by the USA Food and Drug Administration (FDA) in March 1996, has been used with some success in practice. It is a sustained-release intraocular implant consisting of semi-permeable polymers with a 6mg ganciclovir (GCV) pellet. The polymers employed are non-biodegradable and this causes the implant to have the distinct disadvantage of having to be removed from the vitreous humor (VH) once its drug-load has been depleted. It is also extremely complicated to produce the Vitrasert® implant as it requires a number of carefully controlled coating processes. Since it is manufactured as a two-piece device (a suture tab and drug-loaded pellet) there has been several incidences reported where the drug-loaded pellet separated from the suture tab once implanted. This has resulted in significant patient discomfort. In addition, the cost of such a device is approximately $US 5000 which is not an option for the average CMV-R patient with HIV/AIDS living in South Africa or other Developing Countries.

To solve these challenges a novel Donut-Shaped MiniTablet (DSMT) was developed and evaluated as a biodegradable intraocular drug delivery system using poly(lactic-*co*-glycolic) acid polymer combinations for rate-modulated delivery of antiviral drugs (Choonara et al., 2006, 2007) (Figure 1.1).

The DSMT device was manufactured in our laboratories using a special set of punches fitted with a central rod in a Manesty tableting press. In previous studies, the erosion kinetics was assessed by gravimetric analysis and scanning electron microscopy. The device gradually eroded when immersed in simulated vitreous humor (SVH) (pH 7.4, 37°C) and released drugs in a sustained manner. Since the device is bioerodible, there will be no need to remove the device once it has released its entire drug load. The device is simple to manufacture, and is reproducible since it is produced on a conventional tableting press using novel tooling. A digital image of the DSMT device is depicted in Figure 1.1. The novel geometric design and veracity of the DSMT device was retained over 24 weeks of *in vitro* erosion indicating that the device was suitable as a biodegradable drug delivery system. When considering the duration of drug released from the DSMT device, it was found that by the careful selection of the type and concentration of polymer employed in formulating the DSMT device, it was possible to produce a device that could release drug for any period up to 12 months (Choonara et al., 2006, 2007).

Figure 1.1: A digital image depicting the DSMT device in relation to a typical USA one dime coin.

Although *in vitro* release testing can supply useful and valid information regarding the release of drug from the DSMT device, it cannot totally simulate *in vivo* conditions. The safety of the DSMT has also not yet been evaluated. Therefore, the current research focused on the *in vivo* evaluation of the DSMT device in terms of physical and chemical stability characterization (effect of γ-sterilization), intravitreal drug release, toxicity and pharmacokinetics in the New Zealand White Albino rabbit eye model. Knowledge of GCV distribution following administration is important if the disease is to be appropriately treated and damage to ocular tissues by higher concentrations of drug is to be avoided. When GCV is released from the DSMT matrix it must be assumed that the rate of GCV release should be much smaller than the concentration of GCV present in the VH. This assumption is reasonable because if the introduction of an intravitreal prolonged release device is to serve any purpose, the time over which it

releases a useful quantity of drug should be considerably longer than the half-life of the free drug in the VH. Therefore pharmacokinetic studies were undertaken to evaluate the GCV levels reached in the VH after intravitreal implantation of the DSMT device into the New Zealand White Albino rabbit eye. The DSMT device was sutured to the scleral flap where it released GCV over a number of months. Figure 1.2 shows a schematic comparing the DSMT device and the marketed Vitrasert® device implanted in the posterior segment of the human eye. Since the DSMT device is biodegradable, it would not be necessary to remove it once the drug-load is depleted (Athanasiou et al., 1990; Bodmeier et al., 1991; Colo et al., 1992; Bhardwaj et al., 1998; Avery et al., 1999; Dorta et al., 2002). The device is reproducible and easy to manufacture, as it is produced on a conventional tableting press with specialized tooling able to produce a disc-shaped minitablet with a perfect central hole.

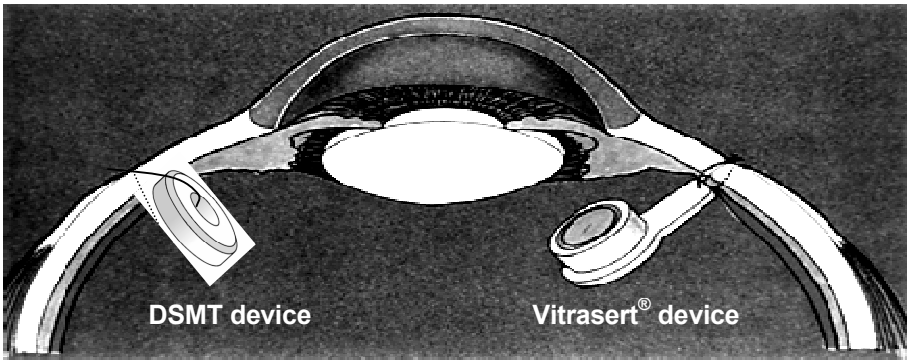

Figure 1.2: Envisaged implantation of the DSMT device in the human eye, (Adapted from Sanborn et al., 1992).

Whenever a new device for delivering drugs to the posterior segment of the eye is being considered, it is to be expected that many pathological parameters such as retinal tissue toxicity must also receive consideration. There is the potential of harm to the eye due to chemical toxicity as a result of polymer degradation and higher concentrations of drug within the posterior segment of the eye. Consequently it is imperative that the safety of the device be accurately evaluated. Biocompatibility tests can be extremely useful. However no one individual test is conclusive proof of compatibility. Therefore, a combination of as many tests as is practical and economically viable was employed in this research to assess the potential toxicity of the DSMT device.

1.2. Aim and Objectives of this Research

This research was approached from an impact viewpoint of the pharmaceutical technology formulation and development of the DSMT device aimed at considering all factors that are responsible for optimization of the DSMT device in terms of its *in vivo* performance. A drug-loaded DSMT device using various poly(lactic-co-glycolic acid) (PLGA) combinations was formulated with GCV employed as the model drug. The device was prepared on a Manesty F3 tableting press, using a novel central rod and punch setup developed in our laboratories. The specific objectives of this research were:

- To determine the possible effects of irradiation sterilization on the physical and chemical stability of the DSMT device.
- To blueprint and develop a surgical procedure for implantation of the DSMT device in the New Zealand White Albino rabbit eye model.
- To develop a stable and sensitive Ultra Performance Liquid Chromatography (UPLC) assay method using 3D chromatography for quantification of GCV from VH samples.
- To assess the safety, biocompatibility or potential toxicity of the DSMT device.
- To pharmacokinetically evaluate the *in vivo* release of GCV from the DSMT device.

1.3. Overview of this Thesis

Chapter 1 of this thesis provides a concise background and introduction to the challenges faced with current intraocular drug delivery and the rationale for undertaking this research. An ingenuous solution to these potential challenges is then defined with reference to previous *in vitro* studies by Choonara et al., (2006; 2007) pertaining to the novel Donut-Shaped MiniTablet (DSMT) device developed for the treatment of a common posterior segment eye disease namely, cytomegalovirus retinitis (CMV-R). Lastly, a summary of the aims and objectives, approach and methodology embarked on our current research is delineated at the end of this Chapter.

Chapter 2 of this thesis provides a comprehensive literature survey on intravitreal implantable device technologies for the treatment of posterior segment eye diseases. This section elaborates on the various approaches taken by other researchers who have developed drug delivery devices for treating the relentless disease and also highlights the pertinent advantages and limitations of these devices, in particular the Vitrasert® device.

Chapter 3 of this thesis describes and evaluates the effects of γ-irradiation on the physical and chemical stability of the PLGA-based DSMT device loaded with $5\%^{w}/_{w}$ GCV and intended for intraocular implantation in the New Zealand White Albino rabbit eye model. The influence of PLGA radiolysis and the identification of possible irradiation mechanisms are also discussed after investigations employing Fourier Transform Infra-red (FTIR) analysis, porositometry, thermal analysis, textural profiling and chemometric model analysis. The DSMT devices were prepared by direct compression technology utilizing novel tablet tooling and γ-irradiated for sterilization prior to implantation. The stability of the GCV-loaded DSMT device was evaluated on the basis of molecular structural transitions, changes in porosity, thermal analysis, physicomechanical profiling and chemometric model analysis. The device was found to be desirably stable with no significant transitions in its physicochemical and physicomechanical properties that could negatively impact the overall, performance of the device.

Chapter 4 of this thesis delineates the pragmatically undertaken *in vivo* animal studies performed in the New Zealand White Albino rabbit eye model once the stability of the DSMT device was established. This

component of the research focused on the *in vivo* investigation of the GCV-loaded biodegradable DSMT device in the rabbit eye model. The DSMT was manufactured with PLGA used as the GCV delivery platform as it displayed superior control of GCV release during previous *in vitro* studies. A total of 12 rabbits were used for the *in vivo* studies. This Chapter details the implantation procedure of the DSMT through the pars plana/peripheral retina of the rabbit eye. The possible adverse effects of the DSMT on ocular tissues are also outlined in terms of histomorphological and slit lamp examinations, the measurement of intraocular pressure and indirect ophthalmoscopy. The *ex vivo* micro-environmental pH variation studies are also discussed with the use of pH-time profiles. The Chapter concludes with a comprehensive discussion of the assay development for GCV content analysis and description of the *in vivo* GCV concentration-time profile obtained after VH and plasma sample retrieval and analysis by a liquid-liquid phase extraction technique and 3D Ultra Performance Liquid Chromatography (UPLC) technology.

Chapter 5 of this thesis enlightens the reader with the *modus operandi* of developing a suitable pharmacokinetic (pK) model and *in vitro-in vivo* (IVIVC) correlation to describe the release of GCV from the DSMT device in the New Zealand White Albino rabbit eye model. This mathematical and computational software-based component of the research focused on compartmental and non-compartmental pK modeling of GCV release from the DSMT device.

Chapter 6 of this thesis discusses the suitability of the novel DSMT device developed and recommendations are provided for future studies in human subjects.

CHAPTER 2

A LITERATURE REVIEW OF INTRAVITREAL IMPLANTABLE DEVICE TECHNOLOGIES FOR THE TREATMENT OF POSTERIOR SEGMENT EYE DISEASES

2.1. Introduction

The design of ophthalmic drug delivery systems is a unique challenge that is restricted by the anatomical position of the eye as well as the functional physiology of the eye tissues. The eye is a relatively isolated organ divided into an anterior and posterior segment with numerous avascular structures (Bourges et al., 2006). In this regard, the efficacy of topical drug delivery via eye-drops is only limited to the treatment of anterior segment eye diseases. The anterior segment includes the cornea, iris, crystalline lens, ciliary body and aqueous humor while the posterior segment comprises the vitreous body, retina, and choroid. Historically, the bulk of ophthalmic research focused on drug delivery to the anterior segment of the eye (Rapoport, 1977; Velez and Whitcup, 1999). Due to the number of protective anterior segment barriers, typically less than 5% of an applied dose via an eye-drop will be delivered to the ocular tissues of the anterior segment and almost negligible quantities to none may enter the posterior segment if required (Laties and Rapoport, 1976; Cunha-Vaz, 1979; Foulds et al., 1980; Cunha-Vaz, 1997).

Various attempts have focused on trying to improve the bioavailability of eye-drop formulations. These include the addition of viscosity and penetration enhancers such as hydrogel-based polymers (Ahmed and Patton, 1985), chelating agents (Schoenwald and Huang, 1983), preservatives (Sieg and Robinson, 1977), surfactants (Liaw and Robinson, 1992), bile salts (Rojanasakul et al., 1992), the use of prodrugs and liposomal carriers (Schoenwald and Ward, 1978), mucoadhesives (Chang and Lee, 1987), thermoreponsive gels (Brechu and Maren, 1993), and colloidal particulate formulations (Grass and Robinson, 1988). These approaches have the ability to prolong the pre-corneal residence time and improve the bioavailability of drugs within the anterior segment (Maren and Jankowska, 1985; Huang et al., 1989). However they have no bearing on improving the delivery of drugs to the posterior segment of the eye where the majority of sight-threatening diseases are likely to emanate and prevail.

Systemic drug administration has been used to treat a few vitreoretinal diseases (Chang et al., 1988; Charles et al., 1991; Urtti et al., 1994). However, previous studies reported that only minimal quantities of drug could reach the eye and hence large doses are required to obtain therapeutic drug levels in the posterior segment of the eye due to the restrictive blood-ocular barriers. Studies have revealed that the systemic route of drug administration for the treatment of posterior segment eye disease results in increased peripheral side-effects due to the large doses required for penetrating the blood-ocular barriers. Thus diseases affecting the posterior segment of the eye are difficult to treat and take longer to combat by employing conventional topical or systemic drug delivery (Maurice, 2001). Therefore research has been directed at specialized drug delivery technologies to the tissues of the posterior segment of the eye (Winfield et al., 1990; van Ooteghem, 1993; Visor, 1994; Lang, 1995; Le Bourlais et al., 1998; Oyster, 1999; Geroski and Edelhauser, 2000; Mort, 2000; Van Santvliet and Ludwig, 2004; Baudouin, 2005; Gulsen and Chauhan, 2005; Hosoya et al., 2005; Salyani and Birt, 2005; Barbu et al., 2006; Choonara et al., 2006; 2007).

2.2. The blood-ocular barriers: An impediment to intraocular drug delivery

The blood-ocular barriers located at the level of the retinal vascular endothelial cells and retinal pigment epithelium inhibits the entry of drugs from the systemic circulation into the retinal tissue. The circumstances at the blood-ocular barriers are better understood considering two main barrier systems present (Figure 2.1). The ***blood-aqueous barrier*** regulates the exchange between the blood and intraocular fluid and concerns primarily the ciliary body where inward movements from the blood into the eye predominate. Aqueous humor is secreted into the posterior segment by the ciliary processes through the pupil into the anterior segment and leaves the eye by bulk flow at the segment angle by the trabecular or uveoscleral routes. Diffusional solute exchange between the aqueous humor and surrounding tissue, the posterior segment, and the vitreous compartment exists (Hayreh et al., 1966). The other well defined barrier is the ***blood-retinal barrier*** responsible for homeostasis of the neuroretina and involves the outward movement of substances from the eye into the blood while the penetration of only a few important metabolic products is allowed into the eye. Hence the vitreous humor is located between the blood-aqueous barrier anteriorly and the blood-retinal barrier posteriorly. The

extent of drug absorption intended to be delivered to the posterior segment of the eye is therefore severely hampered by these physiological barriers (Cunha-Vaz, 1979).

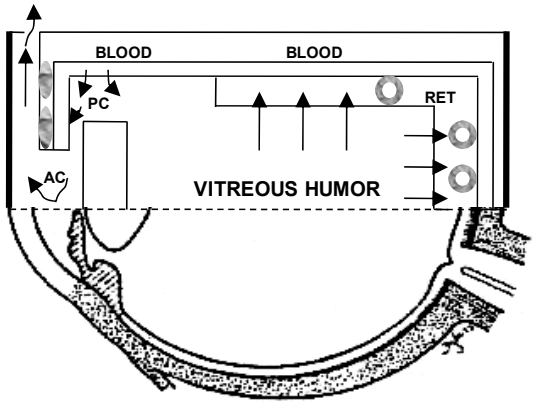

Figure 2.1: Schematic of the blood-ocular barriers, RET (retina); PC (posterior segment); AC (anterior segment), (Reproduced with permission from: Cunha-Vaz, 1979).

2.3. Potential sites for intraocular drug delivery device implantation and mechanisms of drug release

Currently, commercialized ocular drug delivery systems have been limited to the administration by topical and intravitreal routes. However, both clinical and non-clinical studies are ongoing to evaluate systems administered by subconjunctival, sub-tenon's capsule, intrascleral, subretinal, and suprachoroidal routes as well as improvements to topical application by using unique fornix devices or punctual placement (Figure 2.2). Systemic delivery using oral tablets is still a viable alternative to ocular administration, although unique delivery systems may not be preferred as it is usually easier for patients to comply with normal oral medication schedules, even if given more than once a day, instead of undergoing a surgical implantation procedure.

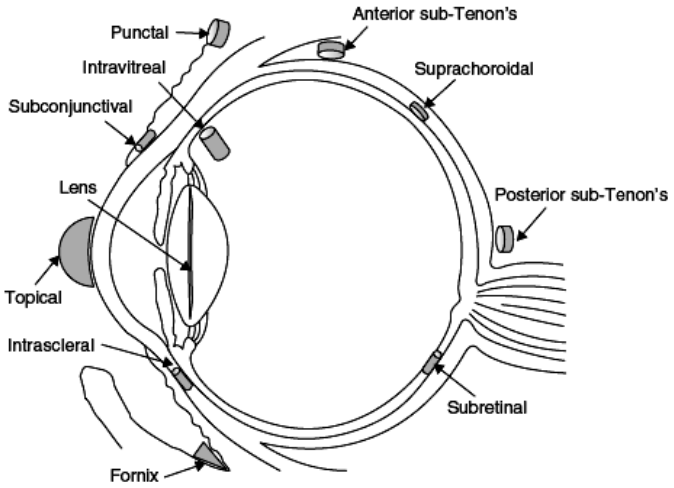

Figure 2.2: Potential sites for ocular drug delivery device administration (Reproduced with permission from Weiner, 1994).

An intraocular device can be designed as either a reservoir or matrix system. Reservoir systems are non-eroding devices that provide superior control of drug release by virtue of a specific physical rate control feature linked with the internal drug reservoir. This feature may be an opening in the device, a porous membrane or a coating through which drug diffusion is retarded. It is easier to achieve zero-order drug release kinetics using a reservoir system as there is only a single rate controlling variable that may impact drug delivery. In order to engineer non-eroding intraocular devices, there are a number of useful biocompatible biomaterials such as the polyimides, polysulfones, polyvinyl alcohols, polyvinylidine fluorides, ethylene vinyl acetates, siloxane polymers, and various methacrylate and ethylacrylate polymers. Alternatively, in a matrix system, drug is co-mixed with the rate controlling polymer. A matrix device can be engineered to produce zero-order drug release kinetics, for example, if the polymer is non-eroding and the release is then governed by polymeric chain relaxation and the dissolution rate of the drug. However, in such a device, the drug concentration must be high enough such that, when erosion occurs from the matrix, it produces sufficient fenestrated channels in the device for aqueous diffusion media to reach the internally located drug particles. In a non-eroding matrix system, the strength or resilience of the device could be compromised as diffused drug produces a series of interconnected voids through the device.

If the polymer in the matrix device is bioerodible then the device may exhibit more complex drug release kinetics due to the erosion factor of the polymer which may contribute independently to the drug dissolution or diffusion behavior, unless the geometry of the device is considered to produce a

constantly eroding drug releasing surface. In addition, biodegradable polymers may erode, either by bulk and/or surface erosion. Poly-lactides, poly-glycolides, and polycaprolactone polymers are the most common biocompatible polymers employed for the design of biodegradable intraocular drug delivery matrices. Surface eroding biodegradable polymers include certain polyanhydrides and polyorthoesters. Generally, for intraocular drug delivery, the selection of a particular system depends on the duration that is anticipated for treatment of the disease site. It is also critical to have drugs with potencies in the µg/day range, to accommodate the limited space in the human eye. Other aspects of ophthalmic drug delivery systems have been presented elsewhere (Weiner, 1994; Kumar, 2000; Chowhan et al., 2002; Edlund and Albertsson, 2002; Divvuri et al., 2003; Davis et al., 2004; Heller, 2005; Hughes et al., 2005; Ludwig, 2005; Ghate and Edelhauser, 2006).

2.4. Various approaches employed for ophthalmic drug delivery to overcome the blood–ocular barriers

A number of approaches for drug delivery to the posterior segment of the eye have been explored over the last few decades (Lloyd et al., 2001). These approaches include direct intravitreal injection of drug solutions, drug-loaded microparticle carriers such as microspheres, nanospheres (Diebold et al., 2007), and liposomes (Moritera et al., 1991; Veloso et al., 1997), transscleral drug delivery devices (Lee et al., 1999; Ambati et al., 2000), targeting of drugs via the systemic circulation (Ogura et al., 1993), and intravitreal devices using polymers (Sanborn et al., 1992; Martin et al., 1994, 1999).

2.4.1. Direct intravitreal injection

Direct intravitreal injection of drugs into the vitreous cavity is employed to achieve higher drug concentrations in the vitreous and the retina (Smith et al., 1992; Akula et al., 1994; Yang et al., 1998; Benz et al., 2006). However, repeated injections are needed to maintain drug concentrations at an effective therapeutic level over a certain period of time since the half-life of drugs in the vitreous is relatively short. Repeated intravitreal injections results in extreme patient discomfort and may lead to complications such as vitreous hemorrhage, infection, and lens or retinal injury. The direct intravitreal injection route of drug administration is able to reduce the systemic side-effects and depending on the formulation approach it may be capable of retarding drug release. However intravitreal injections

introduce further challenges, such as the progression of endophthalmitis and cataract due to repeated injections (Heinemann, 1989) (Figures 2.3a and b).

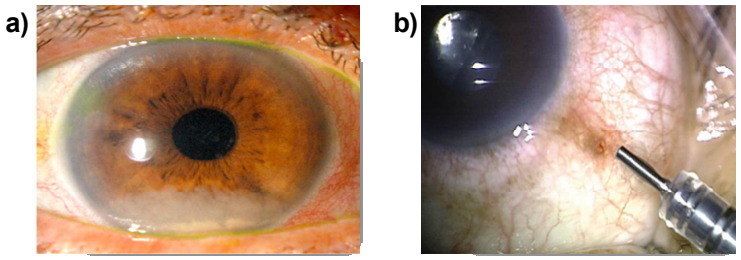

Figure 2.3: Digital images of a) a human eye showing a case of endophthalmitis and b) an intravitreal injection made at the *ora serrata* (Reproduced with permission from Yoon et al., 2009).

Intravitreal injection of sustained-release drug delivery systems such as microspheres (Herroro-Vanrell et al., 2000), lipospheres (Cheng et al., 2000; 2002) and nanospheres (Merodio et al., 2002; Bonferonia et al., 2004; Yasukawa et al., 2004; Kassem et al., 2007; Motwani, et al., 2007) offer attractive options. Colloidal-based systems are capable of delivering drug over a longer period of time than conventional intravitreal formulations used for injection into the vitreous cavity. Microparticles like microspheres or liposomes can be injected into the vitreous cavity with a fine needle and are able to release drug in the vitreous and maintain concentrations at a therapeutic level over a certain period of time (Le Bourlais et al., 1996; Martinez-Sancho et al., 2004). Microspheres of biodegradable polymers such as poly(lactic acid) (PLA) or poly(lactic-co-glycolic acid) (PLGA) have shown to effectively deliver drugs to the vitreous and retina and can be tolerated by the ocular tissues (Kimura et al., 1992; 1994). Microspheres consist of a polymer matrix, which erodes over time releasing drug that is dispersed within the matrix. Drug release kinetics from polymeric microspheres could be controlled by changing the molecular mass of the polymers or the co-polymerization ratio of PLA and PLGA. Bioerodible polymeric microspheres were shown to be effective in the treatment of ocular infections such as cytomegalovirus retinitis (CMV-R) (Moritera et al., 1991; Akula et al., 1994; Veloso et al., 1997). Figure 2.4 depicts scanning electron microscopy (SEM) images of PLGA microspheres developed by Hickey and co-workers (2002).

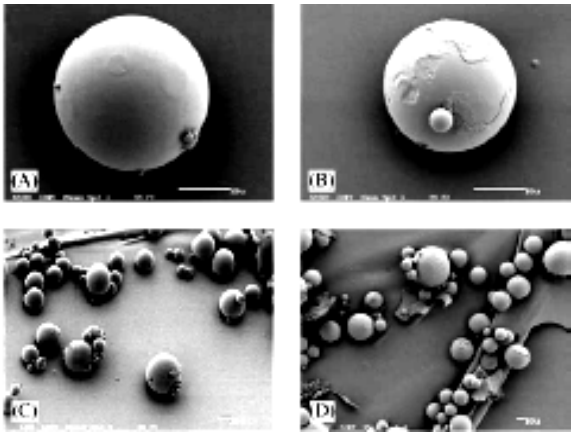

Figure 2.4: SEM images of poly(lactide-co-glycolide) microspheres (Reproduced with permission from Hickey et al., 2002).

The pharmaceutical world is becoming more and more aware of intraocular drug delivery challenges, and revolutionary therapeutic advances are being invented and implemented which may have the potential to vastly improve patient care and quality of life. Among these most promising developments are intravitreal drug delivery devices designed to deliver drugs with precision directly to the vitreous, retina, and choroid (Ashton et al., 1992; 2000).

2.4.2. Intravitreal implantable device technology

Implantable sustained-release intravitreal device technology has been given much impetus due to the perceptible benefits afforded over the use of topical eye-drops, systemic drug administration and direct intravitreal injections as modes of drug delivery to the posterior segment of the eye as described earlier (Yasukawa et al., 2005; Sultana et al., 2006). Solid biocompatible implantable devices for sustained or controlled intravitreal drug delivery to the posterior segment of the eye have been developed employing diverse approaches and includes the use of implantable devices such as osmotic mini-pumps, non-bioerodible and bioerodible drug-loaded pellets, configured capillary fibres, biodegradable scleral plugs, scleral discs, polymeric matrices and scaffolds of various geometries providing unique mechanisms of drug release for the delivery of drugs to the posterior segment of the eye (Ding, 1998; Herrero-Vanrell and Refojo, 2001; Barbu et al., 2005; Choonara et al., 2006; 2007). The intraocular structures are easily (and visually) accessible and are confined and isolated from the systemic circulation by the inner and outer blood-ocular barriers that allow for the local delivery of drugs. Furthermore, the eye benefits from an “immune privilege” particularly observed in the anterior segment and in the sub-retinal space, limiting the risk of an exaggerated inflammatory reaction to foreign antigens and cell graft rejection (Danckwerts

and Fassihi, 1991). In a study by Danckwerts and co-workers (1991), the advantages offered by intravitreal implantable delivery systems have been published and are listed in Table 2.1. However, such systems are not without their risks. These are highlighted throughout the course of this Chapter.

Table 2.1: Advantages offered by intravitreal implantable drug delivery systems.

- Drugs are delivered close to their target sites of action and undesirable effects on other sites in the body are minimized.
- For drugs that cannot be administered by other routes and where compliance is likely to be a major challenge.
- In cases of extreme allergies or side-effects to drugs already administered, immediate removal of implantable devices is possible in contrast to injectable drug delivery systems.
- Less drug is required to treat the disease state, minimizing possible side-effects and enhanced efficacy of treatment.
- Capable of protecting drugs which are unstable *in vivo* and that would normally require frequent dosing intervals.
- The improved sustained release action offers better patient compliance.
- They bypass the blood-ocular barriers allowing higher intraocular drug levels than could be achieved by systemic administration.

(Source: Danckwerts and Fassihi, 1991; Musch et al., 1997)

2.4.2.1. Bioerodible and non-bioerodible intravitreal implantable devices

Bioerodible and non-bioerodible implantable devices have been developed with the drug release kinetics dependant on both the solubility and diffusion coefficient of the drug in the polymer, the drug-loading capacity, the device configuration and the *in vivo* degradation rate of the polymer. There are several major factors to consider during the development of implantable intravitreal drug delivery devices. Biocompatibility is essential and all components are required to be chemically inert, non-carcinogenic, hypoallergenic, and mechanically stable at the implantation site. Furthermore, the material should not be physically or chemically modified by local tissue nor cause any unexpected immune or inflammatory response at the site of implantation (Zaheer et al., 1982; Park and Park, 1996). The overall development of these devices can be both time-consuming and complex, and may consist of various stability and biocompatibility tests.

Non-bioerodible devices are able to offer the advantages of sustained release and reduced host response. However, bioerodible intravitreal drug delivery devices have gained much popularity over non-bioerodible devices due to the fact that they are eventually absorbed or excreted by the body eliminating the need for surgical removal of the device after the drug-load has been depleted thereby increasing patient acceptance and compliance (Wood, 1980; Lewis, 1990). However, developing

bioerodible devices is a more complicated task as numerous variables such as the *in vivo* erosion kinetics of the polymer is required to remain at a constant rate in order to maintain sustained-release of the drug, yet their benefits far supersede these challenges. Furthermore, numerous factors may affect the rate of *in vivo* polymer erosion. Alterations in body pH or temperature may cause a transient increase or decrease in the erosion rate of the device. The surface area of the drug delivery device also plays a significant role in its erosion. As erosion proceeds the surface area of the device decreases. Thus, changes in the shape of the device need to be taken into account during the formulation design. In order to attain uniform and constant release kinetics it is therefore necessary to use geometrical shapes with surface areas that do not drastically change as a function of time during erosion (Graham, 1978). Another challenge with bioerodible devices is the extremely slow diffusion of drug from the polymeric matrix (Danckwerts and Fassihi, 1991). Diffusion of drug usually occurs at a slower rate than the bioerosion of the device and is dependent upon the chemical nature of the polymeric substance utilized in the formulation of the device. This poses a significant challenge to overcome in situations where the drug has a narrow therapeutic index (Dash and Cudworth II, 1998).

2.5. Specialized intravitreal implantable technologies for the treatment of anterior and posterior segment eye disease

2.5.1. A mucoadhesive hydrogel-based thin coiled metallic wire device (Ophthacoil)

Pijls and co-workers (2004; 2005) have developed an intraocular drug delivery device called "OphthaCoil" that is implanted in the conjunctival fornix after ethylene-oxide gas sterilization (Figure 2.5). The device consists of a drug-loaded mucoadhesive hydrogel on a thin coiled metallic wire providing the device with flexibility and integrity. The ends of the coil are capped using a photo-curable cyanoacrylate adhesive. On contact with tear fluid the hydrogel coating swells and drug is released into the tear film. The OphthaCoil device has been shown to be well tolerated in the eyes of Beagle dogs and results have shown that the device is able to release ciprofloxacin for the treatment of bacterial infections in the posterior segment of the eye as well as for conjunctivitis or keratitis over a period of 16 hours (Parks et al., 1993; Pijls et al., 2005). In order to improve the drug-loading capacity and the drug release kinetics two further approaches were explored where the interior of the coil was used as an additional drug reservoir and poly(2-hydroxyethyl methacrylate) and poly(2-hydroxyethyl methacrylate-co-1-vinyl-2-

pyrrolidone) polymeric microspheres were incorporated as drug carriers (Rosemary et al., 2003). *In vitro* drug release profiles revealed a six-fold increase of the drug-loading capacity. Preliminary *in vivo* evaluation of the Ophthacoil device was performed over a 2 hour period to assess the tolerance of the device in the human eye. Ophthalmologic examinations of the eye indicated no signs of irritation. An Ophthacoil device with a drug bioavailability of 50% can be compared to 8-12 eye drops and the researchers foresee several potential applications of the device such as for the treatment of corneal ulcers, severe bacterial conjunctivitis, fungal keratitis and controlled delivery of drugs to the posterior segment of the eye, prior to cataract surgery (Iyer et al., 2006). Depending on the potency of the antibiotic agent, sustained delivery over a minimum of 5 hours could be achieved (Pijls et al., 2004; 2005). It is not surprising that the use of an intraocular device that consists of a metallic core may cause concern even though the wire may be thin (76μm in diameter) and the coil is extremely flexible. However, according to Pijls and co-workers (2005; 2007) who have developed the OphthaCoil device, there is no contact between the metal wire and the ocular epithelium due to the hydrogel coating and the polymer caps. The essential role of the coiled metallic wire is to ensure device integrity throughout the application time window. Further proposed advantages of the Ophthacoil device (owing to the use of a metallic substrate) are the possible removal of the device with a magnet (instead of tweezers) and the enhanced x-ray visibility of the metallic coil, which is a purported safety issue. A disadvantage of the Ophthacoil device is the fact that removal of the device is required after the drug-load is depleted. However, the insertion and removal of the insert could be combined with controlled clinical examinations (Pijls et al., 2007). Reminiscent designs are discussed later in this Section, such as the I-vation® triamcinolone-coated screw that was developed by SurModics (Pty) Ltd. (Eden Prairie, MN, USA), as a vehicle for drug delivery to the posterior segment of the eye.

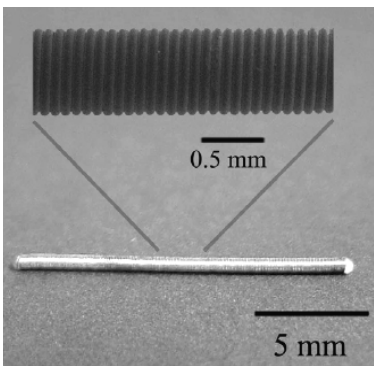

Figure 2.5: Image of the OphthaCoil drug delivery device (Reproduced with permission from Pijls et al., 2007).

2.5.2. An imprinted hydrogel contact lens device

Zero-order or concentration-independent release kinetics is highly desirable from drug delivery devices. Ali and co-workers (2000), have demonstrated zero-order release of low molecular mass, ketotifen fumarate (M_W=425g/mol), from a molecularly imprinted hydrogel device used as therapeutic contact lenses. *In vitro* drug release studies were performed within a novel microfluidic device that was able to simulate the volumetric flow rates, tear volume and tear composition of the eye (Figure 2.6). Imprinted gels with multiple functional monomers and complexation points to the drug demonstrated delayed drug release kinetics compared to less functionalized systems. Under infinite sink conditions, the imprinted contact lenses demonstrated Fickian release kinetics with diffusion coefficients ranging from 4.04×10^{-9} to $5.57\times10^{-10}cm^2/s$ (Ali et al., 2000). The authors reported the highest functionalized gel to exhibit a diffusion coefficient averaging <10 times than minimally functionalized hydrogels and released ketotifen over 5 days with 3 distinct rates of release. Under physiological volumetric flow rates, the release rate was constant for a duration of 3.5 days delivering a therapeutic dose and was fitted to a Power Law model indicating zero-order release with n=0.981±0.006 (R^2=0.99). The device has the potential for molecular imprinting to further tailor the drug release kinetics via the imprinting process. However, it is rather complicated to produce and requires several intricate design processes to affect the reproducibility of the molecular imprinting technology employed. In addition, the device has shown to release drug only up to 5 days with three distinct rates of drug release. This may not be suitable for posterior segment eye diseases that require chronic suppressive maintenance therapy over several weeks to months.

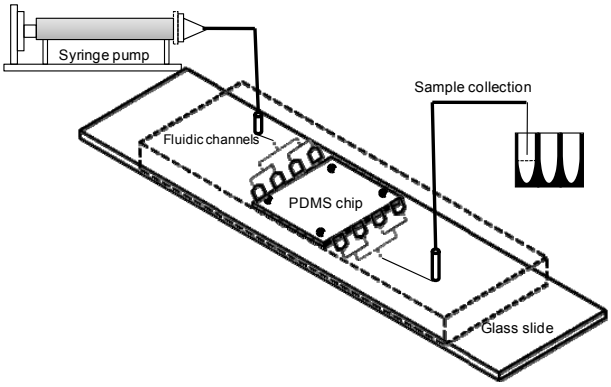

Figure 2.6: Schematic of the micro-fluidic chip design with physiological ocular flow for contact lens drug delivery evaluation (Reproduced with permission from Ali et al., 2000).

2.5.3. A cyclosporine-loaded discoid device

Gilger and co-workers (2000) reported on a discoid intravitreal device developed for the constant release of cyclosporine-A (CsA) in inflammatory episodes of uveitis in horses (Figure 2.7). This was accomplished by measuring clinical signs, intraocular damage, cellular infiltrates, and T-lymphocyte counts in conjunction with the associated level of transcribed cytokine specific mRNA. The effects of the device on recurrent inflammatory episodes in experimental uveitis were determined. Nine healthy horses were immunized peripherally with H37RA-mTB antigen twice, and then received 25mg of H37RA-mTB antigen intravitreally in the right eye and an equal volume of balanced salt solution intravitreally in the left eye. Two weeks later, the animals randomly received either the CsA-loaded device or a placebo in both eyes. One week after implantation of the devices, 25mg of H37RA-mTB antigen was re-injected into the right eye of each animal. Clinical signs of ophthalmic inflammation were graded following injections and implantation. Aqueous and vitreous humor protein levels, infiltrating cell counts, total number of T-lymphocytes, and levels of IL-2 and IFNg-mRNA were significantly less in eyes containing the CsA device compared to the eyes with the placebo. The CsA devices did not completely eliminate the development of a recurrent experimental inflammatory episode in the horse model. However, the duration and severity of inflammation, cellular infiltration, tissue destruction, and pro-inflammatory cytokines RNA transcript levels were significantly less in eyes implanted with the CsA devices (Gilger et al, 2000). Results from the study demonstrated the effectiveness of the CsA delivery device for the treatment of immune-mediated intraocular inflammation. However the efficacy of the device in human subjects is yet to be reported.

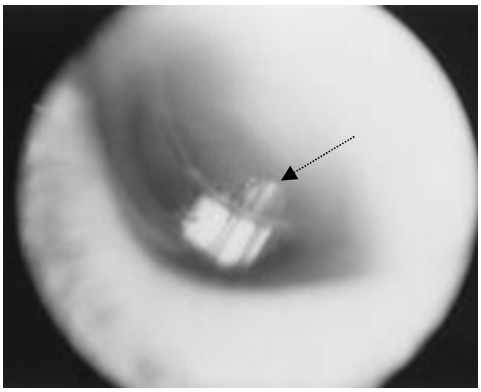

Figure 2.7: Slit-lamp image showing a cyclosporine device in the inferotemporal quadrant. The patient is pseudophakic (Reproduced with permission from Jaffe et al., 1998).

2.5.4. A Gelfoam®-based device for the delivery of insulin

Lee and co-workers (1997; 1999b), have delivered insulin employing an acidified absorbable gelatin sponge-based (Gelfoam®) (Pharmacia & Upjohn Company, Division of Pfizer Inc., NY, USA) intraocular device that can be efficiently absorbed into the systemic circulation without the aid of an absorption enhancer. The Gelfoam® device is soft and pliable and may be worn with contact lenses. The Gelfoam® device is approximately 6mm in diameter with a 2mm thickness and is excised from a slab of Gelfoam® sponge comprising 0.2mg of Zn-insulin dissolved in a 30mL solution of 10%$^{v}/_{v}$ acetic acid in water. The Gelfoam® insulin-loaded device was evaluated in the rabbit eye model. Results suggested that a change in the Gelfoam® upon treatment with acid was responsible for the systemic absorption of insulin from the device. Generally an absorption enhancer is required for the systemic absorption of insulin delivered by the ocular route (Chiou and Chuang, 1989; Yamamoto et al., 1989; Chiou et al., 1990; Chiou, 1991; Hopper et al., 1991; Chiou and Li, 1993; Bartlett et al., 1994a, b; Sasaki et al., 1994; 1995; Morgan 1995; Pillion et al., 1995; Morgan and Huntzicker 1996; Simamora et al., 1996; Negvesky et al., 1999). Lee and co-workers (1997a) showed that the device could provide a uniform blood glucose reduction over 8 hours with the aid of Brij-78 as an absorption enhancer. Furthermore, this group (Lee et al., 1997b) also showed that similar results could be obtained from enhancer-free devices to which acetic acid had been added and removed by evaporation. They have shown that acetic acid enhances the systemic absorption of insulin from the gelatin-based devices by the intraocular route. The pH of tear fluid changed from a pH value of 7 to 5 immediately after the instillation of the acid-treated device and returned to pH 7 within 5 minutes while absorption continued for over 8 hours (Figure 2.8a and b). This indicated that tear pH was not responsible for enhancing the absorption of insulin (Lee et al 1999). Overall, the data suggested that the enhancement of the absorption of insulin is due to a change in the Gelfoam® upon acid treatment. This was confirmed by the devices that were not treated by acid and were inactive whereas those that were acid treated were active. While neither the chemical composition nor the mechanism by which the device functions are clearly understood, it is clear that the interaction of gelatin with dilute acetic acid produces a potent enhancer which promotes the systemic absorption of insulin delivered via the intraocular route. Although the Gelfoam® device is currently employed for the systemic delivery of drugs via the ocular route, future research into the applications of this device may realize its potential for the intraocular delivery of drugs to the posterior segment of the eye.

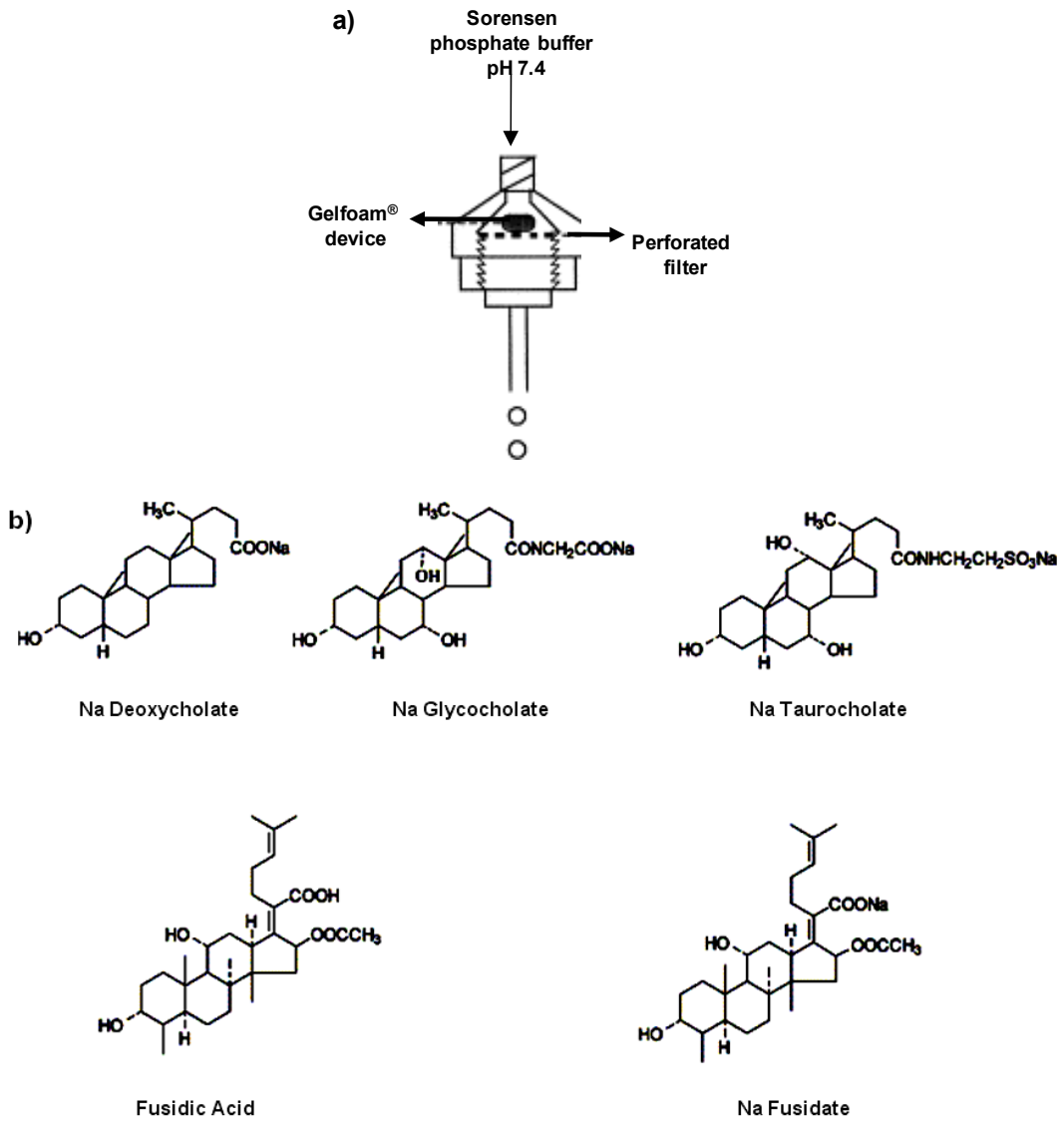

Figure 2.8: a) Experimental set-up for the determination of Zn-insulin concentrations released from the Gelfoam® device and b) chemical structures of the various compounds comprising the Gelfoam®-based device (Reproduced with permission from Lee and Yalkowsky, 1999).

2.5.5. An ethylene vinyl acetate and poly(vinyl) alcohol reservoir device (Vitrasert®)

Non-biodegradable polymers were first used clinically for intraocular sustained release of ganciclovir in the treatment of cytomegalovirus retinitis (CMV-R) (Sanborn et al., 1992; Musch et al., 1997). The Vitrasert® reservoir-type device (Chiron Vision Inc., Irvine, CA, USA), is composed of drug and polymeric coats of polyvinyl alcohol (PVA) and ethylene vinyl acetate (EVA). The device is implanted in patients requiring the treatment of CMV-R. PVA, a permeable polymer regulates the rate of ganciclovir permeation through the device (Figure 2.9). EVA, an impermeable polymer, limits the surface area of the device through which ganciclovir can be released. The device has shown to have no initial burst

effect. The commercially used device requires a 4-5mm sclerotomy at the pars plana for implantation. Furthermore, because the device is non-biodegradable, the drug depleted device needs to be removed during a second surgery in order to implant another device if required. The complications related to multiple implantations are vitreous haemorrhage, rhegmatogenous retinal detachment, endophthalmitis, and cystoid macular oedema with epi-retinal membrane, which occurred in 12% of eyes in one study (Lim et al, 1999). The same type of implant containing dexamethasone, fluocinolone acetonide, or cyclosporine is being tested to treat severe uveitis (Jaffe et al., 1998; 2000; 2000). The sustained release of triamcinolone and 5-fluorouracil (5-FU) was studied in the treatment of experimental proliferative vitreoretinopathy (PVR) (Yang et al., 1998). However, the sustained release of these steroids may cause secondary glaucoma and cataract. Many candidate drugs tested for the treatment of age-related macular degeneration (AMD) may be applicable using the sustained release Vitrasert® device. Furthermore, occasional endophthalmitis and an increased rate of retinal detachments have been reported after implantation of the Vitrasert® device (Bourges et al., 2006). Most patients are expected to experience an immediate and temporary decrease in visual acuity which lasts for approximately 2-4 weeks post-operatively that is attributed to the surgical procedure. Nevertheless, the Vitrasert® device has witnessed the most clinical success to date as an intraocular device and has been extensively used for the treatment of CMV-retinitis. Other devices such as the Retisert® and Medidur® (Bausch & Lomb Inc., Rochester, NY, USA) devices have since been developed and refined based on the clinical success of the Vitrasert® device.

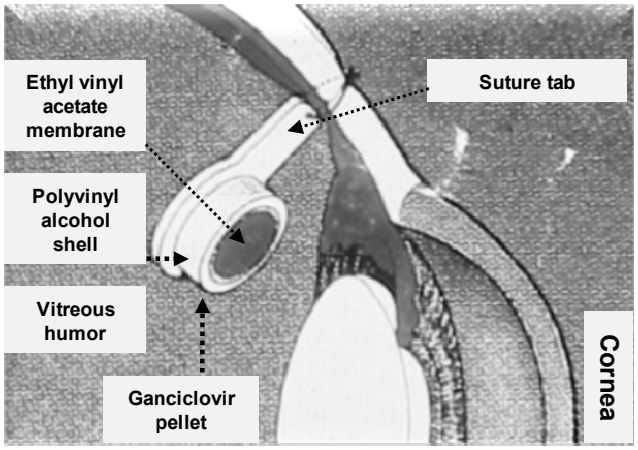

Figure 2.9: Schematic of the non-biodegradable Vitrasert® device implanted in the human eye (Reproduced with permission from Smith et al., 1998).

2.5.6. The Retisert® and Medidur® devices

Retisert® (Bausch & Lomb Inc., Rochester, NY, USA) is a reservoir-based fluocinolone-loaded implant designed to provide drug release over a period of approximately 1,000 days (Figure 2.10). The implant contains 0.59mg of drug, and delivers 0.5µg/day of the corticosteroid, fluocinolone (Kupperman, 2006). However, significant ocular side-effects are noted with the device. The concept of a small quantity of drug can be effective; however, this also highlights the efficacy of the drug delivery device. There have been uveitis and diabetic macular edema (DME) trials undertaken with the Retisert® technology, but currently the device is indicated for uveitis only. While a benefit is seen in both conditions, the ocular side-effects of the device are significant enough that limits its indication to uveitis. The device has shown significant efficacy with 1 year post-implantation (the recurrence rate for uveitis was 5.4% compared with 46% in the control eye). In the case of DME with an extensive cystoid component, complete resolution of fluid was noted 6 weeks after implantation and the pre-existing laser spots that were previously invisible with edema were visible. The challenge is the ocular side-effects of steroids, where a 50% rate of glaucoma was observed which is unacceptable in DME patients. Additionally, cataracts are almost ubiquitous after 3 years of implantation and 93% of eyes require cataract surgery compared to 20% in a control group (Kupperman, 2006). In addition, reported surgical complications of the device have included choroidal detachment, endophthalmitis, hypotony, retinal detachment, vitreous haemorrhage, vitreous loss and exacerbation of intraocular inflammation. When considering such devices, cognisance must be taken of the ultimate risk-benefit ratio. In a recent National Institutes of Health (NIH) sponsored 5-year clinical trial the effectiveness of the Retisert® device as compared with conventional therapy (oral corticosteroids) in the management of posterior uveitis is being evaluated in 400 patients at 20 sites throughout North America. The Medidur® device (Bausch & Lomb Inc., Rochester, NY, USA) also contains fluocinolone, but it is a much smaller device (Figure 2.10). The device is easier to surgically implant and must be performed through a 3.5mm incision with a 25G needle. It is a reservoir-type non-biodegradable implant that is not sutured to the eye wall and floats freely in the vitreous space. A Phase 3 clinical trial is underway for the treatment of uveitis with limited safety data acquired from 20 patients with 900 patients in a larger Phase 3 clinical trial for the treatment of DME (Kupperman, 2006). There are two separate studies under evaluation - one device that releases fluocinolone for 18 months and another for 36 months. Medidur® may thus hold some advantage over Retisert®. It has been shown to have a more favorable ocular hypertension side-effect

profile. This may be due to the positioning of the device relative to the ciliary body and/or the trabecular meshwork (anteroposterior implant localization in the eye). The manufacturers are undertaking investigations to evaluate the validity of this statement.

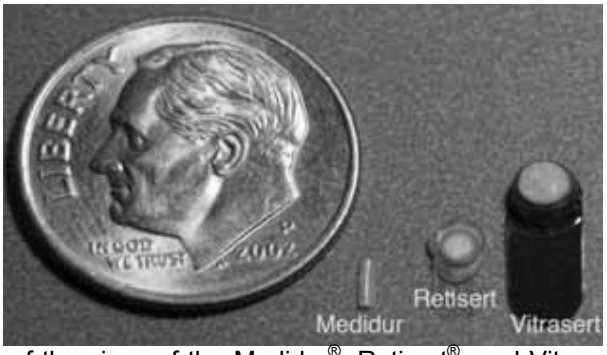

Figure 2.10: Comparison of the sizes of the Medidur®, Retisert®, and Vitrasert® implants (Reproduced with permission from Kuppermann, 2006).

2.5.7. A micro-electromechanical device

A micro-electromechanical (MEM) intraocular drug delivery device was investigated by Li and co-workers (2007), for the treatment of incurable ocular diseases (Figure 2.11). Unlike conventional ocular drug delivery devices, the MEM device is capable of being refilled, features electronic control of drug delivery, and enables targeted intraocular drug delivery. The refillable design permits long-term drug therapy and avoids repetitive surgeries. Electronic control of dosing is achieved by using electrolysis-actuated pumping to deliver drugs directly to the posterior segment of the eye. A flexible transscleral cannula allows targeted delivery to tissues in both the anterior and posterior segments of the eye. The device has demonstrated to provide flow rates suitable for ocular drug therapy from pL/min to L/min. Both continuous and bolus drug delivery modes may be used to achieve accurate delivery of a target volume of 250nL of drug. An encapsulation packaging technique was developed for acute surgical studies and preliminary *ex vivo* drug delivery experiments in porcine eyes were performed. To deliver drug into the eye, the device is actuated by manually depressing the drug reservoir. This action generates an overpressure in the reservoir which in turn causes a check valve in the cannula to open and allow drug to enter the intraocular space (Figure 2.11a). Upon depletion of drug, the drug reservoir is refilled by puncturing the reservoir wall with a syringe needle and emptying the syringe into the reservoir. To achieve variable delivery rates and the ability to select either bolus or continuous delivery, an active device having electrochemically driven drug delivery was also investigated (Li et al, 2007). The drug delivery device consists of an electrolysis pump, drug reservoir, and transscleral cannula. The

electrolysis pump consists of two inter-digitated platinum electrodes immersed in an electrolyte. The electrode geometry improves the pumping efficiency by reducing the current path through the solution which also serves to lower the heat generation (Belmont and Girault, 1994). When current or voltage is applied, with the drug as an electrolyte, electrolysis of water in the drug at the electrodes produces oxygen and hydrogen gases. The gases generated result in an internal pressure increase in the sealed reservoir which causes drug to be released through the cannula and into the eye. Electrolysis is a reversible process and ceases when the applied current or voltage is switched off. This allows the gradual recombination of hydrogen and oxygen to water. Drug is stored in a reservoir integrated on top of the electrolysis pump. Preliminary *ex vivo* testing was performed demonstrating the feasibility of the MEM device for intraocular drug delivery (Li et al 2007). However, the device is extremely difficult to produce and requires significant patient intervention to achieve the required therapeutic efficacy. This may not be suitable for chronic intraocular drug therapy.

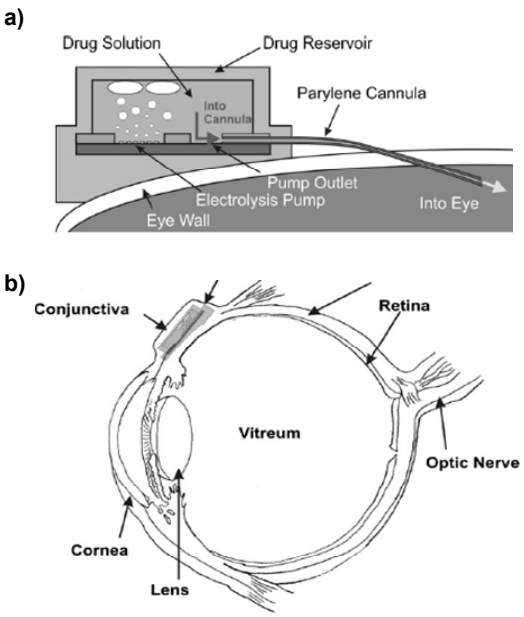

Figure 2.11: Schematic diagrams of a) A cross-section of the micro-electrochemical drug delivery device depicting electrochemical pumping of drug into the eye, and b) illustration of the implanted device under the conjunctiva in the anterior segment of the human eye (Reproduced with permission from Li et al 2007).

2.5.8. Poly(lactic) acid scleral plug devices

Vitreoretinal drug delivery with biodegradable scleral plug devices have been investigated (Figure 2.12). The drug-loaded scleral plugs of various dimensions comprise biodegradable polymers and can be implanted at the pars plana and gradually release effective doses of drugs with polymer biodegradation

over several months. For instance, the biodegradable scleral implant (Figure 2.12a and b) (mass=8.5mg; length=5mm) is prepared from poly(DL-lactide) (PLA) or poly(DL-lactice-co-glycolic acid) (PLGA) and contains various quantities of ganciclovir (GCV). The release profiles of GCV are dependent on the type of polymers used, the polymer molecular mass, and the quantity of GCV loaded. Once implanted the implantation site is replaced with connective tissue. Electroretinography and histological studies revealed minimal retinal toxicity. The implantable scleral plug may be advantageous for diseases such as CMV-R that respond to repeated intravitreal injections and for vitreoretinal disorders such as proliferative vitreoretinopathy that require vitrectomy. Other scleral devices such as the non-erodible, refillable reservoir device and coated coil matrix (Figures 2.12c and d) have also been developed. The devices can be implanted at the pars plana without a suture through a scleral incision. Since it comprises biodegradable polymers or is refillable it does not need to be removed once the drug-load is depleted. Release profiles obtained from the scleral plug devices generally have a tri-phasic release pattern depicted by i) an initial burst effect, ii) a diffusional release phase, and iii) a final burst phase. The duration and the rate of GCV release is affected by the molecular mass and the co-polymeric ratio, the total surface and volume of the matrices, and the drug-loading. Blending of PLA with various molecular masses prolonged the linear release of GCV (Yasukawa et al, 2001). A 10% GCV-loaded scleral implant prepared from PLA (M_w=130,000g/moL) released GCV *in vitro* over a period of six months (Ogura, 1998). The *in vivo* release and biodegradation were studied using 25% GCV-loaded plugs comprising PLGA (75/25; M_w=121,000g/moL) in pigmented rabbits. The GCV concentration in the ED_{50} range of for human CMV-R was maintained in the vitreous for over 3 months and in the retina/choroid for over 5 months. The GCV concentration was greater in the retina/choroid than in the vitreous throughout the study. The scleral plugs showed two distinct phases of biodegradation, a lag-time followed by erosion. During the erosional phase, the mass of PLGA was significantly reduced with the plugs being separated into two pieces at the site of scleral penetration and displaced into the vitreous 10 weeks after implantation. The fragments disappeared from the vitreous and the sub-conjunctival space 5 months after implantation (Kunou et al, 1995). However, scleral plug devices do bring their own disadvantages, such as a second burst in the late phase of drug release. Therefore researchers have explored different geometrical designs in order to circumvent the undesirable drug release kinetics obtained and have investigated the use of scleral discoid-shaped and donut-shaped devices for more controlled drug releasing surface kinetics.

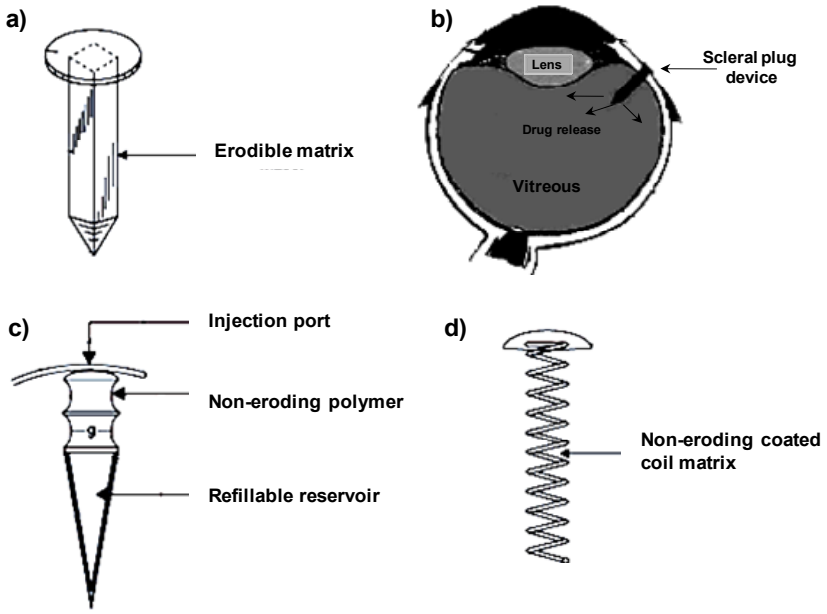

Figure 2.12: Images of a) the scleral plug drug delivery device, b) illustration of the device implanted through the scleral in the human eye, c) non-eroding reservoir device allowing for re-injection of depleted bioactive and d) non-eroding metal coil with a matrix coating (Reproduced with permission from Weiner, 1995; Ogura, 1998; Yasukawa et al., 2001; Varner, 2004).

2.5.9. A scleral discoid device

A scleral discoid device was developed to release triamcinolone acetonide (TA) over several months (Breton et al., 1998; Chan et al., 2004). Scleral disks were manufactured by a compression-molding method using the synthetic polymer, poly(methylidenemalonate) (PMM2.1.2), as the matrix (Figure 2.13). PMM2.1.2 is a synthetic polymer that has been mainly used for the manufacture of particulate systems (Roy et al., 1997). Its use for the development of intraocular implants has been advocated since its non-toxic and biodegradable leading to the formation of ethanol and glycolic acid as by-products (Breton et al., 1994; Lescure et al., 1994). The scleral discoid device displays superior physicomechanical properties adapted for *in vivo* intraocular implantation when high molecular mass PMM2.1.2 (100-150kDa) associated with ethoxylated derivatives of stearic acid (Simulsol^{TM}, Seppic Inc., Fairfield, NJ, USA) or oligomers of methylidenemalonate as a plasticizer are used. After implantation in rabbit eyes, the scleral discoid device displayed ocular biocompatibility. Clinical follow-up and ocular inflammation parameters, such as inflammatory cell counts and protein content in the aqueous humor demonstrated that the devices did not provoke abnormal inflammation. The scleral device was able to release TA in the vitreous and the sclera over a period of 5 weeks. The study by Felt-Baeyens and co-workers (2006), also supported the fact that the scleral route is promising for the treatment of posterior segment eye disease, allowing higher concentrations of drug with minimal side-effects (Felt-Baeyens et

al., 2006). Okabe and co-workers (2003) also developed an intrascleral implant prepared from PVA and EVA containing betamethasone in the form of a disk (4mg in mass, 1mm thick and 4mm in diameter). Their implantable disk was able to release betamethasone at a therapeutic level over a period of 4 weeks without an initial burst-effect. Since intrascleral implantation does not require perforation of the eye wall, the device may reduce several complications noted with other devices that require surgical imposition into the vitreous compartment.

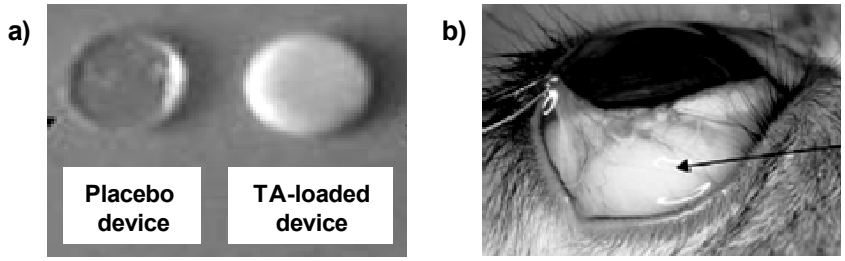

Figure 2.13: Images of a scleral device a) drug-loaded and un-loaded, and b) implanted into the peribulbar space at the sclera of a beagle dog eye model (Reproduced with permission from Felt-Baeyens et al., 2006).

2.5.10. An osmotic minipump device

A posterior segment implantable osmotic minipump device was first developed by Michelson and co-workers (1979). The osmotic minipump was implanted subcutaneously in the temporal region of the rabbit eye model of endophthalmitis. The device had connective tubing directly infusing into the vitreous cavity through a pars plana incision and maintained a calculated dose of the antibiotic gentamicin (0.01mg/h) over 4 days. Other investigators attempted similar pump models (Eliason et al., 1980; Ohkuma and Ryan, 1984), but none of these approaches reached clinical acceptance. More recently, much interest has been focused on uncomplicated slow-release intravitreal implantable devices to treat CMV-R and PVR.

2.5.11. A hyaluronic acid plug device

A hyaluronic acid (HA) intravitreal plug device was developed comprising three different HA esters namely, 100% ethyl ester, 100% benzyl ester and 75% benzyl ester (Figure 2.14). The plugs were implanted through a sclerotomy at 3.5mm from the limbus of rabbit eyes in order to study the *in vivo* biocompatibility and the biodegradation rate (Avitabile et al., 2001). The shaft diameter of the plugs was measured by ultrasound bio-microscopy to assess the *in vivo* biodegradation of the device. Slit lamp microscopy, indirect ophthalmoscopy and electroretinography were performed periodically. The effects

of the device on ocular tissues were also evaluated histologically. All the plugs displayed biocompatibility and underwent slow erosion kinetics. The partial benzyl ester was completely reabsorbed after 15 days. Analysis of variance showed a high correlation between the biodegradation rate and the time of resorption. The biodegradation rate of each device was related to the chemical structure of the three types of HA. The study suggested that the intravitreal plug devices based on HA esters may provide useful biocompatible and biodegradable devices for potential drug delivery in the treatment of posterior segment eye diseases.

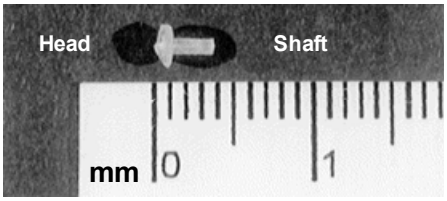

Figure 2.14: Digital image depicting the head and shaft configuration of the hyaluronic acid scleral plug delivery device (≈5mm in length) (Reproduced with permission from Avitabile et al, 2001).

2.5.12. A novel helical device

The I-vation® technology developed by SurModics (Pty) Ltd., (Eden Prairie, MN, USA) consists of a helical coil with an eluting polymer containing triamcinolone. The device provides a way of obtaining controlled release of the common ocular corticosteroid, triamcinolone. The device is implanted through a 25G needle stick and it is self-anchoring within the sclera (Figure 2.15). Initially, there were concerns regarding conjunctival exposure with the metallic screw. However, these challenges were overcome ensuring that the hub of the screw was flush with the scleral surface and not seated at an angle. A prospective, randomized, double-masked multicenter trial is underway to evaluate the technology, using two formulations in 30 patients with DME (Kupperman, 2006).

Figure 2.15: Digital images depicting a) the I-vation® technology from SurModics (Pty) Ltd., (Eden Prairie, MN, USA) consisting of a helical coil with an eluting triamcinolone-loaded polymer, b) the relative size of the device and c) the device implanted through a 25G needle stick and is self-anchoring within the sclera (Reproduced with permission from Kuppermann, 2006).

2.5.13. A micro-machined drug delivery device

The Ocular Drug Delivery Group at the University of California (Irvine, CA, USA) developed a micro-machined intraocular drug delivery device (Figure 2.16). The goal of the project was to use micromachining technology to engineer a passive, programmable, pulsatile drug delivery device, with numerous pulses, yet small enough to be used as an intraocular implantable device. The device was designed with null zones in the polymer and drug-loaded zones. This enables drug levels to cycle up and down in a pre-programmed manner, also allowing native expression of endogenous cytokines and growth factors (Kuppermann, 2006). A pulsatile system is of considerable interest for intraocular drug delivery as the programmed release of a specific dose of drug at a specific time could potentially minimize drug-related side-effects. The overall safety and efficacy of this device is yet to be established.

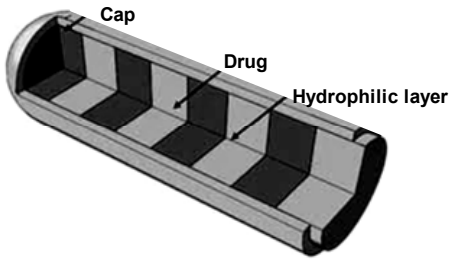

Figure 2.16: A schematic of the micromachined drug delivery device developed by the Ocular Drug Delivery Group at the University of California (Irvine, CA, USA) (Reproduced with permission from Kuppermann, 2006).

2.5.14. Encapsulated cell technology for intraocular delivery

The Encapsulated Cell Technology (Neurotech (Pty) Ltd., Lincoln, RI, USA) ophthalmic device is rather controversial (Figure 2.17). The technology uses ARPE-19 cells, a human retinal pigment epithelium (RPE) cell-line. The cells are commercially available and have been modified to produce ciliary neurotrophic factor (CNTF) and can be designed to produce various growth factors. Neurotech (Pty) Ltd. claims that the cells can produce rhuFab V2, a ranibizumab-like compound (Lucentis®; Genentech (Pty) Ltd., San Francisco, CA, USA). The controversy is that the RPE cells produce other compounds as well and the question is whether these are being disproportionately stimulated. RPE cells that are present in the human eye are able to naturally produce growth factors on a continual basis.

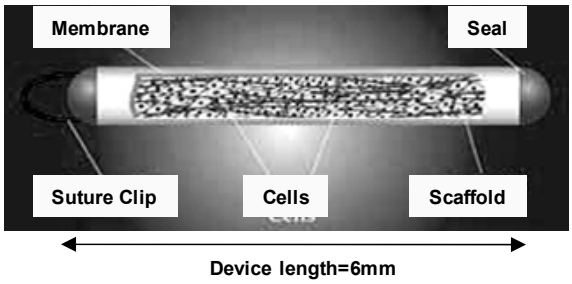

Figure 2.17: An image of the Encapsulated Cell Technology implant that is 6mm long and is surgically placed inside the eye. The CNTF elutes over time and the explants continue to secrete CNTF (Reproduced with permission from Kuppermann, 2006).

2.5.15. The Visulex® non-invasive iontophoretic ocular drug delivery device

The Visulex® technology developed by Aciont Inc., (Salt Lake City, USA) is a non-invasive, iontophoretic ocular drug delivery device that can deliver therapeutically relevant doses of triamcinolone acetonide (TA) (Figure 2.18). Researchers performed iontophoresis of TA phosphate (TAP) on the eyes of healthy New Zealand White rabbits (Hastings et al., 2004; Eljarrat-Binstock and Domb, 2005). An electrical current of 3mA for 20 minutes using a Visulex® sustained-release formulation of TAP, *in vivo* was employed. Hastings and co-workers (2004) conducted an *in vivo* study in the rabbit eye model in order to examine the quantity of TAP delivered into the eye. They dissected the enucleated rabbit eyes and used a High Performance Liquid Chromatography (HPLC) assay to determine the drug distribution in the rabbit ocular tissues. An efficacy study was also conducted to evaluate the Visulex® transscleral drug delivery system in an endotoxin-induced posterior uveitis rabbit model using direct ophthalmologic examination. A contrast agent was visually tracked as part of a precipitating sustained-release depot formed by the Visulex® device at various time intervals with Magnetic Resonance Imaging (MRI) to determine the distribution of drug released from the device. In the pharmacokinetic study, the quantity of TAP delivered into the sclera and retina/choroid regions were approximately 0.03mg from the Visulex® device. Significant levels were also found in similar tissue samples dissected from test eyes at later time intervals. The results of the efficacy study showed a significant improvement in the uveitis score of the eyes treated with the TAP-loaded Visulex® sustained release device (Csaky, 2007). The MRI study showed noticeable distribution of the contrast agent from the precipitating device toward the back of the eye. The Visulex® device can non-invasively deliver a therapeutic dose of TAP for the treatment of posterior segment eye diseases. However, further studies are required to fully evaluate the distribution of drug released over time from the Visulex® device as drug depots within the eye. In addition, the

duration of the drug action attained with the iontophoretic technique is less prolonged than with the controlled release drug delivery devices described.

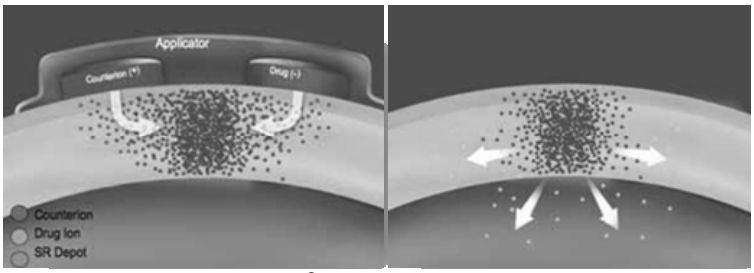

Figure 2.18: Schematic depicting the Visulex® depot-forming technology (Reproduced with permission from Csaky, 2007).

2.5.16. A pellet device comprising a silicone shell

Thalidomide is known to be a potent angiostatic agent. However, its systemic side-effects include peripheral neuropathy, central nervous system (CNS) depression, and embryo toxicity which have resulted in the lowering of dosages administered to patients for the treatment of subretinal neovascularization. Systemic inhibition of angiogenesis in elderly patients may also interfere with the development of collateral circulation, which has a role in the prevention of CNS as well as cardiac ischemic events. Velez and co-workers (1999) have developed an implant that successfully releases therapeutic intraocular doses of thalidomide, and could be used for the treatment of subretinal neovascularization (Figure 2.19). This system, however, has several disadvantages. The outer shell is non-biodegradable. Therefore, after the drug has been released, minor surgery is necessary for the removal of the delivery device from the eye. There is also the possibility that shell rupture may potentially lead to “dose dumping” during therapy. Depending on the type of drug loaded into the reservoir, “dose dumping” may result in toxic side-effects from drug concentrations that exceed maximum safety levels.

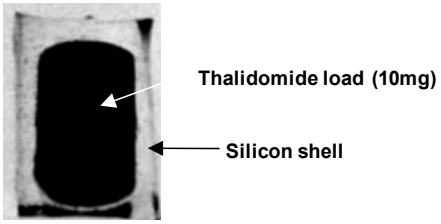

Figure 2.19: Experimental thalidomide implant with a 10mg pellet and a silicone shell (Reproduced with permission from Velez et al., 1999).

2.6. Concluding Remarks

The therapeutic advantages offered by the use of intraocular implantable devices are numerous and significant. In spite of this, the devices that are available have not yet gained widespread acceptance even though a few new products have been commercialized. This situation may change as improved devices such as those described in this Chapter are in various stages of development and are mandated by the emergence of important new drugs that have very short biological half-lives. Intravitreal drug delivery technologies that provide continuous controlled drug release may in time find significant application in the treatment of ophthalmic diseases that, because of epidemiological circumstances, are otherwise difficult to treat effectively. In summary, a reasonable strategy to circumvent the drawbacks of the challenges associated with intravitreal drug delivery is to combine technologies with the necessary balance in order to achieve sustained or controlled intravitreal drug release with patient comfort and ease of manufacturing and use. At this stage, it is apparent that no single intravitreal drug delivery device can fulfil all the clinician's expectations and needs. Thus, intravitreal implantable drug delivery devices are to be specifically designed and adapted to the targeted tissue, the physicochemical properties of the drug to be used, the physicomechanical properties of the polymer-based device and to the desired kinetics of intraocular drug release.

CHAPTER 3

CHARACTERIZATION OF THE DONUT-SHAPED MINITABLET: THE EFFECTS OF IRRADIATION STERILIZATION ON THE PHYSICAL AND CHEMICAL STABILITY OF THE DEVICE

3.1. Introduction

This Chapter aims to describe the development and characterization of the novel ganciclovir (GCV)-loaded Donut-Shaped MiniTablet (DSMT) device. As it is critical that the device remains intact throughout its therapeutic period in the vitreous humor (VH), as well as retain the ability to be reproducible on a tableting press, it is essential that certain fundamental physicochemical and physicomechanical properties of the device are assessed. These studies focused mainly on those properties that could affect the physical and chemical stability of the DSMT as a result of sterilization employing gamma (γ)-irradiation. A thorough understanding and investigation of these properties may ultimately provide a rationale for formulation design and modifications if required. There are numerous investigations that could be undertaken during pharmaceutical characterization studies. However, for this research, investigations were performed in a pragmatic manner and only immediately relevant data was generated to assess the stability of the DSMT device before and after sterilization in accordance with the UK panel on γ-irradiation guidelines for pharmaceutical products. Briefly, these guidelines conform to the agreement between the international standards for medical device sterilization and the guidelines for Gamma and Electron Beam Radiation followed by device manufacturers. The purpose of the validation process is to ensure that certain products are rendered free of viable microorganisms, and thus, is “sterile.” These standards ensure certain predetermined criteria that validates sterilization are met prior to the production of a sterile healthcare product and include, evaluation of materials to be used in the product and its packaging, determination of the product’s radiation stability, sterilization dose selection, product dose mapping, certification of the process and verification of the sterilization dose (European Guideline 3AQ4a, 1992).

As mentioned earlier the development of a prolonged release intraocular implantable device for delivering GCV is interesting for the treatment of posterior segment eye infection such as cytomegalovirus retinitis (CMV-R) (Choonara et al., 2006). Poly(lactic-*co*-glycolic acid) (PLGA) is a

copolymer of lactic and glycolic acids widely used for the preparation of drug delivery devices due to its biocompatibility and biodegradation (Ruiz et al., 1990; Black, 1992; Park and Lake, 1992; Volland et al., 1994; Athanasiou et al., 1996; Sintzel et al., 1997; Bittner et al., 1999). Numerous drug delivery devices comprising hydrophobic biodegradable polymers have received much attention, due to their ability to prolong drug release and protect drugs from premature degradation (Yoshioka et al., 1995; Montanari et al., 1998).

Drug-loaded biodegradable devices have been explored in order to improve the stability, long-term therapy, and targeting of drugs for the treatment of various posterior segment eye diseases (Lewis et al., 1990). However, devices for implantation have to meet the pharmacopoeial requirements of sterility, which has been often neglected during their design. Terminal sterilization is preferred to aseptic processing of such devices in a clean room environment under Good Manufacturing Practice (GMP) conditions, if both sterility assurance and cost are considered. The common sterilization approaches for implantable medical devices are steam, dry-heat, ethylene oxide (EO) gas, and γ-irradiation (Henn et al., 1996; Nijenhuis et al, 1996; Mohr et al., 1999). Among these, steam and dry-heat sterilization are performed at high temperature and may cause severe degradation and hydrolysis of the polymeric device. Therefore, EO gas and γ-irradiation techniques have been preferred for the sterilization of implantable biodegradable polymeric devices. Sterilization is crucial in producing biodegradable devices for clinical applications. However, only a few studies have explored the effects of the sterilization procedure on biodegradable devices composed of PLGA (Volland et al., 1994; Montanari et al., 1998; Faisant et al., 2002). Of those available, the efforts have been focused mainly on the effects of γ-irradiation on drug release and often the physicomechanical properties have been overlooked. Apart from studies showing that the simpler and lower costing EO gas sterilization procedure does not affect the molecular mass of PLGA unlike in γ-irradiation sterilization (Henn et al., 1996), a general lack of knowledge on the micro-mechanical properties of such devices after sterilization may have contributed to the prevailing conception that there are limited approaches for sterilizing biodegradable devices.

PLGA-based devices offer various advantages compared to the use of conventional polymers, such as the possibility to control the resulting drug release rate accurately over prolonged periods of time as well as having superior biocompatibility and complete bioerosion. The effects of γ-irradiation on PLGA and

other drug-loaded devices have been discussed previously and varying results have been reported, depending on the drug utilized (Volland et al., 1994; Bittner et al., 1999). This makes it necessary to investigate the effects of γ-irradiation on newer formulations such as devices intended for intraocular implantation as local toxicity may be related to specific properties that can be affected by the sterilization procedure. The advantages of γ-irradiation sterilization include higher penetrating power due to radiation, lower chemical reactivity, lower measurable residues, smaller temperature rises and fewer variables to control. Ionization radiation such as γ-irradiation is a form of electromagnetic radiation, characterized by high penetration at a very low dose rate that may modify the performance of irradiated drug delivery devices through radiolytic degradation (Hausberger et al., 1995; Montanari et al., 1998; Bittner et al., 1999; Shameem et al., 1999; Woo and Sanforb, 2002). However, there is minimal knowledge available regarding the underlying micro-mechanical transitional mechanisms that may also affect mass transport phenomena that modulate the drug release kinetics from such devices.

Therefore this study explored the effects of γ-irradiation sterilization on the PLGA-based DSMT device that would be suitable for further *in vivo* studies in order to improve the micro-mechanical understanding of the affects of the sterilization procedure on the DSMT device. The influence of γ-irradiation on the selected formulation was assessed using a combination of complimentary characterization techniques such as Scanning Electron Microscopy (SEM), Fourier Transform Infra-Red (FTIR) Spectroscopy, Differential Scanning Calorimetry (DSC), Porositometry and Textural Profiling. These techniques were supported by in-depth Chemometric Model Analysis to further explicate dynamic transitions at the macroscopic and molecular levels.

3.2. Materials and Methods

3.2.1. Materials

Resomer® grade RG504 (i.v.=0.45-0.60dl/g; M_w=55,000g/moL) comprising poly(lactic-*co*-glycolic acid) (PLGA) with a 50% lactide content was selected for this study and purchased from Boehringer Ingelheim, GmbH, (Ingelheim, Germany). Ganciclovir (GCV) was purchased from Hoffmann-La Roche Inc. (Nutley, NJ, USA). Magnesium stearate (Sigma Chemical Corp., St. Louise, MO, USA) was used as a tableting lubricant. A test sieve shaker (Endcotts Octagon 200, London, UK) with a variety of sieves

(Endcotts Test Sieves, Inc., London, UK) of different aperture sizes were used for ensuiring uniformity in particle size for tableting. All other reagents used were of the ultrapure grade.

3.2.2. Preparation of the PLGA-based DSMT device

Special tablet tooling was previously designed in our laboratories and manufactured by Holland Tableting Science Ltd., (Nottingham, England). Further details on the preparation of the DSMT device can be found in a publication by Choonara and co-workers, (2006). Briefly, the punch set comprised a lower and upper punch, die, and central rod. Both the upper and lower punches contained a longitudinal central hole for the insertion of the rod, which enabled a donut-shaped tablet to be compressed around it. All blending was performed using an Erweka AR 400 Cube Blender (Erweka GmbH, Flemington, NJ, USA), and a Manesty F3 eccentric (single punch) tableting press (Oystar Manesty (Pty) Ltd., Merseyside, England) was used for directly compressing the powder blends into the design of a DSMT device. A model TR 104 mass balance (Denver Instrument (Pty) Ltd., Denver, Colorado, USA) was used for all gravimetrical analysis.

3.2.3. Irradiation sterilization of the DSMT device

DSMT device samples were conditioned according to a process described by Hausberger and co-workers (1995). A batch of DSMT devices were weighed (100±0.05mg) and transferred to 2mL glass poly-top sealed cap vials. The vials were labeled and packed surrounded by dry ice into a polyurethane container, assuring a low temperature during the irradiation process. Although γ-irradiation may produce a minimal rise in temperature, maintaining a low temperature avoided a possible acceleration of PLGA hydrolytic degradation. Samples were couriered and irradiated with cobalt (Co)-60 at the γ-irradiation unit of Isotron (Pty) Ltd. (Isando, South Africa). An effective sterilizing dose of 25kGy (commonly known as the industrial overkill) was used for sterilizing the DSMT devices. Placebo and GCV-loaded DSMT devices were irradiated using Co as the irradiation source. Irradiation was performed at room temperature either under vacuum or in air with a 25kGy dose at a dosing rate of 1.3kGy/h. A minimum absorbed dose of 25kGy is regarded as adequate for the purpose of sterilizing pharmaceutical products without providing any biological validation (European Guideline 3AQ4a, 1992).

3.2.4. Surface morphological characterization of the irradiation sterilized DSMT device

The surface morphology of the DSMT device before and after γ-irradiation was analyzed by Scanning Electron Microscopy (SEM). Samples were prepared for photomicrographs by applying a thin layer of colloidal graphite on aluminium stubs and mounting the DSMT devices on graphite to secure them in place during microscopic examination using an electrical potential of 15kV. The devices were then sputter-coated with a thin layer of gold-palladium. Several photomicrographs were produced by scanning fields, selected at different magnifications using a Jeol JSM-840 SEM (Tokyo, Japan). The shape, homogeneity and the degree of surface morphological transitions were identified to assess the influence of γ-irradiation on the DSMT device (N=10).

3.2.5. Chemical structural transition analysis due to irradiation sterilization of the DSMT device

Fourier Transform Infra-Red (FTIR) spectrophotometric analysis was performed on the native GCV and PLGA, the GCV-loaded DSMT device and 1:1 ($^{w}/_{w}$) GCV-PLGA physical mixtures at ambient temperature in the wavelength range of 400-4000cm^{-1} using a Perkin Elmer Spectrum BXII FTIR spectrometer equipped with a Universal Attenuated Total Reflectance and a DynaScan interferometer (Perkin Elmer Life and Analytical Sciences Inc., Shelton, CT, USA). FTIR spectra were recorded on scans of samples at a resolution of 2cm^{-1}. FTIR spectra before and after γ-irradiation were recorded for GCV, PLGA and the DSMT devices. The molecular structure of native GCV, native PLGA, a physical mixture of GCV and PLGA and the compressed GCV-loaded DSMT device were analyzed to elucidate any variations in vibrational frequencies and subsequent polymeric structure as a result of interactions after γ-irradiation.

3.2.6. Porositometric analysis of the DSMT device before and after irradiation sterilization

The potential of PLGA degradation as a result of γ-irradiation may significantly alter the micro-environmental physicochemical and physicomechanical properties of the DSMT device such as the H^{+} concentration within the polymeric matrix. Lactic and glycolic acids produced by degradation of PLGA may lead to a decrease in pH at the centre of the device matrix (Shenderova et al., 1999). As PLGA degradation is catalyzed by H^{+} ions, a micro-pH decrease may lead to autocatalytic effects and thus alter the porosity of the polymer matrix (Spenlehauer et al., 1989; Dunne et al., 2000). Changes in porosity could affect the extent to which the DSMT device is able to imbibe sufficient quantities of

release media for the absorption of OH^- into the matrix and/or the diffusion of monomeric and/or oligomeric acids outward that is desirably rapid to prevent acidic micro-environments and thus suppress any autocatalytic effects of PLGA (Anderson and Shive, 1997; Sansdrap and Mose, 1997). These events occur as a function of the size and porosity of the device. Furthermore, PLGA degradative products initiated by the γ-irradiation process can crystallize within the device resulting in a modification of porosity (Gopferich and Langer, 1995; Park, 1995).

Porositometric analysis was performed employing an ASAP 2020 Porositometer (Micromeritics Instrument Company (Pty) Ltd., Norcross, GA, USA) equipped with research grade ASAP 2020 V3.01 software. Briefly, the surface area and pore structure was analyzed by degassing the sterilized and non-sterilized DSMT device samples (mass=95mg; density=1g/cm^3) in order to remove sample moisture and atmospheric vapor by applying a heat gradient and evacuating with Nitrogen gas (N_2) (hard-sphere diameter=3.860Å; molecular cross-section=0.162nm^2) that was used as a non-adsorbent gas. The overall hold pressure for the evacuation and heating phases during the degassing procedure was maintained at 100mmHg. The sample temperature was then reduced by an adaptive rate technique (continuous) to that of liquid N_2 (-196°C) for gas adsorption (maximum manifold pressure set at 925mmHg) using an isothermal jacket surrounding a sample tube with a warm and cold free-space of 1cm^3. Table 3.1 lists the parameters and settings employed for the porositometric analysis under standard conditions of temperature and pressure (STP: 0°C and 760torr). Adsorption isotherms representing the accumulated molar quantity of N_2 adsorbed and the gas pressure at a single constant temperature was generated. The pressure was expressed as the ratio between the relative actual N_2 pressure (P) and the vapor pressure (P_0) of N_2. The effect of γ-irradiation on the porosity and surface area transitions of the DSMT device was described by linear isotherms, Brunauer, Emmett and Teller (BET) surface area (Brunauer et al., 1938) and Barrett, Joyner and Halenda (BJH) adsorption and desorption relationships generated (Barett et al., 1951). In addition, a modern approach adopted in this study focused on the fundamental principles of statistical thermodynamics in porositometry combined with chemometric and molecular modeling in order to seek a single and unified theoretical understanding of pore formation and transitions applicable over the entire range of the isotherms generated for the DSMT device before and after sterilization.

Table 3.1: Porositometric parameter settings employed for analyzing the DSMT device physical and chemical stability transitions as a result of γ-irradiation sterilization.

Parameter	Settings
Degassing evacuation phase	
Temperature ramp rate	10°C/min
Target temperature	30°C
Evacuation rate	50mmHg/s
Unrestricted evacuation limit	30mmHg
Vacuum set-point	500µmHg
Evacuation time	60min
Degassing heating phase	
Temperature ramp rate	10°C/min
Hold temperature	35°C
Hold time	7200min
Sample analysis phase	
Sample mass	0.95g
Cold free space[a]	56.92cm^3
Analysis absorptive	Nitrogen (N_2)
Analysis bath temperature	-197.46°C
Warm free space[b]	18.61cm^3
Equilibration interval	20s

[a] *Capacity volume computed from the known quantity of N_2 in the partially immerged sample holder*
[b] *Physical free volume of the sample holder*

3.2.7. Analysis of the Tensile Strength and Fracture Energy after sterilization of the DSMT device

The sterilization-induced micro-mechanical transformations of the DSMT device were investigated employing textural profile analysis. Understanding the potential sterilization-induced transformations is significant to ensure device stability and quality. The objectives were therefore to develop a method for direct micro-mechanical analysis of the DSMT device that underwent γ-irradiation in order to establish an understanding of the controlling factors of matrix transformation that may influence the overall stability of the device. Textural analysis was performed employing a TA.XT*plus* Texture Analyzer (TA) (Stable Microsystems, Godalming, Surrey, England) fitted with a 2mm flat-tip cylindrical probe and a 5kg load-cell. The Tensile Strength and Fracture Energy were computed from Force-Distance and Force-Time profiles generated. The TA settings used to generate the necessary profiles and subsequently compute the micro-mechanical properties are listed in Table 3.2. The Fracture Energy provided data on the strength of the surface structure of the DSMT device before and after γ-irradiation and was determined by computing the gradient between the initial Force (anchor 1) and the first point of major

inflection (anchor 2) on a Force-Distance textural profile (Figure 3.1a). This was indicative of primary matrix fracture and was noted as a reduction in force.

Table 3.2: Textural parameter settings employed for physicomechanical property analysis of the DSMT.

Test parameters	Settings	
	Tensile Strength (N/mm^2)	Fracture Energy (J)
Pre-test speed	1.00mm/sec	2.00mm/sec
Test speed	0.50mm/sec	0.50mm/sec
Post-test speed	1.00mm/sec	5.00mm/sec
Compressive distance	0.25mm	-
Compression force	-	40.00N
Sensitivity of trigger force	0.05N	0.05N

Figures 3.1a and b depict typical Force-Distance and Force-Time profiles generated for computing the Tensile Strength and Fracture Energy respectively of the DSMT device before and after γ-irradiation.

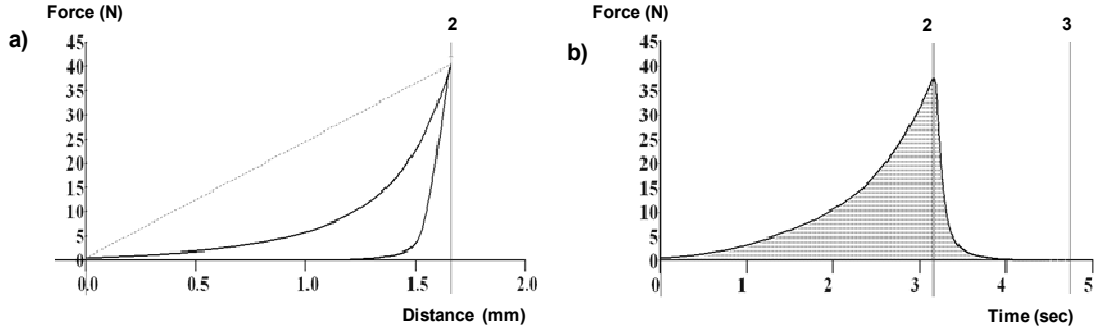

Figure 3.1: Typical textural profiles of a) a Force-Distance and b) a Force-Time curve used in computing the Tensile Strength and Fracture Energy of the DSMT devices before and after irradiation sterilization.

3.2.8. Thermal characterization of the irradiation sterilized DSMT device

The inherent and sequential transient thermal behavior of polymers after γ-irradiation may influence the physicochemical and physicomechanical properties as well as the final performance of the device (Araujo et al., 2003). Therefore, Differential Scanning Calorimetry (DSC) was selected as a practical technique for evaluating a range of different samples and components of the DSMT device in order to assess the influence of the γ-irradiation process on the thermo-energetic properties of native PLGA and GCV as well as the DSMT device. DSC also provided a distinct interpretation of the polymeric thermal transitions with improved sensitivity and the ability to detect glass transition temperatures (T_g) that have minimal changes in heat capacity (Giron, 2002; Lopes et al., 2006; Silver-Junior, 2006). In this research, the direct compression process was used for manufacturing the GCV-loaded DSMT device. DSC

analysis provided qualitative and quantitative data regarding the influence of GCV and PLGA, and the effects of compression of GCV and PLGA to produce the DSMT device. The effect of compression and sterilization on the drug–polymer interactions was also investigated by DSC. Physical mixtures of GCV:PLGA in ratios identical to those used in the manufacture of the DSMT device were used as a control. DSC curves were generated with a Mettler Toledo DSC1, STAR^e System (Columbus, OH, USA). Thermal transitions were assessed in terms of the T_g measured in response to variation in the magnitude of the melting temperature (T_m) and crystallization temperature (T_c) peaks corresponding to the total heat flow (ΔH). The temperature calibration was accomplished with a melting transition of 6.7mg indium (melting point 156°C and ΔH=28.4J/g). The thermal transitions of native GCV and PLGA were compared to a physical mixture of GCV and PLGA as well as ground samples (5mg) of the DSMT device before and after γ-irradiation. Samples of sterilized and non-sterilized DSMT devices (5-10mg) were weighed and sealed in perforated 40μL aluminum pans and ramped within a temperature gradient of 30-400°C under a constant purge of an inert N_2 atmosphere (100mL/min) in order to diminish oxidation. The instrument parameter settings employed comprised a sine segment starting at 150°C with a heating rate of 1°C/min at an amplitude of 0.8°C and a loop segment incremented at 0.8°C and ending at 500°C.

3.2.9. Chemometric modeling of the effects of irradiation sterilization on the DSMT device

The quantitative and qualitative analysis of the DSMT device was developed using chemometric molecular modeling. This approach provided a mechanistic understanding of the device surface geometry in order to analyze the physical stability of the device. Further studies were conducted to model the intensity variations in sterilized and non-sterilized DSMT samples. A model was used to describe the intensity variation as a function of solid fraction and thickness and tested on the PLGA devices. With this model, intensity variations from devices made before and after sterilization conditions were normalized, making the method transferable and facilitating the analysis over the expected range of formulation components and process variation. For complex processes such as compression and ensued by γ-irradiation, factors such as pressure, temperature and ionization may induce transformations within the DSMT device matrix. Induced transformations were analyzed in a quasi-static molecular environment using chemometric software (ACD/I-Lab, V5.11 Structure Elucidator Application (Add-on) biometric software, Advanced Chemistry Development Inc., Toronto, Canada, 2000). The

implicit design of the GCV-loaded DSMT device required customization of the novel donut-shaped geometry with the ability to support the micro-mechanical stability for γ-irradiation and subsequent intraocular implantation of the device. The componential DSMT properties were modulated through computational modeling to establish the effects of γ-irradiation in order to produce a viable GCV-loaded PLGA device. The fundamental modeling parameters were pivoted on the polymer compression, sterilization process, surface properties, macrostructure, micro-mechanical properties, drug-loading and biodegradation of the DSMT device. In order to incorporate fine control within the complexities of three-dimensional (3D) modeling, the physical properties of the sterilized and non-sterilized device such as the transformation in porosity, shape, wall thickness, interconnectivity and networks for GCV diffusion through the matrix was regulated. The DSMT topography was predicted for intraocular implantation with pre-defined micro-architecture and micro-mechanical properties equilibrating ocular tissue as the site of implantation to provide mechanical support during sterilizability prior to function. Suppositional 3D graphical models with potential inter-polymeric interactions before and after γ-irradiation was generated based on the step-wise molecular mechanisms of matrix transformations before and after γ-irradiation of the DSMT device and polymer interconversion as envisioned by the chemical behavior and physical stability. A combination of a computationally rapid Neural Network (NN) and a modified Hierarchal Organization of Spherical Environments (HOSE) code approach were employed as the fundamental algorithms in designing the prototype models. The associated energy expressions were chemometrically designed based on the assumption of the DSMT device behaving initially as a plastic structure with higher states of combinatory energy.

3.3. Results and Discussion

3.3.1. Surface morphological analysis of the γ-irradiated DSMT devices

Samples were selected to explore the influence of γ-irradiation on the surface morphology of the DSMT device (N=10). The analysis was based on the optimized DSMT device sterilized at 25kGy and compared to a non-sterilized device (Figure 3.2). Photomicrographs revealed the transition in surface morphology of the γ-irradiated DSMT samples and that the observed physical transformation played a critical role in instituting the changes in the micromechanical properties of the sterilized DSMT device as deduced by textural analysis studies and supported by the chemometric modeling approach employed

(Figure 3.2). The DSMT surfaces were dissimilar in surface geometry and porosity. The surface morphology of the non-sterilized DSMT device transitioned from a porous, web-like structure (Figure 3.2a), to a more closely packed clustered surface resembling a continuous embedded crystallized surface (Figure 3.2b).

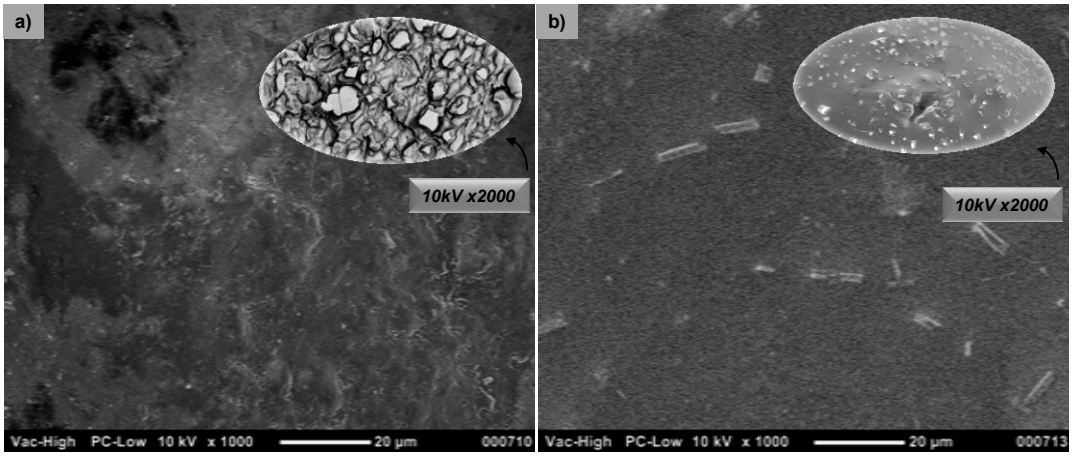

Figure 3.2: SEM images of the surface morphologies of a) a non-sterilized DSMT device and b) a sterilized DSMT device at 25kGy γ-irradiation (×1000 magnification; insert ×2000 magnification; N=10).

A proposed explication for this observation is due to PLGA chain transition during γ-irradiation that subsequently alters the surface geometry or the packing efficiency of the DSMT device (Figure 3.3a and b). This produces a combined lamellar crystalline PLGA structure resulting from chain folding and shear slip of H-bonded polymeric sheets due to the γ-irradiation energy applied as depicted in Figure 3.3c from the time-independent chemometric models derived. The conspicuous differences revealed by the SEM images shown in Figure 3.2 is pivoted upon the effects of the sterilization process on the physical surface configuration and consequently the micromechanical behavior and ability to control drug release from the DSMT device.

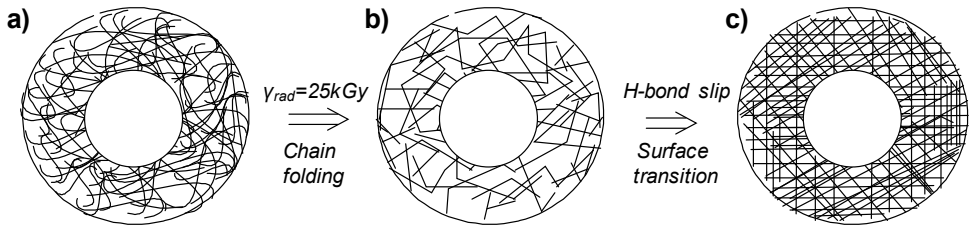

Figure 3.3: Structural models of the surface morphological transitions of the DSMT device upon exposure to γ-irradiation depicting a) the anarchic surface before irradiation, b) morphological changes occurring at intermittent energy levels to a maximum of 25kGy and c) complete lattice surface transition after irradiation.

3.3.2. Porositometric analysis of the DSMT device

Porositometric analysis was undertaken to determine the total exposed surface area of the DSMT device as well as any transition in the volume and distribution of pores and pore size as a result of γ-irradiation sterilization. The DSMT device was analyzed following the BET surface area, BJH method and the t-plot analysis of Lippins, Linsen and de Boer (Lippins et al., 1964). Table 3.3 shows the computed BET surface areas, BJH pore sizes and parametrics of the adsorption and desorption isotherms generated for the non-sterilized and sterilized DSMT devices. A distinct difference was noted between the porositometric values obtained for the sterilized and non-sterilized DSMT devices. The DSMT device displayed a net negative BET total surface area (-0.028±0.022m^2/g; R^2=0.71) after sterilization signifying an approximate 4-fold reduction in pore volume compared to the non-sterilized device which had a BET total surface area of 0.110±0.005m^2/g (R^2=0.99). The BET theory assumes uniform surface coverage with no favored adsorption sites and that N_2 is more strongly attracted to the surface rather than to other N_2 molecules. The typical range of BET-C values is from 5-100. Values <5 as in the case with the sterilized DSMT device (BET-C=2.69; N=3) implied that the gas-gas affinity was competing with the gas-solid affinity as a result of the significantly reduced surface area and minimization of pores after γ-irradiation. The BET-C value for the non-sterilized DSMT device was 15.47 (N=3). The lower surface area was attributed to the surface morphological transitions that occurred as a result of γ-irradiation with an ultimate reduction in porosity (Figure 3.3). This was revealed by the simultaneous qualitative and quantitative analysis of scanning electron micrographs (N=10) and linear isothermal plots generated as depicted in Figure 3.4a-d revealing the significant reduction in the porosity and BET surface area after sterilization of the DSMT device.

The adsorption isotherms for the non-sterilized and sterilized DSMT device displayed distinctly different patterns typically indicative of having relatively large pores for the non-sterilized DSMT (Figure 3.4a) and a subsequent transition to a typical non-porous adsorbent after sterilization of the DSMT device (Figure 3.4b). The absorption isotherm for the sterilized DSMT device (Figure 3.4b) increased comparatively rapidly as the relative pressure approached unity. When the relative pressure was reduced (desorption isotherm) this led to complete retracing of the curve (Figure 3.4b). However, the absence of a hysteresis loop (Figure 3.4b) is not conclusive evidence of non-porosity as certain conical, wedge and close-end pore geometries can also yield isotherms without hysteresis (Barrer et al., 1956). The absorption

isotherm of the non-sterilized DSMT device had the same general shape as the sterilized DSMT device (Figure 3.4a) except that it displayed a wider hysteresis loop instead of retracing the adsorption curve. This behavior is typical of mesoporous and macroporous materials with interconnected pore sizes of >20Å and >500Å respectively. The occurrence of the pronounced hysteresis loop signified the evaporation of N_2 from the pores after condensation from the inward central-core of the pores that are intimately intertwined with the adsorbent surface area and pore geometry. Figures 3.4c and d display the BET linear plots generated with the results reported in Table 3.3.

Table 3.3: Porositometric results obtained for the sterilized and non-sterilized DSMT device.

Parameter	**DSMT**	**DSMT$_{(S:25kGy)}$**
BET total surface area (m^2/g)	0.110±0.005	-0.028±0.022
BET slope (g/cm^3 STP)	36.94±1.83	-212.72±119.75
BET y-intercept (g/cm^3 STP)	2.55±0.25	57.66±17.66
BET-C[d]	15.47	2.69
Q_m (cm^3/g STP)[e]	0.025	-0.006
R^2 (BET plot)	0.99	0.71
Micropore volume (cm^3/g)	-0.000027	[c]*NC*
External surface area (m^2/g)	0.1496	[c]*NC*
R^2 (t-plot)	0.97	[c]*NC*
t-plot slope (cm^3/g.Å STP)	0.0017±0.0010	[c]*NC*
t-plot y-intercept (cm^3/g STP)	-0.018±0.004	[c]*NC*
Pore thickness range[a]	3.5-5.0Å	[c]*NC*
BJH adsorption pore size (Å)[b]	286.22	192.49
BJH desorption pore size (Å)[b]	693.67	482.20

[a]*Calculated employing the Harkins and Jura pore thickness equation*
[b]*Cumulative surface area of pores between 17.000-3000.000Å in diameter (m^2/g)*
[c]*NC=Not Computable as a positive BET surface area was not obtained for the sterilized DSMT devices*
[d]*BET-C=intensity of the N_2-surface interaction*
[e]*Q_m=monolayer surface capacity*

Figures 3.4e-h depict the Halsey Faas corrected BJH adsorptive cumulative pore volumes and BJH desorption dA/dD pore areas of the non-sterilized and sterilized DSMT devices (Halsey, 1948). The Halsey equation (Figures 3.4e and f) was selected as it assumes an adsorbed N_2 monolayer with the same density and packing as normal N_2. The preferred analytical representative expression of the standard adsorption isotherm at higher relative pressures is shown in Figures 3.4e and f. The pore size and pore volumes were significantly reduced after γ-irradiation of the DSMT device. Pore sizes displayed reduced values indicating a uniform and low quantity of pores despite variances caused by γ-irradiation (Figure 3.4e and f). This observation is ideal as the DSMT is intended for the controlled and sustained delivery of GCV. Thus having a negligible porosity that is supported by the γ-irradiation

process, the DSMT device would rely specifically on matrix erosion as a mechanism for GCV release rather than the influx of release media through fluid-filled pores (Figures 3.4g and h). The lower distribution of pores can also be attributed to a homogenously dispersed system with few air molecules entrapped during compression that can be attributed to the presence of the unique central rod used in producing the DSMT device. This created multi-directional radial forces obliterating the significant presence of pores. While the pore volume in both formulations was relatively low, the presence of larger macropores in the non-sterilized device led us to conclude that pore size may have affected the more rapid release of GCV. The non-sterilized DSMT devices had a BJH adsorption of 286.22Å and BJH desorption of 693.67Å which is much larger than the sterilized devices (BJH adsorption of 192.49Å and a BJH desorption of 482.20Å). Therefore GCV release from the sterilized DSMT devices was more controlled than non-sterilized devices as described in Chapter 4 of this thesis.

Since every adsorbate-adsorbent system yields a unique adsorption isotherm the concept of standard isotherms were employed by superimpositioning and normalization (Gregg and Sing, 1982). This led to the generation of t-plot isotherms as a means of determining the volume of micropores (<20Å), detecting the presence of mesopores and quantifying the thickness of the adsorbed N_2 layer of the external surfaces and the walls of any pores that are present within the DSMT device structure. For t-plot isotherms, the quantity of N_2 adsorbed (V_a) was profiled against the thickness (t) of the adsorbed N_2 layer (Figure 3.5) (Lippins et al., 1964). Extrapolation of the linear isotherm to the extent of N_2 adsorption provided the micropore volume. In order to describe the thickness of the adsorbed N_2 layer the Harkins and Jura thickness equation was employed (Figure 3.5) (Harkins and Jura, 1944) for determining the surface area of the DSMTdevice without the use of a molecular area which is a requirement if the BET method was used. The quantity of N_2 adsorbed was related to the statistical thickness of the adsorbed N_2 film by the equation shown in Figure 3.5. As shown in Table 3.3 t-plot volumes were only obtainable for the non-sterilized DSMT device with a micropore volume of -000027cm^3/g over a pore thickness range of 3.5-5.0Å. As expected the t-plot parametrics for the sterilized DSMT device could not be determined due to the negative micropore volume revealing the lack of micropores. This is further depicted in Figure 3.5 in which extrapolation of the linear t-plot (R^2=0.97) resulted in a negative intercept (-0.018±0.004cm^3/g). This revealed that the γ-irradiation process did not affect the porosity of the DSMT device in the micropore region.

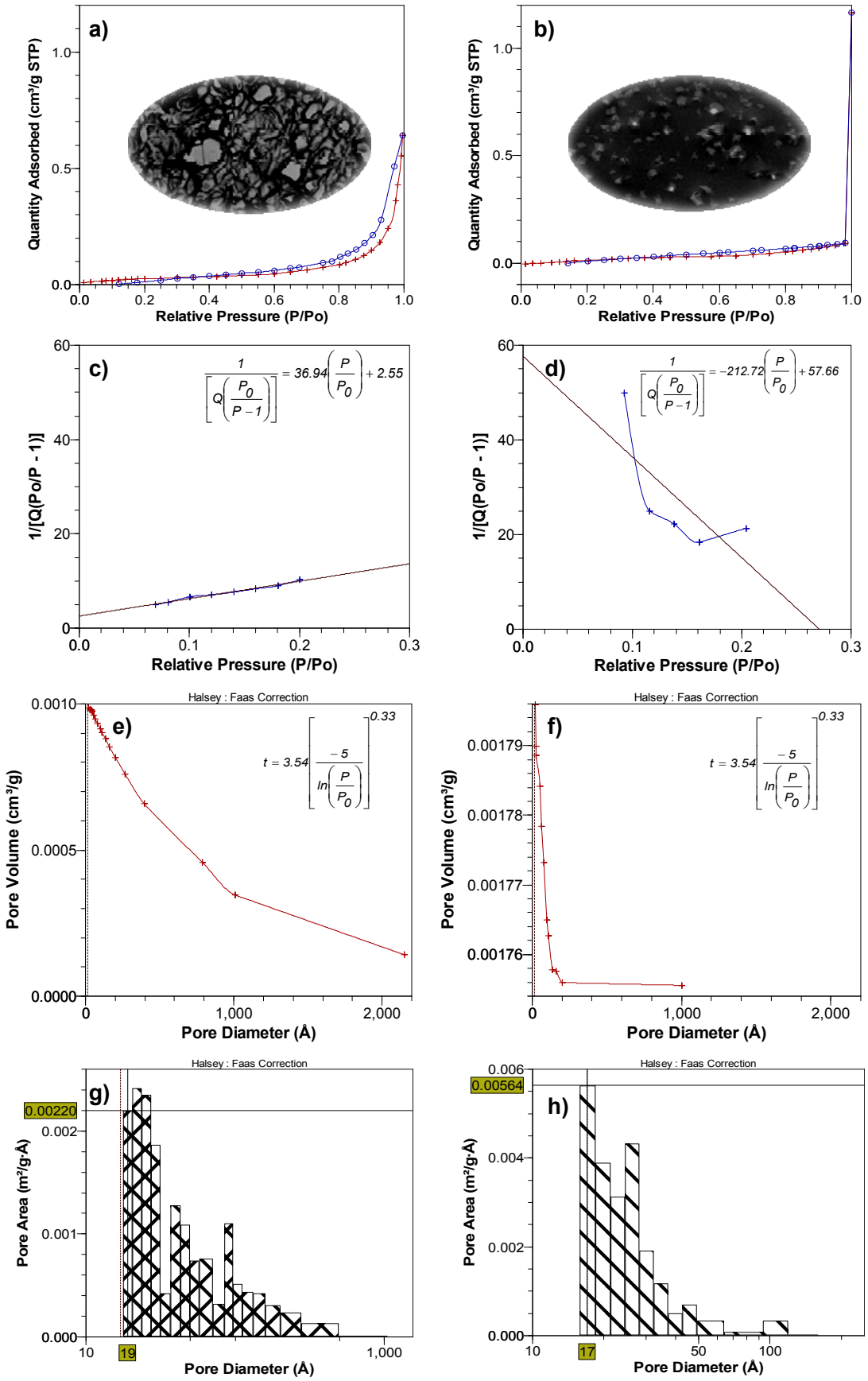

Figure 3.4: Descriptive porositometric plots of a-b) linear isotherms with overlaid photomicrographs (10kV ×2000), c-d) BET surface areas, e-f) BJH adsorption cumulative pore volumes and g-h) BJH desorption dA/dD pore areas of the non-sterilized and sterilized DSMT devices respectively.

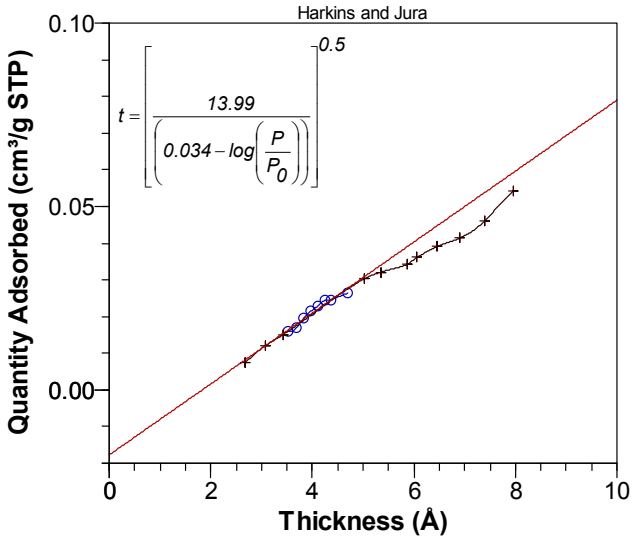

Figure 3.5: Typical t-plot generated for the sterilized DSMT device (N=3; SD<0.01 in all cases).

Pores are known to twist, turn, broaden, narrow and have rugged walls and other distorted shapes. Therefore, a practical alternative is required to undertake dynamic modeling for the application of mathematical analysis. This provided an accurate method for describing the DSMT device with fewer computations. The porosity determinations in this study assumed the pores within the DSMT device to be right cylinders (90° to the horizontal) with variable lengths/slits of infinite extent and parallel walls in a single layer of atoms with a continuum of interaction potential formed as shown by the molecular models in Figure 3.6. Figure 3.6 describes molecular models of the pair-wise interaction energy between PLGA chains during pore minimization for the sterilized DSMT device. It should be noted that isotherm profiles may vary and therefore detailed examination in accordance with thermodynamic and other processes such as chemometric modeling is required to elicit the desired information of surface area and pore structure.

Regarding the sterilized DSMT device, γ-irradiation at 25kGy may have exceeded the yield pressure of PLGA, resulting in increased energy generated and dissipation above the T_g value. The excess energy induced molecular structural changes and resulted in surface deformation of the matrix that led to stress relief at heterogeneous stress loci distributed within the DSMT device after direct compression. Consequently stress relaxation and surface disruption occurred on a micro-level to alter the morphology, porosity and micro-mechanical properties of the sterilized DSMT device. Based on the model, an estimation of the transformation potential on the physical properties of PLGA is possible. The combined effects of two major factors such as pressure and γ-irradiation energy on inducing transformations within

the DSMT matrix was investigated. The simplest system to model in terms of geometry was that of a single pore represented by two parallel α and β PLGA chains with stress loci at a distance H (Figure 3.6a). The pore is formed and three-dimensionally optimized with an average pore size of 200Å as a single component followed by pore division as a result of thermodynamic and density-dependant equilibrium potential on the surface of the DSMT device (Figure 3.6b-d). Results showed that pressure alone is unlikely to induce the polymorphic-like transformations within the DSMT matrix (Figure 3.2). The effects of the γ-irradiation energy must be considered in compaction-induced transformation after sterilization. The central hole further significantly alters the porosity in a uniform and multi-directional manner in view of the increased surface area of the DSMT device over a conventional discoid tablet matrix as represented by Equations 3.1 and 3.2 respectively. The larger surface area exposure is crucial and significantly alters the micro-mechanical profile as depicted by the chemometric models in Figures 3.6 and 3.7 as well as the porosity results shown in Figure 3.4.

$$A = \frac{\pi}{4} h \times (D^2 - d^2) \qquad \textit{Equation 3.1}$$

$$A = \frac{\pi}{4} D^2 h \qquad \textit{Equation 3.2}$$

Where, A=surface area, h=height of solid, D=total diameter and d=diameter of the central hole in the case of the DSMT device.

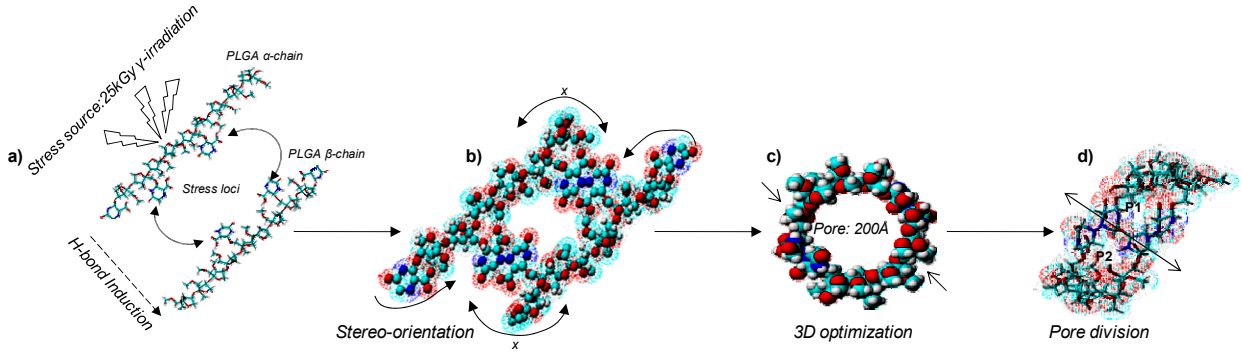

Figure 3.6: Chemometric models of segmental surface transitions occurring after γ-irradiation of the DSMT device depicting a) the application of γ-irradiation as a source of stress loci nativity to two sterilized PLGA strands, b) the induction of surface pore formation and shape optimization, c) a complete pore formed at minimum energy levels (for maximum stability) in a 3D optimized state and d) further pore-division with a geometric fit-model in the coiled state showing the molecular pore volume.

Instead of traditional kinetic or phenomenological approaches, it is also preferable to use chemometric model-based statistical theory that allows relating the linear isotherms generated to the microscopic properties of the system such as the solid-solid interaction energy parameters, the mechanism of pore formation, the pore size and the pore geometry. Figure 3.7 depicts the chemometric energy paradigms and molecular structural models mechanistically describing the influence of the γ-irradiation process on the energy gain and dissipation within the DSMT device matrix after γ-irradiation of the DSMT device. The adsorption isotherms generated also conveys data regarding the energetic heterogeneity of the DSMT surface. Even completely non-porous surfaces are composed of regions that have greater or lesser affinity for adsorbing N_2 molecules and this energetic non-uniformity influences the shape of the isotherm. Therefore determining the distribution of the chemometric energy paradigms afforded an additional means of characterizing the DSMT surface transitions as a result of sterilization. The DSMT acquired a constant energy source during γ-irradiation and energy decay was subsequently induced through PLGA strand decoiling with minimal energy retained after γ-irradiation (Figure 3.7a). The instant energy decay profile of the matrix and the retained energy profile modeled were for the γ-irradiation with energy conservation from the developed and inherent energy status of the process (Figures 3.7b and c).

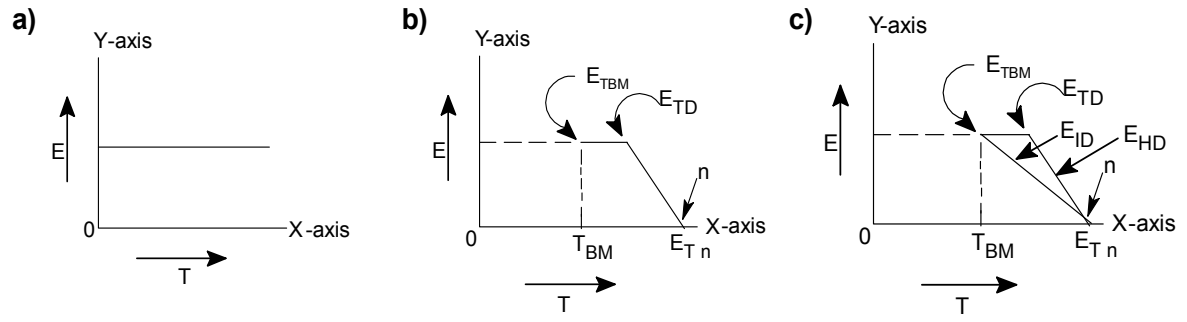

Figure 3.7: Chemometric energy paradigms and molecular structural models depicting the influence of the γ-irradiation process on the DSMT device matrix where, a) constant energy requirement by the DSMT matrix during γ-irradiation, b) energy decay through decoiling with minimal energy retained after γ-irradiation and c) instant energy decay profile of the matrix, where, E_{ID}= instant energy decay, E_{HD}=hold energy decay, E_{TD}=energy decay point with E_{HD}., E_{TBM} energy requirement till irradiation complete, TBM= irradiation time, E_{Tn} end-point energy relationship at n point of time.

3.3.3. Assessment of the physicomechanical properties of the DSMT device

The physicomechanical transitions of the PLGA-based DSMT device interacting with the γ-irradiation process were analyzed. The extent of physicomechanical modification was quantified in order to predict the dynamic transitions for flexibility and reproducibility of the DSMT device after sterilization. The PLGA in the DSMT device interacted with the γ-irradiation by means of polar-hydrophobic interactions and hydrogen bonding. The physicomechanical properties of the matrices were governed by the PLGA molecular mass, PLGA concentration, and sterilization reaction time. The ability of the DSMT devices to absorb energy was found to correlate with the sterilization process. Non-sterilized samples had an increased Fracture Energy of the devices during textural probe penetration. On the contrary, γ-irradiated devices displayed an increased resistance to fracture by the textural probe penetration indicating that excess energy was absorbed by the DSMT devices during sterilization resulting in crystalline matrices with higher fracture energies and Tensile Strength. The general trend revealed was that the γ-irradiated DSMT device was less susceptible to fracture and had positive physicomechanical transitions. Hence, the sterilized devices were more crystalline and hence less prone to degradation *in vivo*, thus superiorly retarding the release of GCV. The Tensile Strength of the DSMT device was determined from axio-radial compression tests performed on a Texture Analyzer equipped with a 5kg load-cell and a 2mm cylindrical probe in order to accurately measure the maximum penetration force *(F)*. Together with the measured diameter and thickness of the DSMT device, the Tensile Strength (σ_t) was calculated using Equation 3.3 (Fell and Newton, 1970).

$$\sigma_t = \frac{2F}{\pi dt} \qquad \textit{Equation 3.3}$$

Where, *F*= maximum penetration force (N) with *d*= diameter of the DSMT device and *t*= thickness of the DSMT device.

Table 3.4 lists the force values (N) generated from penetration and the Tensile Strength of the DSMT compacts. The Tensile Strength of the compacts indicated that the material formed moderately softer compacts after γ-irradiation.

Table 3.4: Textural analysis values obtained for the non-sterilized and sterilized DSMT devices.

Formulation Type	Tensile Strength (N/mm^2)	Fracture Energy ($N.s^{-1}$)
DSMT	26.396±1.062	151.301±6.089
$DSMT_{(S: 25kGy)}$	24.426±1.184	140.009±6.785

This observation highlights the important differences in the mechanical properties of the non-sterilized and sterilized DSMT devices, which is temperature and pressure dependant in their response to applied mechanical stress and this observation will subsequently be explained in a stepwise manner.

Powder compaction and compressibility is a key phenomenon for the production of solid dosage forms such as tablets (Shotten et al., 1976; Doelker, 1978; Jones, 1978; Barra and Doelker, 1998). In this study, the physicomechanical properties such as the robustness of the DSMT device, propensity to fragment during manufacture or subsequent handling and porosity when sterilized may have a significant effect on the *in vivo* performance of the device. Hence, the compressibility behavior of the constituents of the DSMT device such as the PLGA has been previously analyzed (Choonara et al., 2006). Powder compaction is a complex process, involving granule movement and re-orientation within the powder bed, together with deformation or fracture, resulting in increased contact area and intergranular bonding (Shotten et al., 1976; Doelker, 1978; Jones, 1978). This can be affected by the modulus and strain behavior of PLGA (i.e. elastic, plastic deformation or brittle fracture), as well as geometric factors such as surface rugosity, shape and size distribution of the powder introduced into the die cavity prior to compression (Krycer and Pope, 1982; Doelker, 1983; Marshall, 1986; Doelker, 1988; Rippie, 1990). The compaction behavior also depends on friction; both between powder granules and with the compaction die surfaces (Celik, 1992; Wray, 1992).

The combination of these factors generally results in variations of density and strength within compacted matrices, which may depend on their shape and can result in fragmentation faults such as chipped edges, delamination or capping. Nevertheless, and notwithstanding the considerable research effort that has been motivated by the importance for pharmaceutical tablet manufacture, a complete understanding of the compaction physics during manufacture of the DSMT device still eludes us. Numerous variables such as the solid-state properties and inherent deformation behavior of the PLGA, granule size, granule shape, and most significantly the tooling geometry and process

conditions can affect the attributes of the resulting DSMT device. Moreover, while it is generally accepted that granule rearrangement at a relatively low packing fraction is superseded by various relative quantities of deformation and fragmentation at higher compaction pressures and with the use of novel donut-shaped tooling as in this study, no direct evidence of densification mechanisms have been observed. The physics of this process is elaborated on henceforth from a postulated viewpoint.

3.3.4. Postulated locale on the axial to radial force transmission during DSMT compression

Theoretically, the radially transmitted force or pressure (stress) may essentially intervene in two ways during compression of PLGA into the DSMT device and this is depicted by a model related to the axial and radial force transmission (Figure 3.8). Figure 3.8 shows the stresses operating on the powder blend under compression when using the novel DSMT tooling. The friction force (F_d) is the force lost to the die wall and represents the difference between the two vertical forces.

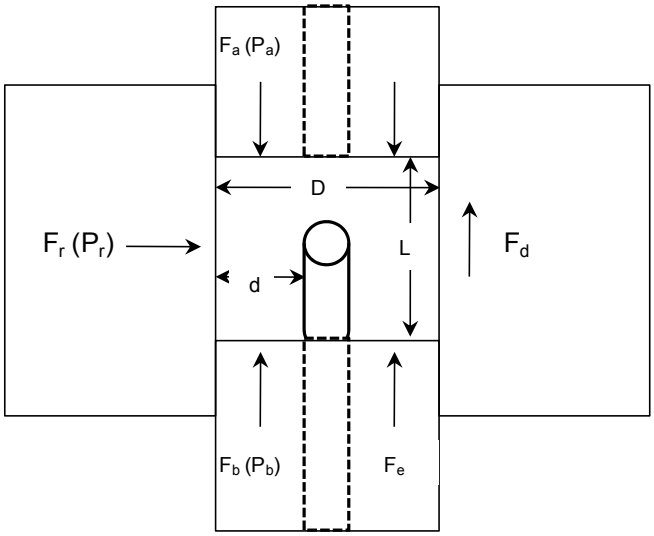

Figure 3.8: A schematic depicting the forces and pressures operating on the powder blend under compression in a punch and die assembly with the protrusion of the novel central rod employed for producing the DSMT device. Where, $F_a(P_a)$=applied force (pressure) by the upper punch, $F_b(P_b)$=force transmitted by the lower punch (in a single-punch press), F_d=force lost to the die (i.e. the axial frictional force operating during compression), $F_r(P_r)$=radial force arising from the horizontal expansion of the mass in response to the axial compressive force (pressure) and is reduced as a result of the residual force absorbed by the central rod, F_e=ejection force on the lower punch during expulsion of the DSMT out of the die, D=die diameter and d=diameter of the central rod, L=height of the compact.

3.3.4.1. Axial transmission

The radial stress generated by axially pressing a body in a die is present in the numerous equations proposed to describe die-wall friction. In the simple model of pressing from one end in a stationary cylindrical die, these equations relate the pressure applied by the upper punch (P_a), to the pressure

transmitted to the lower punch *(P_b)*, a well known derivation is that of Unckel, (1945) that can be modified as in Equation 3.4 to account for the central rod.

$$\frac{P_a}{P_b} = e^{4\mu\eta L/(D-d)} \qquad \textit{Equation 3.4}$$

Where μ= the coefficient of die-wall friction, η= the stress ratio, defined as the ratio between the radial pressure *(P_r)* and the applied pressure *(P_a)*, *L*= the compact length, and *D-d*= the diameter provided for the DSMT die representing the displacement of the central rod within the die cavity. As μ= the coefficient of friction between the powder mass and the die wall, then Equation 3.5 applies.

$$F_d = \mu F_r \qquad \textit{Equation 3.5}$$

Where, F_d=force lost to the die (i.e. the axial frictional force operating during compression), μ= the coefficient of die-wall friction and F_r= radial force arising from the horizontal expansion of the mass in response to the axial compressive force (reduced in the case of the DSMT device production due to the residual force absorbed by the central rod).

These basic equations describe an exponential decay of the applied pressure down the compact length and postulate constant μ and η values. However, it has been suggested that μ and η may vary along the length of the compact according to the conditions of relative interfacial movement or modification of tablet tooling, even though the product $\mu\eta$ could remain constant (Train et al., 1962). This could explain the experimentally observed uneven Tensile Strength between conventional PLGA matrices and the DSMT device produced. Both, axial and radial stress gradients are present although short compacts are expected to be reasonably homogenous along the compression axis, especially when the die is lubricated. In contrast, the radial distribution of the axial pressure on the upper and lower punch may show parabolic and symmetric patterns about the lateral central axis of the die alongside the central rod (Thompson, 1981). The general conclusion from analyzing these models is that geometrical changes may alter the relative radial pressures and the coefficient of friction, μ,

affects the intrinsic properties of the compacted device such as the Tensile Strength and Fracture Energy of the DSMT device.

3.3.4.2. Radial transmission

Long (1960; 1962) elucidated the theoretical significance of radial versus axial pressure cycles. Two types of the Long's compression cycles were predicted according to the behavior of the material compressed in addition to that of a perfectly elastic body (Figure 3.9). In both cases, line OA (or OA') is representative of perfect elastic behavior of a solid isotropic compact of material that is if the axial pressure *(P_a)* is released, the radial pressure *(P_r)* would return along this to zero. When the axial pressure exceeds the elastic limit (yield pressure) points A or (A'), yield begins and the slope changes according to the failure behavior of the material.

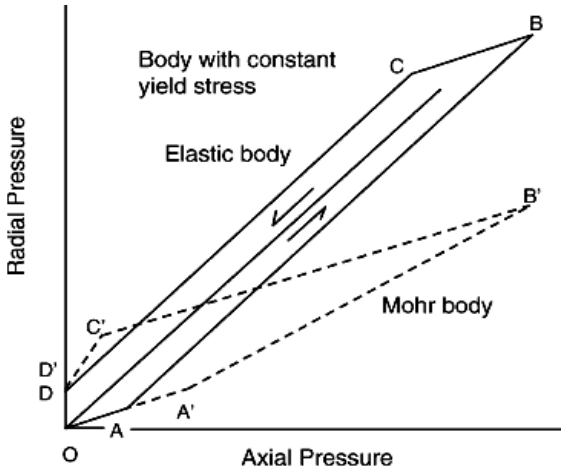

Figure 3.9: Theoretical radial pressure cycles for an ideal elastic body, a body with constant yield stress and a Mohr body, where A-A'= yield points, B-B'=maximum applied pressure, C-C'= yield points of decompression and D-D'= residual die-wall pressures (Source: Long, 1960).

For a body with a constant yield stress (strength) in shear, the difference between the axial pressure and the radial pressure remains constant and the slope of the line AB will equal unity. For a Mohr body, i.e. a body with a shear stress depending on the value of the normal stress, after a maximum axial pressure is reached (points B and B'), decompression occurs and the compact is no longer forced to yield but recovers elastically. The line BC (or B'C') will be parallel to OA (OA'). At point C (or C') the induced radial pressure exceeds the axial pressure and yield once again occurs. In the case of a material with a constant yield stress in shear, the line CD will be parallel to line AB. In the case of a Mohr body, the slope of the line C'D' is the reciprocal of line A'B' due to stress inversion. Once the

axial pressure has returned to zero but ejection has not yet occurred, the compact will remain under a residual radial pressure (Carstensen and Toure, 1980; Parrott, 1990). Several reasons may explain such deviations and is outlined in Table 3.5 (Long, 1960; 1962).

Table 3.5: Potential reasons for deviations in the radial and axial pressure cycles of a powder blend under compression.

- In the case of a perfectly hydrostatic body A (A') coincides with O and C (C') with B (B'). The cycle degenerates into a single straight line (Long, 1960).
- A compacted powder is not a solid and therefore the isotropic compact and its yield stress cannot be the same. Thus, segment OA (OA') may be curved as porosity continuously decreases and point A (A') may not always be visible. Plastic flow may be confined to the interparticulate regions (Carless and Leigh, 1974). Thus, instead of the slope of the OA (OA') segment, it may be better to consider the rest of the cycle where a reasonable degree of densification has occurred.
- If the applied pressure has not been large enough to reach the elastic limit i.e. point A (A'), yield will not occur and the change of slope at point C (C') will not be observed and also affects the magnitude of the residual radial pressure.
- If the applied pressure has not been sufficiently high, the CD (C'D') segment may be missing from the cycle, thus affecting the residual radial pressure.
- Die elasticity also affects the shape of the radial compression cycle (Long, 1962). This may be a concern when the die volume is reduced to position the central rod when producing the DSMT device. Two different situations have to be considered. First, the cycle is complete and only the slopes of lines OA (OA') and BC (B'C') are reduced. The magnitude of the residual radial pressure is unchanged. Second, the cycle is incomplete and line CD (C'D') is absent and line BC (B'C') continues to intercept the radial pressure axis, causing higher residual radial pressures.

Adapted from: Long, (1960; 1962)

This justifies performing compression studies at sufficiently high applied pressures and comparing various polymer grades at a given relative inherent viscosity (Marshall, 1986; Choonara et al., 2006). Friction arising from the polymeric material and the die (die-wall friction), the central rod and between particles (interparticulate or internal friction) operates during tableting. However, internal friction is of significance only at low applied pressures, i.e. during particle slippage and rearrangement, and is not a decisive factor in the tableting process. In contrast, the friction between the powder mass, the die wall and the central rod is a pivotal issue when a sufficient radial pressure has been generated, i.e. beyond a certain consolidation ratio as in the case of the DSMT device.

Friction is present and varies during compression, decompression, pre-ejection and ejection of tablets. Challenges often arise in the compression and decompression phases but become evident only at ejection (Hiestand et al., 1977; Schrank-Junghani et al., 1984). Friction phenomena occurring

during tableting may be estimated through various parameters such as the ratio of the maximum lower punch force to the upper punch force *(F_d)*, the ejection force *(F_e)*, the residual lower punch force, the work of friction, and the work of ejection that may be calculated from the upper and lower punch force measurements using an instrumented tableting press (Doelker, 1994). Factors influencing the friction conditions at the die also affect the radial transmission of the applied pressure. Thus, the presence of the central rod may reduce both the interparticle friction and friction at the die-wall, and hence particles compact more tightly and homogeneously. The result is a decrease in the coefficient of die-wall friction, μ, and an increase in radial stress transmission, η. A consequence is that the product $\mu\eta$ in Equation 3.4 may not be influenced by the presence of the central rod. However, the only way to discriminate between the two effects is to monitor the die-wall pressure using a modified instrumented tableting press in order to measure η and then calculate μ for the DSMT compression cycle.

Apart from the tablet tooling and the product to be compressed, numerous manufacturing conditions may in practice also influence the friction coefficient measurements (Strijbos, 1976; 1977). These include the method of tablet production (unique or continuous) and applied pressure. The effect of internal lubrication (i.e. adding a lubricant to the powder mass) or that of external lubrication (i.e. pre-lubricating the die and central rod). In the former case, 0.5%$^{w}/_{w}$ magnesium stearate was added to a DSMT device formulation. In the latter case, the magnesium stearate was dusted onto the internal die cavity and the central rod before compression. Both internal and external lubrication acted favorably on the DSMT tableting process. The presence of the central rod generally showed an improvement of the tablet mechanical strength. For conventional equi-dimensional PLGA matrices, the radial conversion during compression was lower in the absence of a central rod with an increased die-wall pressure. An opposite trend may be observed for the DSMT device with a potential increase in radial transmission and a slightly reduced residual die-wall pressure absorbed by the presence of the central rod. Other studies are generally in line with the results obtained in this study (Shotton and Obiorah, 1975; Obiorah and Shotton, 1976; Obiorah, 1978). It is evident that a superior radial transmission of pressure alone is not sufficient to explain compactibility. On the other hand, tablet formation is also related to a higher residual die-wall pressure, but the strongest tablets are not associated with the highest residual die-wall pressure (Doelker and Shotton, 1977). Probably, the

effect of the central rod and that of material hardness play a prominent role on the axial to radial pressure transmission.

In addition, the donut geometry also has a significant bearing on the micro-mechanical attributes of the DSMT device. Physical factors such as particle-particle, particle-die and particle-rod contact surface areas during compression are significantly increased. This may induce a gradient for increased tablet consolidation and explained the Tensile Strenght and Fracture Energy results reflected in Table 3.4. The surface tension affected by the donut shape as compared to a conventional discoid tablet is also increased and therefore less critical pharmaceutical excipients such as binder was needed to produce the robust DSMT matrix. The increase in surface tension led to superior consolidation and stability of the DSMT device. However, the net change is almost negligible or very small due to compensation of energy by the outward surface of the donut matrix overriding the increase in inward surface tension. This may or may not affect an approximate 2-5% increase in Tensile Strenght or Fracture Energy of the donut shaped matrix depending on the rugosity of the matrix polymer selected (Figure 3.10).

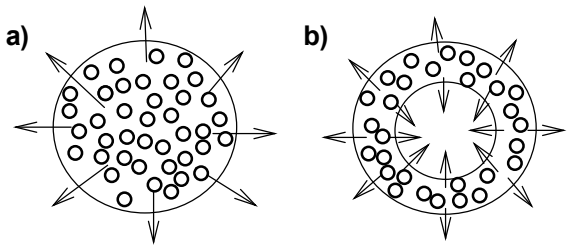

Figure 3.10: Schematic diagrams depicting the differences in surfaces available for interaction and subsequent consolidation during compression between a) a conventional tablet matrix and b) a donut shaped tablet matrix of equal diameter.

Interest in die-wall instrumentation is continuing. However, when examining the literature dealing with radial pressure measurement during compression of pharmaceutical materials, one is confronted with numerous inconsistencies (Hoag, 2003). One reason is the technical difficulties of die instrumentation and calibration that lead to discrepancies in the results reported for similar products. Another reason is that the models used for interpreting data have been proposed mostly for conventional solid, isotropic bodies and not for specialized geometrical matrices such as the DSMT device. Based on literature examination and on textural profiling results from this study die-wall instrumentation may be useful for compaction studies and for elucidating the friction phenomena during compaction and compression of PLGA into the DSMT device. In this respect, the residual die-wall pressure is of

significance as the success of the DSMT device formation is determined by the decompression and ejection phases and more emphasis should be placed on analyzing the kinetics of time-dependent deformation in the later period of the compression cycle as a result of the central rod. In addition, mathematical relationships that consider the material compressibility (volume reduction under pressure) have been proposed, but as for the relation between the DSMT matrix strength (material compactibility) and the compression parameters inferred from die-wall monitoring, suitable models still require development as initiated in Figure 3.11.

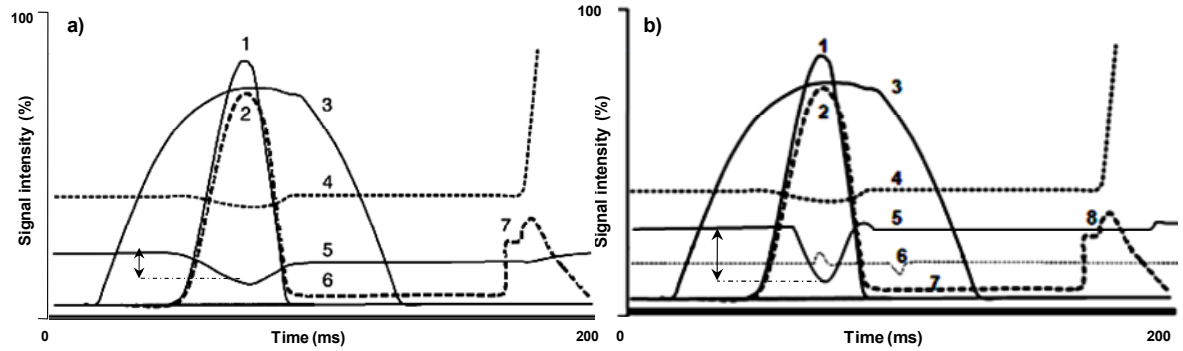

Figure 3.11: A model depicting typical digitalized signals from an instrumented tablet press of the compression/decompression tableting cycles of a) a conventional tablet matrix and b) a DSMT device, where, *1a* and *b*=upper punch forces, *2a* and *b*=lower punch forces, *3a* and *b*=upper punch displacements, *4a* and *b*=lower punch displacements, *5a* and *5b*=die-wall force of conventional tablet matrix and DSMT device, respectively, *6a*=residual lower punch force, *6b*=central rod friction during DSMT compression and decompression, *7a*=ejection force of conventional tablet matrix, *7b*=residual lower punch force after DSMT compression and *8*=ejection force after DSMT compression.

3.3.5. Thermal analysis of the irradiation sterilized DSMT device

The superimposed thermal profiles generated are shown in Figure 3.12. The DSC curve for native GCV shows a first exothermic peak in the range of 150-160°C that was characteristic of disordered crystallization or an amorphous drug phase (Yonemochi et al., 2005). A second endothermic event in the range of 360-380°C may be attributed to GCV decomposition immediately after melting. The DSC curve for pure PLGA is also shown in Figure 3.12. From the DSC curve of PLGA it was possible to observe two thermal events. The glass transition temperature (T_g) of PLGA occurred in the range of 50-60°C with an enthalpy of relaxation of 0.05mW/mg and a midpoint of 55°C. The endothermic degradation of PLGA occurred on a single step in the range of 360-380°C. The physical and chemical interactions between GCV and PLGA were also studied with the aim of predicting the thermal behavior of the biodegradable GCV-loaded DSMT device before and after γ-irradiation sterilization. Thus,

physical-mixtures of GCV and PLGA with identical proportions to the GCV-loaded DSMT device were analyzed by DSC.

The T_g of PLGA occurred in the range of 50-60°C, followed by an exothermic event in the range of 150-160°C due to hydration of GCV present in the sample. The notable exothermic shift to a higher ΔH may be due to the possible dissolution of the GCV fraction during the PLGA melting phase while heating. In previous studies this was well characterized when polymers with low melting point/glass transitions were used (Arias et al., 1998; Naima et al., 2001; Yamashita et al., 2003; Bikiaris et al., 2005). Consequently as seen in this study the appearance of the GCV:PLGA physical mixture melting point was at a lower temperature range than that of native GCV (360-380°C), with premature melting in the range of 320-340°C. The endothermic decomposition of PLGA occurred in the temperature range of 310-330°C. After characterizing the thermal properties of the native GCV and PLGA as well as the physical mixture, DSC analysis was performed on the groung samples (5mg) of the sterilized and non-sterilized GCV-loaded DSMT devices (Figure 3.12). The beginning and intensity of the thermal events varied between the sterilized and non-sterilized DSMT device samples. The T_g of PLGA occurred in the range of 50-60°C. For both the non-sterilized and sterilized DSMT device an exothermic event typically due to hydration occurred in the range of 150-160°C. For the non-sterilized DSMT device a second endothermic thermal event occurred in the range of 300-360°C due to melting and the onset of decomposition during GCV melting. For the sterilized DSMT devices a third exothermic event was observed in the temperature range of 340-360°C. This distinct event was possibly due to the ionization effects of the γ-irradiation process resulting in a prominent crystallization phase consistent with the DSC curve of native GCV signifying slower decomposition.

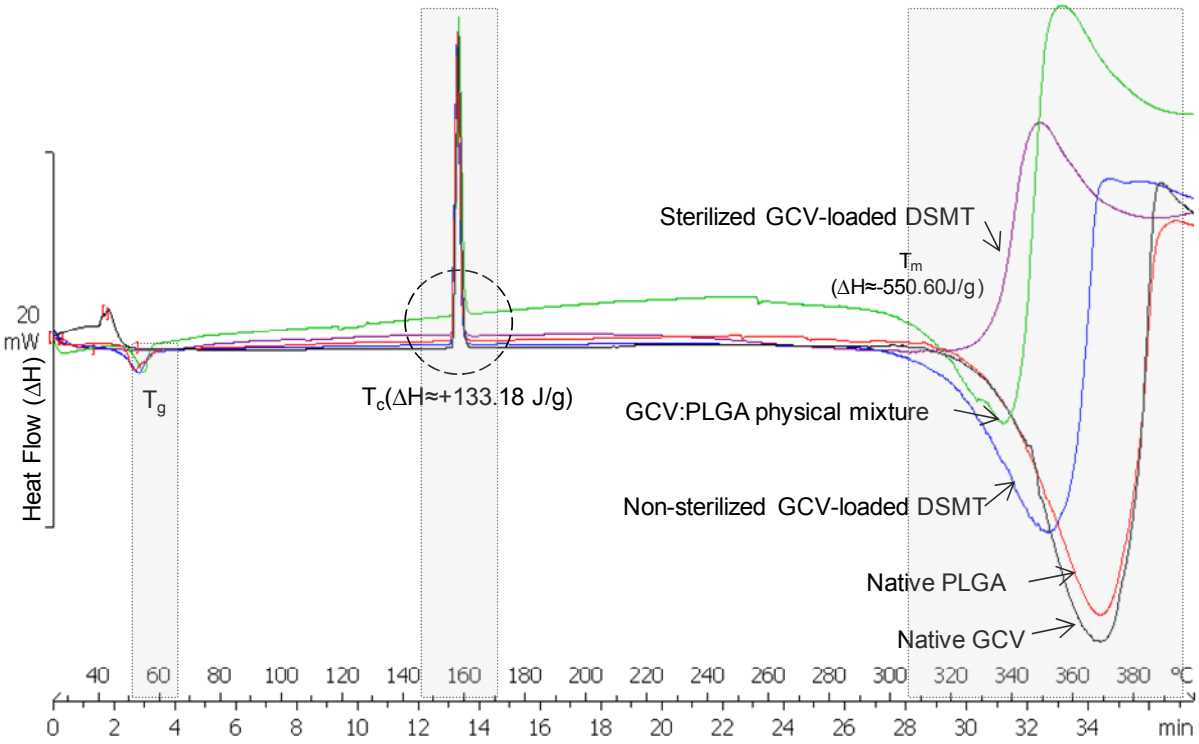

Figure 3.12: Superimposed thermal profiles for native GCV, native PLGA, a GCV:PLGA physical mixture, a non-sterilized GCV-loaded DSMT device and a sterilized GCV-loaded DSMT device, at a temperature range of 30-400°C and a heating rate of 10°C/min (N=3).

In order to evaluate the effect of compression on the drug–polymer interactions and on the stability of the DSMT device, the data obtained from thermal analysis of the compressed GCV-loaded PLGA devices were correlated with the respective physical mixtures. The temperature ranges of the thermal events were similar, indicating that the experimental selected conditions for preparation of the GCV-loaded DSMT device did not change the stability of the drug or polymer. However, the enthalpy values involved in the thermal events obtained for the GCV-loaded DSMT device were different from those determined for the respective physical mixtures. This could be attributed to the various aggregation states of GCV present in different samples. It may be evidenced by a lower relaxation enthalpy identified for the T_g of PLGA in the DSMT devices than those obtained for the physical mixtures. It is well established that polymer compression has different aggregation states than physical mixtures (Corrigan, 1995; Gustafsson et al., 1998; Anshuman et al., 2004; Ohta and Bucktona, 2005). The T_g is a significant parameter to characterize the physicomechanical behavior of glassy amorphous polymers such as PLGA (Vyazovkin and Dranca, 2005; Vyazovkin and Dranca, 2006; Kim et al., 2007). The molecular mobility of the polymeric chains has an important role in deciding the physicomechanical properties, diffusion of drug molecules through the polymeric matrix, and the enthalpy involved in the thermal event may vary with the drug content in the polymeric matrix (Kim et al., 2007).

In this study the T_g remained relatively stable for all combinations of samples and ranged between 50-60°C. From the DSC data obtained, the second thermal exothermic event occurred during hydration and thus an increase in enthalpy values was obtained. The maintenance of the thermal properties of the DSMT device after γ-irradiation is fundamental for assuring the performance of the device once implanted and its ability to behave as expected in controlling the release of GCV. DSC analysis revealed that the thermal properties were similar for both GCV-loaded DSMT devices and the respective GCV:PLGA physical mixtures, demonstrating that the stress conditions during direct compression and γ-irradiation did not affect the thermal properties of the structural components of the DSMT device.

3.3.6. Chemical structural transition analysis

FTIR analysis was performed in this research with an aim to complement the results obtained from the thermal analysis by DSC. The FTIR spectra of native GCV and PLGA are shown in Figure 3.13. The bands of the carboxyl OH group were assigned in the range of 2500-3500cm^{-1}, the tertiary amine at 3527 and 3375cm^{-1}, secondary amine at 3100, CH_2–N stretching at 2705cm^{-1}, ketone C-O at 1708cm^{-1}, C-C bands in the region of 1600 and 1495cm^{-1} and C–bond stretching in the range of 1100-1300cm^{-1}, these values corresponding to the characteristic FTIR of GCV (Figure 3.13). From the FTIR spectra for PLGA it was possible to identify the characteristic absorption bands at 1759cm^{-1}, related to the PLGA ester group, and axial stretching of sp^2 and sp^3 carbons in the range of 2900-3000cm^{-1}, were assigned (Figure 3.13). The FTIR spectra of the GCV-loaded DSMT device and the GCV:PLGA physical mixtures are also shown in Figure 3.13. For both, the GCV-loaded DSMT device and the physical mixtures, the characteristic FTIR bands of the functional groups of GCV and PLGA were established. On the contrary, the ester carbonyl groups of the polymer could react with the amino groups of GCV. However, the maintenance of the FTIR characteristic bands for both, GCV and PLGA, and the absence of any new FTIR bands, indicating modifications in the ester carbonyl and amine functions demonstrate that GCV is only dispersed in the PLGA polymeric matrix. These results are in agreement with the thermal analysis data indicating that there is no significant interaction between GCV and PLGA used to manufacture the DSMT device. In all samples, the FTIR spectra of the DSMT device exhibited a transmission pattern that was the sum of the two components in relation to their abundance indicating that no interactions between GCV and PLGA occurred (Figure 3.13). Moreover, the NH deformation signal recorded at 1534cm^{-1} confirmed the presence of GCV in the PLGA matrix.

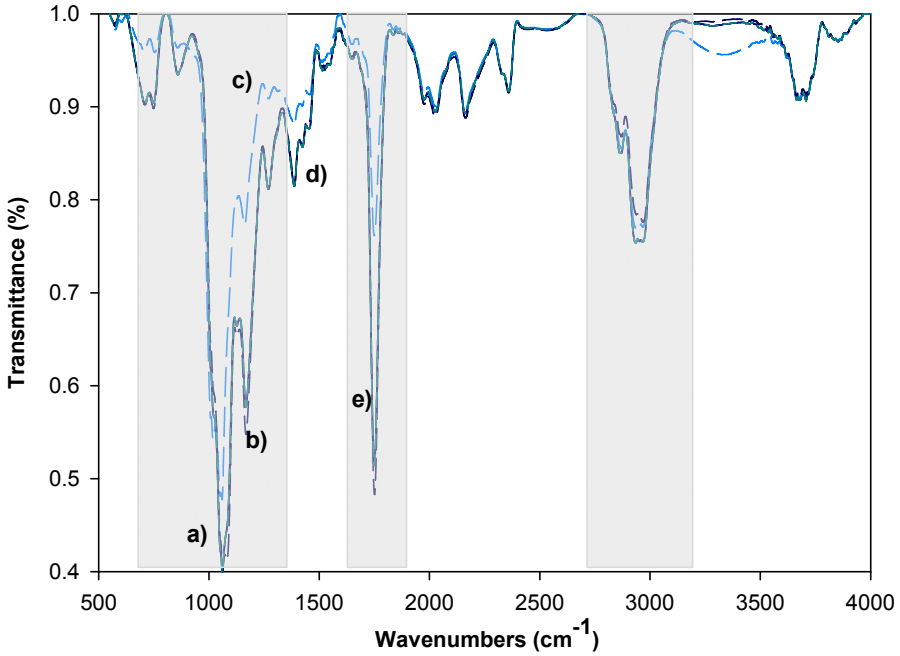

Figure 3.13: Superimposed FTIR spectra of a) native GCV, b) native PLGA, c) a GCV:PLGA physical mixture, d) a non-sterilized DSMT device and e) a sterilized DSMT device.

The results of this research demonstrated that through thermal analysis it was possible to deduce the pre-formulation characteristics of the biodegradable DSMT device produced by direct compression and sterilized by γ-irradiation prior to intraocular implantation. The selected manufacturing and sterilization technique of the DSMT device did not provoke any transformations in the physical and chemical stability of the DSMT device or its components. It was possible to establish a relationship between the thermal behavior of the device, the GCV-loading and subsequent effects of γ-irradiation. It can be concluded that direct compression and subsequent γ-irradiation are efficient and reliable processes for the production of a stable GCV-loaded DSMT device. Irradiation of biodegradable polyesters such as PLGA may induce dose-dependent chain transitions (Figure 3.14) as well as molecular mass reduction thus potentially accelerating degradation of the polymer (Reed and Gilding, 1981). The degradation rate of polymeric biomaterials due to γ-irradiation may be linked to radical formation (Stevels et al., 1996; Nijenhuis et al., 1991). In order to prevent radical-induced degradation, antioxidants such as α-tocopherol and ascorbic acid esterified with palmitin- or stearic-acid are often added to formulations. However these are mainly used as protecting agents for lipophilic materials and thus were not considered in this work.

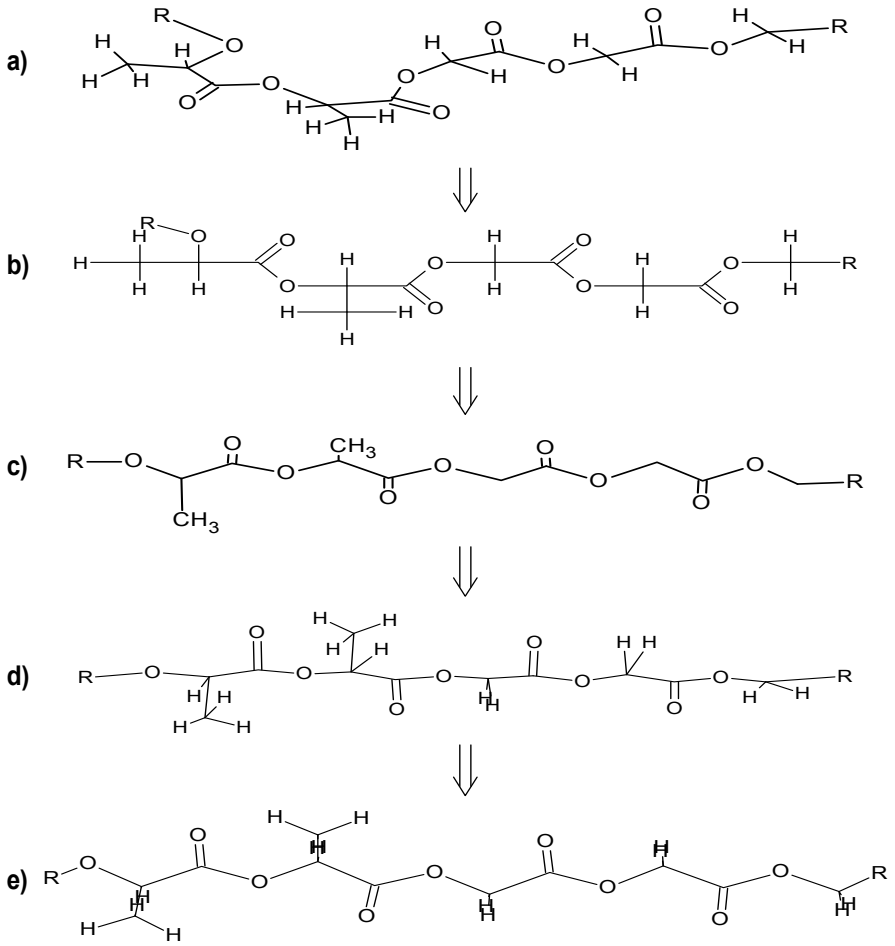

Figure 3.14: Schematic depicting the molecular geometrical changes of PLGA strands after γ-irradiation showing a) a PLGA strand segment at initial stages, b) irradiation-induced energy perturbations resulting in bond re-orientation, ordering and patterning, c) energy emission-stimulated stereochemical changes toward a more stable PLGA conformation, d) intermediatary energy variable conformation between structures c) and e), where e) represents the most stable and least energetic PLGA strand conformation along with patterning of all methylene hydrogens at similar levels of geometrical coordination.

3.3.7. Chemometric simulation of PLGA radiolysis due to the sterilization process

Chemometric models of polymeric transitions under γ-irradiation are depicted in Figure 3.15 with molecular nodes generated by polymer coiling at the quaternary stage of the PLGA structure when γ-irradiation was applied. The super-coiling of the polymer and the decoiling stages are stereo-electronically and structurally compact, thus reducing the surface porosity of the sterilized DSMT device. Figure 3.15 denotes each cycle in the structural decoiling mechanism during γ-irradiation and the postulated nodes generated that are responsible for pore formation (14-point nodes in the model with the polymer interactive morphology linked to the iso-surface for inter-polymeric interactions). The internal cavity in Figure 3.15a is shown as a nodal geometric order in Figure 3.15b. The physicochemical parameters of this specification can mostly be reached in coiled pore formations for any other molecule to mimic the associated bioactivity other than GCV.

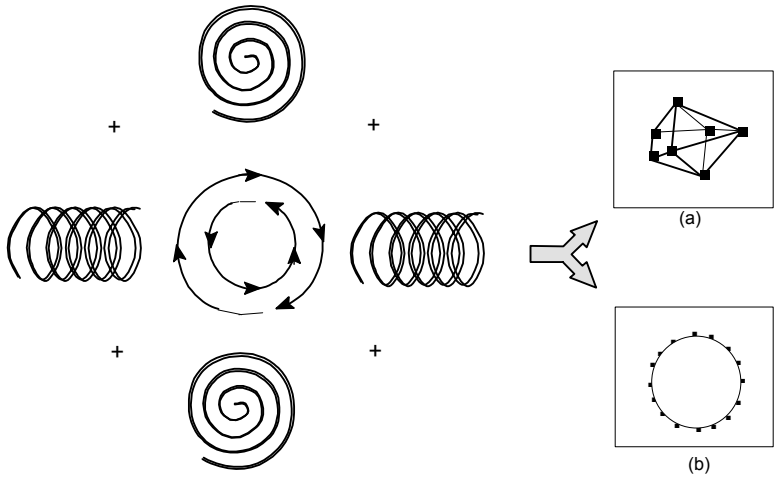

Figure 3.15: Chemometric structural models depicting the influence of the sterilization process on the DSMT device matrix and pore formation after irradiation where the mechanism of pore formation via polymeric decoiling is shown.

Figure 3.16 shows the qualitative relationship of the energy absorption and change of the system at the initial point (E_n) and after irradiation at x levels (E_x). The difference is qualitative, though presumed to be at a higher end that does not permanently damage the polymeric material. The decay of the energy is also comparatively rapid than other conventional sources of energy such as heat or pressure. The plot represents a chemometric qualitative plot indicating the energy supplied to the polymeric device during a short span γ-irradiation energy relay. In Figure 3.16b the qualitative relationship of the energy emission and instant energy loss of γ-irradiation energy packets is depicted. The higher end energy of the polymeric device at E_x is rapidly changed during a short period. The energy can be said to be reflected back with the energy packets or quantas providing an equilibrating molecular effect and distribution of energy within the system. The energy loss is comparatively greater than the gain, though loss occurs in quantized and relatively regular relay packets rather than by erratic convection (as seen with heat loss). Thus the energy loss (E_{xs}) is greater than the net gain of energy (E_{xn}) by γ-irradiation owing to the higher stability of the DSMT device after γ-irradiation rather than employing other sterilization processes.

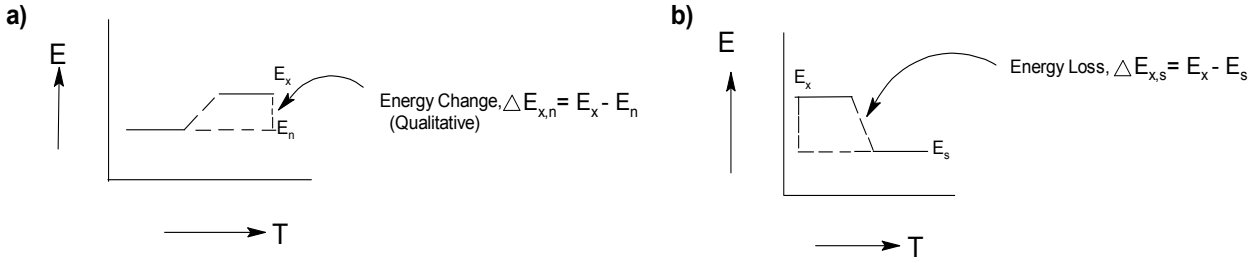

Figure 3.16: Chemometric models depicting the qualitative relationship of a) energy absorption and energy change and b) energy emission and instant energy loss of irradiation energy packets within the DSMT device after γ-irradiation, where *E*=energy; *T*=time E_n=initial energy; E_x=energy applied, E_{xn}=net gain in energy and E_{xs}=net loss in energy.

The copolymer PLGA is an amorphous type material. Amorphous materials do not have distinct melting points but rather go through a T_g phase as observed during the thermal studies performed. Secondly, it is worth mentioning that poly(lactic acid) (PLA) is thermally unstable (Zhang et al., 1992). Hence, the presence of this monomer randomly distributed within the PLGA copolymer backbone structure tends to increase chain flexibility and therefore during high energy processes such as γ-irradiation, it's inclined to contribute to the widening in the copolymer molecular mass distribution and decrease the yield pressure. The yield pressure indicates the point where forces involved in consolidation have essentially been 'broken'. Sterilization of the PLGA-based DSMT device generated significant energy within the internal structure of the device. The excess energy is dissipated and escapes gradually through the surface of the device altering the porosity, morphology and ultimately the physicomechanical properties such as the Tensile Strenght and Fracture Energy.

Since it would have required significant modification of the current testing equipment to permit data to be collected in order to monitor these *in situ* changes in energy, this phenomenon was explored through chemometrical modeling. Presumably at energies above the T_g value, amorphous material would show a transformation in behavior with an increased ductility. Subsequently the device transitioned into a more rubbery state. It is well-known that above the T_g value molecular motions are very rapid which may lead to a decrease in the extent of polymer chain entanglement and an increased mobility of the polymer chain segments, whereas below the T_g value these motions are restricted and are regarded as almost 'frozen'. Figure 3.17 shows chemometric models representing γ-irradiation of the PLGA-based DSMT device within a single molecular voxel. When irregular PLGA strands (Figure 3.17a) are exposed to irradiation the irradiation effects produce networking and layering of the matrix upon exposure to γ-rays.

Energetic transitions are induced as finite plate energy quanta as successive relays to affect stereochemical and molecular geometrical transitions at the atomic binding levels for bond stretching and expansion. This produces varying molecular geometrical or stereo sets of the matricized layers as depicted in Figure 3.17b where the last layer shows the remaining irregular PLGA strands where radiation is still to pass. Eventually the matrix transitions into an ordered configuration as depicted in Figure 3.17c.

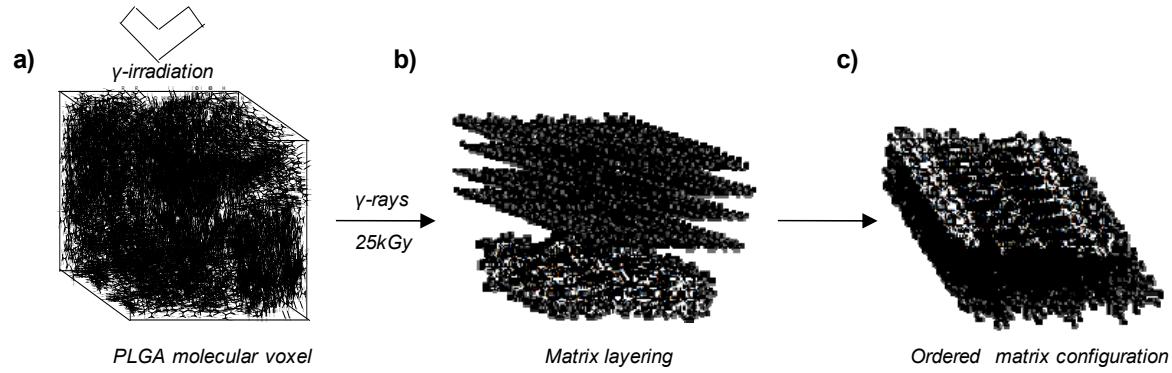

Figure 3.17: Chemometric models representing γ-irradiation of the PLGA-based DSMT device showing a) irregular PLGA strands exposed to irradiation, b) the irradiation effects producing networking and layering of the matrix under γ-rays and c) total layering of the irregular matrix in an ordered configuration.

The DSMT device's morphological changes induced by molecular geometry and limited stereochemical organization patterning is shown in Figure 3.18. Initially a random state PLGA geometry and irregular morphology exists (Figure 3.18a). Once γ-irradiation is applied the initial effects induces polymeric chain disentanglement and re-orientation towards ordered patterning (Figure 3.18b). Complete patterning for the irradiation stance when partial energy from γ-irradiation quanta is being absorbed producing homogenization and equilibrating effects simultaneously with equi-distant pores in the matrix. The minimum energy conformers in a rigidized ordered patterning state after initial irradiation energy effects produces relatively equal energy distribution and solvation-like effects with the emission of excess energy. At this level the system is at a lower energy state in order to achieve stability over a comparatively longer period of time.

The lower energy state of the matrix produces stabilizing effects rather than the patterning and orderliness of the matrix (it is for this reason that excess energy when supplied to the matrix is utilized in patterning, orderliness, equilibrating and near-solvation-and homogenization effects and the overall

energy status of the matrix remains toward baseline. Patterning may be responsible for the longer stability, and is responsible for a high energy kill for the detoxification and sterilization process. The matrix stability is linked to the lower energy state of the matrix which is lost as E^+ from the matrix where E is the original startup energy of the matrix. Alternatively it can be represented as E^- where energy is lost. The energy loss may be due to the quanta of energy exchange at the atomic level emissions/discharges of the surplus energy from the matrix while the irradiation is passed through/reflected from the inner dimensions of the matrix. The current understanding favors the E^+ loss.

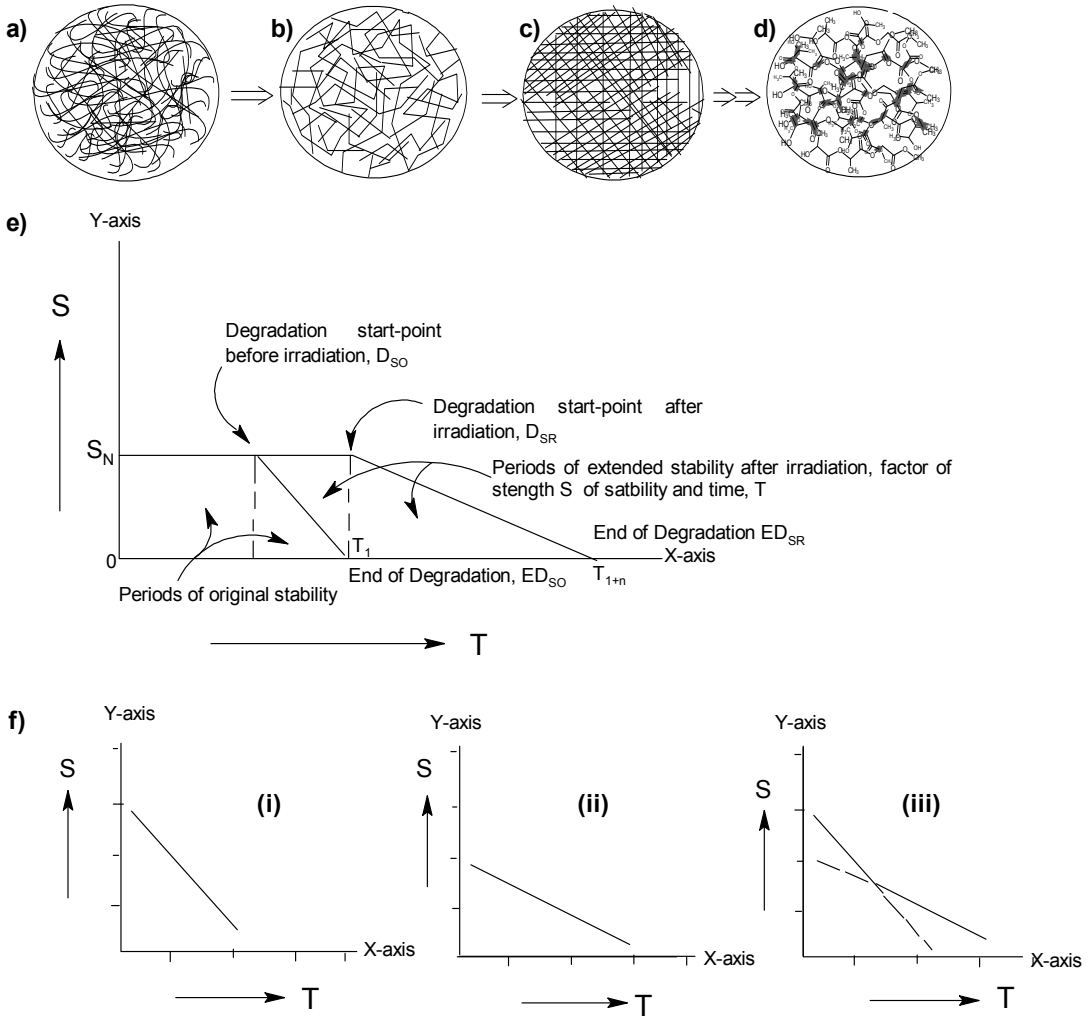

Figure 3.18: Chemometric models depicting the molecular geometry and stereochemical morphological transitions of the DSMT device after irradiation where a) is the random state PLGA irregular morphology, b) initial γ-irradiation effects producing polymeric strand disentanglement, c) complete orderliness of the irradiated matrix, d) minimum energy conformers in rigidized state for prolonged stability, e) stability of the DSMT before and after irradiation, and f) stability depiction as a factor of energy and time whereby, (i) before irradiation, (ii) stability after irradiation (the total energy within the matrix dissipates while the time is extended and (iii) equilibrium point of the energy level and time factor for non-algebraic quantitation of the stability factor.

3.4. Concluding Remarks

Characterization of the γ-irradiated DSMT device revealed that the affected transitions favored the DSMT to be employed as an implantable intraocular device. PLGA can be regarded as suitably stable under compression and γ-sterilization for manufacture of the DSMT device. This is consistent with the broader expectation that amorphous type materials have a higher free energy. In addition this study has shown that as the characterization techniques for biomaterials progress, it is essential to rigorously consider the confounding improbabilities with the data obtained by detailed chemometric and molecular modeling approaches in order to draw comprehensive conclusions on the inherent behavior of the system at a micro-level. The approach employed has proven to be a flexible and powerful research tool for building and exploring models of complex polymeric structural networks subjected to various stresses during manufacture.

CHAPTER 4

IN VIVO EVALUATION OF THE DONUT-SHAPED MINITABLET IN THE RABBIT EYE MODEL

4.1. Introduction

The technology for posterior segment drug delivery has progressed remarkably over the last five decades. Promising developments are implants designed to deliver drugs intravitreally that allow for higher intraocular drug levels (Kulkarni et al., 1962; Hayreh et al., 1966; Yolles et al., 1970; Macoul et al., 1975; Laties and Rapoport, 1976; Rapoport, 1977; Cunha-Vaz JG, 1979; Foulds et al., 1980; Moritera et al., 1991; Okada et al., 1991; Moritera et al., 1992; Giordano et al., 1993; Akula et al., 1994; Hashizoe et al., 1995; Miyamoto et al., 1997; Ding, 1998; Yang et al., 1998; Khoobehi et al., 1999; Einmahl et al., 2000; Yasukawa et al., 2000; Herrero-Vanrell and Refojo, 2001; Geroski and Edelhauser, 2001; Hatefi and Amsden, 2002; Merodio et al., 2002; Jabs et al., 2003; Lallemand et al., 2003; Bonferonia et al., 2004; Lee et al., 2004; Yasukawa et al., 2004; Barbu et al., 2005; Myles et al., 2005; Benz et al., 2006; Choonara et al., 2006; 2007; Kassem et al., 2007; Motwani, et al., 2007; Eperon et al., 2008; Li et al., 2009). The *Vitrasert*® device (Chiron Vision Inc., Irvine, CA, USA) which was approved by the US Food and Drug Administration (FDA) in March 1996, has been used with success in practice for the prolonged release of ganciclovir (Sanborn et al., 1992; Musch et al., 1997). However the device which is implanted through a 4-5mm sclerectomy at the pars plana is non-biodegradable and requires an additional surgical procedure to remove the device from the vitreous humor (VH) once the drug-load has been depleted. Previous studies using pigmented rabbits demonstrated that intraocular devices containing ganciclovir maintained a VH concentration within the therapeutic range for CMV-R for 2-3 months (Moritera et al., 1991; Smith et al., 1992; Sanborn et al., 1992; Kimura et al., 1992; 1994; Harper et al., 1993; Hashizoe et al., 1994; Kunou et al., 1995; 2000; Veloso et al., 1997; Zhou et al., 1998; de Rojas Silva et al., 1999; Tan et al., 1999; Bourges et al., 2006). However most presented with a few disadvantages such as secondary bursts in the late phases of drug release, separation of suture tabs from the drug-loaded pellets and the ease and reliability of securing the devices to the scleral flap has not been ideal.

In an attempt to solve the challenges associated with achieving prolonged release of drug in the posterior segment of the eye and conferring biodegradability to posterior segment intraocular devices, previous studies by Choonara and co-workers (2006; 2007) described a novel biodegradable donut-shaped minitablet (DSMT) employing poly(lactic-co-glycolic) (PLGA) as the polymeric carrier for the model antiviral drug ganciclovir. The DSMT device developed in these previous studies was implanted at the pars plana of the New Zealand White Albino rabbit eye model employing a simple surgical procedure for prolonged intraocular release of ganciclovir in the present study. Therefore the purpose of the current study was to evaluate the DSMT device *in vivo* in the rabbit eye model in order to assess the safety and potential of the DSMT device to provide constant drug release as a suitable and versatile intraocular drug delivery device.

4.2. Materials and Methods

4.2.1. Materials

Resomer® grades RG503 (i.v.=0.32-0.44dl/g; M_w=41,000g/moL) and RG504 (i.v.=0.45-0.60dl/g; M_w=55,000g/moL) consisting of biodegradable poly(lactic-co-glycolic acid) (PLGA) with a 50% lactide content, were purchased from Boehringer Ingelheim GmbH, (Ingelheim, Germany). Ganciclovir (GCV) was purchased from Hoffmann-La Roche Inc. (Nutley, NJ, USA). Acyclovir (ACV) was used as the internal standard for drug content analysis and was purchased from Sigma-Aldrich Co. (St. Louise, MO, USA). Disodium hydrogen orthophosphate ($Na_2HPO_4^-$), sodium chloride (NaCl) and potassium dihydrogen phosphate ($KH_2PO_4^-$) were purchased from Saarchem-Holpro Analytic (Pty) Ltd., (Krugersdorp, Johannesburg, South Africa). All other reagents used were ultrapure grade.

4.2.2. Preparation of the DSMT device

The preparation of the DSMT device has been discussed earlier in this thesis and can be found in Chapter 3, Section 3.2.2. Further details can be read in a research publication by Choonara and co-workers, 2006).

4.2.3. Sterilization of the DSMT device

A terminal sterilization procedure in accordance with the guidelines stipulated by the UK Panel on Gamma and Electron Irradiation, (1987) was used as the preferred method over aseptic processing before implantation into the posterior segment of the rabbit eye model as detailed previously in Chapter 3, Section 3.2.3 of this thesis.

4.2.4. *In vivo* study design

Twelve New Zealand White Albino male rabbits weighing 2.5-3.0kg were used for the *in vivo* animal study (Ethics clearance was obtained from the Animal Ethics Committee of the University of the Witwatersrand for this study, Ethics Clearance No 2006/40/04, see Appendix D and E). The animals were housed individually and were treated in accordance with the Association for Research in Vision and Ophthalmology (ARVO) Resolution on the Use of Animals in Ophthalmic and Vision Research (Rockville, MD, USA). The animals were held in a vivarium for at least one week prior to the surgical procedure (Figure 4.1). The rabbits were divided into two experimental groups of six rabbits each. The first group of six rabbits each received GCV-loaded DSMT devices formulated with Resomer® grade RG503 and the second group of six rabbits each received GCV-loaded DSMT devices formulated with Resomer® grade RG504.

Figure 4.1: A digital image depicting the conditions under which the rabbits were housed in a vivarium according to ARVO Resolution guidelines.

4.2.5. Pre-operative screening of the rabbit eyes

All rabbits were examined by slit-lamp bio-microscopy, tonometry, assessment of the menace response (i.e. reaction to hand motions toward the eye) and indirect ophthalmoscopic analysis through dilated pupils to exclude animals with any pre-existing anterior or posterior segment chorio-retinal abnormalities from the study. The rabbits were anesthetized with an intramuscular combination of ketamine hydrochloride (40mg/kg) (Pfizer, Morris Plains, NJ, USA) and xylazine (10mg/kg) (Bayer Animal Health (Pty) Ltd., Monheim, Germany) in a 4:1 ratio. Pupillary dilation was achieved with a topical instillation of cyclopentolate hydrochloride (2mg/mL) and phenylephrine hydrochloride drops (10mg/mL) (Cyclomydril®, Alcon Laboratories Inc., Fort Worth, TX, USA) 10-15 minutes prior to surgery. Thereafter preoperative facial preparation was undertaken with the right side of the rabbit's eye region shaven in order to improve the ophthalmic surgeon's visibility during surgery. Both eyes of a rabbit were rinsed with balanced saline solution (0.9%$^{w}/_{v}$) and the rabbit was draped in a conventional sterile manner, ensuring that the drapes did not occlude the rabbit's nose or mouth. A description of the ocular appearance of the rabbit eyes and scores based on the severity of clinical signs were recorded. Specific signs graded were, ocular cloudiness (corneal edema, aqueous regions) and ocular discharge. To ensure intraoperative care the rabbits were positioned on a bed, which was equipped with a full-length gel pad. A pillow was placed under the rabbits head to reduce discomfort, and the torso was secured and covered with a warm blanket. A blood pressure monitor was used throughout the procedure and a pulse oximetry probe was placed on the rabbit's penis with electrocardiogram leads. A carbon dioxide monitor was also positioned inside one of the nasal prongs of an oxygen cannula before placing the cannula in the rabbit's nose. Supplemental oxygen was administered throughout the surgical procedure. The rabbit's oxygen saturation remained stable at 100%. A GCV-loaded DSMT device was implanted into the right eyes of rabbits from each group and the left eyes were used as controls. The above procedures were consistent for all animals throughout the *in vivo* experiment.

4.2.6. Surgical procedure for implantation of the DSMT device

The surgical procedure involved implanting the DSMT device into the vitreous cavity via a pars plana (or peripheral retinal) incision. A supero-temporal or supero-nasal fornix-based conjunctival flap was formed and haemostasis was achieved. A circumferential 5-6mm incision was made 2mm posterior to the limbus. The wound was opened to check for full-thickness penetration into the vitreous cavity.

Prolapsing VH was pushed back with the DSMT device and the device was anchored with a 9-0 nylon suture passed through the scleral lip and then through the hole in the center of the device and then through the other scleral lip. Another two or three 9-0 nylon sutures were used to close the wound. The conjunctiva was repositioned but not sutured and chloramphenicol ointment was applied and used daily for 3 days after surgery. The positioning of the device was monitored post-operatively. All animals in this study were treated in accordance with the ARVO Resolution on the Use of Animals in Ophthalmic and Vision Research (Rockville, MD, USA). Figure 4.2 depicts sequential time-frame images of the surgical procedure for implantation of the DSMT device.

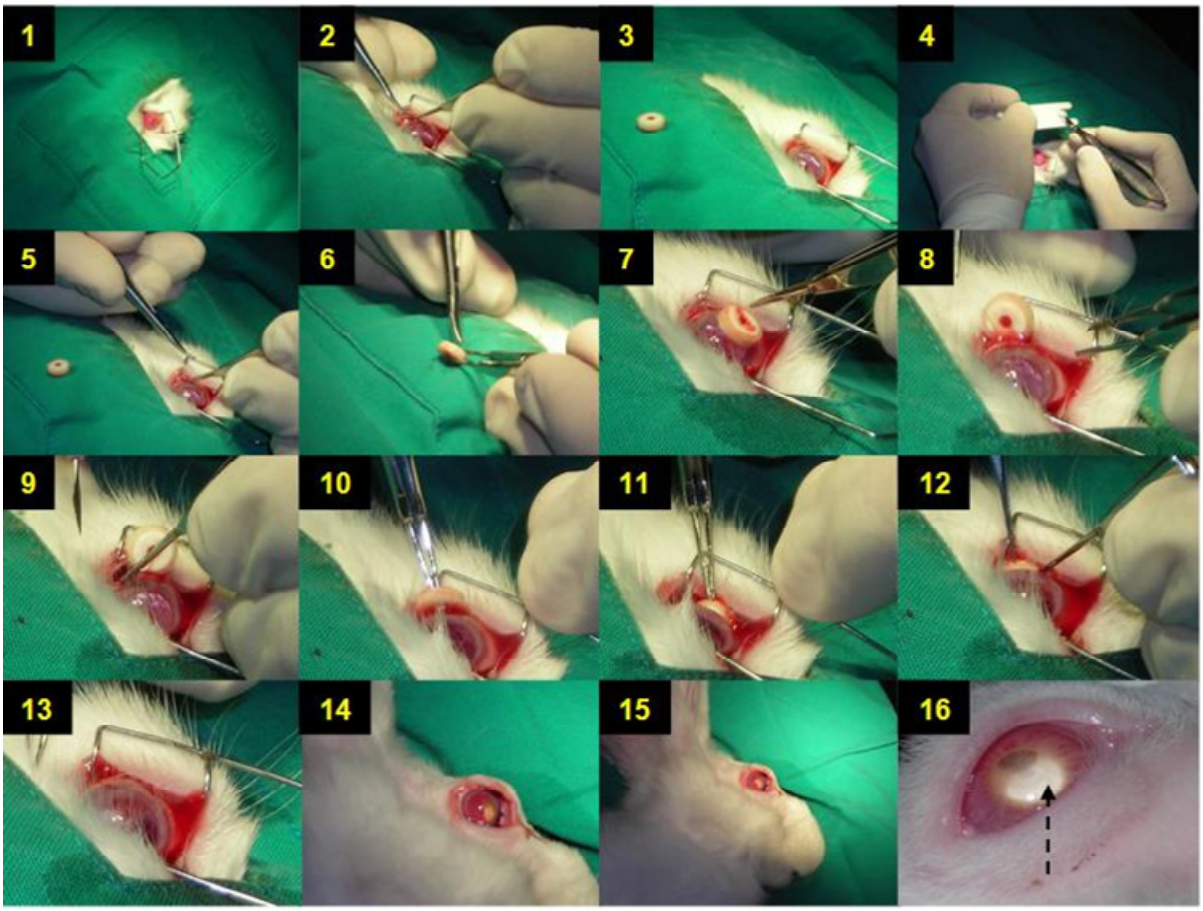

Figure 4.2: Sequential time-frame images of the surgical procedure (±30 min; N=12) and a magnified image of the DSMT device implanted into the superonasal region of the vitreous cavity and visible through the lens of the rabbit eye model at day 3 after implantation (image no.16).

Care was taken to ensure that the DSMT device was positioned without making contact with the lens and in order that the device could be monitored postoperatively. A 9-0 nylon suture was anchored to the scleral incision, tied, and cut short to avoid any irritation to the rabbit. Normal saline solution (NaCl=0.9%$^{w}/_{v}$) was used to rinse the implantation site and the device was inspected with an indirect

ophthalmoscope to confirm correct intravitreal placement. The rabbit's face was then cleaned with sterile water to remove blood and residual preparation solution.

4.2.7. Post-operative monitoring of the rabbits

Any possible adverse effects of the DSMT device on ocular tissues were assessed by clinical observation (eye reflex and retinal examinations) and histological examination (Figure 4.3). Slit lamp examination, tonometric analysis for the measurement of intraocular pressure (IOP) in the test and control eyes of the rabbits and indirect ophthalmoscopic examinations were performed to evaluate the possible toxic effect of the DSMT device before and after implantation. Tissue reaction was monitored clinically by observing changes in the vitreous (vitreous haze) and retina (edema, chorio-retinal atrophy, vascular changes, exudative changes, and necrosis) adjacent to the implanted device. The presence and appearance of the DSMT device was also noted. Although the accuracy of IOP measurement is desirable, it is often the trend of change in IOP that one is most interested in. Numerous tonometers are used in animal experimentation, the accuracy of which has already been established in human eyes. However, when tonometers designed for human eyes are used in rabbits, their suitability is limited by the differences in the corneal anatomy (lack of Bowman's membrane in rabbits), corneal rigidity, and tear film composition. The ideal tonometer selected was a handheld microprocessor-controlled tonometer that is a modified "Mackay-Marg" design of the Tonopen^{TM} XL (Reichert$^{®}$, Depew, NY, USA) due to its accuracy, consistency and low variability in measurements. The instrument uses only the central part of the applanation area for pressure measurement, thereby minimizing the effect of differences in central corneal thickness. Dohadwala and co-workers (1998) have demonstrated that the Tonopen^{TM} XL is the most accurate for IOP measurements in humans and animals. Analysis was performed on the test and control eyes of all rabbits. Findings in an initial examination of all animals were normal, and baseline IOP measurements were recorded. The Tonopen^{TM} XL was first calibrated to the manufacturer's instructions and measurements were repeated until the coefficient of variation was <5%. All tonometric measurements were performed by the same ophthalmic surgeon. To correct tonometry estimates that provide a closer approximation of the actual IOP in rabbits, Equation 4.1 was used as derived by Lim and co-workers (2005) from a linear regression study. Lim and co-workers (2005) demonstrated that the Tonopen^{TM} XL showed the least error in estimation of true pressure. However, there was a high degree of variability in the measurements, especially at higher IOPs, where it

significantly undervalued the IOP and therefore a correction factor was introduced (Equation 4.1). Despite this variability the Tonopen^{TM} XL plays a significant role in cases where the main objective is to report a change in IOP trend rather than an absolute measurement.

Actual IOP (mmHg) = 1.12(Tonopen^{TM} XL) + 3.07 *Equation 4.1*

Where, the term *'(Tonopen^{TM} XL)'* is the IOP reading obtained during the measurement.

Figure 4.3: Digital images depicting the post-operative ophthalmoscopic monitoring procedures (reflex and retinal examinations) undertaken to assess the safety and toxicity of the DSMT device.

4.2.8. Enucleation procedure for evaluation of the DSMT device in the rabbit eye model

A total of two rabbits, one from each group of six were enucleated at pre-determined time intervals. Prior to euthanization retinal examinations was performed and 2mL blood samples were removed from the marginal ear vein. The rabbits were euthanized with an overdose of intravenous sodium pentobarbitone (200mg/kg) (Euthanaze®, Centaur Labs, Johannesburg, South Africa) on days 3, 7, 14, 28, 48, and 72 after implantation. Following euthanasia, VH was aspirated from the eyes using an 18G needle introduced into the VH through the sclera and pars plana 1cm posterior to the limbus. VH from the left eyes (non-test eyes) was used as controls. All VH and blood samples (removed from the marginal ear vein of the rabbits) were stored at -70ºC prior to GCV concentration analysis by Ultra Performance Liquid Chromatography (UPLC). The partially eroded DSMT devices were removed and the ocular tissues from the test and control eyes each comprising the cornea, iris, ciliary body, and sclera, were collected, immersed in glutaraldehyde/formalin (Fisher Scientific®, Pittsburgh, PA, USA) and histopathological examinations were thereafter performed. Figure 4.4 depicts sequential time-frame images of the enucleation procedure.

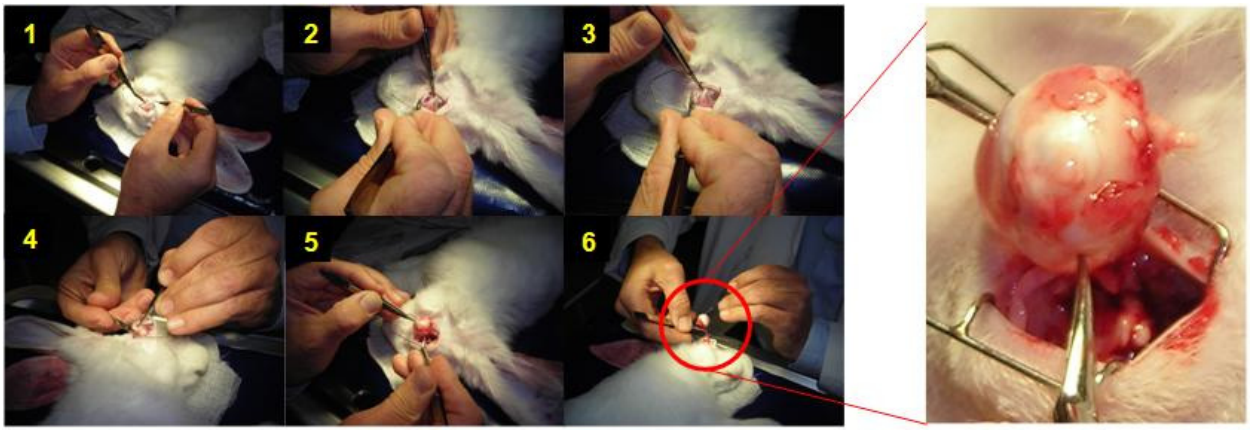

Figure 4.4: Time-frame images of the enucleation procedure (± 30min; N=12).

4.2.9. Histomorphological examination to assess the toxicity of the DSMT device

Possible adverse effects of the DSMT device on the ocular tissues were evaluated by histological examination under light microscopy after histological staining of the test and control eye tissue samples. Once the rabbit eyes were enucleated at 3, 7, 14, 28, 48 and 72 days after implantation and the partially eroded DSMT devices and VH samples were removed, the ocular tissues were immersed in formalin for 24 hours. Globes were then opened at the equator and separated into anterior and posterior segments and the incised specimens were dehydrated, infiltrated, embedded in paraffin, and sectioned with a microtone and stained with hemotoxylin and eosin and assessed microscopically. Ocular tissue were graded by two blinded observers, for extent of tissue destruction (histological grade based on a scoring scheme of 0=normal to 4=no recognizable structure), and type and extent of inflammatory cells present in the iris, iridocorneal angle, and ciliary body.

4.2.10. Influence of the DSMT device on the micro-environmental pH of vitreous humor

The control of enzymatic and structural processes that occur within the posterior segment of the eye and protein-protein interactions are likely to be influenced by changes in pH and ionic concentrations as a result of PLGA degradation into lactic and glycolic acid through cleavage by enzymatic or non-enzymatic hydrolysis (Kuck, 1975; Peracchia and Peracchia, 1980; Summers et al., 1984;). Since the DSMT device is PLGA-based it is crucial to have an accurate measure of the internal pH of the VH, as the degradation of the DSMT device may influence the inherent pH of the VH. Therefore changes in pH within the VH due to degradation of the DSMT device was assessed by *ex vivo* incubation of 5mL fresh VH aspirated from two enucleated rabbit eyes (controls) and swiftly placed into test tubes 10mm in

diameter (Figure 4.5). The test tubes were then incubated for 3 months after immersing a DSMT device in close proximity to the center of the VH. The micro-environmental pH variation in close proximity to the immersed DSMT device (<5mm of the eroding surface) was monitored with a MPT-2 Multi- purpose titrator equipped with a rapid response, liquid filled glass pH micro-electrode supported on a vertical puller (Malvern Instruments Ltd., Worcestershire, UK). The changes in pH were evaluated from a pH-time profile. The electrode calibration standards were adjusted to cover the buffer range from pH 6.1-7.5 with a linear Nernstian response maintained.

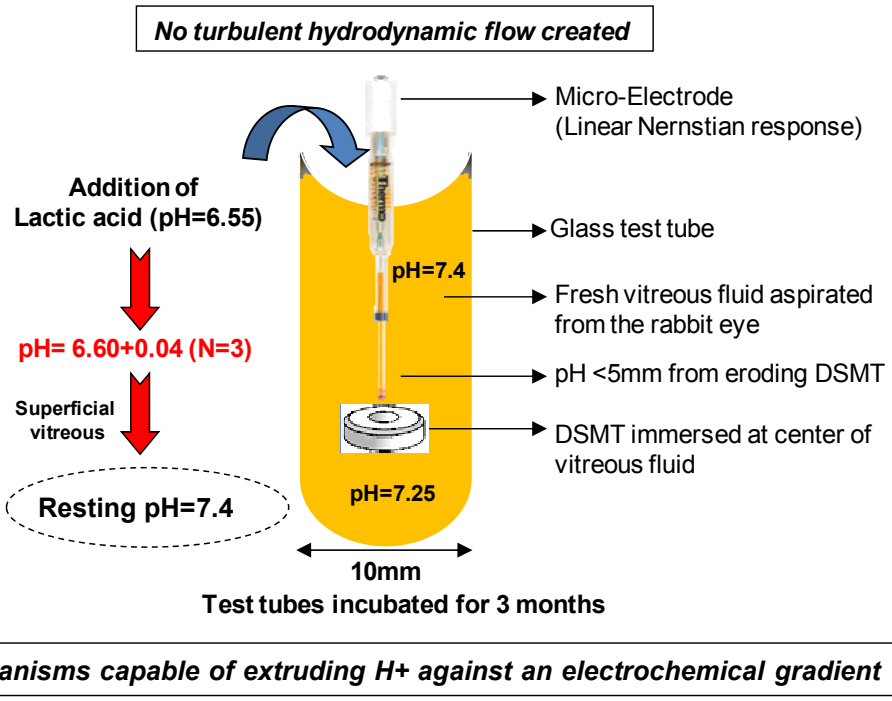

Figure 4.5: A schematic diagram detailing the experimental procedure used to assess the potential for micro-environmental pH changes within the VH as a result of DSMT implantation.

4.2.11. Quantification of *in vivo* ganciclovir released from the DSMT device

4.2.11.1. Preparation of calibration standards

Stock solutions of GCV were prepared (5mg/mL) and aqueously diluted further with deionized water to prepare spiking solutions with GCV concentrations ranging between 0.1-5.0µg/mL. In order to prepare the calibration standards used for generating a standard curve of GCV in VH and for method validation, 100µL aliquots of the spiking solutions and the internal standard solution of ACV (initial concentration of 1mg/mL) were added to inert polypropylene tubes that each contained a 250µL aliquot of blank rabbit

VH previously thawed and centrifuged at 15000*g* for 10 minutes. A liquid-liquid phase extraction methodology was used for the extraction of GCV from the blank rabbit VH in order to prepare a calibration profile. To each calibration standard 250µL of acetonitrile was added to the spiked VH standards in a quantification range of 0.1-5.0µg/mL. The tubes were then capped, vortexed (Vortex-Genie 2, Scientific Industries Inc., Bohemia, NY, USA) for 15 seconds and centrifuged (Optima® LE-80K, Beckman Coulter Inc., Fullerton, CA, USA) at 15000*g* for 10 minutes. Aliquots (300µL) of the supernatants were filtered through a 0.22µm Millipore® filter and transferred to UPLC injection vials. Thereafter 5µL was injected onto the UPLC column for GCV content analysis. The ratio of the peak areas (between the internal standard ACV, and GCV) versus the concentration data for the calibration standards was fitted by linear regression to generate the calibration curve. This procedure generated a set of five calibration standards with concentrations ranging from 0.1-5.0µg/mL of GCV in rabbit VH. The five calibration standards were used to construct a standard linear curve and additional calibration standards were prepared and analyzed for validation runs for precision and accuracy analysis of the assay method. Figure 4.6 displays the standard linear curve constructed for the determination of GCV concentrations form the VH samples in the rabbit eye model (R^2=0.99).

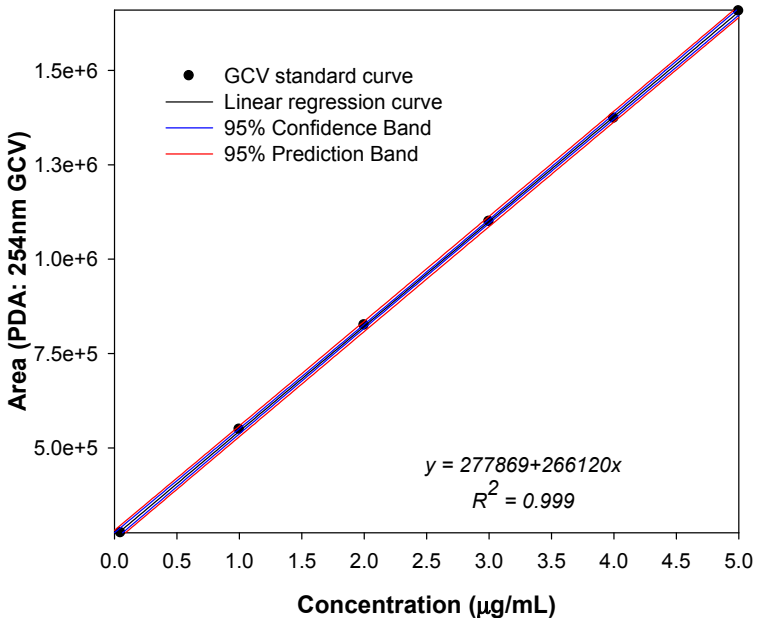

Figure 4.6: Calibration curve of GCV concentrations in blank rabbit VH.

4.2.11.2. Extraction of ganciclovir from the aspirated vitreous fluid samples

Frozen study samples were thawed at room temperature (21±0.5°C) and allowed to environmentally equilibrate. The samples were then centrifuged at 15000*g* for 10 minutes. The sample biological matrix matched the matrix employed for the calibration standards. Aliquots (250µL) of the VH samples were transferred using a graded micro-syringe (±0.5µL) (Hamilton (Pty) Ltd., Bonaduz, GR, Switzerland) into polypropylene tubes. Deionized water (100µL) was added to each tube and the tubes were vortexed for 15 seconds. The same procedure used for the extraction of the calibration standards (with the addition of 250µL acetonitrile) and UPLC injection of calibration standards were applied to the diluted VH samples to ascertain GCV content. An appropriate dilution factor was used to adjust the final GCV concentration obtained (Figure 4.7).

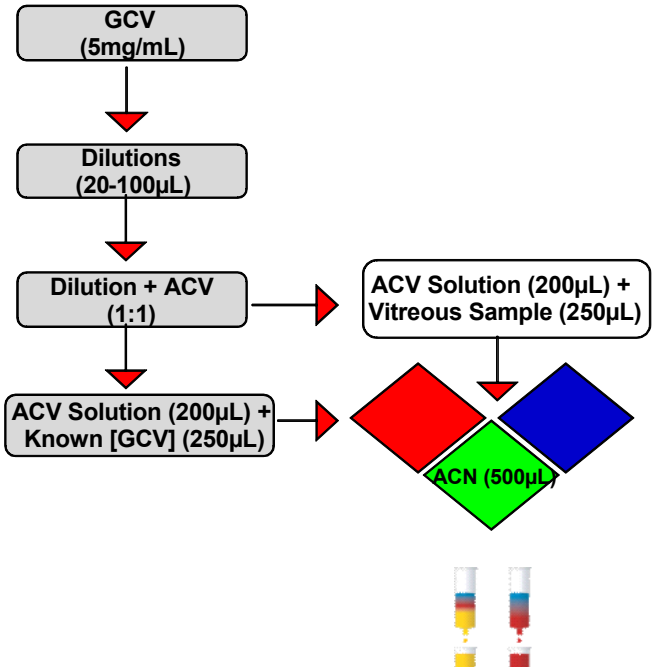

Figure 4.7: A flow diagram detailing the solid phase extraction procedure utilized for GCV concentration analysis for the rabbit VH samples.

4.2.11.3. Chromatographic procedure for ganciclovir concentration analysis

The concentration of GCV released into the rabbit VH from the DSMT device was determined using Ultra Performance Liquid Chromatography (UPLC). Analyses were performed on a Waters® Acquity UPLC™ system (Waters Corp., Milford, MA, USA) consisting of an Acquity UPLC™ binary solvent manager and an Acquity UPLC™ sample manager. Separation of GCV was obtained with an Acquity UPLC BEH C_{18} column (1.7µm; 1×100mm) and a photodiode array (PDA) detector set at 254nm. The

binary mobile phase comprised 0.05M ammonium acetate at a pH of 6.8 and acetonitrile in a ratio of 96:4%$^{v}/_{v}$. A solvent flow rate of 0.25mL/min was maintained with an average initial pressure of 6500psi. The program followed was isocratic and 5µL of the extracted and pre-filtered samples were injected onto the column. The column and sample manager temperature was maintained at 21±0.5ºC. Prior to use, the column was equilibrated by passing 45mL of mobile phase solvent through the system. The eluant was monitored at an analytical wavelength set at 254nm and the entire assay procedure was performed at room temperature (21±0.5ºC). ACV was used as the internal standard. A standard linear curve was used to assess the concentration of GCV released from the device at various time points. The recovery of GCV obtained during the extraction procedure spiked into blank VH samples from the non-test rabbit eyes was 102.69±1.50%, indicating the valid evaluation of GCV concentrations in the VH of the rabbit eye model.

4.2.11.4. Precision, accuracy and ganciclovir stability analysis during assay procedure

To assess the precision and accuracy of the assay method employed aliquots of each of the calibration standards were repeated in each of three assay runs. Furthermore, two calibration standards at each concentration, in addition to those used to generate the standard calibration curves, were prepared and analyzed in each of three runs. The data was then analyzed by ANOVA (Single Factor), (Minitab® Software V14, Minitab Inc., State College, PA, USA) to generate intra-assay and inter-assay coefficients of variation expressed as percentages (CV%). Accuracy was assessed by evaluation of mean recovery, defined as the ratio of mean found concentration to nominal concentration, expressed as a percentage. Recovery of GCV during the extraction procedures in the VH samples was assessed by replicate analysis (N=5) of the lower and upper concentration limits of the calibration standards and compared to those obtained by injection of aqueous solutions of GCV prepared at the same concentrations corresponding to the standards. Both extracted calibration standards and the aqueous samples were injected onto the UPLC column employing the same chromatographic conditions as in the assay method developed. The stability of GCV in frozen VH samples was assessed by periodic analysis of the calibration standards stored under the same conditions as the test samples and at -70ºC. Stability of GCV in the thawed VH samples was evaluated by replicate analysis of the calibration standards at the lower and upper concentration limits.

4.3. Results and Discussion

4.3.1. Preparation of the DSMT device

DSMT devices comprising 5%$^{w}/_{w}$ GCV were prepared employing Resomer® RG503 and Resomer® RG504. Figure 4.8 depicts a digital image showing the typical size of a sterilized DSMT device prior to implantation in the rabbit eye model.

Figure 4.8: Digital image indicating the dimensions of a DSMT device in comparison to a USA one dime coin prior to implantation into the New Zealand White Albino rabbit eye model.

4.3.2. Pre-surgical assessment of rabbit eyes prior to implantation of the DSMT device

Typical photographic evaluation in conjunction with indirect ophthalmoscopy and slit-lamp microscopy was undertaken for pre-surgically assessing the rabbit's eyes prior to implantation of the DSMT device (Figure 4.9). The photographic images of all animals were shown to be superimposable. Magnifications of the images were performed to determine whether subtle variations in capillary diameter occurred. The results of the photographic evaluations, in all cases, revealed that there was no detectable change in the anatomical features of the rabbit eyes and all findings were within normal limits suggesting that the eyes were not irritated.

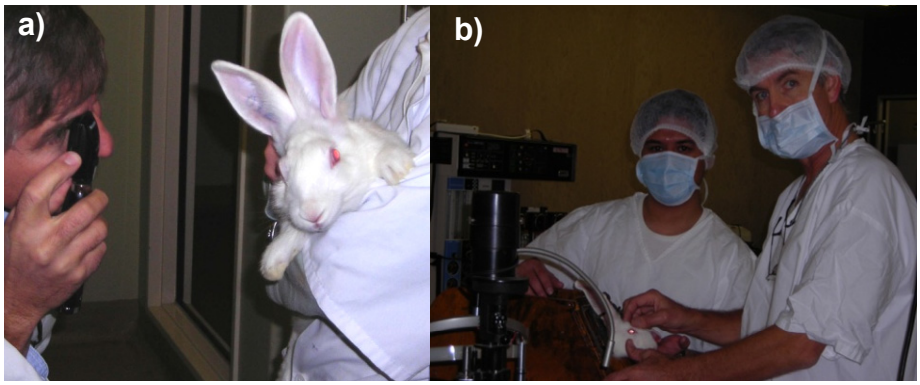

Figure 4.9: Digital images depicting a) indirect ophthalmoscopic examination and b) slit-lamp microscopic examination of the rabbit's eyes prior to implantation of the DSMT device.

4.3.3. Post-surgical assessment of complications after implantation of the DSMT device

The DSMT device appeared to be well tolerated up to a last time point reaching 72 days in the rabbit eye model and was visible by indirect ophthalmoscopic analysis in the supero-temporal quadrant of the eye (Figures 4.10a and b). Of the 12 rabbits studied, three had small postoperative hyphaemas, visible after the surgery and for up to 7 days. Two had vitreous hemorrhages and one had a retinal detachment by two weeks. There were no infections or inflammation and no cataract formation. At day 3 the surgical wound made at implantation was completely healed (Figure 4.10c). Clinically no changes were observed in the VH, retina or choroid such as vitritis, vascular changes, exudative changes, necrosis or traction. Preliminary histological examinations revealed no significant difference between the test and control eyes except for the presence of poorly-formed multi-nucleated giant cell infiltrates around the 9-0 nylon suture site. In addition, no focal disruption of the normal inner retinal architecture was observed. A non-significant inherent anterior segment hemorrhage was detected in one rabbit from the initial experimental group of six rabbits that received a DSMT device formulated with Resomer® RG504. However, this finding was as a result of intraocular pressure variation during the surgery and not directly caused by the presence of the DSMT device. No filtering bleb around the wound or leakage of VH from the wound was observed. The matrix of the DSMT device was visually observed and estimated to swell gradually due to hydrolysis but was not significant to induce any complications. The DSMT device eroded steadily over the 72 day period of the study with minute opaque fragments remaining within the VH space. The biocompatibility of the polymer PLGA has been extensively reported in the intraocular region (Langer et al., 1983; Heller et al., 1984; Lee et al., 1988; Charles et al., 1991; Giordano, et al., 1995; Deshpande et al., 1998; Morita et al., 1998; Einmahl et al., 1999).

Figure 4.10: Post-surgical monitoring and examination of the test and control eyes. Digital images showing a) direct ophthalmoscopic examination after 72 days, b) the patent ophthalmic reflex of a rabbit with a DSMT implanted into the superonasal quadrant of the eye and c) the surgical wound completely healed at day 3.

Slit-lamp examinations showed a normal appearance of the ocular surface in all animals after the DSMT device was removed. It was noted that rabbit 3 had a rather narrow fornix, due to an oriental lid crease. Prior to the experiment, redness was grade I for all rabbits (i.e. no redness) and no changes in redness were observed throughout and after the experiment. All rabbits had a normal appearance of the anterior segment before implantation of the DSMT device and after removal except for one in which an insignificant anterior segment hemorrhage was noted. None of the rabbits showed corneal punctuate staining before installation of the device, or afterwards. On the first postoperative day, the right eyes of the rabbits were mildly red, but no discomfort was noted. Vision in the right eye was graded as normal, with the rabbits not displaying any gross distress or difficulty in identifying their surroundings. Indirect ophthalmoscopic examination detected minimal vitreous hemorrhage and verified that the DSMT device was in the correct position. The rabbits were re-examined initially daily for 7 days and thereafter at weekly intervals after the surgery. At a 1 month postoperative clinical examination, the rabbit's vision was considered normal in both eyes, and the presence of any vitreous hemorrhage had resolved (Figure 4.11).

Figure 4.11: Digital image showing the patent ophthalmic reflex of a rabbit with a DSMT implanted into the superonasal quadrant of the eye.

Tonometric analysis in the rabbit eye revealed that the use of an instrument calibrated for human use resulted in a gross underestimate of IOP measurement in the rabbit eye. Therefore this underestimate was accounted for by the linear regression model of Lim and co-workers (2005). IOP measurements recorded via the use of the Tonopen^{TM} XL revealed a trend of no drastic change in the IOP of the rabbit's eyes after implantation of the DSMT device (Figure 4.12). The mean IOP measurements for all rabbits (N=12) were within a range of 6-8mmHg and in close proximity to the baseline measurements

before implantation of the device and the control eyes. The slight variations noted from the IOP measurements are as a direct result of the technique used to measure the IOP from the rabbit eye model that is dependent on the corneal anatomy (lack of Bowman's membrane in rabbits), corneal rigidity, and tear film composition as reported by Lim and co-workers (2005).

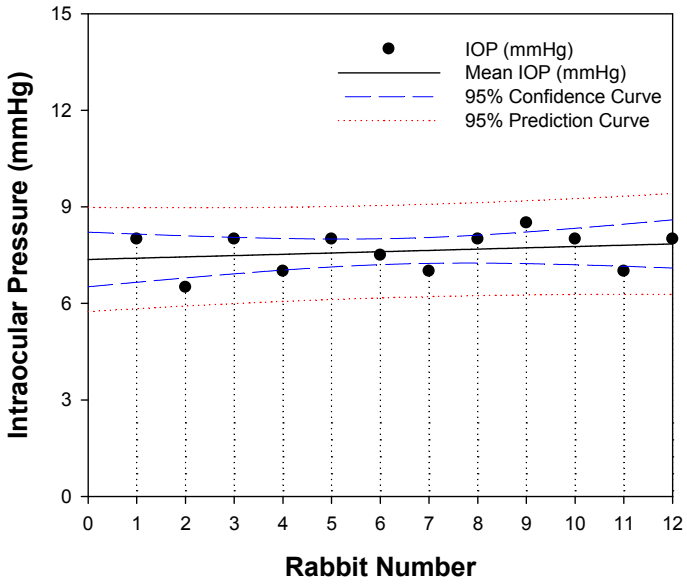

Figure 4.12: Profiles showing the variation in intraocular pressure in relation to the baseline after implantation of the DSMT device in the rabbit eye.

4.3.4. Histological examination and toxicology analysis

A progressive inflammatory response was noted in the ocular tissue, centered predominately around the ciliary body and in the posterior segment (Figure 4.13a). The initial response was that of an acute inflammatory reaction with hemorrhage, edema and a predominately neutrophilic infiltrate (Figure 4.13b). The inflammatory reaction then became more chronic in nature with lymphocytes, occasional eosinophils, plasma cells and fibroblasts noted (Figure 4.13c). A foreign body type giant cell response was also appreciable (Figure 4.13d). The hemorrhage and edema had subsided by day 28. Some foreign material was noted in association with the foreign body giant cell response (day 28). After 72 days, a minimal residual inflammatory response was noted and of significance, there was no evidence of a sympathetic ophthalmitis, no evidence of chronic fibrosis and no histopathologic evidence of damage to the ciliary body or retina. There was no histopathologic evidence of damage to the ocular tissue and no evidence of an exuberant inflammatory response. The retina in the posterior pole remained intact (Gould et al., 1994; Dubielzig et al., 1997; Gilger et al., 1999).

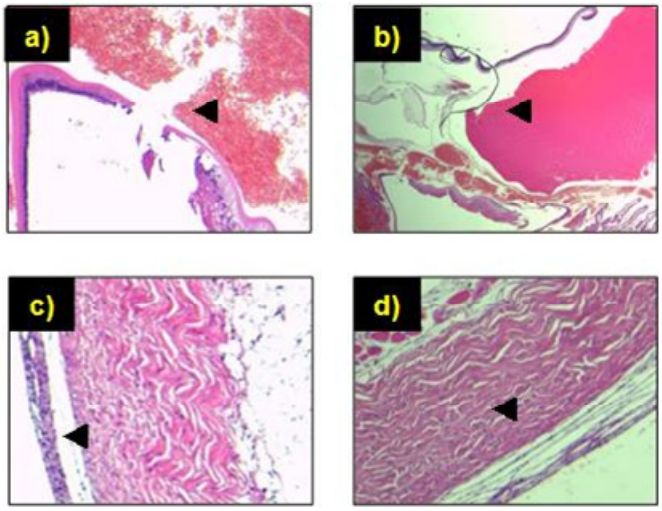

Figure 4.13: Digital images of hemotoxylin and eosin stained histological slides showing a) and b) the sclerotomy after implantation of a DSMT device at 7 days with foreign material noted (suture) and a giant cell response (original magnification ×25); c) and d) residual inflammatory cells infiltrate the matrix and the intact retina at the implantation site after 72 days in the rabbit eye model with no evidence of a sympathetic ophthalmitis, chronic fibrosis or damage to the ciliary body (original magnification ×50).

Fibroblasts, neutrophils and multinucleated giant cells were infiltrating into the matrix pores in the course of degradation, but no significant inflammatory reaction was observed in the VH. No retinal detachment occurred around the DSMT implant. At 3 weeks after implantation, the device begun to erode and was visually evident in the VH. It was also observed that the sclerotomy site had been closed with fibrous connective tissues and the infiltration of inflammatory cells had been further decreased around the sclerotomy site. Furthermore, grading by the two blinded observers for extent of tissue destruction related that all rabbits were given a score of 0 (normal) for the type and extent of inflammatory cells present in the iris, iridocorneal angle, and ciliary body.

4.3.5. Drug extraction and assay procedure

Figure 4.14 depicts a typical UPLC chromatogram showing the simultaneous separation of GCV and ACV (internal standard) from the rabbit VH samples at 3 days after implantation of the DSMT device, where GCV was eluted at approximately 1 minute and ACV at 1.35 minutes. Validation of the assay method indicated that intra-day and inter-day precision and accuracy as well as the recoveries were satisfactory (R^2=0.99; RSD±0.02%; see Appendix G). The assay method developed and validated employed acetonitrile to precipitate proteins from the VH samples. To avoid any deleterious effects of overloading the column with acetonitrile, the injection volume was maintained at 5µL. An Ultraviolet (UV) photodiode array (PDA) detector was used for detection and quantification of GCV levels in the VH samples. ACV was used as the internal standard. The mobile phase concentration of acetonitrile and

ammonium acetate at a pH of 6.8 provided adequate retention of GCV and ACV on the UPLC column. The assay method was validated for the range of GCV concentrations from 0.1-5.0µg/mL in VH. The signal to noise ratio at the lower limit of quantification (0.1µg/mL) was >10.

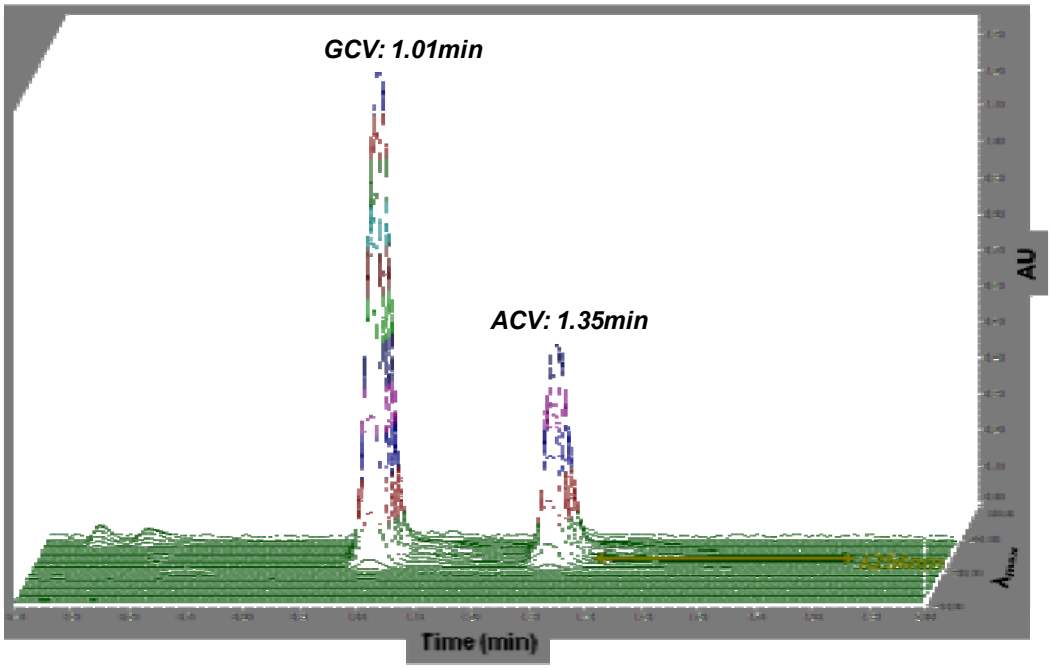

Figure 4.14: Typical 3D Ultra Performance Liquid Chromatogram of GCV and ACV separation from the rabbit VH samples.

Analysis of blank VH samples showed no interfering peaks at the retention times of GCV and the internal standard ACV (Figure 4.14). The precision of the assay method in VH was assessed by determination of the intra-assay and inter-assay coefficients of variation (CV%) of the method from replicates of each calibration standard in each of 3 runs (N=8). The accuracy of the assay method was evaluated from the calibration standards by the mean recovery defined as the ratio of the mean found concentration to the nominal concentration, expressed as a percentage. Absolute recovery of GCV from the VH samples was performed by comparison of peak areas from extracted low and high calibration standards to those from aqueous standards. A CV%=5.38% and mean recoveries ranging from 97.4-101.0% (R^2=0.99) was obtained. These results indicated essentially complete recovery of GCV after the extraction process. Stability studies of GCV in the rabbit VH indicated no changes in GCV concentrations upon storage of the samples frozen over 4 months at -70ºC or upon subjecting the VH samples to three freeze and thaw cycles. A simple UPLC method employing an isocratic gradient has been validated for the determination of GCV in the rabbit VH samples employing ACV as the internal

standard. The validated range and lower limit of quantification (0.1µg/mL) of the method was desirable for further pharmacokinetic studies.

4.3.6. *In vivo* release of ganciclovir in the rabbit eye model from the DSMT device

As expected the DSMT device manufactured employing PLGA grade Resomer® RG504 provided superior control in GCV release than Resomer® RG503 with sustained release of GCV in the VH cavity over a period of 72 days (Figures 4.15 and 4.16). The cumulative release of GCV released from the Resomer® RG504 DSMT device at a constant GCV loading of 5%$^{w}/_{w}$ is shown in Figure 4.15. The cumulative drug release profile was obtained by measuring the percentage of GCV released versus the initial content loaded in the DSMT device (Figure 4.15). The data is consistent with a reduced biphasic profile as noted from the previous *in vitro* study by Choonara and co-workers (2006; 2007), that was primarily due to the rapid release of GCV deposited on the surface of the rigid Resomer® RG504 matrix (Figure 4.15a). However for the current *in vivo* study the DSMT device was initially equilibrated in sterile saline prior to implantation. This additional procedure may have resulted in removal of the patent deposition of GCV molecules on the surface of the device. Thus the release of GCV from the device was constant and controlled by the degradation rate of the polymer. The release rate increased with the decrease of the molecular mass of PLGA. This rate was probably due to the difference in the degradation rate of the polymers. Degradation of PLGA could be influenced by the composition of the lactide and glycolide content with the higher the glycolide content, the faster the degradation rate (Baker et al., 1974).

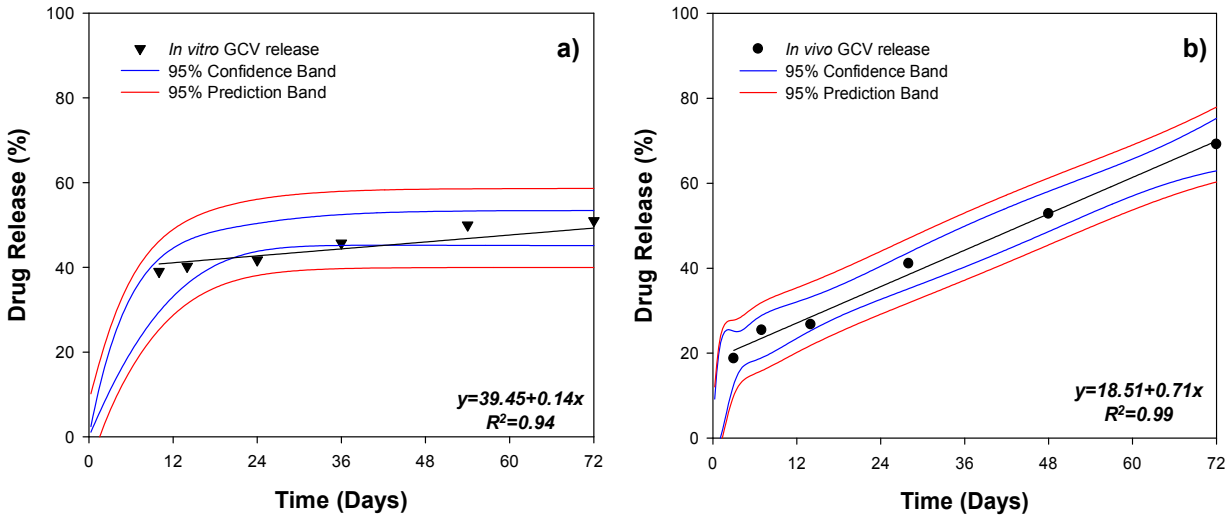

Figure 4.15: Profiles of a) *in vitro* release (Choonara et al., 2006; 2007) and b) cumulative *in vivo* release of GCV from a Resomer® RG504 DSMT device over a period of 72 days (N=6; SD<3.31 in all cases).

Devices formulated with Resomer® grade RG503 displayed a higher quantity of GCV release within the 50% effective dose (ED_{50}) range for the treatment of human CMV-R as compared to DSMT devices formulated with Resomer® grade RG504 (Figure 4.16). The *in vitro* ED_{50} of GCV for human CMV-R has been previously determined to be approximately 0.1-2.75µg/mL (Mar, 1983; Martin, 1983; Smee, 1983; Tocci et al., 1984; Plokin, 1985). The intravitreal GCV concentrations were maintained within the ED_{50} range over 72 days. In comparison to the previous *in vitro* release data obtained, the *in vivo* release profile displayed a reduced initial burst phase with <20% GCV released at day 3, 40% by 28 days, 50% by day 48 and 69% after 72 days in the rabbit eye model. The *in vivo* release data has been represented as semi-logarithmic plots in order to assess the effective levels of GCV reached within the VH in terms of achieving an ED_{50} for the treatment of CMV-R in HIV+ patients (Figure 4.16). Although the DSMT device has maintained the VH concentrations of GCV within the ED_{50} of GCV for 72 days, in order to refine the higher drug release produced by DSMT devices manufactured with Resomer® grade RG503, the Resomer® grade RG504 devices produced more controlled GCV release with a reduced quantity of GCV released over the same period. The GCV concentrations in the systemic circulation and the control eyes were <0.1µg/mL which was the detectable limit of the GCV UPLC assay during the study period.

From the previous *in vitro* drug release study (Choonara et al., 2006), the initial phase of GCV release that was termed as a “burst-release phase” was due to drug particles deposited onto the surface of the DSMT device that subsequently provided an initial spike of approximately 30% *in vitro* release of GCV. The second phase of release (comprising the remainder 60-65% of the drug-load) was regarded as a constant drug release phase that significantly depended on the relatively constant surface area created by the donut-shaped geometry of the DSMT. Interestingly, during the current *in vivo* animal study the initial burst-release phase was significantly reduced (<20%) due to the higher viscosity of the rabbit eye VH (compared to enzyme and protein-free PBS of pH 7.4; 37°C) that subsequently controlled the outward diffusion of GCV during the *in vivo* study. In addition, the pre-treatment of the DSMT device with sterile normal saline solution (NaCl=0.9%$^{w}/_{v}$) prior to implantation facilitated the removal of patent GCV molecules deposited onto the surface of the DSMT device during device manufacture. The release of GCV from the DSMT device which has a constant surface area that is controlled by the erosion mechanisms of the polymer followed constant drug release kinetics. This was primarily as a result of

synchronization of front velocities at the erosion interfaces. For conventional tablet geometries this may not be possible as the total surface area accommodating drug release decreases over time even though hydrophilic swellable/erodible polymers are employed resulting in a deviation from constant drug release kinetics. The absence of a central hole does not allow for compensating the decrease in the releasing surface area of the device due to their asymmetrical design.

Attempts have been made to obtain constant drug release kinetics via the use of semi-permeable membranes and non-erodible polymers such as in the case of the Vitrasert® intraocular device (Smith et al., 1992; Sanborn et al., 1992). These approaches (that may also be restrictive in terms of drug-loading capacity) have been attempted in an effort to minimize the effect of the decreasing releasing surface area on achieving constant drug release kinetics. However, such an approach requires advanced manufacturing technologies due to the complicated asymmetrical design and multi-component device configuration (Heller et al., 1987). Thus, in our present study a simple symmetrical "donut-shaped" geometry was used to provide constant drug release kinetics as an implantable extended release biodegradable intravitreal drug delivery device. The erosion controlled principles of the PLGA used to manufacture the DSMT are exercised with a reduced effect of the releasing surface area over time. Generally, drug release from a matrix occurs from all surfaces (circular faces and lateral areas). During drug release, the releasing surface area decreases over time. However, the DSMT reduces the effect of the releasing surface area laterally. Typically, drug release occurs through the central hole, a lateral area and the circular faces (Figure 4.8) and therefore the DSMT can maintain a constant drug releasing surface area over time. From the general behavior of observed erosion boundaries and diffusion fronts during GCV release from the DSMT, it was evident that the decrease of releasing surface area from the outer lateral area was compensated by the increase of releasing surface area from the central hole. This resulted in a constant drug releasing surface area laterally. After 2 months post-implantation the central hole in the device was still proportionately open although the size of the device was slightly reduced due to erosion. This finding suggested that GCV diffused through channels within the polymer matrix during biodegradation. However the mass of the polymer did not change until the production of oligomers, which were sufficiently small to solubilize by random hydrolytic chain scission.

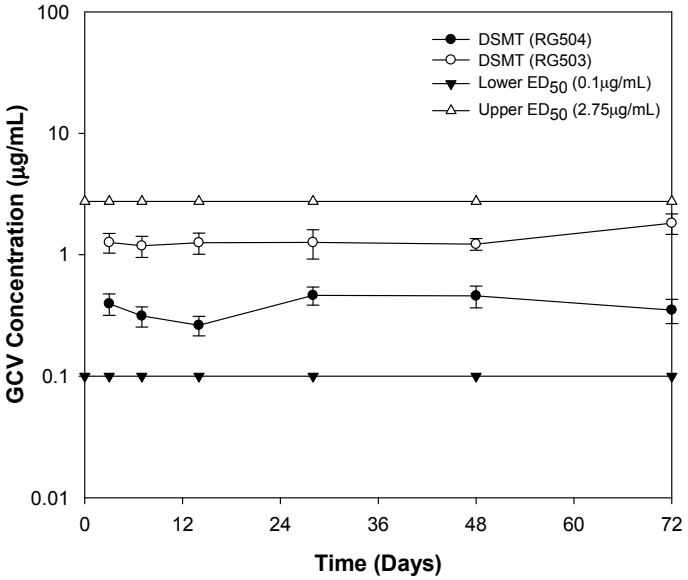

Figure 4.16: Semi-logarithmic plot of GCV released from the DSMT device after 72 days of implantation in the VH of the rabbit eye model (N=12). The upper and lower bounds of the 50% effective dose (ED_{50}) of GCV for human CMV-R replication are also shown.

4.3.7. Micro-environmental pH variation analysis within the vitreous humor

It was usually observed that the superficial VH immediately adjacent to the immersed DSMT device exhibited higher pH values than the VH immediately surrounding the device. The pH, measured as close as possible to the device, was 7.25±0.01 (N=3). The pH electrode was inserted using a Narashige micro-manipulator and was submerged towards the DSMT device by careful hydraulic micro-movements to avoid creating any unnecessary turbulent hydrodynamic flow. A slight drop in pH was routinely recorded as the electrode passed in proximity to the DSMT device with a slightly more acid pH than the entire VH sample (pH 7.20±0.01) around a superficial surface diameter of 5mm (Figure 4.17). The pH, measured away from the superficial layer was 7.40±0.02 (N=3). Attempts were made to perturb the inherent pH of the VH by adding incremental volumes of lactic acid of pH 6.55 (a significantly > volume than would be produced on degradation of the PLGA-based DSMT device in the VH) and incubated for 90 days. Samples were measured before and after incubation. After the lactic acid incubation period the pH recorded within the VH was 6.88+0.02 (N=3) and not significantly different from the resting pH of 7.40. After further addition of lactic acid solution of pH 6.55, the inherent pH was reduced to 6.60±0.04 (N=3). It would appear that the VH was able to maintain its internal pH close to a value of 7.40 in the presence of a more alkaline medium but could not do so in the presence of a largely acidic medium. The effect of lactic and glycolic acid perfusion from PLGA degradation can be seen in Figure 4.17. On exposure to degradation, an alkalinization is observed of some 2 pH units and this is

followed by a return towards the control value of pH 7.40. The characteristic biphasic response was observed in all experiments (N=3) but the amplitude of the pH change recorded was dependent on the position of the pH electrode tip (Figure 4.5). The response was smaller when the electrode was placed close to the DSMT device, presumably because the tip was insulated from pH fluctuation by overlying layers of well-buffered VH. In most experiments the pH overshoots on return to control and very minimal periods of acidosis was noted from which it recovered over an average period of 10 days. The pH of the VH has been measured by a number of indirect techniques. Duke-Elder (1946) found the intraocular fluid to be 'alkaline to litmus' and concluded that indicator methods had generally shown the VH to be more acid than blood. Davison and Luck (1956) obtained a value of 7.20 for the pH of rabbit VH. The present study represents an *ex-vivo* measurement of pH in the rabbit VH. The fact that the pH was found to be slightly higher at 7.40 supports Duke-Elder's (1946) notion that the higher pH values are due to a loss of CO_2, from the eye when the globe is opened. Estimates of pH in mammalian VH by indirect methods range from 7.40 (Bellows, 1944) to 6.9 (Greiner et al., 1981). This indicates the presence of mechanisms capable of extruding H^+ ions against, an electrochemical gradient.

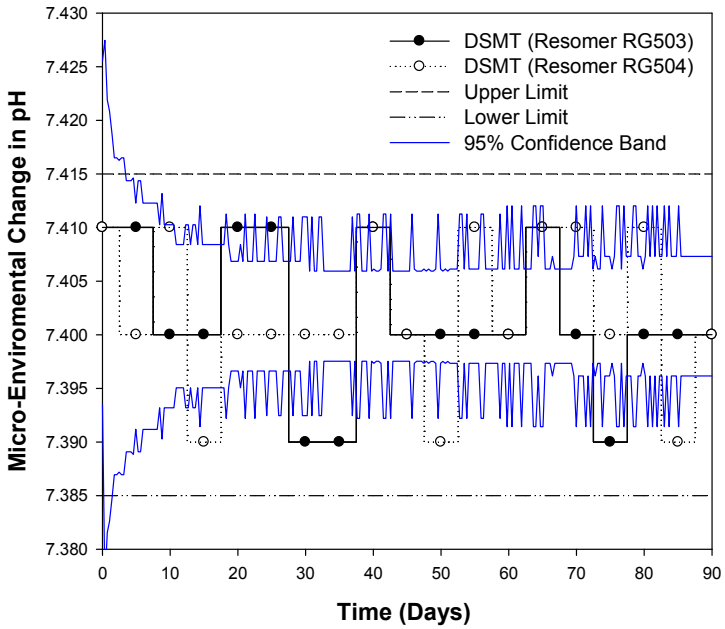

Figure 4.17: *Ex vivo* changes in vitreous pH induced by implantation of the DSMT device. pH transients for electrodes at a superficial surface of 5mm from the submerged DSMT device. For both formulations the initial alkalinization phase (7.41) was followed by an acidic overshoot of pH 7.39 on return to control (7.40).

4.4. Concluding Remarks

In this study we have demonstrated that the biodegradable DSMT device may provide a significant innovation to the current cache of intravitreal drug delivery technologies for the treatment of posterior segment eye diseases such as CMV-R. The DSMT device was well tolerated in the rabbit eye model without any adverse effects or toxicity over the entire duration reaching 72 days in this study. Histopathological examination revealed that the device was non-toxic to intraocular tissue structures. GCV release in the VH of the rabbits from the DSMT device was maintained within the ED_{50} range for the treatment of human CMV-R. Our study has shown that constant drug release can be obtained with the DSMT device due to the unique geometry of the device as well as the use of PLGA with varying molecular mass, lactide:glycolide ratios, drug loading capacities and compressive forces during tableting. The DSMT device is sufficiently flexible and may be used for the effective long-term intravitreal delivery of drugs for the treatment of various posterior segment eye diseases.

CHAPTER 5

EXPLORATORY DATA ANALYSIS EMPLOYING COMPARTMENTAL AND NON-COMPARTMENTAL PHARMACOKINETIC MODELING ANALYSIS

5.1. Introduction

The posterior segment of the eye may be affected by various vision impairing diseases such as viral retinitis, bacterial and fungal endophthalmitis, proliferative vitreoretinal disorders and diabetic retinopathy. Topical and systemic administration of drugs may not deliver effective therapeutic concentrations to the posterior segment of the eye (Lesar and Fiscella, 1985; Geroski and Edelhauser, 2000; Lee et al., 2004). Due to the protective blood-ocular barriers approximately <1% of topically applied drug is available to the anterior segment and only a small fraction of drug present in the anterior segment reaches the posterior segment of the eye (Lee and Robinson, 1986; Lee et al., 2004). In addition, the blood-aqueous and blood-retinal barriers limit the penetration of drug molecules to the internal tissues of the eye such as the retina and choroid from the systemic circulation (Cunha-Vaz, 1979). Direct intravitreal drug administration and intraocular devices have been employed as an effective means of treating the majority of vitreo-retinal diseases proliferating in the posterior segment of the eye (Graham and Peyman, 1974; Cochereau-Massin et al., 1991). Therefore knowledge regarding the distribution and elimination of drug molecules from the vitreous cavity is necessary in order to develop optimal drug therapy. A major limitation in assessing the ocular pharmacokinetics of drugs from *in vivo* animal models such as the New Zealand White Albino rabbit is the fact that a single rabbit must be used for a single time point. Thus in order to obtain a comprehensive pharmacokinetic (pK) profile with minimal variability approximately 6-20 rabbits needs to be sacrificed at each time point as a sufficient number of intervals must be selected to adequately characterize the distribution and elimination processes in the posterior segment of the eye (Schoenwald, 1990).

The application of pK modeling is significant in the drug molecule approval process and the development of novel drug delivery systems. In preclinical studies pK modeling is used to interpret toxicokinetic data and to extrapolate results from animals to man via physiological modeling and allometric scaling. pK modeling assists in the interpretation of dose-response and dose-escalation

studies and therefore has been used in several instances by regulatory agencies to recommend a dose and/or regimen which were not originally studied as part of the clinical program. As further indication of the growing acceptance of the value of pK modeling, the United States Food and Drug Administration (FDA) (1999) have released a document on the "*Guidance for Industry on Population Pharmacokinetics"* (Aarons, 1997). Several International Conference on Harmonization (ICH) guidelines have also been published in this regard (ICH Guidelines, 1999). pK modeling allows one to describe the quantitative relationship between the administered dose or dosing regimen and the observed *in vivo* concentration of the drug (Holford and Scheiner, 1986; Fleishaker and Ferry, 1995; Lima, 1995). Progress in ophthalmic drug delivery has been impressive (Hecht, 1995; Reddy and Ganesan, 1996) and numerous products have been or are currently being developed and these include topical solutions (Nagataki and Mishima, 1980), suspensions (Garny, 1981), ointments, gels (Miyazaki, 1982; Lewis et al., 1986), intravitreal and subconjunctival injectables (Kelly et al., 1989; Barza et al., 1993; Berthe et al., 1994), iontophoretic systems (Friedberg et al., 1991) and intraocular implantable devices (Grass et al., 1984; Choonara et al., 2006; 2007). One of the most significant tools to develop and evaluate these products is with the use of accurate compartmental and non-compartmental pK models. The primary objective of a pK model is to enhance the accuracy of estimating the dynamic state of drug behavior in an actual pre-clinical or clinical situation (Reddy and Ganesan, 1996). Numerous pK models have been reported in the literature and represent varying levels of sophistication with several reviews published on this subject (Mishima, 1981; Maurice and Mashima, 1984; Lee and Robinson, 1986; Schoenwald, 1993; Urtti and Salminen, 1993; Frangie, 1995; Jarvinen et al., 1995).

In the present study compartmental and non-compartmental pK models were explored for potential application to intraocular drug delivery employing the DSMT device (Choonara et al., 2006; 2007). Intravitreal injection and implantable devices for GCV have been used for the treatment of CMV-R in patients with HIV/AIDS (Ussery et al., 1988; Cantrill, 1989; Cochereau-Massin et al., 1991). However, since not only the efficacy but also the toxicity of GCV is influenced by the concentration at the site of action, the local concentration following intravitreal GCV delivery needs to be carefully examined. The pharmacokinetics of intravitreal drug injection has been analyzed by compartmental pK modeling that assumes drug molecules to be uniformly distributed throughout the VH (Ben-Nun et al., 1989). However, this assumption may not be applied to prolonged release drug delivery devices such as the DSMT due

to the constant rate of GCV release and elimination across the surrounding ocular tissues in the posterior segment of the eye. A significant concentration difference may be produced between the surface of the DSMT device and the elimination pathway boundaries such as the retina/choroid/sclera (RCS) membrane and the posterior aqueous segment. The drug concentration and distribution in the VH is influenced by the rate of drug elimination through the RCS membrane and surrounding tissues. The elimination profile of drug in the rabbit eye following intravitreal injection of drug was previously described by a cylindrical vitreous body model (Ohtori and Tojo, 1994; Uno et al., 1994).

Therefore, the primary objective of this study was to characterize and compare the pK fate of GCV released from the DSMT device in the rabbit eye model. The simplest single- and multi-compartment pK models were selected in representation of the posterior segment of the rabbit eye. The cylindrical diffusion/partitioning pK model for predicting the performance of GCV released from the DSMT device was extended. A series of *in vivo* experimental drug release data for determining the most superior pK model and parameter estimates was established. The *in vivo* GCV concentration profiles obtained from animal studies undertaken in the New Zealand White Albino rabbit eye model was compared with several compartmental and non-compartmental pK models and predicted profiles from the pK models using the model parameters determined from *in vivo* experiments. Since the DSMT device is a matrix device with a novel geometric design in which GCV molecules are uniformly distributed throughout the polymer matrix an assumption was made during the pK modeling process that the release rate decreased with increasing time for GCV release.

5.2. Materials and Methods

5.2.1. Materials

For the purposes of this component of the research the DSMT device manufactured using PLGA grade Resomer® RG504 was selected for further kinetic modeling and data analysis due to its ability to provide superior control of GCV release in the vitreous cavity than devices manufactured with Resomer® RG503. The materials used for preparations of the DSMT device have been discussed earlier and can be found in Chapter 3, Section 3.2.1 of this thesis.

5.2.2. Preparation of the donut-shaped minitablet device

The preparation of the DSMT device employing PLGA grade Resomer® RG504 has been discussed earlier in this thesis and can be found in Chapter 3, Section 3.2.2. Further details can be read in a research publication by Choonara and co-workers (2006).

5.2.3. The *in vivo* pharmacokinetic study protocol

The study protocol followed was identical to the procedure delineated in Chapter 4, Sections 4.2.4-4.2.11 of this thesis. All animals were treated in accordance with the Association for Research in Vision and Ophthalmology (ARVO) Resolution on the Use of Animals in Ophthalmic and Vision Research (Rockville, MD, USA).

5.2.4. Pharmacokinetic modeling employing compartmental and non-compartmental algorithms

WinNonLin® software (V5.2.1 with IVIVC Toolkit Build 2008033011, Pharsight Software, Statistical Consultants Inc., Apex, NC, USA) was used as a tool for pK modeling and the computation and estimation of all pertinent pK parameters. Input data comprised *in vivo* GCV release data obtained from the described *in vivo* experimental protocol of DSMT devices manufactured with Resomer® grade RG504 and implanted into six New Zealand White Albino rabbits whereby VH samples were obtained and analyzed via UPLC over a period of 72 days. In vivo data obtained form DSMT devices manufactured with Resomer® grade RG504 were selected for pK modeling as it showed superior control in GCV release as decribed in Chapter 4, Section 4.3.6 of this thesis.

5.2.4.1. pK model structure and selection

Successful pK modeling of the DSMT device (described by a single bolus dose of GCV released over time) is dependent upon the meticulous selection of relevant pK models that are based on the dose and the duration of GCV released in the VH obtained from the *in vivo* VH concentration-time profiles obtained from the *in vivo* studies in the rabbit eye model. Based on the *in vitro* and *in vivo* GCV release dynamics from the DSMT device via exploratory data analysis (EDA) and the pharmacokinetics and pharmacodynamics of the drug GCV, two tentative compartmental (referred to hereunder as pK models A and B) and two non-compartmental (referred to hereunder as pK models C and D) pK models were selected. Prior to pK model fitting to the *in vivo* GCV release data, the EDA

suggested the tentative structure of the pK model and the initial estimates of the pK model parameters. In addition, WinNonlin® was also used to accurately derive the initial parameter estimates in order to avoid data convergence to a local minimum. The *in vivo* GCV release data obtained from the *in vivo* animal study was fitted to the tentative pK models selected in order to confirm or suggest modifications to the pK models chosen. Once a desirable pK model was selected the model was fitted to the *in vivo* experimental data using non-linear regression analysis in order to estimate the pK model parameters and the precision of the pK parameter estimates. Once data iteration was complete the pK modeling process outputs were diagnostically evaluated via pertinent statistical descriptors such as the goodness of fit, correlation between parameters, residual analysis, parameter accuracy and precision, the Schwartz Bayesian Criterion (SBC) (Schwartz, 1978), Condition Number (CN) and Akaike Information Criterion (AIC) (Akaike, 1978). This formed the basis of assessing the suitability of the pK models for fitting the *in vivo* GCV release data from the DSMT device and explicated the data and comparisons of competing pK models. Plots of observed and fitted data superimposed on semi-logarithmic scales as well as residual plots were generated in order to search for the best fitting pK model. The pK parameters were determined using the two compartmental (pK models A and B) and two non-compartmental pK models (pK models C and D) (specifically for sparsely-sampled data obtained from the mean GCV concentrations at various time points after single dose administration) using the GCV release data obtained from the *in vivo* animal studies (Figures 5.1 and 5.2). A WinNonLin® compiled pharmacodynamic (pD) model was also explored for assessing "drug effect data" (Figure 5.3).

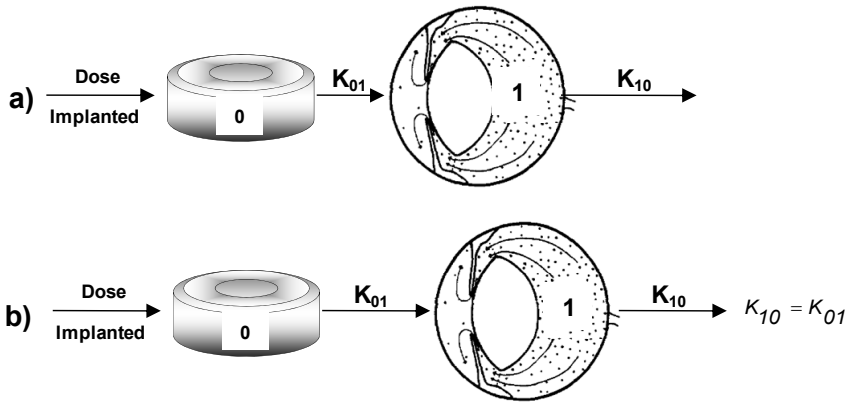

Figure 5.1: Schematics of WinNonlin® compiled one compartmental pK models showing a) no lag-time first-order elimination *(K_{01}<K_{10})* (pK model A) and b) no lag-time first-order elimination (K_{10}=K_{01}) (pK model B).

The concentration of GCV in the VH based on the compartmental pK models A and B can be described by Equations 5.1 and 5.2 respectively. Equation 5.3 represents the estimated GCV clearance parameters for both pK models.

$$C_t = \frac{DK_{01}}{V(K_{01} - K_{10})}[e^{-K_{10}t} - e^{-K_{01}t}] \qquad \textit{Equation 5.1}$$

$$C_t = (\frac{D}{V})Kte^{-K_t} \qquad \textit{Equation 5.2}$$

$$K_{10} = \frac{Cl}{V} \qquad \textit{Equation 5.3}$$

Where, C_t=GCV concentration at time *t, D*=dose implanted, *V*=volume of distribution, *K*=GCV release rate constant (zero-order input), K_{01}=rate at which GCV enters the vitreous compartment from the DSMT device and K_{10}=rate at which GCV leaves the vitreous compartment (first-order elimination).

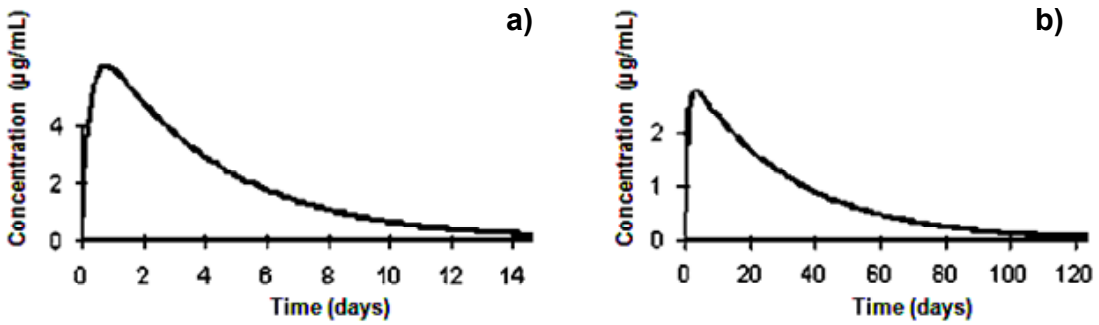

Figure 5.2: Schematics of WinNonlin® compiled non-compartmental pK models of a) VH concentration of GCV via extravascular administration (pK model C) and b) VH concentration of GCV via constant release from the implanted DSMT device (pK model D).

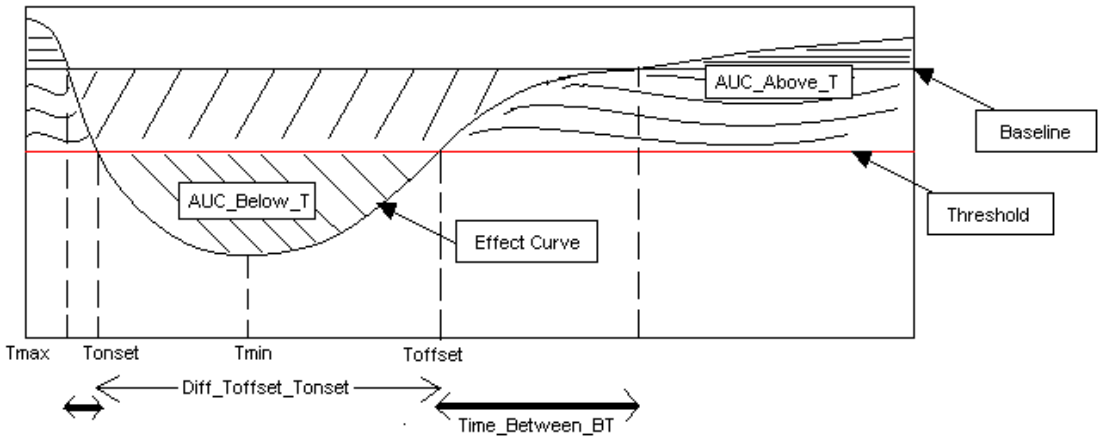

Figure 5.3: Schematic of WinNonlin® compiled pharmacodynamic model for drug effect data estimation.

5.2.4.2. Selection of a suitable algorithm for pK modeling

WinNonLin® software was also used to establish a "best fit" pK model to the *in vivo* release data via estimation of the variance-inflation factors for the pK parameters with the "goodness of fit" as a pertinent statistical criterion for accurate pK parameter estimates. WinNonLin® provided the "least squares" estimates of the various parameters for the pK models employing a linear approximated Levenberg and Hartley modified Gauss-Newton regression algorithm for rapidly minimizing the sum of squared residuals to achieve convergence (Hartley, 1961; Davies and Whitting, 1972; Beck and Arnold 1977). The Levenberg-Hartley (Gauss-Newton) regression algorithm is known to perform well on a wide class of pK modeling processes including ill-conditioned data sets whereby certain pK parameters are absent such as in this case. Although the Gauss-Newton algorithm conventionally requires the estimated variance-covariance matrix of the parameters, the Levenberg-Hartley modification suppresses the magnitude of the change in parameter values between iterations, thus enabling the algorithm to perform well on ill-conditioned data sets. Convergence criteria of 0.0001 were used during the minimization process and a maximum of 50 iterations were allowed. Convergence was achieved with a relative change in the weighted sum of squares (<0.0001).

5.2.4.3. Determination of parameter bounds for pK model estimation

Desirable bounds were set on the admissible pK parameter space resulting in "constrained estimation". This was undertaken in order to achieve the flexibility in obtaining pK parameter estimates that were realistic for models that comprised non-negative parameters for instances where the data set produced a negative actual least squares estimate due to error (also known as unconstrained estimation). Boundary limits on the parameter space prevented the algorithm from deviating. With the Levenberg-Hartley modified Gauss-Newton regression algorithm in WinNonLin®, two successive transformations were used to affect bounding of the pK parameter space. The first transformation was from the bounded space as defined by the input limits to the unit hypercube and the second transformation used the inverse of the normal probability function to delineate an infinite pK parameter space resulting in a transformation of the parameter space (reparameterization) that made the pK modeling process more tractable (Draper and Smith, 1981; Ratkowsky, 1983). Table 5.1 outlines the lower and upper bounds set for the compartmental and non-compartmental pK modeling process.

Table 5.1: Parameter bounds used for constrained and non-constrained pK model estimation.

Parameter	Value	Lower	Upper
Dose time (day)	0	-	-
Bolus dose implanted (µg)	5000	-	-
Length of implantation (day)	72	-	-
Compartmental pK modeling			
Model A			
[a]V (mL)	0.3960	0	0.500
[b]K_{01} (day^{-1})	0.0010	0	0.010
[c]K_{10} (day^{-1})	0.5000	0.1	1.000
Model B			
[d]VF (mL)	0.3960	0	0.800
[e]K (day^{-1})	0.0008	0	1.000
Non-compartmental pK modeling			
Therapeutic window (µg/mL)	-	0.1	2.75
Time bounds (days)	-	0	72
Lamda z	-	28	72

[a]*Volume of distribution of the vitreous compartment*
[b]*The rate at which GCV enters the vitreous compartment from the DSMT device*
[c]*The rate at which GCV leaves the vitreous compartment*
[d]*Volume of distribution based on the terminal phase, where F is the fraction of GCV absorbed*
[e]*Zero-order input or GCV release rate constant from the DSMT device*

5.2.4.4. Establishment of pertinent pK parameters

The apparent rate constants of the terminal-phase elimination rate (via linear regression of the logarithms of the VH concentration-time profiles) (k) and the apparent volume of distribution (V_d) were fitted. Individual estimates of these parameters were obtained and the fits were evaluated by inspection of the residuals. The maximal VH concentration (C_{max}) and time of C_{max} (T_{max}) were calculated from the fitted curves. The clearance (Cl) and the area under the VH concentration-time curve ($AUCt_{0-\infty}$) was calculated by the trapezoidal rule and extrapolated to infinity using standard pK algorithms from the fitted curves. Complete absorption of GCV from the site of DSMT device implantation was assumed. *In vivo* VH drug release profiles of the GCV-loaded DSMT devices were also established by deconvolution through convolution (Dutta et al., 2004).

5.2.5. Pharmacokinetic analysis for *in vitro-in vivo* correlation (IVIVC) establishment

A predictive mathematical model for description of the relationship between an *in vitro* property of the DSMT and a relevant *in vivo* response was developed. WinNonLin® software (V5.2.1 with IVIVC Toolkit Build 2008033011, Pharsight Software, Statistical Consultants Inc., Apex, NC, USA) was used as a tool

for pK computations and estimation of all pertinent pK parameters for the development of a Level A time-scaled *in vitro-in vivo* correlation (IVIVC) (US FDA, 1997). Input data comprised *in vitro* GCV release data obtained from the Resomer® RG504 DSMT devices as well as pK data obtained from the described *in vivo* experiment on the six New Zealand White Albino rabbits whereby VH samples were obtained and analyzed via UPLC.

5.2.5.1. Deconvolution through convolution analysis

Convolution is the prediction of *in vivo* drug concentrations using a mathematical model based on the convolution integral (Levin, 2006). Deconvolution is the estimation of the time course of drug input (in this case the *in vivo* release of GCV) using a mathematical model based on the convolution integral (Levin, 2006). Majority of deconvolution methods used in pK data analysis is to estimate the rate of drug bioavailability in a numerical form. However, analytical deconvolution methods are usually restricted to simple pK models that do not contain shunts and/or time delays, and thus can be approximated by multi-exponential models. Thus the pK conditions described in our *in vivo* study conforms to the requirements of deconvolution through convolution (DTC) as the GCV release from the DSMT device into the VH may be described by simple non-compartmental and/or one-compartmental pK models due to the enclosed environment of the posterior segment of the eye facilitated by the highly restrictive blood-ocular barriers. Therefore this enabled us to determine the numerical and/or the analytical form of the system weighting function approaching the GCV bioavailability rate even under conditions when the deconvolution methods may not be superiorly functional. Furthermore, this approach required neither a special functional form of the weighting function nor equal time intervals of the measurement of the drug concentration profiles, and no preliminary smoothing and/or interpolation of the profiles were necessary. The approach was based on linear system analysis, with linearity defined in the general sense of the linear superposition principle. The concentration, C(t), of GCV within the VH after release from the DSMT device may be represented by Equation 5.4.

$$C(t) = \int_0^t f(\tau) \times g(t-\tau) d\tau \equiv f(t) * g(t) \qquad \textit{Equation 5.4}$$

Where t represents time and (t-τ) represents the time since the quantity of GCV described by f(τ) was introduced into the VH over a interval of time Δτ. f(t) is the function that, when integrated between the limits of t=0 and t, yields the cumulative quantity of GCV released to the impulse input point which is the vitreous cavity and '*' denotes the convolution operation.

Equation 5.5 is the convolution equation that formed the basis for the evaluation of the GCV input rate f(t). The function g(t) was the unit impulse response (disposition function) and was equal to the probability that a molecule that entered the impulse input point (vitreous cavity) at t=0 was present in the VH at time t divided by the volume of the VH. The process of determining the input function f(t) was termed deconvolution as it is required to deconvolve the convolution integral to extract the input function that was embedded in the convolution integral. The unit impulse response function g(t) provided the precise linkage between the GCV-level response C(t) and the input rate function f(t). The principle of DTC was employed via WinNonLin® pK software to determine the input function. The DTC method was an iterative procedure that comprised three steps. First, the input function was adjusted by altering the parameter values. Second, the new input function was convolved with g(t) to produce a calculated GCV-level response and finally the agreement between the observed data and the computed GCV-level data was quantitatively evaluated according to an objective function. The three steps were repeated until the objective function was optimized. Specifically for this data set, a one-compartment model was fit to the observed vitreous GCV concentration-time data to obtain the parameters of the disposition function as shown in Equation 5.5.

$$C(t) = \frac{C_0\left(e^{\lambda \bullet min(\tau,t)} - 1\right)}{\tau \bullet \lambda} \bullet e^{-\lambda t} \qquad \textit{Equation 5.5}$$

Where C_0=the dosing intercept of GCV loaded in the DSMT and λ=the elimination rate constant for a one-compartment pK model (representing the vitreous cavity), and τ=duration of GCV release from the DSMT device.

The observed GCV vitreous concentration-time data were deconvolved using the disposition parameters (λ and C_0) to obtain the input or GCV release rate versus time profile (Equation 5.6). The fractional input versus time profile was used to determine the duration of GCV release.

Observed *in vitro* profile		WinNonLin® estimated disposition function		Inferred input profile
in vitro GCV release profile conc. vs. time^{*-1}		*in vivo GCV release profile conc. vs. time*	=	*GCV release rate profile*

Where $^{*-1}$ *is the deconvolution operator* *Equation 5.6*

5.2.6. Establishment of an *in vitro-in vivo* correlation

The inclusion of *in vitro* dissolution tests in the USP 32 supported the proposition that there is a significant relationship between *in vitro* dissolution and *in vivo* bioavailability. Release rate data, when considered along with data on the drug's solubility, partition coefficient and dissolution constant, can provide an indication of the drug's release potential following administration (Ansel and Popovich, 1990). Dissolution data has been used for predicting *in vivo* performances of drugs (Hanson, 1982), for elucidation of the mechanism of drug release from a drug delivery system and also as a warning for poor drug bioavailability from drug delivery systems that display erratic release patterns in comparative studies (Levy, 1965; Wood, 1966; Gibaldi and Weintraub, 1970; Bergan et al., 1973; Prasad et al., 1983.; Shah et al., 1983). Therefore, it is important that research includes efforts to develop *in vitro* tests that will be valid predictors of relative bioavailability under *in vivo* conditions.

Drug release experiments of the GCV-loaded DSMT device was performed with a modified USP dissolution apparatus at 37±0.5°C using 4mL of simulated vitreous humor (SVH) in each vessel at an agitation rate of 20rpm (Choonara et el., 2006). Samples were removed at predetermined time intervals and analyzed by HPLC. Experiments were run in triplicate and results expressed as a mean % (±SD) dissolved at a given sampling time. The *in vitro* drug release studies were set-up to simulate release of GCV from the DSMT device into the posterior segment of the rabbit eye model. The GCV release data obtained from the *in vivo* study was used to estimate the cumulative GCV release by an adapted Wagner-Nelson method (Axelrod and Reichenthal, 1953; Wagner and Nelson, 1964; Newton et al., 1981; Bonati et al., 1982; Blanchard and Sawers, 1983). VH concentrations of GCV were used to determine the various pK parameters. The fraction of GCV released *in vivo* was calculated by the mean (N=6) VH concentration-time profile and the fraction of GCV released *in vivo* was profiled against the fraction released *in vitro* at corresponding time intervals. The slope, intercept, and correlation coefficient describing the relationship were determined by linear regression and a Levy

plot. It is important to point out that such a correlation is only valid if the given drug is uniformly absorbed (Axelrod and Reichenthal, 1953; Rall, 1980; Newton et al., 1981). In this case the GCV did not require any absorption as drug was immediately available at the enclosed site of action i.e. the vitreous cavity. Thus, the model drug GCV used in the study meets this requirement without any restrictions.

5.3. Results and Discussion

5.3.1. Vitreous humor sampling and drug content analysis

As described in Chapter 4, Section 4.3.5 of this thesis, the UPLC chromatograms of the VH samples retrieved from the rabbits revealed that GCV was successfully eluted with the presence of two distinct chromatographic peaks representing GCV at approximately 1.00 minute and the internal standard ACV at 1.35 minutes after injection. Validation of the assay method indicated that intra-day and inter-day precision and accuracy as well as the recoveries, and relative standard deviation values (%RSD) were satisfactory.

5.3.2. Interpretation of the compartmental pK model analysis

During analysis it was found that 1000 iterations were sufficient to converge release data to a minimum mean square error with a convergence criteria setting of 0.0001. The pK models were further analyzed by the strong parametrical support from statistical descriptors such as the Condition Number (CN) as a measure of the pK model validity (numerical stability) of the fit. The CN is computed as the square root of the ratio of the largest to the smallest eigenvalue of the matrix of partial derivatives of the pK model with respect to the model parameters. For this particular dataset the CN values were 0.100×10^{8} and 0.209×10^{8} for the compartmental pK models A and B, respectively (Table 5.2). Smaller CN values are ‘superior’ to larger values. Figure 5.4 displays the observed and fitted VH concentration-time profiles for the two compartmental models analyzed.

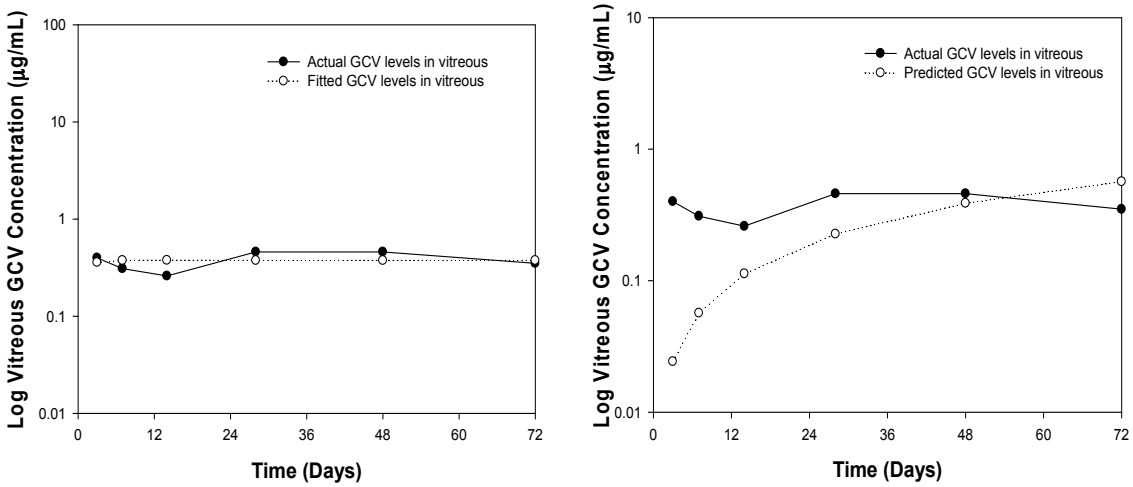

Figure 5.4: VH concentration-time profiles of GCV released from the DSMT device depicting the observed and fitted relationships for a) compartmental pK model A and b) compartmental pK model B (N=6; SD<0.19 in all cases).

In order to assess the accuracy of the pK model fitted and weighting scheme residuals were analyzed. A functional approach for examining the residuals was undertaken by the generation of scatter plots in order to determine whether the residuals tended to be randomly scattered within a lower and upper horizontal band. If the residuals were not randomly scattered, this suggested that either the model or weighting scheme was unsatisfactory (Figure 5.5). The residuals for pK model B had a poor fit of the model to the data (Figure 5.5b). PK model A showed a random scatter in the residuals (Figure 5.5a). In addition, the frequency of altering ± signs (also known as 'iterations' in the residuals) was largest for pK model A than pK model B (there were 17 and 13 iterations, respectively).The absolute magnitude of the residuals, or the amplitude, was also smaller for pK model A. This therefore suggested that pK model A mimicked the *in vivo* data better than pK model B.

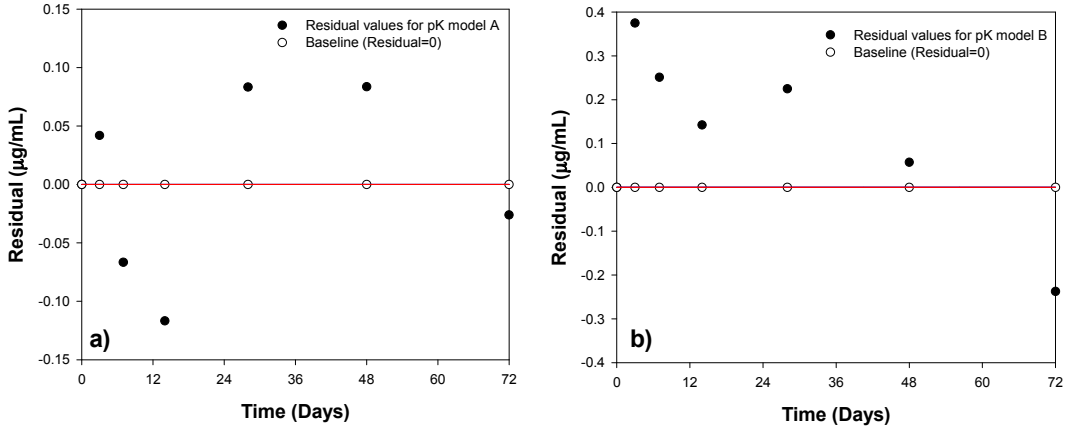

Figure 5.5: Relative residual plots obtained for GCV concentration-time data fitting employing a) compartmental pK model A and b) compartmental pK model B.

Tables 5.2 and 5.3 provide a summary of the pK parameters and goodness-of-fit criteria for each pK model analyzed. PK model A had a lower AIC value than pK model B. Thus, pK model A displayed the most superior fit based upon its lower CN value and uniformly higher parameter precision relative to pK model B (Table 5.2). A uniform weighting scheme for this study performed superiorly due to the relatively small range of the VH concentration data. The pK modeling approach required fewer assumptions and was automated.

Table 5.2: Diagnostic criteria used to assess pK model "goodness of fit" (N=6).

Statistical Descriptor	pK Model A	pK Model B
Corrected Sum of Squared Observations	0.153	0.153
Sum of Squared Residuals	0.344×10^{-1}	0.333×10^{-1}
Correlation (observed vs. fitted)	0.879	0.481
Akaike Information Criterion (AIC)	-17.578	-3.690
Swartz Bayesian Criterion (SBC)	17.741	-3.799
Condition Number (CN)	0.100×10^{8}	0.209×10^{8}

Figure 5.6 shows the convergence profiles obtained for fitting each of the compartmental pK models A and B. In both instances data was converged to a minimum sum of squares that approached zero. PK model A converged earlier than pK model B further signifying the superior fit of the *in vivo* data to the model.

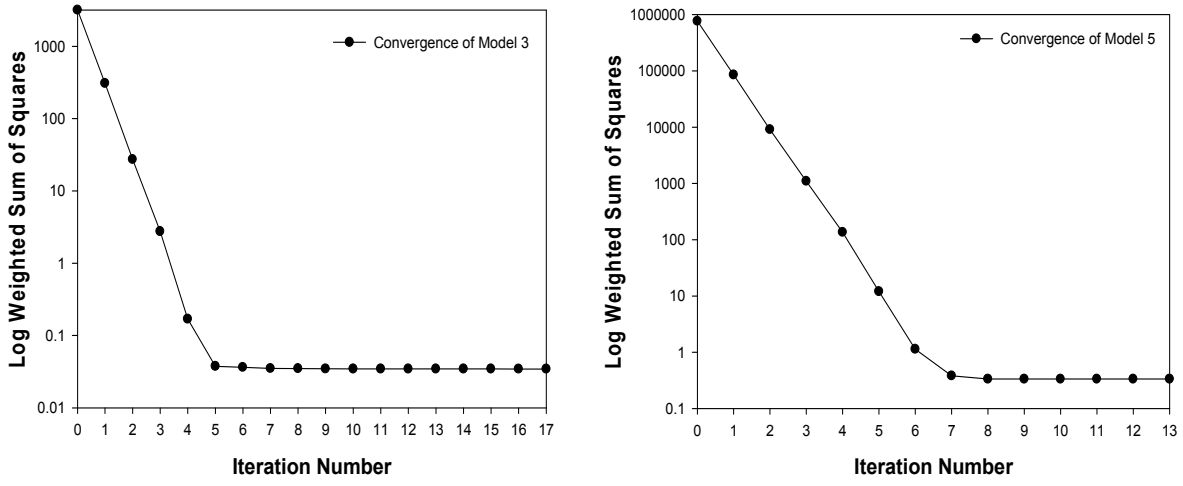

Figure 5.6: Convergence profiles obtained for fitting a) compartmental pK model A and b) compartmental pK model B.

Table 5.3: Summary of estimated secondary parameters for the pK models analyzed (N=6).

Parameter	Estimate	Standard Error	CV%
Compartmental pK model A			
AUC (day.µg/mL)	12.36	1.750	1.418
$K_{01\ HL}$ (day)	22.72	3.220	1.480
$K_{10\ HL}$ (day)	0.694	0.130	1.844
Cl_F (mL/day)	0.405	0.570	1.419
T_{max} (day)	10.41	1.350	1.293
C_{max} (µg/mL)	0.377	0.053	1.418
Compartmental pK model B			
AUC (day.µg/mL)	8.73×10^{9}	3.39×10^{14}	38.80
K_{HL} (day)	7.07×10^{5}	1.37×10^{10}	19.40
Cl_F (mL/day)	1.00×10^{-6}	2.22×10^{-2}	38.90
T_{max} (day)	1.02×10^{6}	1.98×10^{10}	19.50
C_{max} (µg/mL)	3.15×10^{3}	6.12×10^{7}	19.40

5.3.3. Interpretation of the non-compartmental pK model analysis

Results of the non-compartmental pK model analysis are shown in Figure 5.7 and a summary of the estimated pK parameters are listed in Table 5.4 for pK models C and D. As expected the T_{max}, C_{max}, AUC_{all} and AUMC were identical for both non-compartmental pK models. Both models revealed that after 28 days the GCV concentrations reach was 0.46µg/mL and was maintained up to 72 days as noted by the linear AUC-time profile (Figure 5.9). PK model C revealed a 3-point (28-72 days) terminal slope (lambda z) (λ_z) of $0.0066day^{-1}$ and an intercept of -5462 by means of log-linear regression (R^2=0.77) (Figure 5.7). The low λ_z and the relatively high MRT suggested that the VH acted as a drug reservoir. For extravascular pK model C the fraction of GCV absorbed/released could not be estimated. Therefore volume and clearance for the model were actually volume/F or clearance/F where F was the fraction of GCV absorbed/released. Analysis employing pK model D revealed that the λ_z could not be estimated as no parameters could be extrapolated to infinity. The $AUC_{0\text{-}72}$ computed by the linear trapezoidal rule with linear interpolation was 27.165day.µg/mL. The Linear Trapezoidal rule with Linear Interpolation (to find *C** at *t*)* was used as the preferred computational approach for both non-compartmental pK models. Uniform weightings were used for λ_z calculations with the "best fit" method employing log regression used for both models. The lower and upper therapeutic window was 0.10µg/mL and 2.75µg/mL respectively. The λ_z was determined for pK model C and not for pK model D. The MRT parameters were adjusted for the duration of implantation of the DSMT device.

Table 5.4: Final parameter estimates generated from fitting the non-compartmental pK models.

Parameter	Units	Estimated Values	
		pK Model C	pK Model D
R^2	-	0.7734	-
No. points lambda z	-	3	0
Lambda z	day^{-1}	0.0066	-
Lambda z low	day	28	-
Lambda z upper	day	72	-
HL Lambda z	day	104.9384	-
T_{max}	day	28.0000	28.0000
C_{max}	µg/mL	0.46000	0.46000
C_{max} D	µg/mL/µg	0.0001	0.00010
T_{last}	days	72.000	72.0000
C_{last}	µg/mL	0.35000	0.35000
AUC_{last}	day.µg/mL	27.1650	27.1650
AUC_{all}	day.µg/mL	27.1650	27.1650
$AUC_{INF\ obs}$	day.µg/mL	80.1529	-
$AUC_{INF\ D\ obs}$	day.µ/mL/µg	0.0160	-
$AUC_{\%Extrap\ obs}$	%	66.1085	-
Vz_{obs}	mL	9444.0772	-
Cl_{obs}	mL/day	62.3807	-
$AUC_{INF\ pred}$	day.µg/mL	82.3862	-
$AUC_{INF\ D\ pred}$	day.µg/mL/µg	0.0165	-
$AUC_{\%Extrap\ pred}$	%	67.0273	-
Vz_{pred}	mL	9188.0723	-
Cl_{pred}	mL/day	60.6898	-
$AUMC_{last}$	day.day.µg/mL	1006.50	1006.50
$AUMC_{INF\ obs}$	day.day.µg/mL	12737.7119	-
$AUMC_{\%Extrap\ obs}$	%	92.0983	-
$AUMC_{INF\ pred}$	day.day.µg/mL	13232.1472	-
$AUMC_{\%Extrap\ pred}$	%	92.3936	-
MRT_{last}	day	37.0512	2.05120
$MRT_{INF\ obs}$	day	158.9176	-
$MRT_{INF\ pred}$	day	160.6112	-
$Time_{Low}$	day	0.7500	0.75000
$Time_{Dur}$	day	69.250	69.2500
$Time_{Hgh}$	day	0.0000	0.00000
$Time_{InfDur}$	day	265.1609	-
$Time_{InfHgh}$	day	0.00000	0.00000
AUC_{Low}	day.µg/mL	6.96250	6.96250
AUC_{Dur}	day.µg/mL	20.2025	20.2025
AUC_{InfDur}	day.µg/mL	39.7072	-

T_{max}: Time of maximum observed concentration
C_{max}: Maximum observed concentration occurring at T_{max}
T_{last}: Time of last measurable (positive) concentration
C_{last}: Concentration corresponding to T_{last}
AUC_{last}: AUC from the dosing time to the last measurable concentration
AUC_{all}: AUC from the dosing time to the time of the last observation. Here AUC_{last}=AUC_{all}
$AUMC_{last}$: AUMC from the dosing time to the last measurable concentration
MRT_{last}: MRT from the dosing time to the time of the last measurable concentration
RSq: Goodness of fit statistic for the terminal elimination phase
Lambda z: 1st order rate constant of the terminal (log-linear) portion of the curve
Lambda z_{low}: Lower limit on time for values to be included in the calculation of λz
Lambda z_{upper}: Upper limit on time for values to be included in the calculation of λz
HL Lambda z: Terminal half-life
$AUC_{INF\ obs}$: AUC from dosing time extrapolated to infinity based on the last observed concentration
$AUC_{INF\ D\ obs}$: $AUC_{INF\ obs}$ divided by the dose
$AUC_{\%Extrap\ obs}$: % $AUC_{INF\ obs}$ due to extrapolation from T_{last} to infinity
Vz_{obs}: Volume of distribution based on the terminal phase
Cl_{obs}: Total Cl for extravascular administration = Dose/$AUC_{INF\ obs}$
$AUC_{INF\ pred}$: AUC from dosing time extrapolated to infinity based on the last predicted concentration
$AUC_{\%Extrap\ pred}$: % $AUC_{INF\ pred}$ due to extrapolation from T_{last} to infinity
Cl_{pred}: Total Cl for extravascular administration = Dose/$AUC_{INF\ pred}$
$AUMC_{INF\ obs}$: AUMC extrapolated to infinity based on the last observed concentration
$AUMC_{\%Extrap\ obs}$: Percent of $AUMC_{INF\ obs}$ that is extrapolated
$AUMC_{INF\ pred}$: AUMC extrapolated to infinity based on the last predicted concentration
$AUMC_{\%Extrap\ pred}$: Percent of $AUMC_{INF\ pred}$ that is extrapolated
$MRT_{INF\ obs}$: MRT extrapolated to infinity
$MRT_{INF\ pred}$: MRT extrapolated to infinity

The fitted VH concentration-time profiles of GCV release from the DSMT device and the pK model C-fitted λ_z are shown in Figure 5.7. Release of GCV into the vitreous cavity from the DSMT device was controlled with an initial "burst" followed by an uptake with a fitted λ_z of approximately 44 days (range 28-72 days).

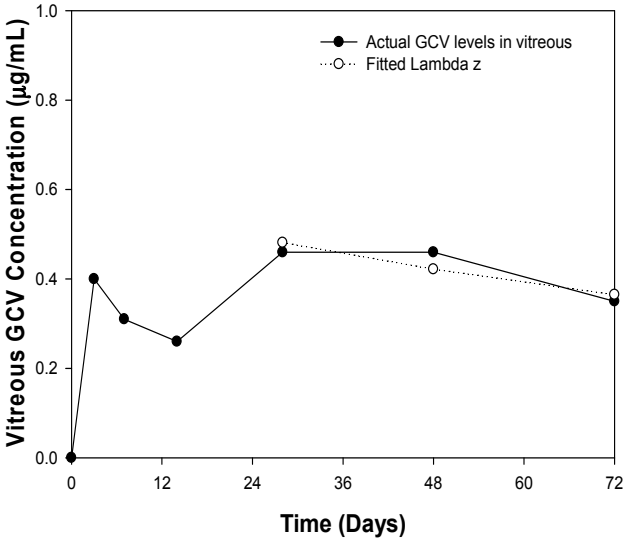

Figure 5.7: The non-compartmental pK model C fitted AUC and terminal $t_{1/2}$ of GCV after implantation of the DSMT device in the rabbit vitreous compartment (N=6; SD<0.16 in all cases).

Results from the pharmacodynamic (pD) model fitting in order to determine the GCV effects are shown in Table 5.5. The pD model utilized fitted the *in vivo* GCV release data relatively well with an R^2=0.82. The input baseline and threshold values represented the ED_{50} of GCV for the treatment of human CMV-R that ranged between 0.1-2.75µg/mL. The AUC below and above the baseline and threshold values were computed. The DSMT device was able to efficiently modulate the release of GCV into the VH with the concentration of GCV remaining below the baseline throughout the 72 days of this study. In addition GCV levels were maintained above the threshold for a period of 71.24 days. This was ideal as there was no evidence of dose dumping or unfounded spikes in GCV release that may contribute to side-effects due to GCV concentrations increasing beyond the baseline. Instances of GCV concentrations below the threshold value only occurred for a duration of 0.76 days.

Table 5.5: Parameter estimates from fitting the pharmacodynamic model for drug effect data.

Parameter	Units	Estimated Value
R^2	-	0.82
T_{min}	day	0.00
T_{max}	day	28.00
Baseline	µg/mL	2.75
$AUC_{>baseline}$	day.µg/mL	0.00
$AUC_{<baseline}$	day.µg/mL	169.92
$Time_{>baseline}$	day	0.00
$Time_{<baseline}$	day	72.00
$Time_{\%<baseline}$	%	100.00
Threshold	µg/mL	100.00
$AUC_{>threshold}$	day.µg/mL	0.021
$AUC_{<threshold}$	day.µg/mL	0.038
$Time_{>threshold}$	day	71.24
$Time_{<threshold}$	day	0.76
$Time_{\%<threshold}$	%	1.05
T_{onset}	day	0.00
T_{offset}	day	0.76
$Time_{between\ BT}$	day	71.24

5.3.4. *In vivo* release of ganciclovir in the rabbit eye model from the DSMT device

The cumulative release of GCV from the DSMT device at a constant GCV loading of $5\%^{w}/_{w}$ is shown in Figure 4.15. The cumulative drug release profile was obtained by measuring the percentage of GCV released versus the initial content loaded in the DSMT device (Figure 4.15). The data is consistent with a reduced biphasic profile as noted from the *in vitro* study by Choonara and co-workers (2006; 2007), that was primarily due to the rapid release of GCV deposited on the surface of the rigid matrix (Figure 4.15a). However for the current *in vivo* study the DSMT device was initially equilibrated in sterile saline prior to implantation. This additional procedure may have resulted in removal of the patent deposition of GCV molecules on the surface of the device. Thus the release of GCV from the device was constant and controlled by the degradation rate of the polymer. The release rate increased with the decrease of the molecular mass of PLGA. This rate was probably due to the difference in the degradation rate of the polymer grades Resomer® RG503 and Resomer® RG504. Degradation of PLGA could be influenced by the composition of the lactide and glycolide content with the higher the glycolide content, the faster the degradation rate (Baker et al., 1974). The DSMT device provided sustained release of GCV in the VH cavity over a period of 72 days as shown in Chapter 4, Section 4.3.6 of this thesis (Figure 4.16). Devices formulated with Resomer® grade RG503 displayed a higher quantity of GCV release within the ED_{50} range for the treatment of human CMV-R as compared to DSMT devices formulated with Resomer® grade RG504 (Figure 4.16).

5.3.5. Deconvolution and relative bioavailability analysis

Deconvolution of observed vitreous GCV concentration-time data against the *in vitro* release profile provided the cumulative *in vivo* release-time profile (Figure 5.8). The individual cumulative release-time profile did not reveal any evidence of dose dumping. The mean cumulative release-time profile presented in Figure 5.8 showed that GCV relative bioavailability was ~70%, and the mean release duration was 72 days. In conjunction with the mean input AUC-time profile (Figure 5.9), this indicated that GCV was released in a zero-order manner. However, the rate of release was marginally high during the initial 3 days after implantation of the DSMT device and tailed off at a zero-order release rate after an average of 10 days, with 70% of the total GCV released after 72 days. The observed release rate-time profile was not unexpected for a zero-order prolonged release device implanted in the vitreous cavity where the extent and rate of release predictably occurs in the VH and a lower extent and slower rate of absorption occurs through surrounding ocular tissues. The duration of GCV release from the DSMT device was 72 days, and the zero-order release rate was 2.02±0.01µg/h for a 5mg GCV-loaded DSMT device. It should be recognized that the 2.02±0.01µg/h release rate represents an approximation of the zero-order rate for the entire duration of release (72 days) (i.e., the rate is faster in the initial few hours after implantation and decreases after 7-10 days).

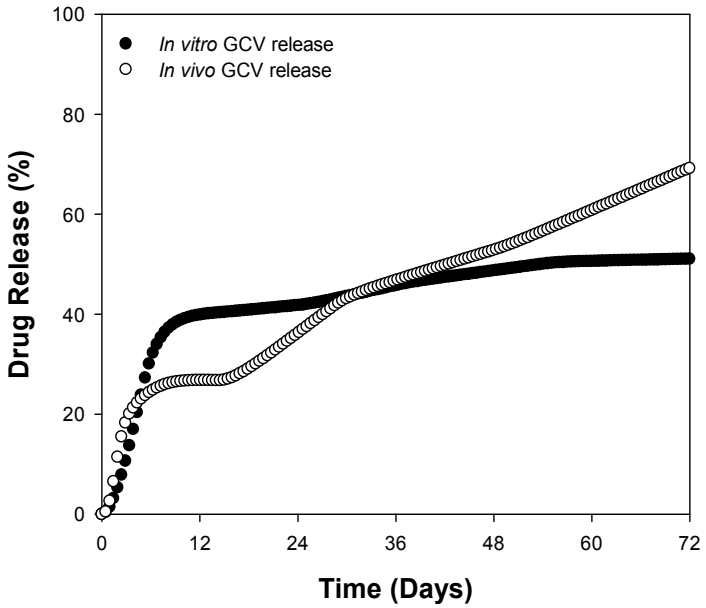

Figure 5.8: Drug release profiles of the *in vitro* GCV release and the observed mean cumulative *in vivo* release profile extracted using deconvolution analysis for single-dose GCV released from the DSMT device.

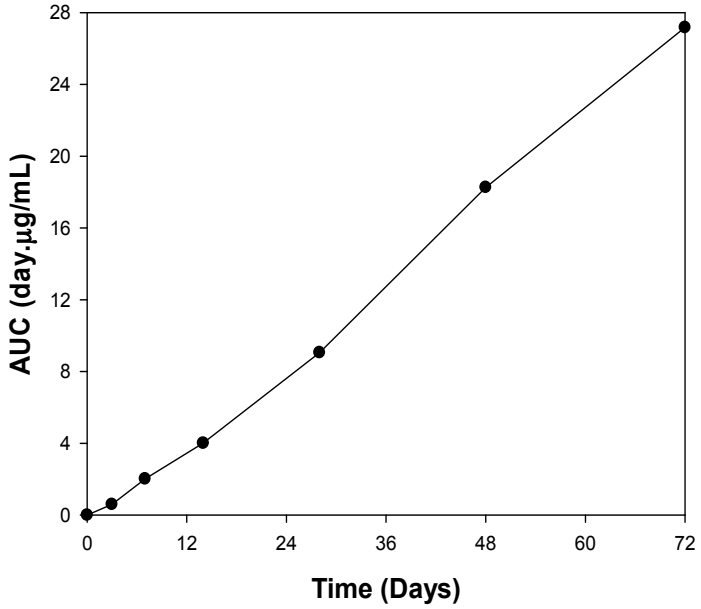

Figure 5.9: Profile showing the cumulative linear increase in GCV concentration over a period of 72 days computed from the AUC of the mean *in vivo* VH concentration-time profile (R^2=0.99).

5.3.6. *In vitro-in vivo* correlation (IVIVC)

The intravitreal transit time for the DSMT device was annulled (t=0 hours) as the device was implanted directly at the site of action. Following evaluation of the pK parameters, the *in vivo* drug release from the DSMT device was calculated employing a Wagner-Nelson method (Figure 5.8). In accordance with the *in vitro* profiles, the DSMT released GCV immediately without any lag-time. *In vitro* GCV release was relatively fast. By comparison, GCV release was more controlled over a longer time period when the DSMT was implanted *in vivo*. To better compare the *in vitro* profiles with those representing the *in vivo* release at corresponding time points and to elucidate the predictive power of the *in vitro* study, *in vivo* GCV release calculated from the mean VH concentration-time profile was described using a Levy plot (Levy et al., 1965). The Levy plot shown in Figure 5.10 demonstrated that the *in vitro* drug release study performed was useful in terms of predicting the *in vivo* GCV release from the DSMT device with a 90% accuracy (R^2=0.90; slope=<1). This can be attributed to the diffusion and bio-distribution of GCV within the vitreous cavity once released from the DSMT device which could not be fully simulated under *in vitro* conditions. Previous authors working on the development of IVIVC's have also observed that, in general, *in vitro* results tend to run ahead of *in vivo* data (Brockmeier and Hattingberg, 1982; Brockmeier et al., 1985).

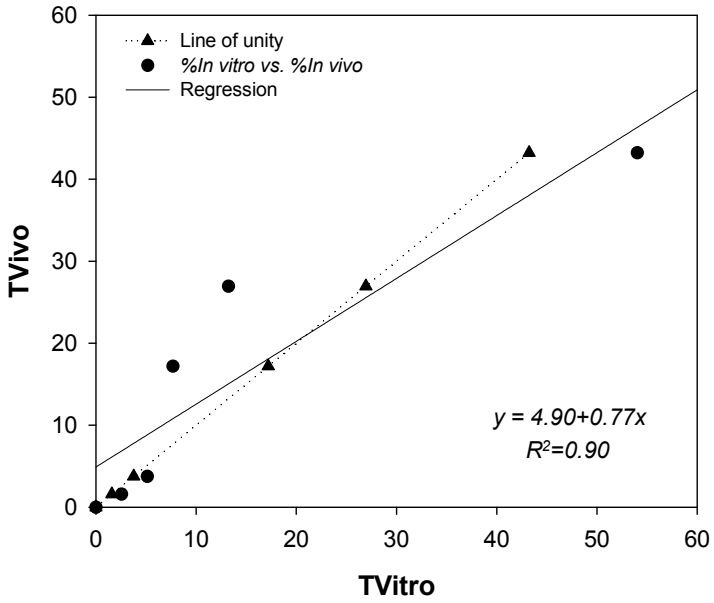

Figure 5.10: Levy plot showing the relationship between the fraction of GCV released *in vivo* and the fraction released *in vitro* (R^2=0.90; slope<1) over corresponding time periods.

A Level A correlation was obtained as a point-to-point relationship was established between the *in vitro* dissolution and the *in vivo* input rate (i.e. *in vivo* dissolution).

5.4. Concluding Remarks

The GCV relative bioavailability was approximately 70%. GCV exhibited superior prolonged release characteristics without any dose dumping. On average 2.02±0.01µg/h of GCV was released into the vitreous cavity from every 5mg GCV-loaded DSMT device over 72 days. Results from this study indicated that the method adopted for the *in vitro* drug release study was sufficiently powerful, convenient and discriminating for predicting GCV release behavior from the DSMT device with a relatively desirable IVIVC obtained in keeping with the complexities of the study conditions. A Levy plot demonstrated that the *in vitro* drug release study performed was useful in terms of predicting the *in vivo* GCV release from the DSMT device with a time-scaled Level A IVIVC correlation obtained (R^2=0.90). The selected pK models are yet to be challenged by testing the pK model on a new set of experimental data for model validation.

CHAPTER 6

CONCLUSIONS, RECOMMENDATIONS AND FUTURE OUTLOOK

6.1. Conclusions

The DSMT device developed throughout this research has proved to be an effective and versatile biodegradable intraocular drug delivery system that provides rate-modulated release of the antiviral model drug GCV to the posterior segment of the eye for the treatment of CMV-R. This has been established from the *in vivo* animal studies undertaken in the New Zealand White Albino rabbit eye model. In keeping with the aims and objectives of this research the following conclusions were achieved:

The effects of irradiation sterilization on the stability of the DSMT device revealed that the affected transitions favored the DSMT to be employed as an implantable intraocular device. PLGA can be regarded as suitably stable under compression and γ-sterilization for manufacture of the DSMT device. In addition, this research has shown that as characterization techniques for biomaterials progress, it is essential to rigorously consider the confounding improbabilities of the data acquired by undertaking detailed chemometric and molecular modeling approaches in order to draw comprehensive conclusions on the inherent behavior of the system at a micro-level.

A blueprint surgical procedure for implantation of the DSMT device in the New Zealand White Albino rabbit eye model has been successfully developed. In this research we have demonstrated that the biodegradable DSMT device may provide a significant innovation to the current cache of intravitreal drug delivery technologies for the treatment of posterior segment eye diseases. The DSMT device was relatively easy to implant within ±30 minutes and was well tolerated in the rabbit eye model without any adverse effects or toxicity over the entire duration reaching 72 days in this study.

A stable and sensitive UPLC assay method utilizing 3D chromatography for quantification of GCV from VH samples was optimized. GCV release in the VH of the rabbits from the DSMT device was maintained within the ED_{50} range for the treatment of human CMV-R. Our research has shown that constant drug release can be obtained with the DSMT device due to the unique geometry of the device.

The DSMT device is sufficiently flexible and may be used for the effective long-term intravitreal delivery of drugs for the treatment of various posterior segment eye diseases.

The safety, biocompatibility or potential toxicity of the DSMT device was assessed via histopathological examination, direct and indirect ophthalmoscopy, intraocular pressure measurements and clinical observation. These studies revealed that the DSMT device was non-toxic to intraocular tissue structures. Pharmacokinetic modeling revealed that the relative bioavailability of GCV in the VH was at least 70% and the device released GCV in a prolonged manner without any dose dumping. On average, approximately 2.02±0.01µg/h of GCV was released into the VH from a 5mg GCV-loaded DSMT device over 72 days.

Results from this study indicated that the method adopted for the *in vitro* drug release study was sufficiently powerful, convenient and discriminating for predicting the GCV release behavior from the DSMT device with a relatively desirable IVIVC obtained in keeping with the complexities of the study conditions. A Levy plot demonstrated that the *in vitro* drug release study previously performed was useful in terms of predicting the *in vivo* GCV release from the DSMT device with a 90% accuracy described by a Level A IVIVC correlation obtained.

6.2. Recommendations

Several implantable intravitreal drug delivery devices have been developed and many more are currently under design. However, none of the marketed products have yet proved to be an all encompassing device that is relatively safe and uncomplicated for patient use, allows for simple implantation procedures to secure the device in the posterior segment of the eye by ophthalmic surgeons, is fully biodegradable and provides zero-order drug release in the vitreal cavity over a period of several months to even years. In order to design an effective intravitreal drug delivery device, the challenges lining the pathway to success must be considered as discussed in this thesis. Firstly, local drug delivery intended for a single eye should not treat the contra-lateral eye. In addition, for certain diseases not limited to the eye, local drug delivery fails to treat the manifestations of extra-ocular disease. Cases in point are infectious diseases such as CMV or ocular inflammatory diseases with

systemic involvement, such as Behçet's disease, Vogt-Kayanagi-Harada disease, and sarcoidosis. Higher intravitreal concentrations of drug attained with intravitreal devices may offer a greater therapeutic effect, but may also be associated with increased ocular toxicity. Drugs that demonstrate safety in the eye over short durations may be toxic upon extended intraocular exposure. Furthermore, the surgical complications of device implantation have been considered, namely, vitreous hemorrhage, retinal detachment, and endophthalmitis. These complications have occurred rather often, especially when surgical penetration of the vitreous cavity is required for device implantation.

Future research should thus focus on the development of devices that are geometrically smaller and do not require full-thickness penetration of the vitreous cavity but rather rely on drug diffusion across the sclera. It is envisaged that the use of nanotechnology would provided this much needed alternative. Device applicability should also be established in the early stages of design. Investigators should identify what a ‘sufficient dose for a reasonable duration’ is for the targeted disease, where ‘sufficient dose’ is the steady-state concentration of drug needed to produce the desired effect in the animal model and, ultimately in humans, and ‘reasonable duration’ is the duration needed to either cure the disease or to ameliorate and maintain suppression of disease symptoms.

Only brief exposure (effective steady-state concentration for a few hours, days, or weeks) is required in cases where the target disease is acute. Contrarily, for chronic conditions, a more prolonged exposure (months or years) to an effective steady-state concentration of the drug is necessitated. Historically it has been acknowledged that biodegradable devices (with relative ease of implantation and lower side-effects profile) are more applicable for short-term (hours, days) or intermediate-term (weeks, months) drug delivery and is all that is required to treat acute disease and where chronic therapy is required (>1 year) non-biodegradable devices may provide superior control of drug release, improved retrievability in the case of serious side-effects, and fewer invasive procedures than a biodegradable device. However, with the advent of several innovative technologies in polymeric and biomaterials science, researchers are continually identifying biocompatible polymeric materials that are capable of providing prolonged drug delivery with the novelty of biodegradability. In addition, the commercialization of intravitreal devices is another significant obstacle, which rests largely on psychological factors inherent to clinicians and patients, who generally feel more at ease with traditional eye-drop therapy.

Several achievements and failures in the marketplace has brought further clarity to the field in recognizing that the development of implantable intravitreal drug delivery devices is not simply a matter of *in vitro* engineering of the device in order to achieve a controlled rate and duration of drug release. Both patient and physician factors are just as critical, if not more significant, in the successful application of the technology. These factors continue to confound scientists in their quest to develop successful intraocular devices that can deliver drug for significantly prolonged periods of time for the treatment of posterior segment eye diseases that require chronic suppressive maintenance therapy. Furthermore, various biomaterials have been employed for designing intraocular drug delivery devices. The use of biomaterials in intraocular drug delivery will inevitably increase in the future as the frontiers of biomaterials science are surpassed. However their biocompatibility and patient comfort will need to be improved in tandem.

6.3. Future Outlook

In light of the above the novel DSMT device certainly opens up a number of new opportunities with regards to innovator drug delivery devices. The device can be modified in numerous ways to produce a drug delivery system demonstrating desirable release kinetics with zero-order drug release, using biodegradable polymers of a suitable inherent viscosity. The device can be applicable to a wide range of bioactives, whereby chronic suppressive therapy is required and intravitreal levels need to be sustained over shorter periods such as several weeks to months or for prolonged release over one to two years. Targeting one of the research outputs such as the United States patent that has been filed for protecting the intellectual property of the DSMT device followed by licensing of the technology to a suitable Pharmaceutical Company promotes the potential for economic growth within the country. Having such technology developed within South Africa would allow the country to compete on an international level in the biotechnology sector against importation of innovator and generic products. Due to the flexibility in the design of the DSMT device there are circumstances where the technology can be applied to several other regions of the human body other than the eye and the period over which bioactives are released is measured in months. An example of such an application is represented by its use as a contraceptive device implanted into the *gluteus maximus* muscle and releases an estrogen or similar compound over a period of between 3-6 months. Another example is the implantation of the device within blood or

lymphatic vessels or intraperitoneally. Figures 6.1-6.3 shows several drawings describing the alternative embodiments of the DSMT device invention.

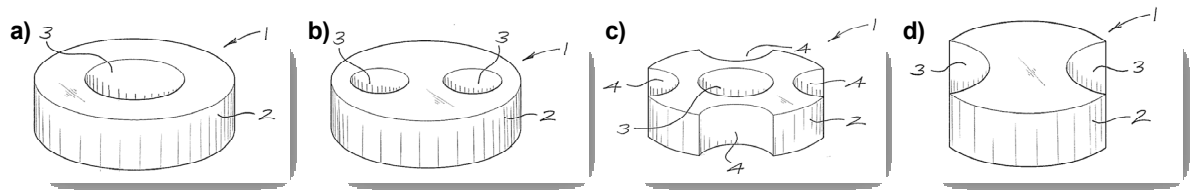

Figure 6.1: Schematic drawings of various embodiments of the DSMT device with a) a side-perspective view of a first embodiment of the invention; b) a second embodiment of the invention; c) a third embodiment of the invention; and d) a fourth embodiment of the invention for the sustained, *in situ*, delivery of a pharmaceutical composition to a human or animal body (US Patent Application # 11/285,035).

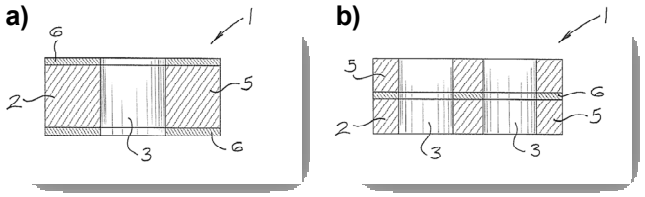

Figure 6.2: Schematic drawings of a) a cross-sectional side view of an embodiment of the invention of Figure 5.1a and b) a cross-sectional side view of and embodiment of the invention of Figure 5.1b.for the sustained, *in situ*, delivery of a pharmaceutical composition to a human or animal body (US Patent Application # 11/285,035).

.

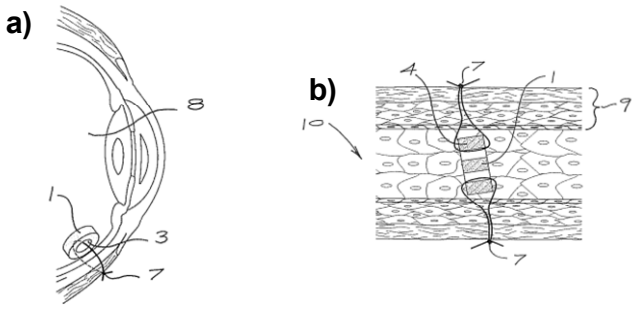

Figure 6.3: Schematic drawings of a) a side-view of the DSMT device of Figure 5.1a sutured within the intraocular cavity and b) within an artery, alternatively a lymphatic vessel as a fifth embodiment of the invention for the sustained, *in situ*, delivery of a pharmaceutical composition to a human or animal body (US Patent Application # 11/285,035).

.

REFERENCES

1. Aarons L 1997. In: Pharmacokinetic and Pharmacodynamic Data Analysis: Concepts and Applications, 2nd ed, Swedish Pharmaceutical Press.

2. Ahmed I, Patton TF 1984. Effect of pH and buffer on the precorneal disposition and ocular penetration of pilocarpine in rabbits. Int J Pharm 19:215-227.

3. Ahmed I, Patton TF 1986. Selective intraocular delivery of liposome encapsulated insulin via the non-corneal absorption route. Int J Pharm 34:163-167.

4. Ahmed I, Patton TF 1987. Disposition of timolol and insulin in the rabbit eye following corneal versus non-corneal absorption. Int J Pharm 38:9-21.

5. Akaike H 1978. Posterior probabilities for choosing a regression model. Ann Inst Math Stat 30:9-14.

6. Akula SK, Peyman GA, Rahimy MH, Hyslop NE, Janney A and Ashton P 1994. Treatment of cytomegalovirus retinitis with intravitreal injection of liposome encapsulated ganciclovir in a patient with AIDS. Br J Ophthalmol 78:667-680.

7. Ambati J, Gragoudas ES, Miller JW, You TT, Miyamoto K, Delori FC and Adamis AP 2000. Transcleral delivery of bioactive protein to the choroid and retina. Invest Ophthalmol Vis Sci 41:1186-1191.

8. Anderson JM, Shive MS 1997. Biodegradation and biocompatibility of PLA and PLGA microspheres. Adv Drug Deliv Rev 28:5-24.

9. Ansel HC and Popovich NG 1990. Peroral solids, capsules, tablets and controlled release dosage forms, In: Pharmaceutical Dosage Forms and Drug Delivery Systems, 5th ed, Lea & Febiger, Philadelphia, 182-195.

10. Anshuman A, Ambike KR, Mahadik AP 2004. Stability study of amorphous valdecoxibInt J Pharm 282:151-162.

11. Araujo AAS, Storpirtis S, Mercuri LP, Carvalho FMS, Filho MS, Matos JR 2003. Thermal analysis of the antiretroviral zidovudine (AZT) and evaluation of the compatibility with excipients used in solid dosage forms. Int J Pharm 260: 303-314

12. Arias MJ, Moyano JR, Gines JM 1998. Study by DSC and HSM of oxazepam-PEG6000 and oxazepam-D-mannitol systems: Application to the preparation of solid dispersions. Thermochim Acta 321:33-41.

13. Athanasiou KA, Niederauer GG, Agrawal CM 1996. Sterilization, toxicity, biocompatibility and clinical applications of polylactic acid/polyglycolic acid copolymers. Biomat 17:93-102.

14. Athanasiou K, Agrawal CM and Niederaurer GG 1990. Sterilization, toxicity, biocompatibility and clinical applications of polylactic acid/polyglycolic acid copolymers. Biomat 17:93-102.

15. Avery M 1999. Intraocular drug delivery systems: New treatments for eye disease, in California Eng Res Paper, ChemE. 185:1-15.

16. Axelrod J and Reichenthal J 1953. The fate of caffeine in man and a method for its estimation in biological material. J Pharmacol Exp Ther 107:519-523.

17. Baker RW, Lonsdale HK 1974. Controlled release: Mechanism and rates, In: Controlled Release of Biologically Active Agents (Tanquary AC, Lacey RE, eds.), Plenum Press, NY, USA, 15-71

18. Barra J, Doelker E 1998. Instrumentation of an eccentric tablet press, In: Munos-Ruiz A, Vromans H (eds), Data Acquisition and Measurement Techniques, Interpharm Press, Inc, Buffalo Grove, USA, pp. 189-238.

19. Barrer RM, Mckenzie N, Reay JSS 1956. Capillary condensation in single pores. J Coll Sci 11:479.

20. Barrett EP, Joyner JG, Halenda PP 1951. The determination of pore volume and area distributions in porous substances. I. Computations from nitrogen isotherms. J Am Chem Soc. 73:373.

21. Barza M, Doft B and Lynch E 1993. Ocular penetration of ceftriazone, ceftazidime, and vancomycin after subconjunctival injection in humans. Arch Ophthalmol 492-494.

22. Beck and Arnold 1977. Parameter Estimation in Engineering and Science. (Beck JV and Arnold KJ, eds.) John Wiley & Sons Inc., NY, USA.

23. Bellows JG 1944. Cataract and abnormalities of the lens. St Louis CV Mosby Co., 540-543.

24. Ben-Nun J, Joyce DA, Cooper RL, Cringle SJ and Constable IJ 1989. Pharmacokinetics of intravitreal injection. Invest Ophthal Vis Sci 30:1055-1061.

25. Benz MS, Albini TA, Holz ER, Lakhanpal RR, Westfall AC, Iyer MN and Carvounis PE 2006. Short-term course of intraocular pressure after intravitreal injection of triamcinolone acetonide. Ophthalmol 113:1174-1178.

26. Bergan T, Qydvin B and Lundo I 1973. Biological availability and *in vitro* release from oral oxytetracycline and tetracycline preparations. Acta Pharmacol Toxicol 33:138-156.

27. Berthe P, Baudouin C, Garraffo R, Hoffmann P, Taburet AM and Lapalus P 1994. Toxicologic and pharmacokinetic analysis of intravitreal injections of foscarnet either alone or in combination with ganciclovir. Invest Ophthalmol Vis Sci 35:1038-1045.

28. Bhardwaj R and Blanchard J 1998. *In vitro* characterization and *in vivo* release profile of poly(DL-lactide-co-glycolide)-based implant delivery system for the α-MSH analog, melanotan. I. Int J Pharm 170:109-117.

29. Bikiaris D, Papageorgiou GZ, Stergiou A, Pavlidou E, Karavas E, Kanaze F, Georgarakis M 2005. Thermochim Acta 439:58-67.

30. Bittner B, Mader K, Kroll C, Borchert HH, Kissel T 1999. Tetracycline-HCl-loaded poly(D,L-lactide-co-glycolide) microspheres prepared by a spray drying technique: influence of gamma-irradiation on radical formation and polymer degradation. J Control Rel 59:23-32.

31. Black J 1992. Biological performance of materials: Fundamentals of biocompatibility, Marcel Dekker, NY, USA, 21.

32. Bodmeier R and Chen H 1991. Evaluation of biodegradable poly(lactide) pellets prepared by direct compression. J Pharm Sci 78:819-822.

33. Bonferoni MC, Chetoni P, Giunchedi P, Rossi S, Ferrari F, Burgalassi S, Caramella C 2004. Carrageenan-gelatin mucoadhesive systems for ion-exchange based ophthalmic delivery: *In vitro* and preliminary *in vivo* studies. Eur J Pharm Biopharm 57:465-472.

34. Bott C, Rudolph MW, Schneider AR, Schirrmacher S, Skalsky B, Petereit HU, Langguth P, Dressman JB and Stein J 2004. *In vivo* evaluation of a novel pH- and time-based multiunit colonic drug delivery system. Aliment Pharmacol Ther 20:347-353.

35. Bourges JL, Bloquel C, Thomas A, et al 2006. Intraocular implants for extended drug delivery: Therapeutic applications. Adv Drug Deliv Revs 58: 1182-1202.

36. Brechu WF and Maren TH 1993. pH and drug ionization affects ocular pressure lowering of topical carbonic anhydrase inhibitors. Invest Ophthalmol Vis Sci 34:2581-2587.

37. Brockmeier D and von Hattingberg HM 1982. *In vitro-in vivo* correlation, a time scaling problem? Arzneim-Forsch 31:248-251.

38. Brockmeier D, Dengler HJ and Voegele D 1985. *In vitro-in vivo* correlation of dissolution, a time scaling problem? Transformation of *in vitro* results to the *in vivo* situation, using theophylline as a practical example. Eur J Clin Pharmacol 28:291-300.

39. Brunauer S, Emmett PH, Teller E 1938. Adsorption of gases in multimolecular layers. J Am Chem Soc 60:309.

40. Cantrill HL, Henry K, Melroe NH, Knobloch WH, Ramsay RC and Balfour NH 1989. Treatment of cytomegalovirus retinitis with intravitreal ganciclovir. Ophthalmol 96:367-374.

41. Carless JE, Leigh S 1974. Compression characteristics of powder: Radial die-wall pressure transmission and density changes. J Pharm Pharmacol 26:289-329.

42. Carstensen JT, Toure P 1980. Compression cycles in tableting. Powder Technol 26:199-204.

43. Celik M 1992. Overview of compaction data analysis techniques. Drug Dev Ind Pharm 18:767-810.

44. Chang SC and Lee VHL 1987. Nasal and conjunctival contributions to the systemic absorption of topical timolol in the pigmented rabbits: implications in the design of strategies to maximize the ratio of ocular to systemic absorption. J Ocul Pharmacol 3:159-169.

45. Chang SC, Chien DS, Bundgaard H and Lee VHL 1988. Relative effectiveness of prodrug and viscous solution approaches in maximizing the ratio of ocular to systemic absorption of topically applied timolol. Exp Eye Res 46:59-69.

46. Charles JB, Ganthier R, Wilson MR, Lee DA, Baker RS, Leong KW, Glasgow BJ 1991. Use of bioerodible polymers impregnated with mitomycin in glaucoma filtration surgery in rabbits. Ophthalmol 98:503-508.

47. Cheng L, Hostetler K, Chaidhawangul S, Gardner MF, Beadle JR, Toyoguchi M et al 2002. Treatment or prevention of herpes simplex virus retinitis with intravitreally injectable crystalline 1-o-hexadecylpropanediol-3-phopho-ganciclovir. Invest Ophthalmol Vis Sci 43:515-521.

48. Cheng L, Hostetler KY, Chaidhawangul S, Gardner MF, Beadle JR, Keefe KS, Bergeron-Lynn G, et al 2000. Intravitreal toxicology and duration of efficacy of a novel antiviral lipid prodrug of ganciclovir in liposome formulation. Invest Ophthalmol Vis Sci 41:1523-1532.

49. Choonara YE, Pillay V, Carmichael T and Danckwerts MP 2006. An *in vitro* study of the design and development of a novel doughnut-shaped minitablet for intraocular implantation. Int J Pharm 310:15-24.

50. Choonara YE, Pillay V, Carmichael T and Danckwerts MP 2007. Studies on a novel doughnut-shaped minitablet for intraocular drug delivery. AAPS PharmSciTech 8:1-7.

51. Chowhan M, Weiner AL, Bhagat H 2002. Drug delivery-ophthalmic route, In: Encyclopedia of Pharmaceutical Technology (Swarbrick J, Boylan JC, eds.), Marcel Dekker, NY, USA, 863-870.

52. Cochereau-Massin I, Lehoang P, Lautier-Frau M et al 1991. Efficacy and tolerance of intravitreal ganciclovir in cytomegalovirus retinitis in acquired immune deficiency syndrome. Ophthalmol 98:1348-1355.

53. Colo GD 1991. Controlled drug release from implantable matrices based on hydrophobic polymers, compression. J Pharm Sci 78:819-822.

54. Corrigan OI 1995. Thermal analysis of spray dried products. Thermochim Acta 248:245-258.

55. Cunha-Vaz JG 1979. The blood-ocular barriers. Surv Ophthalmol 23:279-96.

56. Cunha-Vaz JG 1997. The blood-ocular barriers: past, present, and future. Doc Ophthalmol 93:149-57.

57. Davies and Whitting 1972. A modified form of Levenberg's correction. In: Numerical Methods for Non-linear Optimization. Academic Press, NY, USA, 12.

58. Davis JL, Gilger BC, Robinson MR 2004. Novel approaches to ocular drug delivery. Curr Opin Molec Therapeu 6:195-205.

59. de Rojas Silva MV, Rodriguez-Ares MT, Sanchez-Salorio M, Lamas Diaz MJ, Cuevas Alvarez J, Vila Jato JL, Capeans Tome C 1999. Efficacy of subconjunctival cyclosporine-containing microspheres on keratoplasty rejection in the rabbit. Arch Clin Exp Ophthalmol 237:840-847.

60. Deshpande AA, Heller J, Gurny R 1998. Bioerodible polymers for ocular drug delivery. Crit Rev Ther Drug Carrier Syst 15:381-420.

61. Diebol Y, Jarrın M, Saez V, Carvalho ELS, Orea M, Calonge M, Seijo B, Alonso MJ 2007. Ocular drug delivery by liposome-chitosan nanoparticle complexes (LCS-NP). Biomat 28:1553-1564.

62. Doelker E 1978. Physique de la compression: Interet et limite des machines instrumentees pour loptimisation de la formulation. Pharm Acta Helv 53:182-188.

63. Doelker E 1983. Developments in compression: Compressional tests as an aid in tablet formulation, In: Topics in Pharmaceutical Sciences (Breimer DD, Speiser P, eds.), Amsterdam, Netherlands, 371-386,

64. Doelker E 1988. Recent advances in tableting science. Boll Chim Farm 127:37-49.

65. Doelker E 1994. Assessment of powder compaction, In: Powder Technology and Pharmaceutical Processes (Chulia D, Deleuil M, Pourcelot Y, eds.), Elsevier, Amsterdam, 403-471.

66. Doelker E, Shotton E 1977. The effect of some binding agents on the mechanical properties of granules and their compression characteristics. J Pharm Pharmacol 29:193-198.

67. Dohadwala AA, Munger R, Damji KF 1998. Positive correlation between Tonopen intraocular pressure and central corneal thickness. Ophthalmol 105:1849-1854.

68. Dorta MJ, Santovena A, Llabres M and Farina JB 2002. Potential applications of PLGA film-implants in modulating *in vitro* drugs release. Int J Pharm 248:149-156.

69. Draper and Smith 1981. Applied Regression Analysis, 2nd ed. John Wiley & Sons, NY, USA.

70. Dubielzig RR, Render JA, Morreale RJ 1997. Distinctive morphologic features of the ciliary body in equine recurrent uveitis. Vet Comp Ophthalmol 7:163-167.

71. Duke-Elder WS 1946. Text Book of Ophthalmology, Kimpton, London, 1:464-476.

72. Dunne M, Corrigan I, Ramtoola Z 2000. Influence of particle size and dissolution conditions on the degradation properties of poly(lactide-co-glycolide) particles. Biomat 21:1659-1668.

73. Dutta S, Reed RC and Cavanaugh JH 2004. Absolute bioavailability and absorption characteristics of divalproex sodium extended-release tablets in healthy volunteers. J Clin Pharmacol 44:737-742.

74. Duvvuri S, Majumdar S, Mitra AK 2003. Drug delivery to the retina: Challenges and opportunities. Expert Opin Biol Ther 3:45-56.

75. Edlund U, Albertsson AC 2002. Degradable polymer microspheres for controlled drug delivery, In: Advances in Polymer Science (Albertsson AC, ed.), Springer-Verlag, Berlin, 157:68-112.

76. Einmahl S, Behar-Cohen F, Tabatabay C, Savoldelli M, D'Hermies F, Chauvaud D, Heller J 2000. A viscous bioerodible poly(ortho ester) as a new biomaterial for intraocular application. J Biomed Mater Res 50:566-573.

77. Einmahl S, Zignani M, Varesio E, Heller J, Veuthey JL, Tabatabay C, Gurny R 1999. Concomitant and controlled release of dexamethasone and 5-fluorouracil from poly(ortho ester). Int J Pharm 185:189-198.

78. Eperon S, Bossy-Nobs L, Petropoulos IK, Gurny R, Guex-Crosier Y 2008. A biodegradable drug delivery system for the treatment of postoperative inflammation. Int J Pharm 352:240-247.

79. European Guideline 3AQ4a 1992. The use of ionizing radiation in the manufacture of medicinal products. Official Publications in the European Communities, London.

80. Faisant N, Siepmann J, Oury P, Laffineur V, Bruna E, Haffner J, Benoit JP 2002. The effect of gamma-irradiation on drug release from bioerodible microparticles: A quantitative treatment. Int J Pharm 242:281-284.

81. Fell JT, Newton JM 1970. Determination of tablet strength by the diametrical compression test. J Pharm Sci 59:688-691.

82. Fleishaker JC and Ferry JJ 1995. Pharmacokinetic-pharmacodynamic modeling in drug development: Concepts and applications, In: Handbook of Pharmacokinetic, Pharmacodynamic Correlation (Derendorf H and Hochhaus G, eds.), CRC Press, Bocd Raton, FL, USA, 57-78.

83. Foulds WS, Moseley H, Eadie A, et al 1980. Vitreal, retinal, and pigment epithelial contributions to the posterior blood-ocular barrier. Trans Ophthalmol Soc UK 100:341-342.

84. Frangie JP 199. Clinical pharmacokinetics of various topical ophthalmic delivery systems. Clin Pharmacokinet 29:130-138.

85. Friedberg ML, Pleyer U and Mondino BJ 1991. Device drug delivery to the eye: Collagen shields, iontophoresis and pumps. Ophthalmol 98:7255732.

86. Garny R 1981. Preliminary study of prolonged acting drug delivery system for the treatment of glaucoma. Pharm Acta Helv 56:130-132.

87. Geroski DH, Edelhauser HF 2001. Transscleral drug delivery for posterior segment disease. Adv Drug Deliv Rev 52:37-48.

88. Ghate D, Edelhauser HF 2006. Ocular drug delivery. Expert Opin Drug Deliv 3:275-287.

89. Gibaldi M and Weintraub H 1970. Quantitative correlation of absorption and in vitro dissolution kinetics of aspirin from several dosage forms. J Pharm Sci 59:725-726.

90. Gilger BC, Malok E, Cutter KV, Horohov DW, Allen JB 1999. Characterization of T-lymphocytes in the anterior uvea of eyes with chronic equine recurrent uveitis. Vet Immunol Immunopathol 71:17-28.

91. Giordano GG, Chevez-Barrios P, Refojo MF, Garcia CA 1995. Biodegradation and tissue reaction to intravitreous biodegradable poly(D,L-lactic-co-glycolic)acid microspheres. Curr Eye Res 14:761-768.

92. Giordano GG, Refojo MF, Arroyo MH 1993. Sustained delivery of retinoic acid from microspheres of biodegradable polymer in PVR. Invest Ophthalmol Vis Sci 34:2743-2751.

93. Giron D 2002. Applications of thermal analysis in the pharmaceutical industry. J Therm Anal Calorim 68:335-357.

94. Goepferich A, Langer R 1995. Modeling monomer release from erodible polymers. J Control Rel 33:55-69.

95. Gould L, Trope G, Cheng YL, Heathcote JG, Sheardown H, Rootman D, Liu GS, Menon IA 1994. 50:50 poly(DL glycolic acid-lactic acid) copolymer as a drug delivery system for 5-fluorouracil: A histopathological evaluation. Can J Ophthalmol 29:168-171.

96. Graham RO and Peyman GA 1974. Intravitreal injection of dexamethasone: Treatment of experimentally induced ophthalmitis. Arch Ophthalmol 92:149-154.

97. Grass GM and Robinson JR 1988. Mechanisms of corneal drug penetration II: Ultra-structural analysis of potential pathways for drug movement. J Pharm Sci 77:15-23.

98. Grass GM, Cobby J and Makoid MC 1984. Ocular delivery of Pilocarpine from erodible matrices. J Pharm Sci 73:618-621.

99. Gregg SJ, Sing KWS 1982. Adsorption, surface area and porosity, 2nd Ed., NY, USA.

100. Greiner JV, Kopp SJ, Sanders DR and Glonek T 1981. Organophosphates of the crystalline lens: a nuclear magnetic resonance spectroscopic study. Invest Ophthalmol Vis Sci 21:796-813.

101. Gulsen D and Chauhan A 2005. Dispersion of microemulsion drops in HEMA hydrogel: a potential ophthalmic drug delivery vehicle. Int J Pharm 292:95-117.

102. Gustafsson C, Lennholm T, Nystrom C 1998. Comparison of solid-state NMR and isothermal microcalorimetry in the assessment of the amorphous component of lactose Int J Pharm 174:243-252.

103. Halsey GD 1948. Physical adsorption on non-uniform surfaces. J Chem Phys 16:931.

104. Hanson WA 1982. Handbook of Dissolution Testing, Pharmaceutical Technology Publications, Springfield, Oregon.

105. Harkins WD and Jura G 1944. The relationship between the energy of adsorption of a vapor on a solid and of immersion of the solid in a liquid. J Am Chem Soc 66:1366.

106. Harper CA 3rd, Khoobehi B, Peyman GA, Gebhardt BM, Dunlap WA 1993. Bioavailability of microsphere-entrapped cyclosporine A in the cornea and aqueous of rabbits. Int Ophthalmol 17:337-340.

107. Hartley HO 1961. The modified Gauss-Newton method for the fitting of nonlinear regression functions by least squares. Technometrics 3:269-80.

108. Hashizoe M, Ogura Y, Kimura H, Moritera T, Honda Y, Kyo M, Hyon SH, Ikada Y 1994. Scleral plug of biodegradable polymers for controlled drug release in the vitreous. Arch Ophthalmol 112:1380-1384.

109. Hashizoe M, Ogura Y, Takanashi T, Kunou N, Honda Y, Ikada Y 1995. Implantable biodegradable polymeric device in the treatment of experimental proliferative vitreoretinopathy. Curr Eye Res 14:473-477.

110. Hashizoe M, Ogura Y, Takanashi T, Kunou N, Honda Y, Ikada Y 1997. Biodegradable polymeric device for sustained intravitreal release of ganciclovir in rabbits. Curr Eye Res 16:633-639.

111. Hatefi A and Amsden B 2002. Biodegradable injectable in situ forming drug delivery systems. J Control Rel 80:9-28.Hayreh SS 1966. Posterior drainage of the intraocular fluid from the vitreous. Exp Eye Res 5:123-144.

112. Hausberger AG, Kenley RA, DeLuca PP 1995. Gamma-irradiation effects on molecular weight and *in vitro* degradation of poly(D,L-lactide-co-glycolide) microparticles. Pharm Res 12:851-856.

113. Hecht G 1995. Ophthalmic Preparations, In: Remington: The Science and Practice of Pharmacy (Gennaro AR, ed.) 19th ed. 2, Mack, PA, USA, 1563-1576.

114. Heinemann MH 1989. Long-term intravitreal ganciclovir therapy for cytomegalovirus retinopathy. Arch Ophthalmol 107:1767-1772.

115. Heller J 1984. Biodegradable polymers in controlled drug delivery. Crit Rev Ther Drug Carrier Syst 1:39-90.

116. Heller J 1987. Fundamentals of polymer science, In: Controlled Drug Release (Robinson JR, Lee VH, eds.), Marcel Dekker, NY, USA, 139-177.

117. Heller J 2005. Ocular delivery using poly(orto esters). Adv Drug Del Rev 57:2053-2062.

118. Henn GG, Birkinshaw C, Buggy M 1996. A comparison of the effects of γ-irradiation and ethylene oxide sterilization on the properties of comparison molded poly-D, L-lactide. J Mater Sci: Mater Med 7:591-595.

119. Herrero-Vanrell R and Refojo MF 2001. Biodegradable microspheres for vitreoretinal drug delivery. Adv Drug Del Rev 52:5-16.

120. Herroro-Vanrell R, Ramirez L, Fernandaz-Carallido A, et al 2000. Biodegradable PLGA microspheres loaded with ganciclovir for intraocular administration. Encapsulation technique, *in vitro* release profiles, and sterilization process. Pharm Res 17:1323-1328.

121. Hiestand EN, Wells JE, Peot CB, Ochs JF 1977. Physical process of tableting. J Pharm Sci 66:510-519.

122. Hoag SW 2003. Die wall instrumentation: design and application in compaction. AAPS Annual Meeting and Exposition, Salt Lake City, 2003.

123. Holford NH and Scheiner LB 1986. Kinetics of pharmacologic response, In: Pharmacokinetics: Theory and Methodology (Rowland M ad Tucker G, eds.), Pergamon press, 1899212.

124. Hosoya T, Baccus SA, Meister M 2005. Dynamic predictive coding by the retina. Am J Ophthalmol 140:969.

125. Huang AJW, Tseng SCG and Kenyon KR 1989. Paracellular permeability of corneal and conjunctival epithelia. Invest Ophthalmol Vis Sci 30:684-689.

126. Hughes PM, Olejnik O, Chang TS, Lin JE, Wilson CG 2005. Topical and systemic drug delivery to the posterior segments. Adv Drug Del Rev 57:2010-2032.

127. International Conference on Harmonization, ICH Guidelines, The Federal Register, March 1995-February 1999.

128. Jarvinen K, Jarvinen T and Urtti A 1995. Ocular absorption following topical delivery. Adv Drug Deliv Rev 16:3319.

129. Jones TM 1978. Preformulation studies to predict the compaction properties of materials used in tablets and capsules. Acta Pharm Technol Suppl 6:141-159.

130. Kassem MA, Rahman AAA, Ghora MM, Ahmed MB, Khalil RM 2007. Pharmaceutical nanotechnology nanosuspension as an ophthalmic delivery system for certain glucocorticoid drugs. Int J Pharm 340:126-133.

131. Kelly JA, Molyneux PD, Smith SA and Smith SE 1989. Relative bioavailability of pilocarpine from a novel ophthalmic delivery system and conventional eyedrop formulations. Br J Ophthalmol 73:360-362.

132. Khoobehi B, Stradtmann MO, Peyman GA, Aly OM 1990. Clearance of fluorescein incorporated into microspheres from the cornea and aqueous after subconjunctival injection. Ophthalmic Surg 21:840-844.

133. Khoobehi B, Stradtmann MO, Peyman GA, Aly OM 1991. Clearance of sodium fluorescein incorporated into microspheres from the vitreous after intravitreal injection. Ophthalmic Surg 22:175-180.

134. Kim SH, Chung JW, Kang TJ, Kwak SY, Suzuki T 2007. Determination of the glass transition temperature of polymer/layered silicate nanocomposites from positron annihilation lifetime measurements. Polymer 48:4271-4277.

135. Kimura H, Ogura Y, Hashizoe M, Nishiwaki H, Honda Y, Ikada Y 1994. A new vitreal drug delivery system using an implantable biodegradable polymeric device. Invest Ophthalmol Vis Sci 35:2815-2819.

136. Kimura H, Ogura Y, Moritera T, Honda Y, Wada R, Hyon SH, Ikada Y 1992. Injectable microspheres with controlled drug release for glaucoma filtering surgery. Invest Ophthalmol Vis Sci 33:3436-3441.

137. Krycer I, Pope G 1982. The interpretation of powder compaction data: A critical review. Drug Dev Ind Pharm 8:307-342.

138. Kuck JFR 1975. Composition of the lens, In: Cataract and Abnormalities of the Lens (Bellows JG, ed.), Grune and Stratton, NY, USA, 6995.

139. Kulkarni RK, Pani KC, Neuman C, Leopard F 1966. Polylactic acid for surgical implant. Arch Surg 93:839-843.

140. Kumar MNVR 2000. Nano and microparticles as controlled drug delivery devices. J Pharm Pharmaceut Sci 3:234-258.

141. Kunou N, Ogura Y, Hashizoe M, Honda Y, Hyon S-H, Ikada Y 1995. Controlled intraocular delivery of ganciclovir with use of biodegradable scleral implant in rabbits. J Control Rel 37:143-150.

142. Kunou N, Ogura Y, Yasukawa T, et al 2000. Long-term sustained release of ganciclovir from biodegradable scleral implant for the treatment of cytomegalovirus retinitis. J Control Rel 68:263-271.

143. Labbé A, Dupas B, Hamard P, Baudouin C 2005. *In vivo* confocal microscopy study of blebs after filtering surgery. Ophthalmol 112:1-9.

144. Lallemand F, Felt-Baeyens O, Besseghir K, Behar-Cohen F and Gurny R 2003. Cyclosporine A delivery to the eye: A pharmaceutical challenge. Eur J Pharm Biopharm 56:307-318.

145. Lang JC 1995. Ocular drug delivery conventional ocular formulations. Adv Drug Deliv Rev 16:39-43.

146. Langer R, Peppas N 1983. Chemical and physical structure of polymers as carriers for controlled release of bioactive agents: A review. Rev Macromol Chem Phys 23:61-126.

147. Laties AM, Rapoport SI 1976. The blood-ocular barriers under osmotic stress: studies on the freeze-dried eye. Arch Ophthalmol 94:1086-1091.

148. Le Bourlais C, Acar L, Zia H, Sado PA, Needham T, Leverge R 1998. Ophthalmic drug delivery systems-recent advances. Prog Retinal Eye Res 17:33-58.

149. Lee DA, Leong KW, Panek WC, Eng CT, Glasgow BJ 1988. The use of bioerodible polymers and 5-fluorouracil in glaucoma filtration surgery. Invest Ophthalmol Vis Sci 29:1692-1697.

150. Lee SB, Geroski DH, Prausnitz MR and Edelhauser HF 2004. Drug delivery through the sclera: Effects of thickness, hydration, and sustained-release systems. Exp Eye Res 78:599-607.

151. Lee TW and Robinson JR 2004. Drug Delivery to the Posterior Segment of the Eye II: Development and Validation of a Simple Pharmacokinetic Model for Subconjunctival Injection. J Ocul Pharmacol Ther 20:43-53.

152. Lee VHL and Robinson JR 1986. Review: Topical ocular drug delivery: Recent developments and future challenges. J Ocul Pharmacol 2:677108.

153. Lesar TS and Fiscella RG 1985. Antimicrobial drug delivery to the eye. Drug Intel Clin Pharm 19:642-654.

154. Levin M 2006.Pharmaceutical process scale-up. In: Drugs and the Pharmaceutical Sciences (Levin M, ed), Taylor & Francis, 118:464.

155. Levy G, Leonards J and Procknal JA 1965. Development of *in vitro* tests which correlate quantitatively with dissolution rate-limited drug absorption in man. J Pharm Sci 54:1719-1722.

156. Lewis DD 1990. Controlled release of bioactive agents from lactide/ glycolide polymers. In: Biodegradable polymers and drug delivery systems (Chasin M, Langer R, eds.), Marcel Dekker, NY, USA, 1-41.

157. Lewis RA, Schoenwald RD, Bartknecht CF and Phelps CD 1986. Aminozolamide gel: A trial of a topical carboic anhydrase inhibitor in ocular hypertension. Arch Ophthalmol 104:8422844.

158. Li N, Zhuang C, Wang M, Sun X, Nie S, Pan W 2009. Liposome coated with low molecular weight chitosan and its potential use in ocular drug delivery. Int J Pharm in press available online 25 June 2009.

159. Liaw J and Robinson JR 1992. The effect of polyethylene glycol molecular weight on corneal transport and the related influence of penetration enhancers. Int J Pharm 88:125-140.

160. Liaw J, Rojanasakul Y, Robinson JR 1992. The effect of drug charge type and charge density on corneal transport. Int J Pharm 88:111-124.

161. Lim KS, Wickremasinghe SS, Cordeiro MF, Bunce C and Khaw PT 2005. Accuracy of Intraocular Pressure Measurements in New Zealand White Rabbits. Invest Ophthalmol Vis Sci. 46, 2419-2423.

162. Lima JJ 1995. Pharmacokinetics and Pharmacodynamics, In: Encyclopedia of Pharmaceutical Technology (Swarbrick J and Boylan JC, eds.), Marcel Dekker, NY, USA 12:29952.

163. Lippins BC, Linsen BG, de Boer JH 1964. Pore systems in catalysts. I. Adsorption of nitrogen; apparatus and calculation. J Catalysis 3:32.

164. Lloyd AW, Faragher RGA and Denyer SP 2001. Ocular biomaterials and implants. Biomat 22:769-785.

165. Long WM 1960. Radial pressure in powder compaction. Powder Metall 6:73-86.

166. Long WM 1962. Die design and related questions in powder compaction. Spec Ceram 17:327-340.

167. Lopes LB, Scarpa MV, Pereira NL, Oliveira LC, Oliveira AG 2006. Braz J Pharm Sci 42:497-504.

168. Ludwig A 2005. The use of mucoadhesive polymers in ocular drug delivery. Adv Drug Del Rev 57:1595-1639.

169. Macoul KL, Pavan-Langston D 1975. Pilocarpine Ocusert® system for sustained control of ocular hypertension. Arch Ophthalmol 93:587-590.

170. Mar EC 1983. Effect of dihydroxy-2-propoxyl-methylguanineon human CMV replication *in vitro*. Antimicrob Agents Chemother 24:518-521.

171. Maren TH and Jankowska L 1985. Ocular pharmacology of sulfonamides: The cornea as barrier and depot. Curr Eye Res 4:399-408.

172. Marshall K 1986. Compression and consolidation of powdered solids, In: The Theory and Practice of Industrial Pharmacy, 3rd ed. (Lachman L, Lieberman HA and Kanig JL, eds.), Lea & Febiger, PA, USA, 66-99.

173. Martin DF, Ferris FL, Parks DJ, Walton RC, Mellow SD, Gibbs D et al 1997. Ganciclovir implant exchange. Timing, surgical procedure, and complications. Arch Ophthalmol 115:1389-1394.

174. Martin DF, Kupperman BD, Wolitz RA, Palestine AG, Li H and Robinson CA 1999. Oral ganciclovir for patients with cytomegalovirus retinitis treated with a ganciclovir implant. N Engl J Med 340:1063-1070.

175. Martin DF, Parks DJ, Mellow SD, et al 1994. Treatment of cytomegalovirus retinitis with an intraocular sustained-release ganciclovir implant: A randomized controlled clinical trial. Arch Ophthalmol 112:1531-1539.

176. Martin, JC 1983. 1-3dihydrodoxy-2-propoxyl-methyl-guanine: A new potent and selective anti-herpes agent. J Med Chem 26:759-761.

177. Martinez-Sancho C, Herrero-Vanrell R and Negro S 2004. Optimization of acyclovir poly(D,L-lactide-co-glycolide) microspheres for intravitreal administration using a factorial design study. Int J Pharm 273:45-56.

178. Maurice D 2001. Review: Practical issues in intravitreal drug delivery. J Ocul Pharmacol Ther 17:393-401.

179. Maurice DM and Mashima S 1984. Ocular pharmacokinetics, In: Handbook of Experimental Pharmacology: Pharmacology of the Eye (Sear ML, ed.), Springer-Verlag, NY, USA, 69:19-116.

180. Maurice DM and Srinivas SP 1992. Use of fluorimetry Park, in assessing the efficacy of a cation-sensitive gel as an ophthalmic vehicle: Comparison with scintigraphy. J Pharm Sci 81:615-619.

181. Merodio M, Irache JM, Valamanesh F, Mirshahi M 2002. Ocular disposition and tolerance of ganciclovir-loaded albumin nanoparticles after intravitreal injection in rats. Biomat 23:1587-1594.

182. Mishima S 1981. Clinical pharmacokinetics of the eye. Invest Ophthalmol Vis Sci 21:5044541.

183. Miyamoto H, Ogura Y, Hashizoe M, Kunou N, Honda Y, Ikada Y 1997. Biodegradable scleral implant for intravitreal controlled release of fluconazole. Curr Eye Res 16:930-935.

184. Miyazaki S, Ishii K and Tdkada M 1982. Use of fibrin film as a carrier for drug delivery: A long-acting delivery system for pilocarpine into the eye. Chem Pharm Bull 30:340553407.

185. Mohr D, Wolff M, Kissel T 1999. Gamma irradiation for terminal sterilization of 17-estradiol loaded poly-(D, L-lactide-co-glycolide) microparticles. J Control Rel 61:203-217.

186. Montanari L, Costantini M, Signoretti EC, Valvo L, Santucci M, Bartolomei M, Fattibene P, Onori S, Faucitano A, Conti B, Genta I 1998. Gamma irradiation effects on poly(DL-lactide-co-glycolide) microspheres. J Control Rel 56:219-229.

187. Morita Y, Saino H, Tojo K 1998. Polymer blend implant for ocular delivery of fluorometholone. Biol Pharm Bull 21:72-75.

188. Moritera T, Ogura Y, Honda Y, Wada R, Hyon SH, Ikada Y 1991. Microspheres of biodegradable polymers as a drug delivery system in the vitreous. Invest Ophthalmol Vis Sci 32:1785-1790.

189. Moritera T, Ogura Y, Yoshimura N, Honda Y, Wada R, Hyon SH, Ikada Y 1992. Biodegradable microspheres containing adriamycin in the treatment of proliferative vitreoretinopathy. Invest Ophthalmol Vis Sci 33:3125-3130.

190. Mort M 2000. Multiple modes of drug delivery. Mod Drug Discov 3:30-32.

191. Motwani SK, Chopra S, Talegaonkar S, Kohli K, Ahmad FJ, Khar RK 2008. Chitosan-sodium alginate nanoparticles as submicroscopic reservoirs for ocular delivery: Formulation, optimization and *in vitro* characterization. Eur J Pharm Biopharm 68:513-525.

192. Myles ME, Neumann DM and Hill JM 2005. Recent progress in ocular drug delivery for posterior segment disease: Emphasis on transscleral iontophoresis. Adv Drug Deliv Rev 57:2063-2079.

193. Nagataki S and Mishima S 1980. Pharmacokinetics of instilled drugs in the human eye. Int Ophthalmol Clin 20:33-49.

194. Naima Z, Siro T, Juan-Manuel GD, Chantal C, Rene C, Jerome D 2001. Eur J Pharm Sci 12:395-404.

195. Newton R, Broughton LJ, Lind MJ, Morrison PJ, Rogers HJ and Bradbrook ID 1981. Plasma and salivary pharmacokinetics of caffeine in man. Eur J Clin Pharmacol 21:45-52.

196. Nijenhuis AJ, Colstee E, Grijpma DW, Pennings AJ 1996. High molecular weight poly(L-lactide) and poly(ethylene oxide) blends: Thermal characterization and physical properties. Polymer 37:5849-5847.

197. Nijenhuis AJ, Grijpma DW, Pennings AJ 1991. Highly crystalline as-polymerized poly(L-lactide). Polym Bull 26:71-78.

198. Obiorah BA 1978. Possible prediction of compression characteristics from pressure cycle plots. Int J Pharm 1:249-255.

199. Obiorah BA, Shotton E 1976. The effect of waxes, hydrolyzed gelatin and moisture on the compression characteristics of paracetamol and phenacetin. J Pharm Pharmacol 28:629-632.

200. Ohta M, Bucktona G 2005. A study of the differences between two amorphous spray dried samples of cefditoren pivoxil which exhibited different physical stabilities Int J Pharm 289:31-38.

201. Ohtori A and Tojo K 1994. *In vivo*/*in vitro* correlation of intravitreal delivery of drugs with the help to computer simulation. Biol Pharm Bull 17:283-290.

202. Okada H, Doken Y, Ogawa Y 1996. Persistent suppression of the pituitary-gonadal system in female rats by three-month depot injectable microspheres of leuprorelin acetate. J Pharm Sci 85:1044-1048.

203. Okada H, Inoue Y, Heya T, Ueno H, Ogawa Y, Toguchi H 1991. Pharmacokinetics of once-a-month injectable microspheres of leuprolide acetate. Pharm Res 8:787-791.

204. Oyster CW, Amthor FR, Takahashi ES 1993. Dendritic architecture of on-off direction-selective ganglion cells in the rabbit retina. Vis Res 33:579-608.

205. Oyster CW, Takahashi ES, Collewijn H 1972. Direction-selective retinal ganglion cells and control of optokinetic nystagmus in the rabbit. Vis Res 12:183-193.

206. Park JB, Lakes RS 1992. Biomaterials: An introduction, Plenum Press, NY, USA, 162.

207. Park TG 1995. Degradation of poly(lactic-co-glycolic acid) microspheres: Effect of copolymer composition. Biomat 16:1123-1130.

208. Parrott EL 1990. Compression, In: Pharmaceutical Dosage Forms: Tablets, (Lieberman HA, Lachman L and Schwartz JB, eds.), Marcel Dekker, NY, USA 2:201-243.

209. Peracchia C and Peracchia LL 1980. Gap junctional dynamics: Reversible effects of hydrogen ions. J Cell Biol 87:719-727.

210. Plokin, SA 1985. Sensitivity of clinical isolates of human CMV to 1,3-dihydroxy-2-propoxylmethyl guanine. J Infect Dis 152:832-834.

211. Prasad V, Shah V and Knight P 1983. Importance of media selection in establishment of *in vitro-in vivo* relationship for quinidine gluconate. Int J Pharm 13:1-7.

212. Quigley HA, Pollack IP, Harbin TS Jr 1975. Pilocarpine Ocuserts®: Long-term clinical trials and selected pharmacodynamics. Arch Ophthalmol 93:771-775.

213. Rall TW 1980. Central nervous system stimulants, In: The Pharmacological Basis of Therapeutics, 6th ed., (Goodman A and Gilman G, eds.), Macmillan Publishing Co. Inc, NY, USA, 592-607.

214. Rapoport SI 1977. Osmotic opening of blood-brain and blood-ocular barriers. Exp Eye Res Suppl:499-509.

215. Ratkowsky D 1983. Nonlinear Regression Modeling. Marcel Dekker, NY, USA.

216. Reddy IK and Ganesan MG 1996. Ocular therapeutics and drug delivery: An Overview, In: Ocular Therapeutics and Drug Delivery: A Multi-Disciplinary Approach (Reddy IK, ed.), Technomic Publishing Co., Inc. Lancaster, PA, USA, 3-29.

217. Reed AM, Gilding DK 1981. Biodegradable polymers for use in surgery-poly(glycolic)poly(lactic acid) homo and copolymers 2. In vitro degradation. Polymer 22:494-498.

218. Rippie EG 1990. Compression of solids and compressed dosage forms, In:, Encyclopedia of Pharmaceutical Technology (Swarbrick J and Boylan JC, eds.), Marcel Dekker, NY, USA, 149-165.

219. Rojanasakul Y, Wang LY, Bhat M, Glover DD, Malanga CJ and Ma JKH 1992. The transport barrier of epithelia: A comparative study on membrane permeability and charge selectivity in the rabbit. Pharm Res 9:1029-1034.

220. Ruiz J, Busnel J, Benoit J 1990. Influence of average molecular weights of poly(DL-lactic acid-co-glycolic acid) copolymers 50/50 on phase separation and in vitro drug release from microspheres. Pharm Res 7:28-34.

221. Sanborn GE, Anand R, Torti RE, Nightingale SD, Cal SX, Yates B, Ashton P, Smith T 1992. Sustained-release ganciclovir therapy for treatment of cytomegalovirus retinitis: Use of an intravitreal device. Arch Ophthalmol 110:188-195.

222. Sansdrap P, Moes AP 1997. *In vitro* evaluation of the hydrolytic degradation of dispersed and aggregated poly(D,L-lactide-co-glycolide) microspheres. J Control Rel 43:47-58.

223. Schoenwald RD 1990. Ocular drug delivery: Pharmacokinetic considerations Clin Pharmacokinet 18:2555269.

224. Schoenwald RD 1993. Ocular pharmacokinetics/pharmacodynamics. In: Ophthalmic Drug Delivery System (Mitra AK, ed.), Marcel Dekker, NY, USA, 833110.

225. Schoenwald RD 1993. Pharmacokinetics in ocular drug delivery. In: Biopharmaceutics of Ocular Drug Delivery (Edman P, ed.), CRC Press, Bato Raton FL, USA, 1599191.

226. Schoenwald RD and Huang HS 1983. Corneal penetration behavior of fl-blocking agents I: physicochemical factors. J Pharm Sci 72:1266-1272.

227. Schoenwald RD and Ward R 1978. Relationship between steroid permeability across excised rabbit cornea and octanol-water partition coefficients. J Pharm Sci 67:786-788.

228. Schrank-Junghani H, Bier HP, Sucker H 1984. The measurement of die wall forces to determine the minimum concentration of lubricant needed for tablet formulations. Acta Pharm Technol 30:224-234.

229. Schwarz G 1978. Estimating the dimension of a model. Annals of Stat 6:461-464.

230. Shah VP, Prasad VK, Alston T, Cabana BE, Gural RP and Meyer MC 1983. Phenytoin I: In vitro correlation for 100mg phenytoin sodium capsules. J Pharm Sci 72:306-308.

231. Shameem M, Lee H, Burton K, Thanoo BC, DeLuca PP 1999. Effect of gamma-irradiation on peptide-containing hydrophilic poly(D,L-lactide-co-glycolide) microspheres. PDA J Pharm Sci Technol 53:309-313.

232. Shenderova TG, Burke SP, Schwendeman 1999. The acidic microclimate in poly(lactide-co-glycolide) microspheres stabilizes camptothecins. Pharm Res 16:241-248.

233. Shotton E, Hersey JA, Wray PE 1976. Compaction and compression, In: The Theory and Practice of Industrial Pharmacy, 2nd ed., (Lachman L, Lieberman HA and Kanig JL, eds.), Lea & Febiger, PA, USA, 296-320.

234. Shotton E, Obiorah BA 1975. Effect of physical properties on compression characteristics. J Pharm Sci 64:1213-1215.

235. Sieg JW and Robinson JR 1977. Vehicle effects on ocular drug bioavailability II: Evaluation of pilocarpine. J Pharm Sci 66:1222-1228.

236. Silva-Junior AA, Formariz TP, Scarpa MV, Oliveira AG 2006. J Basic Appl Pharm Sci 27:119-126.

237. Sintzel MB, Merkli A, Tabatabay C, Gurny R 1997. Influence of irradiation sterilization on polymers used as a drug carriers-A review. Drug Dev Ind Pharm 23:857-879.

238. Smee, DF 1983. Anti-herpes activity of the acyclovir nucleoside 1,3-dihydroxy-2-propoxylmethyl guanine. J Antimicrob Agents Chemother 23:676-682.

239. Smith TJ, Pearson PA, Blandford DL, Brown JD, Goins KA, Hollins JL, Schmeisser ET, Glavinos P, Baldwin LB, Ashton P 1992. Intravitreal sustained-release ganciclovir. Arch Ophthalmol 110:255-258.

240. Spenlehauer G, Vert M, Benoit JP, Boddaert A 1989. *In vitro* and *in vivo* degradation of poly(D,L-lactide/glycolide) type microspheres made by solvent evaporation method. Biomat 10:557-563.

241. Stevels WM, Ankone MJK, Kijkstra PJ, Feijen J 1996. Stereocomplex formation in ABA triblock copolymers of poly(lactide) (A) and poly(ethylene glycol) (B). Macromol Chem Phys 196:3687-3694.

242. Strijbos S 1976. Friction between a powder compact and a metal wall. Sci Ceram 8:415-428.

243. Strijbos S, Rankin P, Wassink RJK, Bannink J, Oudemans GJ 1977. Stresses occurring during one-sided die compaction of powders. Powder Technol 18:187-200.

244. Sultana Y, Aqil M, Ali A 2006. Ion-activated, gelrite-based *in situ* ophthalmic gels of pefloxacin mesylate: Comparison with conventional eye drops. Drug Deliv 13:215-219.

245. Sultana Y, Jain R, Aqil M, Ali A 2006. Review of ocular drug delivery. Curr Drug Deliv 3:207-217.

246. Summers L, Slingsby C, White H, Narebor M, Afoss D, Miller L, Mahadevan D, Lindley P, Driessen H and Blundell TL 1984. The molecular structure and interactions of bovine and human d-crystallines, In: Int. Symp. On Human Cataract Formation, 21936, Pitman Press, Bath, UK.

247. Tan DT, Chee SP, Lim L, Lim AS 1999. Randomized clinical trial of a new dexamethasone delivery system (Surodex®) for treatment of post-cataract surgery inflammation. Ophthalmol 106:223-231.

248. Thompson RA 1981. Mechanics of powder pressing: I. Model for powder densification. Am Ceram Soc Bull 60:237-243.

249. Tocci, MJ, Livelli TJ, Perry HC, Crumpacker CS, Field AK 1984. Effects of the nucleoside analogue 2-nor-2'-deoxyguanosone on human cytomegalovirus replication. Antimicrob Agents Chemother 25:247-252.

250. Train D, Carrington JN, Hersey JA 1962. The pressing of polymers in cylindrical dies. Ind Chem 38:77-80.

251. Unckel H 1945. Vorgange beim pressen von metallpulvern. Arch Eisenhuttenwesen 18:161-167.

252. Uno K, Ohtori A and Tojo K 1994. Drug transport in the vitreous body of rabbits *in vitro*. J Eye (Atarashii Ganka) 11:607-609.

253. Urtti A and Salminen L 1993. Minimizing systemic absorption of topically administered ophthalmic drugs. Sur Ophthalmol 37:4355456.

254. Urtti A, Rouhiainen H, Kaila T and Saano V 1994. Controlled ocular timolol delivery: systemic absorption and intraocular pressure effects in humans. Pharm Res11:1278-1282.

255. US FDA Guidance for Industry 1997. Extended release oral dosage forms: Development, evaluation and application *in vitro*/*in vivo* correlations. US Department of Health and Human Services, Food and Drug Administration, Centre for Drug Evaluation and Research.

256. Ussery FM, Gibson SR, Conklin RH et al 1988. Intravitreal ganciclovir in the treatment of AIDS-associated cytomegalovirus retinitis. Ophthalmol 95:640-648.

257. Van Ooteghem M 1995. In: Preparations Ophtalmiques, ed. Galenica, Technique and documentation. Lavoisier, Paris.

258. Van Santvliet and Ludwig A 2004. Determinants of eye drop size. Surv Ophthalmol 49:197-213.

259. Velez G and Whitcup SM 1999. New developments in sustained release drug delivery for the treatment of intraocular disease. Br J Ophthalmol 83:1225-1229.

260. Veloso AA, Zhu Q, Herrero-Vanrell R, Refojo MF 1997. Ganciclovir-loaded polymer microspheres in rabbit eyes inoculated with human cytomegalovirus. Invest Ophthalmol Vis Sci 38:665-675.

261. Visor GC 1994. Drug design strategies for ocular therapeutics. Adv Drug Deliv Rev 14:269-279.

262. Volland C, Woll M, Kissel T 1994. The influence of terminal γ-sterilization on captopril containing poly(DL-lactide-co-glycolide) microspheres. J Control Rel 31:293-305.

263. Vyazovkin S, Dranca I 2005. Physical stability and relaxation of amorphous indomethacin. J Phys Chem B 109:18637-18644.

264. Vyazovkin S, Dranca I 2006. Probing beta relaxation in pharmaceutically relevant glasses by using DSC. Pharm Res 23:422-428.

265. Wagner JG and Nelson E 1964. Kinetic analysis of blood levels and urinary excretion in the absorptive phase after single doses of drug. J Pharm Sci 53:1392-1403.

266. Weiner AL 1994. Polymeric drug delivery systems for the eye, In: Polymeric site specific pharmacotherapy (Domb AJ, ed.), John Wiley & Sons Ltd, NY, USA, 316-346

267. Weiner AL, Carpenter-Green SS, Soehngen EC, Lenk RP, Popescu MC 1985. Liposome-collagen gel matrix: A novel sustained drug delivery system. J Pharm Sci 74:922-925.

268. Weiner AL, Missel PJ, Chastain JE, Yaacobi Y, Mitra AK, Kompella UB et al 2006. Administration of anecortave acetate in a finite element physiologic ocular pharmacokinetic model. Invest Ophthalmol Vis Sci 47: ARVO E-Abs 5084.

269. Weiner AL, Sinnett K, Johnson S 1995. Tack for intraocular drug delivery and method for inserting and removing the same. US Patent 5,466,233.

270. Woo L, Sandford CL 2002. Comparison of electron beam irradiation with gamma processing for medical packaging materials. Radiat Phys Chem 63:845-850.

271. Wood JH 1966. *In vitro* evaluation of physiological availability of compressed tablets. Pharm Acta Helv 42:129-132.

272. Wray PE 1992. The physics of compaction revisited. Drug Dev Ind Pharm 18:627-658.

273. Yamashita K, Nakate T, Okimoto K, Ohike A, Tokunaga Y, Ibuki R, Higaki K, Kimura T 2003. Int J Pharm 267:79-91.

274. Yang CS, Khawly JA, Hainsworth DP, Chen SN, Ashton P, Guo H, Jaffe GJ 1998. An intravitreal sustained-release triamcinolone and 5-fluorouracil co-drug in the treatment of experimental proliferative vitreoretinopathy. Arch Ophthalmol 116:69-77.

275. Yasukawa T, Kimura H, Kunou N, Miyamoto H, Honda Y, Ogura Y, Ikada Y 2000. Biodegradable scleral implant for intravitreal controlled release of ganciclovir. Arch Clin Exp Ophthalmol 238:186-190.

276. Yasukawa T, Ogura Y, Sakurai E, Tabata Y, Kimura H 2005. Intraocular sustained drug delivery using implantable polymeric devices. Adv Drug Del Rev 57:2033-2046.

277. Yasukawa T, Ogura Y, Tabata Y, Kimura H, Wiedemann P, Honda Y 2004. Drug delivery systems for vitreoretinal diseases. Prog Retinal Eye Res 23:253-281.

278. Yolles S, Eldridge JE, Woodland JHR 1970. Sustained delivery of drugs from polymer/drug mixtures. Polym News 1:9-15.

279. Yonemochi E, Hoshino T, Yoshihashi Y, Terad K 2005. Thermochim Acta 432:70-75.

280. Yoshioka S, Aso Y, Kojima S 1995. The effect of γ-irradiation on drug release from poly(lactide) microspheres. Rad Phys Chem 46:281-285.

281. Zhang X, Wyss UP, Pichora D Goosen MFA 1992. An investigation of poly(lactic acid) degradation. J Bioact Compat Polym 9:80-100.

282. Zhou T, Lewis H, Foster RE, Schwendeman SP 1998. Development of a multiple-drug delivery implant for intraocular management of proliferative vitreoretinopathy. J Control Rel 55:281-295.

Appendix A: Research Publications

1: An *in vitro* study of the design and development of a novel donut-shaped minitablet for intraocular implantation, Yahya E. Choonara, Viness Pillay, Trevor R. Carmichael and Michael P. Danckwerts, *International Journal of Pharmaceutics, 310, 15-24, 2006.*

Available online at www.sciencedirect.com
SCIENCE DIRECT®
International Journal of Pharmaceutics 310 (2006) 15–24
INTERNATIONAL JOURNAL OF PHARMACEUTICS
www.elsevier.com/locate/ijpharm

An in vitro study of the design and development of a novel doughnut-shaped minitablet for intraocular implantation

Yahya E. Choonara [a], Viness Pillay [a], Trevor Carmichael [b], Michael P. Danckwerts [a,*]

[a] University of the Witwatersrand, Department of Pharmacy and Pharmacology, 7 York Road, Parktown 2193, Johannesburg, Gauteng, South Africa
[b] Department of Ophthalmology, Faculty of Health Sciences, 7 York Road, Parktown 2193, Johannesburg, Gauteng, South Africa

Received 26 August 2005; received in revised form 13 October 2005; accepted 15 October 2005
Available online 7 February 2006

Abstract

A novel doughnut-shaped minitablet (DSMT) was developed and evaluated as a biodegradable intraocular drug delivery system for rate-modulated delivery of antiviral bioactives. The DSMT device was manufactured using a special set of punches fitted with a central-rod in a Manesty tableting press. The DSMT device released the antiretrovirals foscarnet and ganciclovir at a first-order rate. The erosion kinetics was assessed by gravimetric analysis and scanning electron microscopy. The device gradually eroded when immersed in simulated vitreous humor (SVH) (pH 7.4, 37 °C) and released bioactives in a sustained manner. The novel geometric design and veracity of the DSMT device was retained even after 24 weeks of erosion. When considering the duration of the bioactive released from the DSMT device, it was found that by the careful selection of the type and concentration of polymer employed in formulating the DSMT device, it was possible to produce a device that could release drug for any period up to 12 months.

Keywords: Cytomegalovirus retinitis; Doughnut-shaped minitablet (DSMT); Extended release; Polylactide-*co*-glycolide (PLGA); Biodegradation; Intraocular implantation

1. Introduction

Disease due to cytomegalovirus (CMV) is among the most common opportunistic infections in patients with the acquired immune deficiency syndrome (AIDS). The virus can give rise to multiple organ disease and may cause infections such as colitis, esophagitis, encephalitis and pneumonitis, but retinitis accounts for 75–85% of CMV infections in patients (Jabs et al., 2003). CMV retinitis (CMV-R) causes severe visual loss and needs medical treatment for an optimal clinical outcome. It is a serious sight-threatening infection that occurs in approximately 25% of patients with AIDS. If left untreated the disease follows a relentless course which inevitably results in blindness (Smith et al., 1992).

Prospective epidemiological studies have estimated the risk of CMV-R in patients with CD4+ counts less than 100 cells/mm^3 at approximately 10% per year, and in those with CD4+ counts less than 50 cells/mm^3 at approximately 20% per year. Patients with CD4+ counts above 200 cells/mm^3 have rarely developed CMV-R. However, this could change in the future with widespread use of highly active antiretroviral therapy that dramatically changes absolute CD4+ counts (Lin et al., 2002; Holbrook et al., 2003).

Both eyes can be infected at different times with more than one focus of retinitis. Retina that is destroyed by the virus is irreversibly lost and blindness occurs as soon as areas that are critical for vision, including the macula, maculopapillary nerve fibre layer bundle and optic nerve head, become infected (Holland et al., 1987, 1989). In the early stages of CMV-R, patients may notice changes in vision, floating particles or loss of peripheral vision. The disease is not associated with light sensitivity, pain, or redness of the eye. Patients with AIDS should be screened regularly as early diagnosis and efficient management are essential to preserve visual function, and preservation of visual function is a major objective to assure good quality of life (Yasukawa et al., 2000).

2: Studies on a novel donut-shaped minitablet for intraocular drug delivery, Yahya E. Choonara, Viness Pillay, Trevor R. Carmichael and Michael P. Danckwerts, *AAPS PharmSciTech, 8(4), 1-7, 2007.*

AAPS PharmSciTech 2007; 8 (4) Article 118 (http://www.aapspharmscitech.org).

Studies on a Novel Doughnut-Shaped Minitablet for Intraocular Drug Delivery

Received: March 1, 2007; Final Revision Received: August 1, 2007; Accepted: August 1, 2007; Published: December 28, 2007

Yahya E. Choonara,[1] Viness Pillay,[1] Trevor Carmichael,[2] and Michael P. Danckwerts[1]

[1]University of the Witwatersrand, Department of Pharmacy and Pharmacology, Medical School, Johannesburg, Gauteng, South Africa

[2]University of the Witwatersrand, Department of Ophthalmology, Medical School, Johannesburg, Gauteng, South Africa

ABSTRACT

The objective of this study was to evaluate the effect of 2 independent formulation variables on the drug release from a novel doughnut-shaped minitablet (DSMT) in order to optimize formulations for intraocular drug delivery. Formulations were based on a 3^2 full-factorial design. The 2 independent variables were the concentration of Resomer (% wt/wt) and the type of Resomer grade (RG502, RG503, and RG504), respectively. The evaluated response was the drug release rate constant computed from a referenced marketed product and in vitro drug release data obtained at pH 7.4 in simulated vitreous humor. DSMT devices were prepared containing either of 2 model drugs, ganciclovir or foscarnet, using a Manesty F3 tableting press fitted with a novel central-rod, punch, and die setup. Dissolution data revealed biphasic drug release behavior with 55% to 60% drug released over 120 days. The inherent viscosity of the various Resomer grades and the concentration were significant to achieve optimum release rate constants. Using the resultant statistical relationships with the release rate constant as a response, the optimum formulation predicted for devices formulated with foscarnet was 70% wt/wt of Resomer RG504, while 92% wt/wt of Resomer RG503 was ideal for devices formulated with ganciclovir. The results of this study revealed that the full-factorial design was a suitable tool to predict an optimized formulation for prolonged intraocular drug delivery.

KEYWORDS: PLGA, kinetic modeling, controlled release, factorial design.

INTRODUCTION

Response surface methodology (RSM) is a rapid technique used to empirically derive a functional relationship between an experimental response and a set of input variables. It reduces the number of experimental runs necessary to establish a mathematical trend in the experimental design allowing for determination of the optimum level of experimental factors required for a given response.[1] Reducing the number of experiments by optimizing a formulation during development of a drug delivery device may also lead to significant reductions in production costs. RSM is widely used to optimize process parameters, especially in determining optimum conditions for investigations in large-scale drug design and delivery.[2] It has been applied to pharmaceutical systems such as the preparation of particulate carriers like gelisphere matrices[3] and microspheres.[4] It is necessary to have a clear understanding of how preparation conditions and inherent characteristics of excipients employed in pharmaceutical formulations are influenced by potential interactions between various factors in order to optimize a formulation.

Intravitreal implants have been investigated for the controlled release of antiviral bioactives to treat posterior segment eye disease. They can be fabricated from poly(lactide-co-glycolide) (PLGA), a biodegradable and biocompatible polymer, and implanted into the vitreous cavity of the eye with the advantage of being degraded and eliminated from the body once its drug load has been depleted. This polymer has been used for the preparation of various implants, sustained-release preparations, and inserts for their administration through parenteral, oral, dermatological, pulmonary, nasal, and ocular routes.[4-7]

Intravitreal implants of ganciclovir have also been demonstrated to be more effective than intravenous and intravitreal injections for the treatment of ocular pathologies such as cytomegalovirus retinitis (CMV-R), which can lead to irreversible blindness. Successive intraocular injections are poorly tolerated with risks such as endophthalmitis, cataract, retinal detachment, and vitreous hemorrhage. These inconveniences have been overcome by the use of drug delivery systems that are able to promote prolonged release of the bioactive into the vitreous cavity such as biodegradable implants. Implants, however, could constitute a poor delivery device if control of the release of the bioactive material was poor. By modifying the implants' formulation parameters, such as the type and concentration of polymer employed, it is possible to exert control on the in vitro release profile.

In a previous study by Sanborn and coworkers,[8] developed a nonbiodegradable intraocular implant, namely, the Vitrasert device, which was approved by the United States Food and Drug Administration (FDA) in March 1996. The device

Corresponding Author: Viness Pillay, University of the Witwatersrand, Department of Pharmacy and Pharmacology, Medical School, 7 York Road, Parktown, 2193, Johannesburg, Gauteng, South Africa. Tel: +2711 717-2274; Fax: +2711 642-4355; E-mail: viness.pillay@wits.ac.za

3: A review of implantable intravitreal drug delivery technologies for the treatment of posterior segment eye diseases, Yahya E. Choonara, Viness Pillay, Michael P. Danckwerts, Trevor R. Carmichael and Lisa C. du Toit, *Journal of Pharmaceutical Sciences, in press, October, 2009.*

JPS09-336.R2(21987)

REVIEW

A Review of Implantable Intravitreal Drug Delivery Technologies for the Treatment of Posterior Segment Eye Diseases

YAHYA E. CHOONARA,[1] VINESS PILLAY,[1] MICHAEL P. DANCKWERTS,[1] TREVOR R. CARMICHAEL,[2] LISA C. DU TOIT[1]

[1]Department of Pharmacy and Pharmacology, University of the Witwatersrand, 7 York Road, Parktown, 2193, Johannesburg, Gauteng, South Africa

[2]Department of Ophthalmology, University of the Witwatersrand, 7 York Road, Parktown, 2193, Johannesburg, Gauteng, South Africa

Received 27 May 2009; accepted 16 September 2009

Published online ? ? ? ? in Wiley InterScience (www.interscience.wiley.com). DOI 10.1002/jps.21987

ABSTRACT: Intravitreal implantable device technology utilizes engineered materials or devices that could revolutionize the treatment of posterior segment eye diseases by affording localized drug delivery, responding to and interacting with target sites to induce physiological responses while minimizing side-effects. Conventional ophthalmic drug delivery systems such as topical eye-drops, systemic drug administration or direct intravitreal injections do not provide adequate therapeutic drug concentrations that are essential for efficient recovery in posterior segment eye disease, due to limitations posed by the restrictive blood-ocular barriers. This review focuses on various aspects of intravitreal drug delivery such as the impediment of the blood-ocular barriers, the potential sites or intraocular drug delivery device implantation, the various approaches employed for ophthalmic drug delivery and includes a concise critical incursion into specialized intravitreal implantable technologies for the treatment of anterior and posterior segment eye disease. In addition, pertinent future challenges and opportunities in the development of intravitreal implantable devices is discussed and explores their application in clinical ophthalmic science to develop innovative therapeutic modalities for the treatment of various posterior segment eye diseases. The inherent structural and functional properties, the potential for providing rate-modulated drug delivery to the posterior segment of the eye and specific development issues relating to various intravitreal implantable drug delivery devices are also expressed in this review.
 J Pharm Sci 9999:1–25, 2009
Keywords: intravitreal implants; device technology; posterior segment eye disease; blood-ocular barriers; localized drug delivery; biomaterials; biodegradable polymers; vitreous humor

INTRODUCTION

The design of ophthalmic drug delivery systems is a unique challenge that is restricted by the anatomical position of the eye as well as the

Correspondence to: Viness Pillay (Telephone: 27-11-717-2274; Fax: 27-86-517-6890; E-mail: viness.pillay@wits.ac.za)
Journal of Pharmaceutical Sciences, Vol. 9999, 1–25 (2009)

4: Characterization of a donut-shaped minitablet: The effects of irradiation sterilization on the physical and chemical stability of the device, Yahya E. Choonara, Viness Pillay, Michael P. Danckwerts, Riaz A. Khan, Lisa C. du Toit and Trevor R. Carmichael, *AAPS PharmSciTech, submitted, October 2009.*

5: *In vivo* evaluation of a novel donut-shaped minitablet in the rabbit eye model, Yahya E. Choonara, Viness Pillay, Michael P. Danckwerts, Trevor R. Carmichael, Lisa C. du Toit, Carla Wanblad and Simon J. Naylor, *Journal of Controlled Release, submitted, October 2009.*

6: Exploratory data analysis from a donut-shaped minitablet device employing compartmental and non-compartmental pharmacokinetic modeling analysis, Yahya E. Choonara, Viness Pillay, Michael P. Danckwerts, Trevor R. Carmichael and Lisa C. du Toit, *Current Drug Delivery, submitted, October 2009*

Appendix B: Conference abstracts presented

1: American Association of Pharmaceutical Scientists, Los Angeles Convention Centre, Los Angeles, California, United States of America, November 16-20, 2009.

The Influence of Gamma-Irradiation Sterilization on a PLGA-based Intraocular Drug Delivery Device

Y. E. Choonara[1], V. Pillay[1], M. P. Danckwerts[1], T. R. Carmichael[1]
[1]University of the Witwatersrand

Purpose:

This study characterized the effects of γ-irradiation on a PLGA-based Doughnut-Shaped MiniTablet (DSMT).

Methods:

Novel tablet tooling comprising a central-rod enabled a ganciclovir (GCV)-loaded doughnut-shaped PLGA device to be compressed on a Manesty F3 tableting press. The devices were sterilized in sealed polyurethane containers (γ-irradiation; Co-60; 25kGy) prior to analysis. FTIR spectroscopy was performed on native GCV and PLGA, GCV-loaded DSMTs and 1:1 GCV-PLGA physical mixtures (400-4000cm^{-1}). Porositometry involved sample degassing with N_2 and reducing the temperature to LN_2 (-196°C) for gas adsorption. Adsorption isotherms and T-plots were generated. Textural profile analysis assessed the Matrix Hardness (MH) and Fracture Energy (FE) and thermal characterization was performed on samples ramped between 30-400°C (N_2 atmosphere).

Results:

The transition to compact surface morphologies of the γ-irradiated DSMTs altered the micromechanical properties (producing lamellar crystalline structures) due to chain folding and shears slip of H-bonded polymeric sheets during irradiation. T-plot volumes ranged between -0.000892 and -0.001076 for the non-sterilized and sterilized DSMTs respectively, revealing that porosity in the micropore region was not affected. Non-sterilized DSMTs had a larger BJH_a=315.31Å and lower FE and MH values (FE=148.18±2.00N/m; MH=26.53±0.91N) than the sterilized DSMTs (BJH_a=234.60Å) indicating the excess energy absorbed during sterilization resulting in more crystalline matrices. Thermal profiles had exotherms characteristic of disordered crystallization of GCV (150-160°C; ΔH=+133.18J/g) and an endotherm attributed to decomposition after melting (360-380°C; ΔH=−163.85J/g). A T_g of PLGA (50-60°C) and an enthalpy of relaxation (0.05mW/mg) and degradation (360-380°C) was also noted. Physical-mixtures of GCV and PLGA also had a T_g (50-60°C), followed by a hydration exotherm (150-160°C). For the sterilized DSMTs, an exotherm resulting from ionization during γ-irradiation was observed (340-360°C). FTIR spectrograms revealed fingerprint molecular groups of carboxylic OH- (2500-3500cm^{-1}), tertiary amines (3527cm^{-1}), CH_2–N stretching (2705cm^{-1}) and C-O (1708cm^{-1}), corresponding to GCV. For PLGA the absorption bands at 1759cm^{-1}, and axial stretching of sp^2 and sp^3 carbons (2900-3000cm^{-1}) were assigned in agreement with thermal data indicating that no interaction between GCV and PLGA after γ-irradiation.

Conclusions:

Characterization of the γ-irradiated DSMT devices revealed that the affected transitions favored the DSMT to be employed as an implantable intraocular device.

2: American Association of Pharmaceutical Scientists, Atlanta World Congress Centre, Atlanta, Georgia, United States of America, November 16-20, 2008.

A biodegradable Doughnut-Shaped Minitablet for sustained intraocular release of ganciclovir

Y. E. Choonara[1], V. Pillay[1], M. P. Danckwerts[1], T. Carmichael[1], C. Wanblad[1], S. Naylor[2], V. M. Ndesendo[1]
[1]University of the Witwatersrand, [2]National Health Laboratory Services

Purpose.

To evaluate the toxicity and potential of using a biodegradable doughnut-shaped minitablet (DSMT) for intraocular sustained release of ganciclovir (GCV) in a rabbit eye model.

Methods.

Specially designed core-rod tooling was used to directly compress GCV-loaded PLGA matrices into doughnut-shaped minitablets (5×2mm). Six New Zealand White Albino rabbits were used for *in vivo* drug release studies. A DSMT was implanted through the pars plana of the right eyes. Vitreous samples from the left eyes were used as controls. GCV concentrations from vitreous samples obtained from euthanized rabbits at 3, 7, 14, 28, 48 and 70 days after implantation was measured by Ultra Performance Liquid Chromatography. Enucleated test and control eyes were histopathologically examined to ascertain the effect of the DSMT device on ocular tissues. Eyes were fixed in 10% buffered formalin for 24 hours, then bisected and processed in their entirety for histological assessment employing a hemotoxylin and eosin staining technique.

Results.

Semi-logarithmic plots revealed that GCV concentrations in the vitreous initially exceeded the therapeutic range (ED_{50}) for viral suppression in the human eye (0.10-2.75µg/mL) and thereafter remained within the therapeutic window for a period of 70 days after implantation. In contrast with previous *in vitro* release studies, the *in vivo* study displayed a reduced initial burst with 20% GCV released at day 3 followed by a steady phase of diffusional drug release of 69% after 70 days. Histological studies revealed a progressive inflammatory response centered predominately around the ciliary body and in the posterior chamber. An initial acute inflammatory response was noted with haemorrhage, oedema and neutrophilic infiltration that became chronic with lymphocytes, eosinophils, plasma cells and fibroblasts. The haemorrhage and oedema subsided by day 28. After 70 days, a minimal residual inflammatory response was noted and of significance there was no evidence of sympathetic ophthalmitis, chronic fibrosis or damage to ocular tissue.

Conclusion.

Results revealed that no ocular tissue toxicity was observed as a result of intraocular implantation of the DSMT device and therefore may be promising for the sustained intravitreal delivery of GCV.

3: 29th Annual Conference of the Academy of Pharmaceutical Sciences of South Africa, Hunters Rest Resort, Magaliesburg, Johannesburg, South Africa, September 22-26, 2008.

A ganciclovir-loaded intraocular device implanted in rabbit eyes for the potential treatment of human cytomegalovirus retinitis

Yahya E. Choonara[1], Viness Pillay[1]*, Michael P. Danckwerts[1], Trevor R. Carmichael[2], Simon Naylor[3] and Carla Wanblad[3]

[1]University of the Witwatersrand, Department of Pharmacy and Pharmacology, 7 York Road, Parktown, 2193, Johannesburg, South Africa

[2]University of the Witwatersrand, Department of Neurosciences, 7 York Road, Parktown, 2193, Johannesburg, South Africa

[3]University of the Witwatersrand, Department of Anatomical Pathology, 7 York Road, Parktown, 2193, Johannesburg, South Africa

Introduction

An *in vivo* investigation of a biodegradable doughnut-shaped minitablet (DSMT) containing ganciclovir (GCV) in a New Zealand White Albino rabbit eye model.

Methods

Specially designed punches were used to manufacture the DSMT. PLGA was used as the GCV delivery platform as it displayed superior control of GCV release *in vitro*. Twelve rabbits were used for the *in vivo* studies. The DSMT was implanted through the pars plana/peripheral retina of the right eye and sutured with 9-0 nylon. Vitreous from the left eye was used as controls. Possible adverse effects of the DSMT on ocular tissues were assessed clinically for changes in the vitreous (vitreous haze) and retina (oedema, chorio-retinal atrophy, vascular changes, exudative changes, and necrosis) adjacent to the implanted device, histological examination, slit lamp examination, measurement of intraocular pressure and indirect ophthalmoscopy. The *ex vivo* micro-environmental pH variation in close proximity (≤5mm from the eroding surface) of the DSMT was monitored with a Multi-Purpose Titrator (MPT-2) equipped with a rapid response glass pH microelectrode (Malvern Instruments, UK) calibrated with buffered control Ringer solutions. The electrodes were adjusted to cover a buffer range from pH 6.1-7.5 with a linear Nernstian response. Variations in pH were evaluated from pH-Time profiles. Two rabbits were euthanized on days 3, 7, 14, 28, 48 and 70. The residual devices, vitreous, plasma samples and ocular tissue were retrieved and stored at -70ºC prior to GCV concentration analysis by 3D UPLC technology (Waters® Acquity UPLC™ System, Manchester, UK). The recovery of GCV spiked into placebo vitreous and serum samples was 97.4-105.0% indicating a valid evaluation of GCV concentration in the vitreous and serum.

Results

Standard curves were used to assess the quantity of GCV released (R^2=0.99). *In vivo* release profiles were obtained by computing the percentage of GCV released versus the initial content loaded. In contrast to previous *in vitro* release studies, the *in vivo* release displayed a reduced initial burst with 20% GCV released at day 3 followed by a steady phase of diffusional release of 40% by 28 days, 50% by day 48 and 69% after 70 days in the rabbit eye model. The DSMT was well tolerated in the eye. Of the twelve rabbits, three had small postoperative hyphaemas, visible after the surgery and for up to a week, two had vitreous hemorrhages and one had a retinal detachment by two weeks. There were no infections or inflammation and no cataract formation. Semi-logarithmic plots of GCV revealed that GCV concentrations were maintained between the 50% effective dose (ED_{50}) for human cytomegalovirus replication over 70 days.

Conclusions

The device could be produced and inserted reasonably easily. It has shown to release GCV steadily for a period of up to 70 days *in vivo* by which time 69% of GCV had been released.

4: 29th Annual Conference of the Academy of Pharmaceutical Sciences of South Africa, Hunters Rest Resort, Magaliesburg, Johannesburg, South Africa, September 22-26, 2008.

Development of a highly sensitive UPLC assay method for the determination of ganciclovir in rabbit serum and vitreous humour

Yahya E. Choonara, Viness Pillay*, Michael P. Danckwerts and Trevor R. Carmichael
University of the Witwatersrand, Department of Pharmacy and Pharmacology, 7 York Road, Parktown, 2193, Johannesburg, South Africa

Introduction
To develop a highly sensitive quantitative assay method to accurately determine ganciclovir (GCV) concentrations in the vitreous and serum of New Zealand White Albino rabbits employing semi-automated Ultra Performance Liquid Chromatography (UPLC) for the simultaneous three dimensional analyses of GCV and acyclovir (ACV) as an internal standard.

Methods
GCV spiking solutions were prepared (5%$^{m}/_{v}$) ranging from 0.1-0.5mg/mL. For the calibration standards 100µL of each spiking solution and ACV (1%$^{m}/_{v}$) were added to 1.5mL polypropylene tubes containing 250µL of either blank rabbit vitreous or serum previously thawed and centrifuged at 15000xg for 10 minutes and 0.5mL acetonitrile. A set of 5 calibration standards ranging from 1.0-5.0mg/mL of GCV in rabbit vitreous and serum was generated for preparing standard curves and for validation runs, precision and accuracy analysis. Frozen study samples were thawed at room temperature (21±0.5°C) and centrifuged at 15000xg for 10 minutes. The sample matrices and the extraction process matched the calibration standard matrices. Aliquots (250µL) of vitreous and serum samples obtained from the rabbits were transferred to 1.5mL polypropylene tubes and vortexed for 15 seconds. The quantity of GCV in the vitreous and serum was determined by isocratic baseline separation of GCV and ACV using UPLC technology (Waters® Acquity UPLC™ System, Manchester, UK) comprising a binary solvent and sample manager, a BEH C_{18} column (1.7µm; 1×100mm) and a PDA detector set at 254nm. 3D chromatographic separation confirmed the complete separation of GCV and ACV. The mobile phase comprised 0.05M ammonium acetate/acetonitrile (96:4%$^{v}/_{v}$) with a flow rate of 0.4mL/min (6500psi; delta<20) and 1µL of sample injected onto the column at 21±°C.

Results
GCV and ACV were eluted at 1.0±0.2min and 1.2±0.2min after extraction from the vitreous and serum samples respectively. Assay method validation analysis revealed that intra- and inter-day precision and accuracy were satisfactory (R^2=0.99; CV=5.38%) over the range of GCV concentrations between 0.01-0.05mg/mL in rabbit vitreous and serum. The signal to noise ratio at the lower limit of quantification (0.01mg/mL) was >10. For validity testing of the linear regression model, the weighting factors were selected to be proportional to the reciprocal of the standard deviation which was optimal under least square estimation with all R^2 values >0.99. Three dimensional chromatographic analysis of blank vitreous and serum revealed no interfering peaks at the retention times and UV wavelengths of GCV and ACV (200-400nm). The accuracy of the assay method was evaluated from the calibration standards with mean recoveries ranging from 97.4-105.0%.

Conclusions
A simple UPLC method employing an isocratic gradient was validated for the determination of GCV in rabbit vitreous and serum samples. Run times were significantly shorter compared to typical HPLC. The validity of using rabbit vitreous and serum as a surrogate matrix for the preparation of calibration standards was demonstrated with complete recovery of GCV. The assay method has proved to be rugged, precise, accurate, and well suited to support further pharmacokinetic studies.

5: Faculty of Health Sciences Research Day, University of the Witwatersrand, Johannesburg, South Africa, 20th August 2008.

A Ganciclovir-Loaded Intraocular Device Implanted in Rabbit Eyes for the Potential Treatment of Human Cytomegalovirus Retinitis

Purpose

An *in vivo* investigation of a biodegradable doughnut-shaped minitablet (DSMT) containing ganciclovir (GCV) in a rabbit model.

Methods

Specially designed punches were used to manufacture the DSMT. PLGA was used as the GCV delivery platform. Six New Zealand White Albino rabbits were used for the study. The DSMT was implanted through the pars plana/peripheral retina of the right eye. Vitreous from the left eye was used as a control. Rabbits were euthanized on days 3, 7, 14, 28, 48 and 72. The residual devices and vitreous fluid were retrieved and stored (-70ºC) prior to UPLC analysis.

Results:

In contrast with previous *in vitro* release studies, the *in vivo* release displayed a reduced initial burst with 20% GCV released at day 3 followed by a steady phase of diffusional release over the remainder 67 days. The DSMT was well tolerated in the eye. Of the six rabbits, three had small postoperative hyphaemas, visible after the surgery and for up to a week. Two had vitreous haemorrhage and one of these had a retinal detachment by two weeks. There were no infections, inflammation and cataract formation.

Conclusions: The device has shown to release GCV steadily for a period of up to 72 days by which time 69% of the drug had been released.

6: Annual Meeting of the Association for Research in Vision and Ophthalmology, Fort Lauderdale, Florida, United States of America, April 27-May 1, 2008.

Control/Tracking Number: 08-A-3703-ARVO
Activity: Abstract
Current Date/Time: 12/11/2007 12:15:51 AM

An *In Vivo* Investigation Into A Novel Biodegradable Polymeric Device For Intravitreal Insertion

Author Block *T.R. Carmichael[1A], Y.E. Choonara[1B], V. Pillay[1B], M.P. Danckwerts[1B], S. Naylor[1C].*
[A]Ophthalmology, [B]Pharmacy, [C]Pathology, [1]University of the Witwatersrand, Johannesburg, South Africa.

Abstract:

Purpose: An *in vivo* investigation of a novel biodegradable doughnut-shaped minitablet (DSMT) containing ganciclovir (GCV) in a rabbit model. The *in vitro* study showing effective drug release from the device has been previously published.

Methods:
Specially designed punches were used to manufacture the DSMT. A high viscosity grade of Resomer® (RG 504) was used as it had showed the slowest release *in vitro*. Six New Zealand White Albino rabbits were used for the initial *in vivo* drug release studies. The DSMT was implanted through the pars plana/peripheral retina of the right eye and sutured with 9-0 nylon using a technique similar to that used for a Vitrasert® implant. Vitreous from the left eye was used as a control. The rabbits were euthanized on days 3, 7, 14, 28, 48 and 72 and the devices and vitreous were retrieved from enucleated eyes and stored at -70°C prior to GCV concentration analysis. Analyses were performed on a Waters Acquity UPLC™ system (Waters, Manchester, UK) consisting of an Acquity UPLC™ binary solvent manager and an Acquity UPLC™ sample manager. The recovery of GCV spiked into placebo vitreous samples during the extraction procedure was 102.69%, indicating the valid evaluation of the drug concentration in the vitreous.

Results:
A linear standard curve was used to assess the quantity of ganciclovir released from the device at various time points. A profile was obtained by measuring the percentage of GCV released versus the initial content in the device. In contrast with the previous *in vitro* release profiles, the *in vivo* release profile displayed a reduced initial burst with 20% GCV released at day 3 followed by a steady phase of diffusional release of about 40% by 28 days, about 50% by day 48 and 69% after 72 days in the rabbit eye model. The DSMT was well tolerated in the eye. Of the six rabbits, three had small postoperative hyphaemas, visible after the surgery and for up to a week. Two had vitreous hemorrhage and one of these had a retinal detachment by two weeks. There were no infections or inflammation and no cataract formation.

Conclusions: The device could be produced and inserted reasonably easily and cheaply and may be developed to release other medications such as steroid or antibiotics. It was shown to release GCV steadily for a period of up to 72 days by which time 69% of the drug had been released.

Author Disclosure Information: **T.R. Carmichael**, None; **Y.E. Choonara**, None; **V. Pillay**, None; **M.P. Danckwerts**, None; **S. Naylor**, None.
Reviewing Codes: 232 intravitreal/periocular local therapies
Presentation Preference: Poster #1, Paper #2
Keywords: 425 antiviral drugs; 759 vitreous; 503 drug toxicity/drug effects
Clinical Trial and Newsworthy:
Clinical Trial: No
Newsworthy: Yes
Clinicians: True

7: 28th Annual Conference of the Academy of Pharmaceutical Sciences of South Africa, Club Mykonos Resort, Langebaan, Cape Town, September 4-7, 2007.

An *in vivo* investigation into the intraocular implantation and histomorphological characterization of a novel biodegradable polymeric device

[1]Yahya E. Choonara, [1]Viness Pillay*, [1]Michael P. Danckwerts, [2]Trevor Carmichael, and [3]Simon Naylor
[1]*University of the Witwatersrand, Department of Pharmacy and Pharmacology, 7 York Road, Parktown, 2193, Johannesburg, South Africa*
[2]*University of the Witwatersrand, Department of Neurosciences, 7 York Road, Parktown, 2193, Johannesburg, South Africa*
[3]*University of the Witwatersrand, Department of Anatomical Pathology, 7 York Road, Parktown, 2193, Johannesburg, South Africa*

Purpose
This study focused on the *in vivo* implantation of a novel biodegradable doughnut-shaped minitablet (DSMT) and the histomophological assessment of post-surgical inflammatory infiltrates in the rabbit eye model.

Methods
Preparation of the device: Tablet tooling consisting of a lower and upper punch, die, and central-rod was used. Both punches contained a central hole for insertion of a rod that enabled a doughnut-shaped minitablet to be compressed. Devices were gamma sterilized at a minimum intensity of 25kGy with a routine dose reading of 27.2kGy.
In vivo study design: Six New Zealand White Albino rabbits were used. A placebo device was implanted into the left eye, and a ganciclovir-loaded DSMT into the right eye. Vitreous samples (2mL) and devices were removed at 3, 7, and 21 days after surgery from enucleated eyes and stored at -70°C for further analysis by UPLC. Retinal examinations were performed before implantation and euthanasia.
Surgical implantation of the device: The DSMT was placed into the vitreous via a pars plana (or peripheral retinal) incision. Under general anaesthesia, a supero-temporal or superonasal fornix-based conjunctival flap was formed and haemostasis achieved. A 5-6mm circumferential incision was made 2mm posterior to the limbus. The wound was opened to check for full-thickness penetration into the vitreous. Prolapsing vitreous was pushed back with the DSMT and the device was anchored with a 9-0 nylon suture passed through the scleral lip and then through the hole in the DSMT. Another two or three 9-0 nylon sutures were used to close the wound. The conjunctiva was repositioned and chloramphenicol ointment was applied. Positioning of the DSMT was monitored post-operatively.
Histomorphological characterization: Possible side effects of the DSMT on ocular tissues were assessed histologically. At each time point eyes were enucleated and immersed in 10% neutral buffered formalin. Globes were incised at the equator, dehydrated, infiltrated, embedded in paraffin, sectioned with a microtome and stained with hemotoxylin and eosin to assess the extent of inflammatory cell infiltrates.

Results
The DSMT appeared to be well tolerated and visible by indirect ophthalmoscopic analysis in the superotemporal quadrant of the eye. Clinically no changes were observed in the vitreous, retina and choroid. Retinal detachments or vitreous haemorrhages were absent for the duration of this study and preliminary histological examinations revealed no significant difference between control and treatment eyes except for poorly-formed multi-nucleated giant cell infiltrates around the nylon suture site. Furthermore, no focal disruption of the normal inner retinal architecture was observed. A non-significant inherent anterior chamber haemorrhage was detected in one rabbit due to intraocular pressure variation during surgery. In conclusion preliminary in vivo studies in the rabbit eye model revealed that implantation of the DSMT is non-toxic to ocular structures for a period within 42 days after implantation as confirmed by clinical observation and histopathological analysis.

8: Annual Meeting of the American Association of Pharmaceutical Scientists, San Antonio, Texas, United States of America, October 29-November 2, 2006.

Direct compression of a novel intra-ocular poly(DL-lactide-co-glycolide) (PLGA) implant: Investigation of the micromeritic parameters

Y.E. Choonara, V. Pillay and M.P. Danckwerts
Department of Pharmacy and Pharmacology, University of the Witwatersrand, 7 York Rd. Parktown 2193, Johannesburg, South Africa

Purpose:
The aim of this study was to investigate the suitability and effect of the micromeritic properties on the flowability of PLGA used in the formulation of a novel doughnut-shaped minitablet (DSMT) implant, employing direct compression.

Methods:
Particle size, shape, and flowability of various viscosity grades of PLGA (Resomer®) were studied. A sieving technique utilizing a series of stacked electroformed brass meshes was applied for elucidating a particle size distribution analysis. The rugosity of particles was characterized by scanning electron microscopy (Jeol-840 SEM). Flowability was evaluated using the convoluted angle of repose (θ) method. Particle size was analyzed via a frequency distribution polygon in order to visually represent the distribution of particle sizes amid various polymer samples examined. The geometric mean sizes (M) and geometric standard deviations (σ_g) were determined from cumulative distribution curves and the overall shape factor (S_o) was assessed; the interquartile coefficient of skewness ($IQCS$) and the measure of kurtosis (k) was computed to quantify symmetry of the distributions.

Results:
SEM images revealed distinct particle morphologies (round, elliptic to parallelogram shaped) and diverse particle geometry (S_o= 0.29-0.57) which contributed to variable flowability (θ=28.98±3.11). An increase in the geometric mean diameter (M=250.47±0.32) provided a lower angle of repose (θ=28.62±0.49). Size analysis showed positively skewed distributions ($IQCS$=+0.411) with 71% of particles falling in the mean size range of 169-356 µm for the PLGA samples analyzed. These size distributions were regarded as pharmaceutically tight (σ_g=1.764).

Conclusion:
The data suggests that the flowability of the various PLGA grades examined is influenced by their micromeritic properties. The size distributions were relatively tight, and thus not much refining is required in pre-compression stages during fabrication of the DSMT. These properties confer PLGA as suitable for direct compression in formulating the novel DSMT.

9: 1st Symposium on Biomaterials Science and Applications in South Africa, University of the

Witwatersrand, 4th September, 2006.

A Novel Doughnut-Shaped Minitablet (DSMT) for Intraocular Implantation in HIV+ patients

Yahya E. Choonara [a], Viness Pillay [a], Trevor Carmichael [b], Michael P. Danckwerts [a]
[a] *University of the Witwatersrand, Department of Pharmacy and Pharmacology, 7 York Road, Parktown 2193, Johannesburg, Gauteng, South Africa*
[b] *Department of Ophthalmology, Faculty of Health Sciences, 7 York Road, Parktown 2193, Johannesburg, Gauteng, South Africa*

Background: Cytomegalovirus retinitis (CMV-R) is a common cause of visual loss in individuals with AIDS. If left untreated it may lead to blindness. Intravenous ganciclovir is effective, but requires frequent dosing and has serious systemic side effects. Intravitreal therapy has become a useful option but is still a highly invasive and difficult route to administer. The pharmaceutical world is aware of this challenge, and therapeutic advances are being made that have the potential to improve patient care and quality of life. Promising developments are intraocular implants that deliver drugs directly to the vitreous and retina. An implantable system called *Vitrasert*® has been developed, however it is complicated to produce, very expensive and has the disadvantage of having to be removed from the eye once its drug loaded has been depleted, as it is not bioerodible/bioabsorbable.

Objectives: This study focuses on the formulation and process variables used in the design and development of a novel biodegradable doughnut-shaped minitablet (DSMT) as a device for rate-controlled intraocular delivery of Ganciclovir (GCV) and Foscarnet (FOS), two routinely employed antivirals for the treatment of CMV-R.

Results: DSMT's were prepared utilizing various grades of PLGA (Resomer®) consisting of different quantities of GCV and FOS. Preformulation, drug release, and biodegradation studies were conducted. Formulations were compressed using a novel central-rod punch and die system. *In vitro* drug release studies were performed in simulated vitreous humour (SVH) (pH 7.4; 37°C) using a novel dissolution method. Samples were analyzed by HPLC. Process variables, namely compressibility and flowability were studied. The Brinell Hardness Number (BHN) was computed to confirm the reproducibility of different compression forces employed. SEM was used to evaluate the surface morphology of pre- and post-DSMT dissolution samples. *In vitro* release studies demonstrated that DSMT's released GCV and FOS in a biphasic manner over 6 weeks. There was an initial burst effect (35% in 24 hours) followed by a sustained lag-period (42% over 936 hours) and then a release phase to completion. Resomer® RG504 provided a slower release rate due to its higher inherent viscosity (0.45-0.60 dl/g). The BHN values for both polymers reflected that compressibility was consistent (148.54 N/mm^2; CV=1.5%). Resomer® RG504 (θ=12.18 ± 0.88) showed a superior flowability over RG502 (θ=29.77 ± 1.06). SEM studies at time t_0 reflected a compact and smooth surface. After 24 weeks of exposure to SVH, the implants retained their shape, and became porous due to matrix erosion.

Conclusion: DSMT's provide flexible, yet rate-controlled intraocular drug release and may be advantageous for *in situ* drug treatment of CMV-R in HIV+ patients.

Appendix C: Patent Publication

HAMILTON BROOK SMITH REYNOLDS
Intellectual Property Law

Hamilton, Brook, Smith & Reynolds, P.C.
530 Virginia Road P.O. Box 9133
Concord, MA 01742-9133

T 978.341.0036
F 978.341.0136
www.hbsr.com

David E. Brook
David.Brook@hbsr.com
978.341.0036 x3211

June 12, 2007

Mr. Llewellyn Parker
Bowman Gilfillan John & Kernick
165 West Street
P.O. Box 785812
Sandton, 2146
South Africa

Re: U.S. Patent Application No.: 11/288,035
Filing Date: November 28, 2005
Title: Biodegradable Implantable Drug Delivery Device
Inventors: Yahya E. Choonara, Michael P. Danckwerts, and Viness Pillay
Your Reference No.: P15953US00/LP/hh (1106881)
Our Docket No.: 3989.1000-000

US 20070122449A1

(19) **United States**

(12) **Patent Application Publication**
Choonara et al.

(10) **Pub. No.: US 2007/0122449 A1**
(43) **Pub. Date: May 31, 2007**

(54) **BIODEGRADABLE IMPLANTABLE DRUG DELIVERY DEVICE**

(76) Inventors: **Yahya E. Choonara**, Parktown (ZA); **Michael P. Danckwerts**, Parktown (ZA); **Viness Pillay**, Parktown (ZA)

Correspondence Address:
HAMILTON, BROOK, SMITH & REYNOLDS, P.C.
530 VIRGINIA ROAD
P.O. BOX 9133
CONCORD, MA 01742-9133 (US)

(21) Appl. No.: **11/288,035**

(22) Filed: **Nov. 28, 2005**

Publication Classification

(51) **Int. Cl.**
A61F 2/02 (2006.01)

(52) **U.S. Cl.** **424/426**

(57) **ABSTRACT**

The invention relates to biodegradable and implantable devices for the in situ delivery of a pharmaceutical composition to a human or animal that comprise a generally discoid body, having at least one aperture through which the body is anchorable by suture, and that are formed from biodegradable polymeric compositions. The invention relates to methods of manufacturing devices for the in situ delivery of a pharmaceutical composition to a human or animal that comprise a generally discoid body, having at least one aperture through which the body is anchorable by suture, and that are formed from biodegradable polymeric compositions. The invention relates to a therapeutic method that comprises inserting a biodegradable and implantable device that comprises a generally discoid body, having at least one aperture through which the body is anchorable by suture, and that is formed from a biodegradable polymeric composition, into a body cavity of a human or animal.

UNITED STATES PATENT AND TRADEMARK OFFICE

APPLICATION NUMBER	FILING OR 371(c) DATE	FIRST NAMED APPLICANT	ATTY. DOCKET NO./TITLE
11/288,035	11/28/2005	Yahya E. Choonara	3989.1000-000

CONFIRMATION NO. 1293

21005
HAMILTON, BROOK, SMITH & REYNOLDS, P.C.
530 VIRGINIA ROAD
P.O. BOX 9133
CONCORD, MA01742-9133

Title: Biodegradable implantable drug delivery device

Publication No. US-2007-0122449-A1
Publication Date: 05/31/2007

NOTICE OF PUBLICATION OF APPLICATION

The above-identified application will be electronically published as a patent application publication pursuant to 37 CFR 1.211, et seq. The patent application publication number and publication date are set forth above.

The publication may be accessed through the USPTO's publically available Searchable Databases via the Internet at www.uspto.gov. The direct link to access the publication is currently http://www.uspto.gov/patft/.

The publication process established by the Office does not provide for mailing a copy of the publication to applicant. A copy of the publication may be obtained from the Office upon payment of the appropriate fee set forth in 37 CFR 1.19(a)(1). Orders for copies of patent application publications are handled by the USPTO's Office of Public Records. The Office of Public Records can be reached by telephone at (703) 308-9726 or (800) 972-6382, by facsimile at (703) 305-8759, by mail addressed to the United States Patent and Trademark Office, Office of Public Records, Alexandria, VA 22313-1450 or via the Internet.

In addition, information on the status of the application, including the mailing date of Office actions and the dates of receipt of correspondence filed in the Office, may also be accessed via the Internet through the Patent Electronic Business Center at www.uspto.gov using the public side of the Patent Application Information and Retrieval (PAIR) system. The direct link to access this status information is currently http://pair.uspto.gov/. Prior to publication, such status information is confidential and may only be obtained by applicant using the private side of PAIR.

Further assistance in electronically accessing the publication, or about PAIR, is available by calling the Patent Electronic Business Center at 703-305-3028.

Pre-Grant Publication Division, 703-605-4283

JUN - 7 2007
DEB/KAC

Appendix D: University of the Witwatersrand Animal Ethics Screening Committee (AESC) Clearance Certificates and Ethical Approval

AESC 3

STRICTLY CONFIDENTIAL

UNIVERSITY OF THE WITWATERSRAND, JOHANNESBURG

ANIMAL ETHICS SCREENING COMMITTEE

CLEARANCE CERTIFICATE NO:

2002	4	5

APPLICANT: Professor M Danckwerts

DEPARTMENT: Pharmacy & Pharmacology

PROJECT TITLE: Intraocular Therapy for Cytomegalovirus Retinitis

Species	Number	Expiry Date
Rabbits	60	2004

i) Approval is hereby given for the experiment described in the above application.

The use of these animals is subject to AESC Guidelines for the use and care of animals, is limited to the procedures specified in the application form, and to:

APPROVED

SIGNED D.A. Gray
(Chairman: Animal Ethics Screening Committee)

DATE:28 February 2002

ii) I am satisfied that the persons listed in this application are competent to perform the procedures therein, in terms of Section 23(1)(c) of the Veterinary and Para-veterinary Professions Act (19 of 1982)

SIGNED
(Registered Veterinarian)

DATE: 28 February 2002

NOTE:

First-time users of the CAS should contact the Director of the CAS in order to familiarise themselves with the facilities available, and the procedures required by the CAS for the carrying out of experiments.

UNIVERSITY OF THE WITWATERSRAND, JOHANNESBURG

STRICTLY CONFIDENTIAL

ANIMAL ETHICS SCREENING COMMITTEE (AESC)

CLEARANCE CERTIFICATE NO. 2006/40/04

APPLICANT: Mr YE Choonara

SCHOOL: Therapeutic Sciences
DEPARTMENT: Pharmacy
LOCATION: Medical School

PROJECT TITLE: In vivo evaluation of a novel doughnut-shaped minitablet for intraocular implantation

Number and Species

60 rabbits

Approval was given for to the use of animals for the project described above at an AESC meeting held on 20060425. This approval remains valid until 20080424.

The use of these animals is subject to AESC guidelines for the use and care of animals, is limited to the procedures described in the application form and to the following additional conditions:

SOP requires either Dr Meyer or Kennedy be present at surgical procedures. A pilot must first be done for each procedure.Number of animals to be used must be discussed. After report back all animals could be approved.

Signed: D. A. Gray (Chairperson, AESC) Date: 06/06/06

I am satisfied that the persons listed in this application are competent to perform the procedures therein, in terms of Section 23 (1) (c) of the Veterinary and Para-Veterinary Professions Act (19 of 1982)

Signed: _____ (Registered Veterinarian) Date: 12/06/06

cc: Supervisor: Professor V Pillay
Director: CAS

Works 2000/tain0015/AESCCert.wps

AESC 2008

Please note that only typewritten applications will be accepted. Should additional space be required for section "I" and/or "j", please use the back of this form.

ANIMAL ETHICS SCREENING COMMITTEE

MODIFICATIONS AND EXTENSIONS TO EXPERIMENTS

a. Name: Yahya E. Choonara

b. Department: Pharmacy and Pharmacology

c. Experiment to be **extended**

	AESC NO:		
Original AESC number	2006	40	04
Other M&E's : None			

d. Project Title: *In vivo* evaluation of a novel doughnut-shaped minitablet for intraocular implantation

e.	Number and species of animals **originally approved**:	60	New Zealand White Rabbits
f.	Number of additional animals **previously allocated on M&Es**:	0	No additional animals required
g.	Total number of animals **allocated** to the experiment to date:	30	
h.	Number of animals **used** to date:	18	

i. Specific extension requested:

The study is not yet complete and the current ethics clearance application has expired.

j. Motivation for extension:

The study has begun in Mid-June 2007 and was scheduled to begin at the beginning of 2007. Due to unforeseen logistical issues the study begun at a later date. Furthermore, the device implanted into the rabbit eye is intended for the sustained release of drug over several months. Due the promising results achieved thus far the study has continued longer than anticipated as a single study is completed over a 70-80 day period in which time drug levels are still achieved. The current experiment will be completed toward the end on June 2008 and we propose the next experiment to continue over the next 6-12 months depending on the performance of the device. In each experiment the concentration of the polymer is altered to vary the drug release rate from the device within the eye. In this regard we would like to extend the ethics clearance/approval for another 2 year period.

Date: 8th May 2008 Signature:

RECOMMENDATIONS:

APPROVED

Date: 08/05/08 Signature: Chairman, AESC

Appendix E: Results of Animal Health Analysis for Disease Screening

CENTRAL ANIMAL SERVICE

Tel: 011717-1312
Fax: 011 643-4318

DEAR ANIMAL USERS

It is with great satisfaction that we can inform Central Animal Service users of the positive outcome of our animal disease surveillance program.

Central Animal Services sent a batch of 20 rats, 20 mice and 20 rabbits, a statistically representative sample from our stock animals, to Golden Vetpath for disease screening. This was done to check that the animals supplied to researchers are all in good health.

Golden Vetpath is a division of Idexx Laboratories and has a sister company in Germany called Biodoc.

All the serology tests were done by Biodoc and a full post mortem, histopathology and bacteriology were conducted by Vetpath.

The results were as follows:

- The rats, mice and rabbits were free of any infectious viral or bacterial diseases.
- There was no indication that any of the animals were infected or carried mycoplasma.

The surveillance program will continue on a bi-annual basis and the next batch of animals will be sent for surveillance in the next few months. We feel confident that we can maintain the health status of our animals so that you as the researcher can continue to do high standard research.

We will keep you updated on the results of our health monitoring on a regular basis.

Kind regards

Erika Vercuiel (Principle Vet Nurse) and the CAS team
11th February 2008.

Appendix F: Isotron Certificates of DSMT Device Sterilization

Isotron
SOUTH AFRICA (PTY) LTD
(Reg. No. 1998/024219/07)
5 Waterpas Street
Isando Extension 3
P.O. Box 3219
Kempton Park 1620
Tel: (011) 974-8851
Fax: (011) 974-8986
Email: info@isotron.co.za
Gamma Radiation Processing

Certificate of Gamma Irradiation

Certificate Number
56242

This is to certify that
ISOTRON SOUTH AFRICA (PTY) LTD

Has given an irradiation treatment in accordance with:

- The national and international quality assurance system standards: ISO 9001:2000
- The precision and accuracy of the dosimetry system used is traceable to International Standards.

to the following goods (as described by the Manufacturer):

Customer	UNIV OF WITWATERSRAND DEPT OF PHARMACY	Customer order no.	Irradiation completion date
Isotron control number (Internal order number)	63871 / 1	YAHYA02	27/07/2007
Isotron stock code	000 025 TR01	Conforms to the Specified Irradiation Dose of:	
Product description	TRIAL SAMPLE 25KGY.D	Minimum:	25.0 kGy
		Maximum:	kGy
Quantity of containers	Mass of containers Kg	Routine Dose Reading:	25.8 kGy
1	1.00	Ref. Dose Mapping:	

Date 27/07/2007 Product Released By Quality Department

ISO-9 REV: 08

Isotron
SOUTH AFRICA (PTY) LTD
(Reg. No. 1998/024219/07)
5 Waterpas Street
Isando Extension 3
P.O. Box 3219
Kempton Park 1620
Tel: (011) 974-8851
Fax: (011) 974-8986
Email: info@isotron.co.za
Gamma Radiation Processing

Certificate of Gamma Irradiation

Certificate Number
57058

This is to certify that
ISOTRON SOUTH AFRICA (PTY) LTD

Has given an irradiation treatment in accordance with:

- The national and international quality assurance system standards: ISO 9001:2000
- The precision and accuracy of the dosimetry system used is traceable to International Standards.

to the following goods (as described by the Manufacturer):

Customer	UNIV OF WITWATERSRAND DEPT OF PHARMACY	Customer reference no.	Irradiation completion date
Isotron control number (Internal order number)	64509 / 1	64176	22/08/2007
Isotron stock code	000 025 TR01	Conforms to the Specified Irradiation Dose of:	
Product description	TRIAL SAMPLE 25KGY.D	Minimum:	25.0 kGy
		Maximum:	kGy
Quantity of containers	Mass of containers Kg	Routine Dose Reading:	25.8 kGy
1	1.00	Ref. Dose Mapping:	

Date 22/08/2007 Product Released By Quality Department

ISO-9, REV: 08

Appendix G: UPLC Chromatograms for assay method validation and drug content analysis